INTERNET OF DRONES DEPLOYMENT FOR INTELLIGENT TRANSPORTATION SYSTEM APPLICATIONS

BY

GAMIL ABDULLAH MOHSEN AHMED

A Dissertation Presented to the

DEANSHIP OF GRADUATE STUDIES

KING FAHD UNIVERSITY OF PETROLEUM & MINERALS

DHAHRAN, SAUDI ARABIA

In Partial Fulfillment of the
Requirements for the Degree of

DOCTOR OF PHILOSOPHY

In

COMPUTER ENGINEERING

APRIL 2022

KING FAHD UNIVERSITY OF PETROLEUM & MINERALS

DHAHRAN 31261, SAUDI ARABIA

DEANSHIP OF GRADUATE STUDIES

This dissertation, written by GAMIL ABDULLAH MOHSEN AHMED under the direction of his dissertation adviser and approved by his dissertation committee, has been presented to and accepted by the Dean of Graduate Studies, in partial fulfillment of the requirements for the degree of **DOCTOR OF PHILOSOPHY IN COMPUTER ENGINEERING**.

Dissertation Committee

Dr. Tarek Sheltami (Adviser)

Dr. Ashraf Mahmoud (Member)

Dr. Marwan Abu-Amara (Member)

Dr. Mohamed Deriche (Member)

Type text here

Dr. Ansar Yasar (Member)

Dr. Aiman El-Maleh
Department Chairman

Dr. Suliman Al-Homidan
Dean of Graduate Studies

Date

To my beloved parent's souls

ACKNOWLEDGMENTS

First and foremost, I would like to express my deepest gratitude to Allah Almighty as with the blessing this project has successfully been concluded. I would like to express my deepest appreciation to my advisor Prof.Tarek Sheltami for his constant support. He has always been there to listen and answer my questions, read and review my report. I also thank my thesis committee members: Dr.Ashraf Mahmoud, Dr. Marwan Abu-Amara, Dr. Mohammed Dirrish, and Dr.Ansar Yasar for their insightful comments and advice on my thesis and final defense. I am also grateful to all my family members for their continuous support. Also, to my children who have been a constant source of inspiration with their enthusiasm and positivity. My sincere appreciation goes to Ibb university, the Higher Education Ministry of Yemen, and King Fahd University of Petroleum and Minerals (KFUPM) for providing me with the opportunity to continue my graduate studies. Special thanks to Computer Engineering Department at KFUPM for their invaluable support.

Contents

List of Tables

List of Figures

LIST OF ABBREVIATIONS

AFV	Average Fitness Value
AMN	Aerial Mesh Network
AODV	Adhoc On Demand Distance Vector Routing Protocol
AOI	Area Of Interest
APs	Access Points
BS	Base Station
BSM	Basic Safety Message
CPP	Coverage Path Planning
DEM	Digital Elevation Model
DSDV	Destination-Sequenced Distance-Vector Protocol
DT	Duration Time
E2ED	End-to-End delay
FGA	Fast Geometric Avoidance Algorithm
IoD	Internet of Drones
IoD2V	IoD-to-Vehicle
IPSO	Improved Particle Swarm Optimization

ITS	Intelligent Transportation Systems
MILP	Mixed Integer Linear Programming
MPR	Multi-Point Relay
NLOS	Non-Line-Of-Sight
NOCs	Number of Collisions
OLSR	Optimized Link State Routing
OSM	Open Street Map
P2P	Point to Point
PDR	Packet Delivery Ratio
POIs	Point of Interests
PSO	Particle Swarm Optimization
RREQ	Route Request
RSSI	Received Signal Strength Indicator
RSUs	Road Side Units
SEA	Safety Ensure Approach
SPSO	Standard PSO
SRTM	Shuttle Radar Topology Mission
U2U	UAV-to-UAV
V2I	Vehicle-to-Infrastructure
V2V	Vehicle-to-Vehicle
V2X	Vehicle-to-Every thing

VANET	Vehicular Ad hoc Networks
VRP	Vehicle Routing Problem
WAVE	Wireless Access in Vehicular Environments
WHO	World Health Organization

DISSERTATION ABSTRACT

NAME:	Gamil Abdullah Mohsen Ahmed
TITLE OF STUDY:	Internet of Drones Deployment for Intelligent Transportation System Applications
MAJOR FIELD:	Computer Engineering
DATE OF DEGREE:	April, 2022

Intelligent Transportation Systems (ITS) is a leading technology endowed with cutting-edge technological advances to provide traffic safety and efficiency, and to integrate vehicles and infrastructures with the cooperative vehicular technique by utilizing the future trends. The emergence of Internet of Drones (IoD) has attracted much attention lately as it is used in a multitude of applications. However, the design of IoD deployment and coverage path planning has been hampered by underline limitations and challenges, which motivate the quest for efficient solutions. To cope with such challenges, this thesis analyzes the most recent collision-free path planning protocols and UAVs deployment approaches to identify some of their potential gaps and then proposes efficient mechanisms to fill such gaps. First, this *thesis proposes energy efficient path planning approaches to avoid multiple static and dynamic obstacles of different sizes. More importantly, the results validate the efficiency and accuracy of the proposed algorithms in a sparse and dense environment that involves high collision risk with obstacle relative speeds up to 10 meters/second. Second, this thesis proposes two novel dynamic IoD collaborative communication approaches for VANETs assistant, namely, IoDAV, 3DIoDAV, in two and three-dimension terrain, respectively, to enhance the VANETs connectivity. In the former approach, the flat terrain is assumed while the impact of terrain elevation on communication is considered in the latter by proposing a 3D propagation model for an efficient IoD-to-Vehicle (IoD2V) communication in 3D space. The simulation results demonstrate that the proposed IoDAV approach allows finding the optimal IoD positions throughout the time based on the vehicle's movements. Besides, the simulation results of 3DIoDAV show the ability of the proposed approach in detecting the terrain obstacles and thus, guarantees to dispatch the IoD nodes into the most appropriate locations in 3D space that minimize the impact of terrain obstacles on communication. Third, routing protocols are analyzed and AODV is found to be a suitable routing protocol in IoD network. Finally, this thesis proposes a mathematical model for coverage and path planning based on mixed-integer linear programming (MILP) formulation.The results are compared with the heuristic approach, and demonstrate the importance of using the heuristic approach in large-scale problem sizes.*

ملخص الرسالة

الاسم: جميل عبد الله محسن أحمد

عنوان الدراسة: نشر إنترنت الطائرات بدون طيار لتطوير تطبيقات نظام النقل الذكي

التخصص: هندسة الحاسب الآلي

تاريخ الدرجة العلمية: رمضان 1443

حظيت أنظمة النقل الذكية باهتمام كبير باعتبارها تقنية رائدة تتمتع بأحدث التطورات التكنولوجية لتوفير السلامة والكفاءة في التدريب واستخدام الاتجاهات المستقبلية لدمج المركبات والبنى التحتية مع تقنية المركبات التعاونية. جذب ظهور إنترنت الطائرات بدون طيار الكثير من الاهتمام مؤخرًا ويتم استخدامه في العديد من التطبيقات. ومع ذلك ، فان تصميم نشر الطائات بدون طيار وتخطيط مسار التغطية يواجه بالعديد من القيود والتحديات، التي تحفز البحث عن حلول فعالة. للتعامل مع مثل هذه التحديات ، تحلل هذه الأطروحة أكثر بروتوكولات تخطيط المسار الخالية من الاصطدامات وأساليب نشر الطائرات بدون طيار لتحديد بعض الفجوات المحتملة ، ثم تقترح آليات فعالة لسد هذه الفجوات. أولاً تقترح هذه الأطروحة طريقتين لتخطيط مسار لسرب من الطائرات بدون طيار للعمل في البيئة الثابتة والمتحركة، لتجنب العديد من العوائق الثابتة والمتحرك ذات الأحجام المختلفة ضمن نطاق اكتشاف محدود ومسار كامل مع تقليل استهلاك الطاقة. وتظهر النتائج كفاءة ودقة الخوارزميات المقترحة في بيئة متفرقة وكثيفة تنطوي على مخاطر تصادم عالية مع سرعات نسبية للعوائق تصل إلى 10 أمتار / ثانية. ثانيًا، لتعزيز اتصال شبكة المركبات المخصصة، تقترح هذه الأطروحة طريقتين جديدتين للاتصال التعاوني الديناميكي للطائرات بدون طيار لمساعد شبكة المركبات المخصصة ، وهما 3DIoDAV وIoDAV ، في تضاريس ثنائية وثلاثية الأبعاد، على التوالي. في النهج الأول ، يُفترض أن الأرض المسطحة بينما تُؤخذ في الاعتبار تأثير ارتفاع التضاريس على الاتصال في الأخير من خلال اقتراح نموذج اتصال فعال ثلاثي الأبعاد بين الطائات بدون طيار في الجو والمركبات على الارض ويسمى (IoD2V) في مساحة ثلاثية الأبعاد. يتم إجراء عمليات محاكاة مكثفة بناءً

على الإشارة المستقبلة في المركبات على الارض وذلك لفحص أداء النماذج المقترحة. توضح نتائج المحاكاة أن نهج IoDAV المقترح ينشر الطائرات بدون طيار في مواقع أفضل بشكل مستمر بناءً على حركات السيارة ويحقق تغطية أفضل وجودة أفضل للإشارة المستقبلة من خلال إيجاد أنسب موضع .للطائرات بدون طيار. إلى جانب ذلك ، تُظهر نتائج المحاكاة لنموذج 3DIoDAV قدرة النهج المقترح في اكتشاف عوائق التضاريس، وبالتالي تضمن إرسال الطائرات بدون طيار إلى أنسب المواقع في مساحة ثلاثية الأبعاد لتقليل تأثير عوائق التضاريس على الاتصال. أخيرًا ، تقترح هذه الأطروحة نموذجًا رياضيًا للتغطية وتخطيط المسار بناءً على صياغة البرمجة الخطية المختلطة، وتتم مقارنة النتائج بالنهج الاستدلالي وتوضح أهمية استخدام النهج الاستدلالي في أحجام المشكلات واسعة النطاق.

CHAPTER 1

INTRODUCTION

Recently, Intelligent Transportation Systems (ITS) have emerged as an efficient way of enhancing travel security, providing more choices to travelers, and improving the performance of transportation systems. The smartness measurement for smart city is related to its traffic monitoring, disaster management, quality of life, healthcare, air quality, energy consumption, public safety, and other services. Thus, to make cities smarter, the advanced information and communication technology is combined with a better transportation infrastructure together in ITS to pave the way for providing novel services in ITS environments. The aims is to making traffic more efficient, convenient, and safe, addressing professional goals such as changing the way we drive to reduce fuel consumption and accidents. This will eventually promote road safety, minimize transportation problems such as congested roads, and will in general help at making cities more sustainable. The distribution of some services and facilities everywhere and reducing the services cost while achieving a good infrastructure is an important aspect in the smart cities. Furthermore, the harmful effects on the environment and awareness raise due to the congestion and inefficient vehicles. It is worth mentioning that the development in telecommunications and computing technologies has accelerated the researches towards smart transportation [1]. This fast growth of paradigm is characterized by an open architecture that allows transportation objects to interact and cooperate in executing a wide range of tasks [2]. Besides, enabling a plethora of applications such as intelligent guidance and collision avoidance, provides comfort and convenience as well as increases safety during driving. Therefore, the ITS is expected to play a significant role in future smart cities [3]. In fact, the safety is the biggest motivation in most research in transportation systems. The World World Health Organization (WHO) [4] reported that "more than 1.2 million people die every year due to road accidents. Another 20 to 50 million are injured in crashes".

Furthermore, the overall transportation system automation cannot be achieved through vehicles automating only. Indeed, other components of the end-to-end transportation system and road also need to be automated such as rescue teams, field support team, road surveys, and traffic police using UAVs. An example of collaboration of UAVs swarm deployment for traffic monitoring of a smart city is illustrated in Fig1.1.

The ITS model includes Vehicular Ad hoc Networks (VANET) that provides an important services such as traffic management and navigation, as well as safer road. VANET is a wireless communications network that provides an enhancement Vehicle-to-Vehicle (V2V) communications and driving. The Vehicle-to-Every thing (V2X) communication model includes V2V and Vehicle-to-

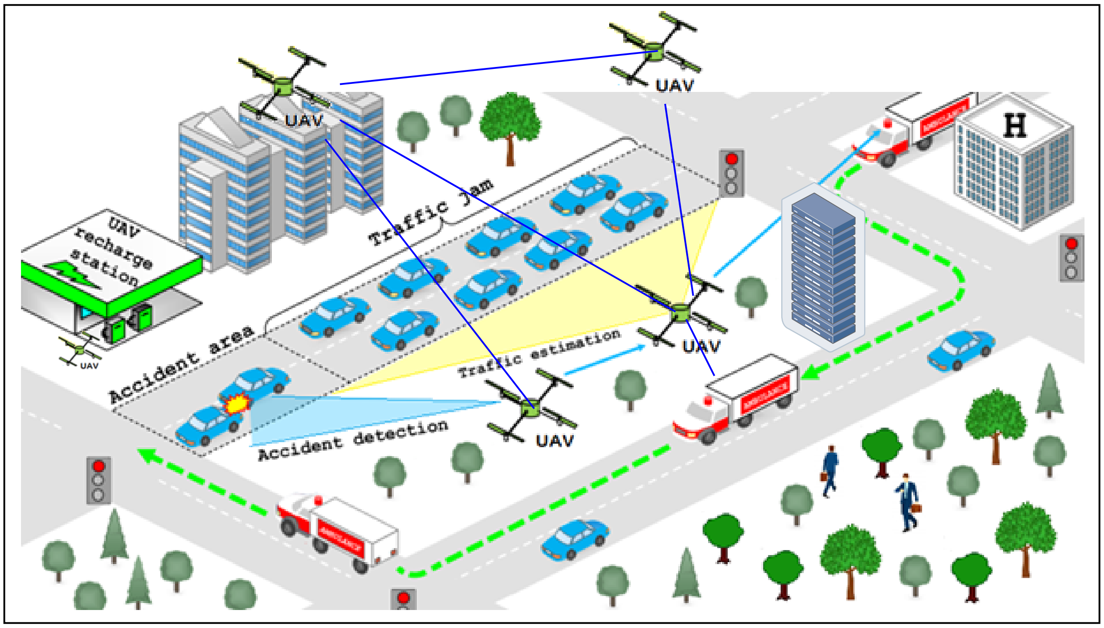

Figure 1.1: Collaboration of UAVs swarm deployment for traffic monitoring of a smart city.

Infrastructure (V2I) communications in which the vehicles act as relays to provide collaborative driving between connected vehicles on the road. VANET makes use of two different technologies depending on the application: Ad hoc communications through the 802.11p standard, and infrastructure networks that use cellular networks or Wi-Fi. In infrastructure networks, a base station is deployed based on a centralized network topology, and the data is delivered from/to the vehicles on the ground for real-time transportation information, safety, control data, and entertainment. The communication channel between vehicles and infrastructures facilitates efficient and safe V2I and V2V communications. Reliable and efficient transmission amongst vehicles and Road Side Units (RSUs) is a prime concern of ITS [5]. The design of an efficient communication system has pertained to underlying limitations such as heterogeneity, high mobility, and channel variation. To cope with such limitations, the dedicated Base Station (BS) is brought to the road edge by proposing the RSU. Another challenge to consider in V2X communications is when the area lacks infrastructure support. Although vehicle communications can rely on many wireless access technologies [6], for example the use of 4G LTE technology to support communications in areas with limited infrastructure such as rural areas. The main problems usually arise when communications take place in areas that have no infrastructure support at all. Ad-hoc communications are the preferred networking approach in vehicular scenarios, since the multiple vehicles have to be included in information dissemination. It has to be noted that although the deployment in direct Wi-Fi is easy and fast, it provides only single hop communications. Therefore, the services provided by ITS cannot be fully deployed using this technology.

Over the last few years, research in Internet of Drones (IoD) formation has gained a broad-spectrum attention in various complex applications due to its unique features such as agility, mobility, flexibility, and quick deployment at a target area that allow it to navigate a rough and remote area that humans cannot access [2], [7]. Therefore, for applications that require highly complex tasks, which individual drone can't perform effectively, IoD can be used to accomplish such tasks efficiently. On the other hand, the rapidly growing popularity of IoD for consumer applications dramatically increases the number of accidents involving drones. The drone faces two types of environment obstacles during its mission, namely, static and dynamic obstacles. For the former, locations of obstacles are known and fixed, while the locations of obstacles are changeable in the letter, and they may appear suddenly in front of the drone [8]. Thus, for drones to complete their missions, the prime concern is the mission's safety. Without preventing collision among drones and with obstacles, safety is not guaranteed. The main challenge in IoD formation is the need for an efficient and effective collision avoidance protocol in static and dynamic environments, which is very important in civilian and military applications [2].

The terrain coverage is one of the most important tasks of drones, which has been engaged in many applications, such as disaster management, photography, and intelligent agriculture [9]. In such applications, planning an efficient flight path is a critical issue due to limited onboard battery-powered that limits the flight time of a drone.

The path planning can be classified into two types, namely, point to point path planning and Coverage Path Planning (CPP). In the former, the path connects a set of consecutive points from start point to the destination point without considering the coverage of Area Of Interest (AOI), while the path covers the whole region by passing through all points of AOI from starting point, i.e., depot, to the endpoint and returning to the depot while detecting and avoiding obstacles [10]. The goal of the CPP mechanism is to seek an optimal collision-free flight path so that full coverage of a given region is guaranteed under specific constraint conditions which is a complicated global optimum problem.

Among different types of drones, a quadrotor drone is becoming popular and mainly utilized in a variety of applications due to its low cost, simple design, small size, and ability to hover in place. Moreover, many applications involve commercial quadrotor UAVs such as search and rescue, monitoring, and surveillance photograph [11], [12]. In this thesis, the terms UAV and drone are used interchangeably.

1.1 Thesis Motivation

Despite the advancement in today ITS in some countries, these ITS are still limited inside cities and most roads have no sort of infrastructure supporting for vehicular networks. Furthermore, as the technology advances, drones become increasingly autonomous and gain new capabilities. On the other hand, in high drones density and increasingly complex mission situations, drones pose new threats as they get closer to each other or obstacles. Also, control and communication become more complex and difficult to manage. In addition, these IoD may merge from different directions, where the risk of catastrophic collision increases. For instance, in certain situations like an urban environment, the drones are tasked to fly through such an environment and must quickly navigate around considerable obstacles while avoiding the collision. Another scenario, in a forested environment, the drone has to travel throughout the tree lines and has to avoid collisions. In such applications, the drone needs to be endowed by an efficient approach to respond quickly and avoid collision with nearby obstacles, while planning its flight path. Although several works have been done to avoid static and dynamic obstacles, the researchers test their approaches using a small number of obstacles in large environments where the probability of collision is very low making their approaches suitable for light environment applications and they are not guaranteed to work in dense environments.

This thesis analyzes the most common existing collision-free path planning and IoD deployment mechanisms for identifying some of their potential gaps and then attempt to propose more effective algorithms to fill these gaps. The remaining of this subsection is devoted to explain the collision avoidance and IoD deployment strategies.

1.1.1 IoD Collision-Free Static Path Planning

In highly dense environment where static and dynamic obstacles fill the region, drones density and increasingly complex mission situations, drones pose new threats as they get closer to each other or obstacles. In highly congested terrain, dynamic and static obstacles have a critical impact on IoD performance. One of the critical challenges in IoD missions is to avoid obstacles for successfully and safely completing tasks. As drones density increases, the probability of intra-collision increases and the collision avoidance becomes a challenging task that need to be addressed. In dynamic path planning, complete information about the environment may not be available ahead of time, so incomplete knowledge about dynamic obstacles is assumed. In this case, the obstacle has to be detected during the mission, which requires real-time path optimization or dynamic path planning in which a complete path is not available. But rather an optimal path information within the drone's field's of view. Besides, each member requires to maintain a specific minimum distance from other drones in the formation [13].

Generating a safe path that is collision-free for IoD formations is the key challenging task in dense swarm and environment constraints. These shortcomings motivate the quest for a solution where IoD should be endowed by an intelligent and accurate collision avoidance algorithm in which IoD paths are modified to guarantee drones' safety.

1.1.2 IoD Energy Efficient Static and Dynamic Collision-Free Path Planning

Despite the distinct features of UAVs and their increasing popularity, inherent limitations still hinder the full potential of their applications. The main limitation is the limited lifetime of on-board batteries which limits its flight time [14]. As a result, most applications can not reach their full potentials. Moreover, for a long path where the drone needs to perform its mission in a large area, the energy consumption by UAV should be minimized to generate a safety path and reach its destination. To clarify the picture, if the energy of the UAV is improved, the UAV can accomplish more tasks in a shorter time. Conversely, if the drone is not endowed by an efficient energy mechanism, it needs to perform more recharge cycles which increases the mission time. For this reason, reducing the energy consumption during the drone mission is a key challenging problem. To tackle this challenge, UAV should be endowed by energy model so that the collision-free paths are generated with minimum energy.

1.1.3 2D IoD Assisted-VANENT

VANETs have gradually emerged as a leading technology to deliver the data from/to the vehicles on the ground for real-time transportation information, entertainment, safety, and control data [15], [16]. The design of an efficient communication system has pertained by underlying limitations such as heterogeneity, high mobility, and channel variation. To cope with such limitations, the dedicated base station (BS) is brought to the road edge by proposing the RSU [17]–[19]. But, fixed RSU is limited by environment constraints that reduce the probability of the Line-Of-Sight (LOS) condition. This problem can be addressed by increasing the number of RSUs, resulting in a high deployment cost. Moreover, the vehicles in the VANET network are allowed to follow a restricted road and communicate with each other and with stationary stations alongside the road. However, the dynamic movement of vehicles causes frequent topology changes; therefore, the connectivity of a large number of vehicles is intermittent [20]–[22].

Recently, IoD has seen a significant consideration due to its high potential influence. It can be integrated with other architectures to bring a plethora of applications to our life such as telecom, military, rescue, search, and monitoring as mentioned above. Unlike static infrastructures on the ground, IoD can achieve a better LOS condition toward ground users when acting as a relay network. Therefore, It provides an effective and efficient temporary communication in the emergency situation in which the terrestrial infrastructures are damaged or unavailable. Due to the above distinctive traits of the IoD paradigm, V2V communication can be enhanced by deploying a swarm of UAVs as a relay network to establish a reliable wireless communication between vehicles in VANETs.

The deployment of the IoD network has been studied in the literature for coverage problems. However, such deployment has been restricted by underline challenges. Although deploying IoD at a high altitude provides a better LOS condition, the distance between the IoD network and vehicles on the ground increases which in turn increases the path loss.

1.1.4 3D IoD Assisted-VANENT

The terrain features have a significant impact on IoD-to-Vehicle (IoD2V) communication because the height of the terrain can act as an obstacle and causes signal attenuation. As a result, the IoD2V communication will experience the effect of multipath propagation.

1.1.5 IoD Energy Efficient Coverage Path Planning

The coverage problem for terrain is one of the most essential tasks of IoD, which has been engaged in many applications, such as disaster management, photography, and intelligent agriculture [9], [23]. In such applications, planning an efficient flight path is a critical issue due to limited onboard battery-powered that limits the flight time of a drone. Although adapting the swarm of drones in coverage path planning achieves flexibility enhancement and cost reduction in practical applications development, carrying out their path planning in a complex and large-scale environment increases the complexity of collaborative control and decision-making systems [24]. Such strategies have a significant impact on coverage problem efficiency because generating trajectories require several constraints and high levels of coordination, which are highly dependent on the positions of UAVs.

1.1.6 IoD Routing Protocols

Routing protocols are essential In IoD network to exchange packets, and play a significant role to enable reliable UAV-to-UAV (U2U) communications for the IoD network. However, developing these protocols in highly dynamic topology changes becomes a challenge. The extreme change in topology causes intermittent disconnection of the network. The restriction range between the drones and the base station is another challenge. Hence, dynamic topology, and high mobility of drones make the development of a routing protocol to ensure reliable communication is difficult to achieve in UAV network [25]–[27]. On the other hand, the UAV network shares many similarities with the traditional ad hoc network. Therefore, traditional routing protocols can be utilized as the basis to provide UAV swarm communication.

1.2 Thesis Objectives

This thesis aims to propose a new approach enabling drones to collaborate and intelligently be deployed to enhance the coverage of VANET network. Besides, the IoD swarm will be able to avoid drones collision. To meet our objective, this thesis proposes energy-efficient collision avoidance mechanisms and optimal IoD deployment solutions that are able to mitigate the IoD formation related shortcomings and assist the VANET network. To quantify these aims, the objectives are abstracted as follows:

- IoD Energy-Efficient Static and Dynamic Collision-Free Path Planning

UAVs consume considerable energy while planning the path and avoiding obstacles. One of the main concern is energy limitation as IoD nodes are battery powered which limits the flight time. This makes energy a precious resource that should be minimized during mission. Another concern is the collision of UAV either with terrain or with other UAVs in the formation. For safety mission, collision should be addressed for drones to accomplish their tasks. This objective is achieved in [2], [7].

- 2D IoD Optimal Deployment Solution

This is another key point to be considered which aims to provide a connectivity of VANET network where IoD acts as a rely network and can be deployed at optimal location to enhance the communication of VANET network. The IoD nodes are endowed with optimization mechanism to autonomously decide on their locations and altitudes to maximize the coverage area of application. This objective is achieved in [28].

- 3D IoD Air-to-Ground Simulation Model

The terrain has a significant impact on communication, where building, hills, and mountains act as obstacles and hinder or attenuate the transmitted signal. Thus, considering theses terrain elevations allows to efficiently dispatch the IoD into the most appropriate location that minimize the effect of terrain on communication. This objective is achieved in a journal paper accepted in Electronics.

- IoD Routing Protocols

This is also an important key for analyzing different multi-hops routing protocols suitable for drones' deployment and path planning. A draft under preparation to be submitted.

- Mathematical Model for Collision-free Coverage Path Planning

The key aim is to develop a mathematical model for path planning and coverage based on Mixed Integer Linear Programming (MILP) formulation, and compare it with heuristic approach for different problem sizes. This objective is achieved in a journal paper submitted to a special issue ”Digital Twins in Smart Transportation and Mobility” in Computer Modeling in Engineering Sciences.

1.3 Thesis Main Contributions

- IoD Static Collision-Free Path Planning via IPSO

IoD Static Path Planning via Improved Particle Swarm Optimization (IPSO) is presented in Chapter 3. The aim is to enhance the optimality and rapidity of three-dimensional IoD path generation by improving the PSO algorithm. The results exhibit significant improvement in convergence speed as well as an optimal solution, which proves the ability of the proposed method to generate a safety path for IoD formation without collision with terrain obstacle and among drones. Also, this work presents thorough analysis considering the optimality and rapidity of IPSO in generating collision-free paths for IoD. The proposed approach is implemented using matlab software. Then the strength and shortcoming are evaluated according to the obtained results. Besides, the proposed approach outperforms CIPSO [29] in terms of optimality and convergence.

- IoD Energy-efficient static and dynamic Collision-free Path Planning

It is presented in Chapter 4. The proposed approach aims to work online in a dense environment in which a drone flies through a narrow passage due to several static and dynamic obstacles filled the terrain. Therefore, the feasible paths from current locations for all drones in IoD formation are not always guaranteed. To guarantee a feasible paths for all drones in the formation, the proposed approach puts some drones in a hovering state for some time. Furthermore, the drone can backtrack when hovering in place is not possible. It is also noteworthy that, the drone is allowed to fly vertically if hovering and backtracking are not possible to avoid crashing with nearby obstacles, which increases the ability to avoid collisions. It also provides an energy-efficient path generation to obtain a collision-free path with minimum energy requirement. The algorithm is able to avoid the following collisions:

(1). Drone-to-drone collision avoidance.

(2). Drone-to-static obstacles collision avoidance.

(3). Drone-to-dynamic obstacles collision avoidance.

The proposed approach is implemented using matlab software. Besides, the proposed approach outperforms the work in [30] in terms of considering IoD formation and the number of collisions (NoCs).

- 2D Collaborative IoD-Assisted VANETs (IoDAV)

IoDAV is presented in Chapter 5. The aim is to dynamically dispatch the IoD, used as a relay network, at optimum coverage base-on cars' locations using Received Signal Strength Indicator (RSSI). In this work, the IPSO algorithm in Chapter 3 is implemented to achieve the aforementioned objectives so that sufficient signal strength towards all isolated vehicles on the ground can be achieved by the IoD network to guarantee the best coverage at each specific time. Moreover, the connectivity of the IoD network is addressed by the proposed optimization approach where the objective function includes the connectivity to be achieved for a better solution. Based on the vehicles' distribution on the ground, the proposed approach dispatches the IoD nodes to the most appropriate locations in real-time. The main assumption is that lack of infrastructures exists in the environment and the connectivity among vehicles is minimum. For example, in urban area, the buildings may obstruct the line of sight and the connectivity among vehicles is lost. Besides, the movement of UAVs in IoD aims to explore the 3D space to offer the connectivity for ground vehicles. The proposed approach is implemented using SUMO, VIENS, in OMNET++ network simulator. Then through the obtained results, the strength and shortcoming are evaluated. Besides, the IoDAV is compared against VANET without drone, i.e, No IoD and with static deployment IoD, i.e., FIoD. Finally, IoDAV outperforms NIoD and FIoD in terms of normalized overall coverage and average RSSI.

- 3D Collaborative IoD-Assisted VANETs (3DIoDAV)

3DIoDAV is presented in Chapter 6. The aim is to enhance the communication of vehicles on the ground and reduce the impact of terrain obstacles on communication. In doing so, a three-dimensional propagation model for IoD2V communication to assist the communication quality between IoD in air and cars on the ground is proposed and used in IoD assisted VANETs. Towards this end, the optimal deployment of IoD nodes is obtained by the optimization algorithm implemented, i.e., IPSO. The proposed 3D propagation model is added to the objective function to evaluate the signal quality at receivers 'sides, i.e., vehicles on the ground in which the effect of high-level terrain on communication is considered in calculating the received signal. As a result, the IoD nodes are dispatched to the most appropriate locations that minimize the impact of terrain obstacles on the transmitted signals and enhance the LOS condition between sender and receiver. The proposed approach is implemented using SUMO, VIENS, in OMNET++ network simulator. The effect of the terrain is considered by extracting the elevation information of the terrain from the Digital Elevation Model (DEM) file and then using it in calculating the received signal strength. Besides, the 3DIoDAV is compared against free-space pathloss model and IoDAV model. The results show the ability of the 3DIoDAV to detect the terrain obstacles and properly evaluate the received signal quality. Besides, the 3DIoDAV approach can retrieve the terrain information and considers it in the communication of IoD in the air and vehicles on the ground, which provided a high level of realism results.

- IoD Energy-efficient Collision-free Coverage Path Planning

It is presented in Chapter 7. The key aim is to develop a mathematical model for path planning and coverage based on mixed-integer linear programming. An optimization formulation of single and multi-UAVs collision-free coverage path planning is derived. The CPP problem is formulated as a minimization problem, where the energy consumption is used as the objective to be minimized. The proposed approach is capable of reducing energy consumption which in turn reduces the required number of drones to cover the ROI.

- IoD Routing Protocols

IoD Routing Protocols are presented in Chapter 8. The key aim is to evaluate the performance of some proactive and reactive routing protocols and identify the appropriate routing protocol that can be applied in our proposed mechanisms. The results show that the AODV routing protocol can adapt to topology change due to its natural reactive.

1.4 Thesis Organization

The reminder of this thesis is divided into eight chapters as follows. **Chapter 2** provides overview of efforts documented in various literature for UAVs path planning solution in static and dynamic environment. It also provides an overview of UAVs deployment for VANETs assistance. Besides, some routing protocols adopted in UAV network are also surveyed. **Chapter 3** discusses the proposed three-dimensional faster and more accurate path planning algorithm using improved PSO. The improvements include (1) the use of a chaos logic map for initializing particles, (2) The development of an adaptive mutation strategy to balance local and global search, and (3) enhancing the algorithm execution process by replacing inactive particles with new fresh particles to push the solution toward global optima and allow the algorithm to overcome sticking in local optima. It also presents the performance evaluation of the IPSO.

Chapter 4 describes IoD online path planning in a dynamic environment. It provides an energy-efficient path generation to obtain a collision-free path with minimum energy requirement. The chapter outlines the energy model for a quad rotor drone. **Chapter 5** presents an optimal deployment of IoD for VANETs assistance. The chapter describes the proposed optimization algorithm to obtain the optimal deployment of IoD in a dynamic vehicular communications environment to allow providing communication among vehicles on the ground. It also provides conducting extensive simulation experiments to test the model performance and to evaluate the proposed model. The framework architecture model is developed for simulation with its validation. **Chapter 6** discusses a 3D IoD-to-Vehicles simulation model for IoD-Assisted VANET. A novel IoD2V communication model is proposed to characterize the 3D communication between the IoD network in the air and the VANETs network on the ground. It also describes 3D collaborative IoD architecture (3DIoDAV) to maximize the coverage area and enhance the quality of the received signal at a receiver side. The IPSO is implemented so that an adequate signal is guaranteed toward isolated vehicles. Besides, the proposed 3D propagation model is utilized by the objective function of IPSO so that the impact of terrain on communication is considered in the IoD deployment. The framework architecture model is developed for simulation with its validation. **Chapter 7** presents the mixed integer linear programming for coverage path planning. A novel approach is proposed to fully cover the target region with minimum energy consumption. Besides, single UAV, as well as cooperative multi UAVs, are involved to cover a single region. The region is decomposed into sub-regions depending on the number of available drones. The sub-regions allocation is proposed to assign the sub-regions to the UAVs. Furthermore, small-scale and large-scale problems are analyzed. A simulated annealing metaheuristic approach for coverage path planning is implemented and compared with the exact solution, i.e., CPLEX solver, and greedy approach. **Chapter 8** discuses and reviews the related routing protocols for UAVs network and studies the performance analysis for three routing protocols, namely, AODV, OLSR, and DSDV. **Chapter 9** discuses and reviews the contributions of this thesis and outlines the scope for possible future work.

CHAPTER 2

LITERATURE REVIEW

In this chapter, collision-free path planning protocols, UAV deployment approaches, and UAV routing protocols are reviewed and analyzed.

2.1 Collision-Free Static Path Planning

The UAVs' path safety has attracted remarkable research attention. Several approaches have been proposed in drone collision avoidance. In IoD formation path planning, the main challenge is to perform optimal path planning to allow the drones to accomplish their tasks safely.

Several path planning approaches with collision avoidance were proposed in the literature. However, only the studies of collision avoidance between drones acquire more attention.

In [31]–[33], effective approaches for path planning based on potential fields were proposed. However, the interaction between repulsive and attractive fields should be established globally to generate the flyable path. Therefore, these methods were easily be stuck in local optima and did not guarantee to generate a feasible path if the obstacles and the destination are close to each other.

Furthermore, the works [34]–[39] were simple path planning algorithms based on Graph Theory such as Voronoi diagram algorithm, probabilistic road maps algorithm, A* algorithm, and rapidly-exploring random trees based algorithm. These algorithms were rarely considering dynamic constraints in addition to computationally expensive and storing cost maps in advance which was required by these methods. Therefore, these algorithms are not appropriate for practical situations.

Recently, significant progress has been made in population based evolutionary algorithms [40], [41]. These algorithms have the ability to obtain the global optima in a flexible and effective way. The application of Swarm Intelligence (SI) in the field of optimization has become very popular because of the quality of its solutions, global exploration, and speed [42], [43]. The optimization method tries to find an input that can minimize the performance index so as to avoid obstacles [44], [45]. These algorithms rely on computational to avoid collision. Thus, many optimization techniques are proposed to address this computational complexity. Drone path planning has been attracted by many researchers to use this class of techniques. The commonly used algorithms mainly include Particle Swarm Optimization (PSO) [46], [47], artificial bee colony (ABC) [48], ant colony (ACO) [49], and genetic algorithm (GA) [50]. Among these algorithms, PSO is utilized extensively due to its global convergence for all particles and ease of implementation. The standard PSO algorithm may get stuck in local optima and suffers from premature convergence. To overcome these limitations, numerous studies on PSO have been carried out on different aspects such as the structure of the algorithm, and selection of parameters. In [51], an adaptive decision operator was combined with PSO to overcome its slow convergence. a 3D path planning was then generated. The improved PSO results showed the advantages of the proposed method. Moreover, some researchers focus on theoretical improvement and analysis of PSO. These improvements include enhancement of initial population by introducing chaotic maps. Also, the Gaussian mutation mechanism is introduced into PSO to address the local optima issue and the premature convergence [52]. Additionally, the factors that impact the PSO performance are comprehensively analyzed. The authors pointed out that four key aspects are required to improve PSO, namely, selection of parameters, initialization of population, the structure of topology, and combination with hybrid methods.

The author in [46] proposed a fitness-based multi-role framework. Based on the current fitness values for particles, any particle was allowed to learn from different exemplars and play different roles.

The authors in [53] proposed a path planning approach to guide the drone from the start location to the end location. A predefined path was planned off-line and the drone follows the path while avoiding collision with obstacles. This optimality was achieved by combining path control with collision avoidance control. Then these mechanisms were solved independently and the movement strategy was designed by combining them together. They compute the track errors from geometric relation between predefined path and drone, which was used in track control law design. The collision avoidance approach calculates the best avoidance maneuvering using angles and zones' risk.

2.2 Dynamic Collision-Free Path Planning

The reviewed static path planning discussed above can not cope with dynamic environment. The dynamic environment requires online path planning, where the environment information is not known in advance.

In this subsection, different dynamic path planning approaches will be reviewed. In geometric methods, the distance between drone and obstacle is calculated using the speed of the drone and the locations of drone and obstacle. The Fast Geometric Avoidance Algorithm (FGA) based on collision probability, kinematics, and limitations of navigation was proposed in [54] by combining the start time selection from critical avoidance and geometric avoidance. To avoid multiple obstacles, different threat levels can be assigned to avoid those obstacles sequentially based on a critical time of avoidance which reduced the computational time compared to other similar works.

Virtual fields around obstacles are assumed in a potential field or force-field approach. The virtual repulsive or attractive forces by these fields are assumed to generate collision avoidance [55]. In [56], a virtual force field was proposed to detect dynamic obstacles. The authors claimed that the efficiency was degraded due to the lack of taking the motion of obstacles into account in the traditional force field approach. The proposed prediction of obstacle force field, determined by frequency modulated continuous wave radar equipped in an unmanned ground vehicle, was utilized to resolve the loss efficiency which solved the weakness of the traditional 1D virtual force approach. Furthermore, the time to the collision was obtained by using the velocity of the obstacle. In [57], a new APF mechanism under dynamic conditions for collision-free trajectories was proposed. Moreover, the conservation field was enhanced and the field vector direction was obtained based on the angle of the drone path and the angle of position vector from drone to obstacle. In this approach, the other drones were considered as dynamic obstacles. However, the approach didn't consider a 3D environment. Generally speaking, in virtual field approaches, the interaction between repulsive and attractive fields should be established globally to generate a flyable path. Besides, they are easily stuck in local optima. Therefore, these methods did not guarantee feasible paths if the obstacles and the destination were close to each other.

In [58], the collision-cone approach was used to develop a minimum effort guidance law to guide the UAV to a waypoint while avoiding multiple obstacles. The positions of the obstacles were estimated using an extended Kalman filter; an algorithm that provides estimates of some unknown variables, and a 2-D passive vision system.

In [59], a novel approach based on particle swarm optimization was proposed to plan the path for an autonomous vehicle in a dynamic environment. The equipped sensors were utilized to collect the data on the environment. Besides, different terrain types were assigned by different weights. Then different navigation possibilities through the terrain were classified based on assigned weights.

Finally, the optimal path was selected based on this classification. Moreover, the particle swarm optimization approach was used in [60] to develop a path planning algorithm for multiple UAVs with communication systems and constraint sensors. The solutions were updated and iterated in a finite time step, which improved the optimality of the solution. However, the premature convergence of PSO was not addressed. In [61], the ant colony algorithm was utilized with a minimum time search algorithm to ensure the successful calculation for obtaining collision-free search trajectories for drones. PSO can be used with model predictive control for static and dynamic threat avoidance during reconnaissance missions. However, these methods require a termination criterion to guarantee a convergence time, and they are computationally intensive. Thus, they are difficult to be applied in real-time scenarios. In [62], A combination of particles optimization algorithm and sense-and-avoid approach was used for multi UAV path planning with state constraints and control. The dynamic constraints were included in the model in order to prevent collision with obstacles. Furthermore, the multi UAV online trajectories were simulated by using Receding Horizon Control (RHC) with the application of a 3D-ducted fan UAV.

In [30], the authors modeled the path of a drone using quadratic Bezier curves. The optimization problem for path planning with different objective functions was proposed. Also, a receding horizon approach was used in which a trajectory was constrained to address obstacle collision in a 2D environment. The proposed approach was tested in a dense environment. However, the approach is applied in the 2D environment only. Also, IoD formation was not considered.

The drone's flight limitations and energy constraints have directly impacted the performance of path planning approach. Thus, they attract the significant attention of researchers. In [63], an energy model derived from real measurements for coverage path planning was proposed. This model focused on the impact of different factors on a drone's energy consumption. Different maneuvering activities like flying horizontally, flying vertically up and down, turning, and hovering were considered in the real experiments. Moreover, power consumption was obtained as a function of the UAV's speed. They measured the power consumed during such operations and the fitting curves were estimated. In [64], a grid-based technique was used to avoid obstacles in a 2D solution. A coverage path for UAVs was planned with minimum energy consumption. The cost function in [65] was enhanced using a new Energy-Cost Function that gained 17% in energy compared with [65].

2.3 2D IoD Deployment for Area Coverage

Recently, various technologies have been introduced to complement the services of the IoT [66]. The deployment of UAVs in IoT offers unprecedented potentials [67].

The deployment strategy has become useful in wireless networks to obtain the best performance [68]. We classify the literature into two types namely, RSU deployment and UAVs assisted deployment.

- **RSU Deployment**

In [69], the placement algorithm of BS was proposed for network capacity maximization. However, the performance of information dissemination was impacted by nodes placement that act as a relay node. In [70], the authors discussed the optimal placement of RSU to improve the intersection connectivity. The best position of RSU can be found by the proposed scheme using the reports from vehicles within the RSU communication range. In [71], the RSU deployment to maximize the number of connected vehicles is proposed. The average report time from vehicles is minimized by the placement strategy proposed in [72]. Nevertheless, the terrestrial obstacles hinder the transmitted signal when located between sender and receiver which limits V2I communication. The flying RSU is a promising technique to cope with terrain obstacles and provide communication between vehicles on the ground which can be achieved using UAVs.

- **UAVs Deployment**

The UAV has the potential for acting as wireless BS or RSU to relay information between nodes in the ground networks especially when the terrestrial infrastructure capacity is not adequate for request handling in hot-spot areas. Furthermore, in remote and harsh environments, deploying ground BSs becomes difficult and inefficient. Such an environment can be covered using drones to extend the coverage of the network.

To tackle the limitations of low energy IoT nodes, UAVs are employed in [73] as a data collector and energy supplier. An efficient deployment approach to support better coverage for the ground users is proposed in [74] in which drones are considered as wireless base stations. The probability of download coverage is defined as a function of the UAV's height and antenna gain. Furthermore, the circle parking theory is used, and the 3D locations of drones that maximize the drone's lifetime and achieve the maximum coverage for the whole region are calculated. The work in [75] analyzed the optimal deployment of UAVs in a multi-level and multi-dimensional assisted network. The distributed approach was based on a potential game approach. Moreover, self-organized behavior where local and global policies participated in decision making for each UAV was utilized

Recently, significant progress has been made in population-based evolutionary algorithms to obtain the best position of UAVs to assist the ground network. In [76], the authors propose an optimization for resource allocation and joint access selection where UAVs are acting as aerial BS. The ground BS allocates its resource based on the access selection decision of UAV. Based on allocated communication resources, drones decide their selection strategy. In [77], a 3D placement strategy of UAV is proposed by optimizing the problem for coverage and throughput maximization with the drone's memory constraint consideration. The optimization problem aims to obtain the optimal position of the drone. The authors in [78] proposed a mechanism to obtain the best position of drone in a disaster scenario to support the nodes' connectivity in indoor buildings. A strategically located drone is utilized to cover all users inside the building so that the minimum transmitted power is maintained. In [79], the optimal placement of UAV can be obtained using PSO algorithm. The aim of the work is to maximize the coverage area while the drone capacity is still considered in the scope of the disaster and public safety. In [80], the brainstorm optimization algorithm is used to obtain the optimal position of UAVs for coverage quality improvement of the network. Furthermore, the use of the available number of UAVs was mentioned in [81] for covering all the targets while minimizing the rate of data dissatisfaction between end devices and their communication services. However, their research work didn't include it. In [82], the bio-inspired algorithms with multi-objective were proposed to obtain the optimal UAVs flight path. The proposed algorithm included several objectives such as energy, sensing ability, associated risk, and flight time. Moreover, the optimal height of a 3D placement of available UAVs is illustrated in [83]. The authors consider three objectives to be optimized namely target coverage, Quality of Service (QoS), and energy consumption. Furthermore, four optimization algorithms are utilized to solve placement problems. To maintain the connectivity of UAVs, the authors create a grid-based connectivity network called Aerial Mesh Network (AMN). However, they consider only static coverage in which drones hover to a given target area. Also, the covered targets are static, i.e, they don't move during the mission. Additionally, the work optimizes the altitude of drones to generate a near-optimal height deployment of drones to cover the target devices and achieve QoS and minimum transmission data energy consumption.

- **2D IoD-Assisted VANETs Deployment**

In urban terrain, the infrastructures and buildings constrain the communication and movement of vehicles [84]. Recently, some works have investigated the integration of UAVs and ground networks, i.e., UAV-assisted, to enhance the ground networks' performance, such as coverage of the target area and received signal strength.

The use of drones in VANET assisted achieves a great improvement in the VANET connectivity, because the UAVs can fly at a high altitude beyond all the infrastructures of terrestrial allowing the movement of UAVs to be much less influenced by terrestrial constraints. Furthermore, fewer influences on the drones' transmission in the air are due to terrestrial obstacles. Based on these advances, UAV becomes an appropriate VANET assistant. Various schemes on the deployment of UAVs to support the vehicular communication are proposed. The author in [85] proposed a drone position algorithm in which the quality of services communication is offered to vehicles in the ground.

To obtain the optimum connectivity between the drones and vehicles, the best position of the UAVs so that adequate signals can be transmitted to the ground vehicles is needed. In paper [86], an urban VANET routing solution was proposed. It ensured reliable and alternative paths when the main path failed. Further, in [87], the incidents are detected on the urban road by deploying the UAVs to provide the vehicle emergency guidance. Moreover, the end-to-end delay is reduced among cars by designing a hybrid vehicle drone ad-hoc network in [88]. In paper [89], the deployment of LTE connectivity for drones is studied. Some challenges are highlighted such as LOS propagation in the sky. In [90], the terrestrial infrastructure is replaced with a drone to minimize the V2I delay on the straight road. The authors in [91] proposed using a drone to improve the packet delivery ratio and reduce the delay. In [92], the drones are used to select the optimal path as an alternative path to achieve the stability and distribution of the cars. In [28], a novel IoD collaborative communication approach has been proposed to improve the communication of the VANET network. The UAVs are optimally deployed to maximize the coverage area and improve the quality of the received signal. Although the proposed approach achieves an optimal value of coverage area, the simulation is conducted in a flat area and the impact of high-level terrain is neglected.

2.4 3D IoD Assisted VANETs Deployment

Some works have investigated the integration of UAVs and ground networks. Specifically, drone-to-vehicle communications have been addressed using simulations; however, these simulations have been performed applying flat scenarios, in which the effect of 3D communication between UAV and ground network has been neglected. It is worth mentioning that a fewer works have taken into account the impact of the terrain or environment in their simulations.

In this subsection, we will review the related UAV-Assisted VANET works that consider the terrain elevation on communication.

The work in [93], includes a Digital Elevation Model (DEM) to detect the obstacles formed by terrain. Moreover, to evaluate the performance of the aerial platform, three propagation models were used, which are Single Knife Edge, Deygout, and Bullington, for supporting mobile cars to broadcast alerts in emergency situations. Two different altitudes, i.e., 40m, and 100m, were implemented. The simulation illustrated reasonable results for 100m altitudes. However, the scenario included only one car moving in the ground and one drone hovering in the same place. In [94], optimal deployment of UAV to provide 3D communication between a UAV and three cars on the ground was proposed. The PSO algorithm was utilized to obtain the best position of the UAV so that sufficient received signal strength was maintained at the receivers. The simulation model included 3D communication to test the communication performance by including the implementation of DEM to indicate the terrain obstacles. The implementation included three cars moving on the ground and one drone placed in the optimal location. Nevertheless, the swarm of drones was not considered in these works.

2.5 MILP Formulation for Coverage Path Planning

Coverage path planning has been studied extensively in the literature, including UAV energy, terrain shape, and internal obstacles. The optimization solutions for the energy efficiency coverage path planning problem aim to develop new control algorithms and coverage path planning that reduce the UAV's energy consumption during its mission. The flight time is extended, and the energy consumption is minimized through minimum-energy paths design followed by aerial vehicles. These approaches enhance the UAV energy consumption in many ways, as they can be easily implemented. For real situations, it is specifically important to realize that UAV operates in the outdoor environment or under the battery-powered limitation [95]. In such a situation, a UAV might need to recharge multiple times to complete coverage for a large region.

In [63], a coverage path planning algorithm was proposed for a single UAV, where the speed-energy model for the drone was used for energy calculation as discussed above. In [96], the AOI was covered using one rotary-wing drone. The proposed approach worked offline and used an approximate cell decomposition with the grid base technique. Each cell was assigned a positive number that represented the percentage of area. It tried to obtain the shortest path and the least number of turns to reduce energy consumption. In [97], the best path for data collection was studied where the flight time and data collection time were considered. Further, brute force, and two heuristic algorithms, were proposed to solve the CPP problem. Moreover, various decomposition approaches were introduced in [98], such as graph, cellular, and grid-based approaches for UAV CPP. The decomposition approaches as mentioned above were utilized to segment the AOI into sub-areas to obtain the sub-optimal coverage path for a drone.

In [99], an energy-aware CPP algorithm for drones was proposed. The energy model for UAV was derived by carrying out a set of experiments at different conditions of operation such as acceleration, deceleration, and constant speed. The AOI is divided into cells and the drone flied through a grid center to cover it. A zigzag pattern was proposed to reduce the number of turns, which reduces the mission consumption energy. However, the obstacles collision avoidance was not considered. Additionally, a CPP problem was formulated as a traveling salesman problem in [100], where the optimal path was obtained to minimize the path length and time windows for multiple salesman problems. In [101], an online

CPP algorithm was suggested by utilizing dynamic programming (DP) to enhance performance in terms of energy efficiency and adaptability. The limitation of this work is that the region was decomposed into big cells, and the cells that include any obstacle are completely avoided. In [102], an inspection of the 3D structure approach was proposed using multi-objective optimization. The energy consumption and coverage were considered in the objective function. The main drawback is that the energy saving can be achieved for partial coverage.

An energy-aware coverage path planning mechanism was proposed in [103]. The 2D grid partitioning was utilized for region decomposition. Moreover, different irregular and regular regions were considered and covered by one drone. The start point, turning positions, and scan direction were determined. The trajectory was planned in an offline mode and the area coverage, completion time, and energy-saving were studied. However, the collision avoidance of obstacles in the areas of interest was not considered.

The work in [104] included studying full exploration with an energy cost using a model approximated with the path length. A method of linear programming to determine a collision-free path was proposed in [105], [106]. The points between the start and endpoints were continuously adjusted to build the path. The main limitation of the work is that forbidden zones were not considered in the design.

The heuristic mechanisms are widely studied in the literature for coverage path planning problems, such as particle swarm optimization [107], [108], Tabu search [109], simulated annealing [110], and genetic algorithm [111], [112]. Such approximation methods are utilized specially for large problem sizes.

In [113], a genetic algorithm was proposed to solve the CPP problem. The objective was to minimize the UAV energy consumption to complete a mission. Reducing the number of turns was proposed to allow the UAV to optimize the flight path and minimize the energy consumption. However, collision avoidance was not considered. In [114], coverage path planning was proposed using a multi-population genetic algorithm, where the problem was formulated as a traveling salesman problem. The drone was tasked to cover multiple regions and came back to the depot following the shortest path. However, the number of UAVs is only one, and they cannot be adapted to regions with multiple UAVs. In [115], the genetic algorithm with a near-optimal sequence of CPP was implemented. To reduce the energy consumption of the robot, the fitness function computed the efficiency of the chromosome. Further, the authors in [116] implemented a genetic algorithm and simulated annealing algorithm to generate multiple local-global coverage trajectories. To reduce the computation cost, both algorithms were processed in parallel. The particle population movements, swarm intelligence algorithm, are utilized in CPP for finding the shortest path or providing the optimal coverage solution. The PSO is a population meta-heuristic approach, inspired by the social behavior of the natural population swarming [117]. In [118], the smooth CPP trajectory was generated using an online manner based on PSO in a high-resolution grid map.

2.6 IoD Routing Protocols

The routing protocols have been studied by many researchers in different network types; MANET, VANET, and FANET. The optimal solution is found to forward data using different approaches and assuming different hypotheses. The objective is to ensure an acceptable level of packet loss, keep the network overhead under controllable levels, and achieve high throughput. Several studies focus on performance analysis of routing protocol in MANET [119], as well as in FANET [120]. In [121], radio propagation models and various routing protocols were compared. In [122], different routing protocols for the VANETs scenario were reviewed. Also, the challenges and open issues for research directions were presented. The data dissemination in MANETs and VANETs was presented in [123] via mobile software agents. A geographic information about the nodes was utilized to support Agents' decisions about migrating among the network nodes so that the desired dissemination of data was achieved. For comparing and contrasting the levels of intelligent decision, three unique information completeness levels were utilized. In [124], an ideal protocol for VANET was examined using several network metrics in AODV, GPSR, and DSDV topologies. SUMO and NS-2 were utilized to visualize the nodes for urban mobility without the road layout. The results showed that AODV performed better packet delivery ratio, throughput, and delay. In [125], AODV, DSR, and Cluster-Based Routing Protocol (CBRP) were studied for VANETs, specifically at road intersections. The scenario included different number of vehicle nodes and traffic densities. At sparse scenarios, AODV, DSR, and CBRP performed well. In dense scenario, CBRP outperformed AODV and DSR protocols with less packet loss.

In [126], the Ad Hoc networks routing protocols were studied. The work considered many performance metrics such as normalized routing load, throughput, received packets, and end-to-end delay with different speeds and pause times.

In paper [127], the reliable energy-aware routing in mobile Ad Hoc networks was proposed. The reliability and energy awareness were ensured in MANET by the proposed routing protocols.

In [128], a new routing protocol was proposed in which the data mining technique in route was used in the selection process from source to destination. The one-hop neighbor was selected in the proposed routing based on some parameters like link expiration time, speed, node lifetime, and trip time. The selection process helped to select stable one-hop neighbor from the source node to the destination which improved the route discovery mechanism.

The work in [129] evaluated two relevant routing protocols named AODV and OLSR performance in VANET using the NS3 simulation tool. The propagation model used is fading propagation model. The statistical analysis indicated that the difference between AODV and OLSR performance was not significant.

The authors in [130] focused on routes design for UAVs. An extensive review of the routing protocols was presented. Moreover, the performance of routing protocols was analyzed and compared in detail.

In [131], the performance test and comparison were carried out on DSR, AODV, OLSR, and GRP. The performance metrics like traffic received, network delay, throughput, and data dropped w.r.t. simulation time were analyzed and compared. The results explained that among all performance metrics, no routing protocol achieved optimal performance and according to the required performance metric, a suitable routing protocol could be selected.

In [132], OLSR and AODV routing protocols were analyzed and compared in terms of overhead, throughput, and end-to-end delay at various speeds and packet sizes. It provided an idea to evaluate the routing protocols in the UAV network. The paper showed that high dynamic mobility makes the use of OLSR difficult.

In [133], the authors enhanced OLSR to meet the dynamic changes in topology and rapid mobility of nodes. They calculated link expiration time with the help of applying GPS. Furthermore, the residual energy of nodes and multiple metrics were utilized to select the most suitable relay node. The improved OLSR with expected transmission count (OLSR-ETX) performed better than the traditional OLSR in terms of end-to-end, overhead, packet transmission, and delay.

CHAPTER 3

IOD SWARM STATIC PATH PLANNING

3.1 Chapter Motivation

As the technology advances, drones become increasingly autonomous and gain new capabilities. On the other hand, in high drones density and increasingly complex mission situations, drones pose new threats as they get closer to each other or obstacles. When the probability of collisions between swarms increases, collision avoidance becomes a challenging task and IoD should have a proper mechanism to prevent or avoid potential collisions. However, this challenge has not been fully solved. Generating a safe path that is collision-free for IoD formations is the key challenging task in dense swarm and environment constraints. Furthermore, building paths for IoD formations using deterministic approaches require massive storage capacity and long execution time. Thus, appropriate optimizations and improvements are required to solve such problem. Meta-heuristic approaches have been widely used to solve NP hard problems such as PSO, genetic algorithm, simulated annealing, and evolutionary algorithm. PSO has gained attention due to its intelligent evolution process. Despite the advantages of the PSO algorithm, it still suffers from a premature convergence problem and may get stuck in local minima when used to solve complex problems. Although the literature works have achieved an improvement on drone's collision avoidance and path planning, some works neglect IoD formation, and consider only one drone. Additionally, other works failed to avoid static obstacles, specially those are close to the destination. Besides, some problems of particle swarm optimization are not fully addressed such as premature convergence and convergence speed.

3.2 Chapter Contributions

To tackle limitations discussed above, this thesis proposes a three-dimensional faster and accurate path planning algorithm. The proposed approach addresses some problems of particle swarm optimization by improving a traditional PSO. The improvements include initial population improvement, adaptive mutation, and speeding up the PSO convergence which improves rapidity and optimality of 3D IoD paths generation. The IoD trajectories are planned with collision avoidance consideration. Moreover, the proposed approach generates optimal safety paths for IoD from start locations to the destinations. The results show noteworthy improvement in optimal solution and convergence speed. The improvements can be summarized as follow.

- The use of chaos logic map for initializing particles.
- The development of an adaptive mutation strategy to balance local and global search.
- Enhance the algorithm execution process by replacing inactive particles by new fresh particles to push the solution toward global optima and allow the algorithm to overcome sticking in a local optima, resulting in fast and accurate collision-free paths for UAVs in 3D space.

This chapter is the result of a collaboration with Dr. Ashraf Mahmoud from Computer Engineering Department, Prof. Ansar Ul-Haque Yasar from Transportation Research Institute, Hasselt University, Belgium. The work has been published in Transportation Research Part A: Policy and Practice 142, 260-278, 2020.

3.3 Traditional Particle Swarm Optimization (PSO)

A population based meta-heuristic search algorithm such as PSO has been widely applied to a variety of problems. The algorithm starts from initial random candidate solution of position and velocity and then the position and velocity are updated iteratively until a global optimal solution is found [51], [134], [135]. For each particle in the swarm, the searching direction is represented by velocity that is dynamically updated by three components; its previous value, its best position (personal best), and the global best position. The particle's new position is obtained from the previous position value and the current velocity value. The new position is then assessed using a fitness function. If the new location of the particle is better than the previous location then it is stored as a personal best position. The global best position is obtained by comparing the new position with other all positions of particles. If it is the best of all, it will be stored as the global best position. Mathematically, the positions and velocities of particles are updated using the following formulas :

$$\nu_{t+1} = \omega\nu_t + c_1 r_1 (pBest_t - x_t) + c_2 r_2 (gBest_t - x_t), \tag{3.1}$$

where c1 and c2 are acceleration coefficients that help to pull the particles towards the personal best (pBest) and the global best (gBest) positions, respectively. Also r1 and r2 are a uniform random number $\in$ [0,1], and ω is the inertia that balances the exploitation and exploration where large values tend to facilitate global exploration and small values facilitate local search or exploitation.

Then the position of particles is calculated using the following formula:

$$x_{t+1} = x_t + \nu_{t+1}. \tag{3.2}$$

Fig. 3.1 shows the graphical representation of evolution of particles in PSO. In two-dimensional space, if we assume that number of path way-point is N then for each particle pi, the position and velocity can be represented as follow:

$$pi = (pi, 1, ..., pi, N) = pi(x_1, y_1), ..., pi(x_N, y_N) \tag{3.3}$$

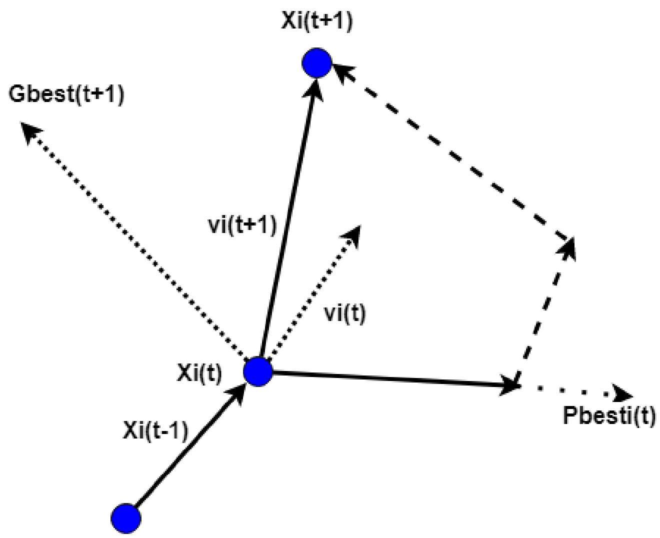

Figure 3.1: Graphical representation of evolution SPSO.

$$vi = (vi, 1, ..., vi, N) = vi(x_1, y_1), ..., vi(x_N, y_N) \tag{3.4}$$

where p_i, v_i is the position and velocity of ith particle respectively. The pseudo code of standard PSO is illustrated in Algorithm 1.

Algorithm 1 Pseudo code of standard PSO algorithm

```
begin
    initialization:
    initialize randomly PSO parameters
    while Termination condition not reached do
        Evaluate fitness of each particle
        for i ← 1 to PopSize do
            Find pBest_i andgBest_i
            for k← 1 to number of dimensions of particle do
                Update the velocity of particle using Eq.(3.1)
                Update the position of particle using Eq.(3.2)
            end
        end
    end
    Repeat until ideal best is obtained or run out of time
end
```

3.4 IoD Path Planning Description

To plan the path of IoD formation, some factors must be taken into account such as terrain area including obstacles in the terrain and IoD formation. The mission environment may include obstacles such as mountains, buildings, radars and other threats. Moreover, the IoD formation includes many drones flying in this environment. Thus, the IoD formation should be able to avoid colliding with these obstacles. To do so, objective function should include all these threats and obstacles and it should be able to reflect the impact of them on performance.

The whole IoD formation can be represented as follow:

$$(p_1, v_1), (p_2, v_2), ..., (p_N, v_N) \tag{3.5}$$

To describe a three dimensional path planning problem, let N is the number of way points for each particle, then the i^{th} particle's position and velocity vector can be respectively written as follow

$$pi = pi(x_1, y_1, z_1), pi(x_2, y_2, z_2), ..., pi(x_N, y_N, z_N). \tag{3.6}$$

$$vi = vi(x_1, y_1, z_1), vi(x_2, y_2, z_2), ..., vi(x_N, y_N, z_N). \tag{3.7}$$

To use PSO meta-heuristic, we need to formulate the problem and select the environment dimension. In this section, the environment dimension will be specified and the representation of candidate solution will be discussed. Furthermore, the required objective function will be illustrated.

3.4.1 IoD Path Representation

The aim of using optimization algorithms for path planning is to find a feasible path for drone from the starting point to the destination point in a complex environment. In this case, the path should be constructed to be used by algorithm and the flying space should be bounded. The location in 3D path planning can be represented as done in [51]

$$(x, y, z)|x_{min} \leq x \leq x_{max}, y_{min} \leq y \leq y_{max}, z_{min} \leq z \leq z_{max}. \tag{3.8}$$

where $x_{min}, y_{min}, z_{min}$ are the lower bounds of the flying space and $x_{max}, y_{max}, z_{max}$ are the upper bounds of the flying space.

3.4.2 Obstacle Model

In this work, the space boundaries and locations of obstacles are assumed to be known in advance. We model the obstacle as a half sphere as in [136], where:

$$O_k = (x_k, y_k, z_k, r_k), \tag{3.9}$$

where x_k, y_k, z_k are the three-dimensional coordinate of kth obstacle and r$_k$ is the corresponding radius of the obstacle, and

$$x_k = r_k \cos(\theta) \sin(\phi) + x_{k0}, \tag{3.10}$$

$$y_k = r_k \sin(\theta) \sin(\phi) + y_{k0}, \tag{3.11}$$

$$z_k = r_k \cos(\phi) + z_{k0}, \tag{3.12}$$

where x_{k0}, y_{k0}, z_{k0} is the center coordinate of kth obstacle, $\theta \in [0\ 2\pi]$, and $\phi \in [0\ \frac{\pi}{2}]$

3.4.3 Design of the Objective Function

The objective function is a mathematical term which illustrates the contribution of different variables to a specific value in order to optimize them. Thus, the generated value by objective function is either maximized or minimized by the optimization algorithm. Moreover, multi-objective function deals with more than one variable. Furthermore, finding a feasible path in IoD formation is an optimization problem with multi-objective function. It includes length of the path, terrain constraints, and collision avoidance with obstacles and with other drones in the swarm. Therefore, the objective function can be expressed as follow:

$$Obj\_Func = f_{pl} + f_{Oc} + f_{mc}, \tag{3.13}$$

where f_{pl} is a function of path length, f_{Oc} is a function of likelihood of colliding, and f_{mc} is a function of member collision. The aim is to minimize these quantities.

- Path length minimization

In some missions, the longer path is not desirable because drone is limited power and longer path is power consuming for drone. Thus, the shortest path is preferable. To evaluate the path length, the following path length ratio in [134] is used.

$$f_{pl} = \frac{\sum_{i=1}^{N_w-1} \sqrt{(x_{i+1} - x_i)^2 + (y_{i+1} - y_i)^2 + (z_{i+1} - z_i)^2}}{\sqrt{(x_{N_w} - x_1)^2 + (y_{N_w} - y_1)^2 + (z_{N_w} - z_1)^2}}, \tag{3.14}$$

where N_w is the number of path way points, $(x_1, y_1, z_1), (x_{Nw}, y_{Nw}, z_{Nw})$ are start and end point respectively, and (x_i, y_i, z_i) is the ith path way point.

This ratio is more admissible than relative distance and it is always $\geq$1 since the denominator represents the shortest straight line distance between start and end point. Therefore, the smallest value reflects the shortest path.

- Obstacle cost

The safe path of IoD formation is the path that does not go through obstacles. If even one point in the solution goes through an obstacle, this solution is penalized with high cost. On one hand, the path cost is significantly decreased when the distance between path and center of obstacle greater than radius of obstacle. On the other hand, the cost increases if the distance between center of obstacle and path is less than radius of obstacle. Thus, the cost function of obstacle can be expressed as follow:

$$f_{Oc(t)} = \sum_{i=1}^{N_w} \sum_{j=1}^{k} e^{-\alpha \frac{D_t(i,j)}{R_j}}, \tag{3.15}$$

where R_j is the radius of jth obstacle,

$$D_t(i,j) = \sqrt{(x(i) - x_O(j))^2 + (y(i) - y_O(j))^2 + (z(i) - z_O(j))^2}, \tag{3.16}$$

where (x,y,z) are the way point of path and (x_O,y_O,z_O) are the center of obstacles, and $\alpha \in$ [0,1] is the control parameter. Increasing α reduces the cost compared with other variables and vice versa.

- Drone member collision cost

As IoD formation density increases, the drones get closer to each other which increases the probability of drone collision. Therefore, drone collision avoidance should be considered by the objective function when planning trajectories for drones. Thus, when IoD paths are generated, it is essential to test whether drones are getting too close while flying in their respective path. Assuming path$_i$ is a path for drone$_i$ and path$_V$ are paths for other drones in the space. Then every point in path$_i$ should be compared with every point of other paths (path$_V$). To do so, a safety distance $\bar{d}$ should be maintained between paths.

The cost function of drone collision can be written as follows:

$$f_{mc(t)} = \sum_{i=1}^{N_w} \sum_{j=1}^{N} e^{-\alpha \frac{D_t(i,j)}{\bar{d}}}, \tag{3.17}$$

where

$$D_t(i,j) = \sqrt{(x_i - x_j)^2 + (y_i - y_j)^2 + (z_i - z_j)^2}, \tag{3.18}$$

(x_i, y_i, z_i) are the way point of path$_i$ and (x_j, y_j, z_j) are the corresponding point in other paths. It can be seen from the model that the cost of member collision of path$_i$ depends mainly on the distance between path$_i$ and other paths. Since the safety distance should be held, the cost will increases if the distance between paths is $\leq \bar{d}$. On the other hand, as the distance between paths increases, the cost function decays very quickly.

3.5 IoD Path Planning Algorithm Description

In this section, the improved PSO will be explained in detailed and the path planning algorithm for IoD formation will be demonstrated.

3.5.1 Improved PSO (IPSO)

One main limitation of the Standard PSO (SPSO) is being stuck in local optima and suffering from premature convergence when addressing a complex problem

[137]. Therefore, to avoid being trapped in local optima and to search for the global optima in more accurate and faster way, we propose enhancements to SPSO. These are (1) improved initialization stage of swarm particles, (2) better updating strategy, and (3) replacement of inactive particles.

- Chaos based particles initialization

Population meta-heuristic PSO is initialized using a random distribution. Moreover, the quality of distribution for initial solution plays a vital role in pushing the search towards the optimal solution. As mentioned in [29], when initial distribution is more uniform, the swarm maintains rich diversity and thus has a higher chance for faster convergence. Thus, the chaos-initialization improves the PSO performance because it helps to diversify the IoD formation. Fig. 3.1 in [29] illustrates the advantage of logistic map by comparing it with random distribution for 10,000 times which shows that the distribution of logistic is more uniform than random.

We use the simplest logistic map for IoD formation initialization as presented in [52]

$$X_{n+1} = \mu X_n(1 - X_n), \tag{3.19}$$

where X_n represent the n^{th} chaotic variable, μ is a bifurcation coefficient.

- Replacing inactive particles

During the iteration, some particles become inactive in which they lose their ability to search in local or global (i.e don't find a better position) which may cause premature convergence. In this case, we propose to replace the inactive particles with fresh ones to avoid getting stuck in local minima and push the search toward a global minima. For doing so, if a particle finds a better position, the corresponding trail is cleared and a trail timer is incremented each time in iteration if the particle cannot find a better position. When the iteration completes, the trail is checked if it exceeds threshold. If so, the corresponding particle is replaced by a fresh one.

- Adaptive mutation strategy

During the optimization process, the convergence and searching are the main objectives for PSO to find the optimal solution. In other word, searching or exploration should dominate the first stage of iterations so that it enriches the diversity, and convergence should dominate the second stage of iterations. To improve the IoD formation exploration and premature convergence, the adaptive mutation is designed as follows:

$$x(t+1) = x(t) + \epsilon\nu(t+1), \tag{3.20}$$

where ϵ selects how fast the particle moves. A big ϵ value allows the system to move quickly to best-known regions, but makes it hard to do fine-grained optimization [138]. On the other hand, a small value of ϵ tweaks the solution and accelerates the convergence. Thus, to balance the optimization process, the particle should explore the space and make big jumps towards the better spaces at the beginning. In the later iterations, the speed of particles should be decreased for fast convergence. Therefore, ϵ should change adaptively with iteration as follow:

$$\epsilon = \epsilon_{max} - \frac{(\epsilon_{max} - \epsilon_{min})t}{MaxIt}, \tag{3.21}$$

where ϵ_{max}, ϵ_{min} are constant value, and $\epsilon_{max} > \epsilon_{min}$, t is current simulation time, and MaxIt is total simulation time.

- Social acceleration coefficient

The acceleration c1 and c2 indicate the weight of stochastic acceleration term. When c1 and c2 are multiplied by random vectors r1 and r2, they have a controllable stochastic impact on IoD formation velocity. Moreover, they represent the weight of sharing information. For example, if c1=c2=0, then a particle relays on its knowledge. But, if c1>c2, then particles trend toward local attractor pBest while if c2>c1, then particles trend toward global attractor gBest. In this work, we select c1 and c2 based on running experiment in their range c_{min} to c_{max} then choose c1 and c2 that achieve both exploitation and exploration.

- Inertia Weight (ω)

The optimization algorithm success is based on balancing local and global search. For this reason, inertia weight is utilized to balance exploration and exploitation search. For more clarification, large value of ω leads to exploring the space while small value facilitates exploitation. Thus, some works adapt ω linearly [52].

$$\omega(t) = \omega_{min} + \frac{MaxIt - t}{MaxIt} * (\omega_{max} - \omega_{min}), \tag{3.22}$$

where MaxIt is maximum simulation time, t is current simulation time, and ω_{min} and ω_{max} are minimum and maximum value of inertia, respectively.

Algorithm 2 Improved PSO algorithm

Limit: Threshold of trail, Max_Iteration: maximum iteration

INITIALIZATION:

initialize c1,c2, initialize position and velocity with logistic map by Eq3.19

begin

    iter=0

    Calculate fitness value and obtain gBest and pBest

    while *Iter<Max_Iteration* **do**

        Update ϵ by Eq3.21, ω by Eq3.22.

        for $i \leftarrow 1$ **to** *PopSize* **do**

            Update the particle velocity by Eq3.1, position byEq3.20

            Calculate fitness of generated particle

            if *particle is inactive* **then**

                Increment its trail

            else

                Clear its trail, Update gBest and pBest

            end

        end

        for $i = 1 :$ **to** *PopSize* **do**

            if *trail(i)>limit* **then**

                Replace inactive particle by new fresh one, Clear its trail

            end

        end

        Increment Iter

    end

    Repeat until ideal best is obtained or run out of time

end

3.5.2 Path Planning Algorithm for IoD Formation

Algorithm 2 is an improved version of PSO. It consists of many parts. The algorithm start with the initialization part that is responsible for initializing all variables such as acceleration coefficients c1 and c2. It is also responsible to create initial solution, i.e., position and velocity of all particles.

The path planning generator receives parameters and environment constraints and returns the feasible paths for all drones with corresponding average fitness. To increase the search efficiency, some improvements of traditional PSO are added. Additionally, ϵ and ω are adaptively changed with iteration as discussed above. At the end of each iteration, the trail is checked for all particles and replace the inactive particle by fresh one if its trail exceeds the threshold. Then the algorithm is repeated until an ideal best is obtained or run out of time. Fig. 3.2 illustrates the flow chart for the developed algorithm.

3.6 Simulation Results and Discussions

The simulation is an effective way to verify the analytical results [139]. It is noteworthy to describe in detail how the simulation results are recorded in the figures. In this section, the simulation of proposed method will be illustrated for fixed and variable altitudes. Then the results will be compared with traditional PSO and recent work CIPSO [29]. The matlab environment is used for simulation.

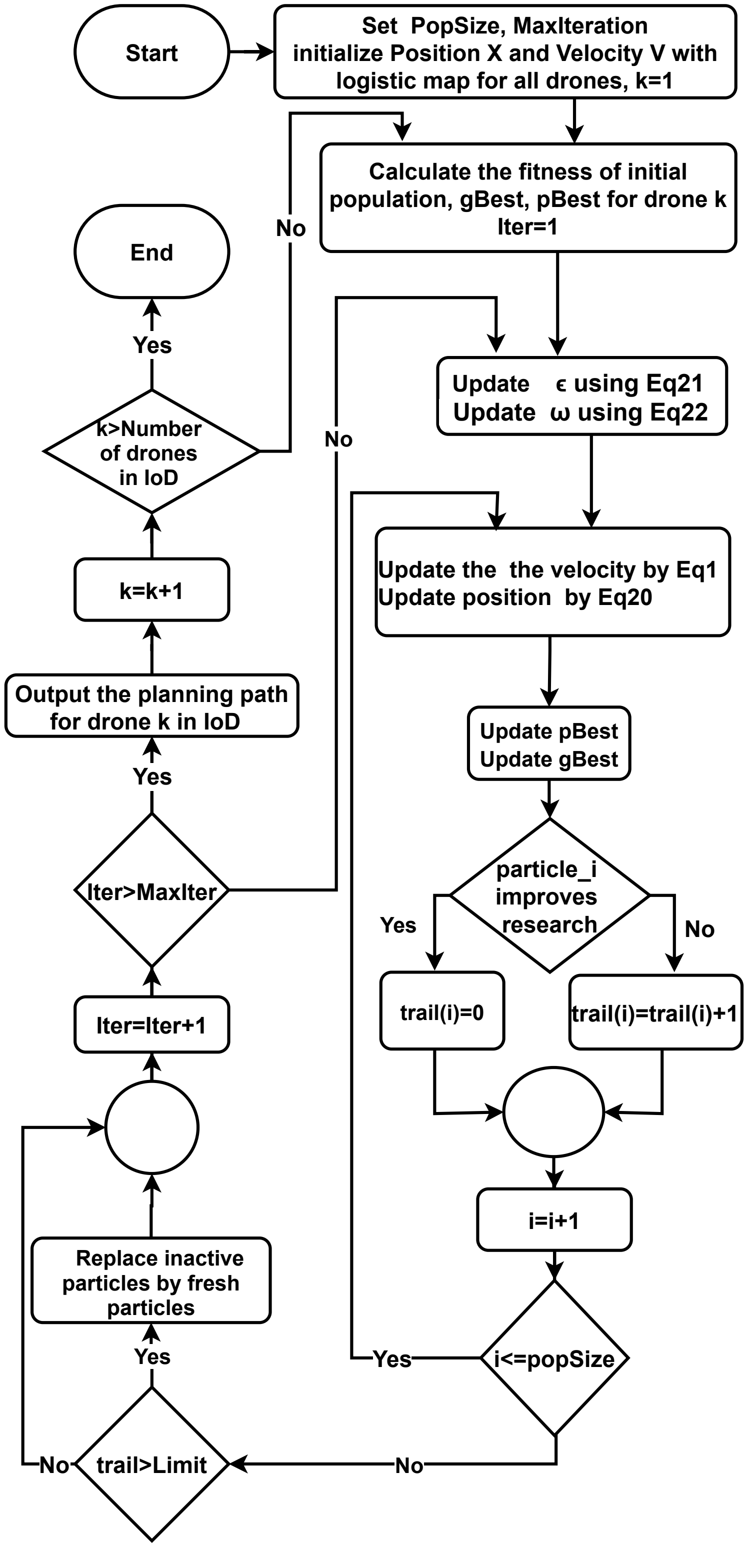

Figure 3.2: Flow chart for IoD path planning (IPSO).

3.6.1 Fixed Drones Altitude

In fixed altitude, the dimension z is constant while x and y are allowed to change.

- Parameters setting

Table 3.1: Drones start and end points

Drones	Start Point (xs,ys,zs)	Destination Point (xd,yd,zd)
Drone 1 (x,y,z)	(300,800,500)	(15000,1000,500)
Drone 2 (x,y,z)	(300,2800,500)	(15000,4000,500)
Drone 3 (x,y,z)	(300,4800,500)	(15000,4800,500)
Drone 4 (x,y,z)	(300,4800,500)	(15000,10000,500)
Drone 5 (x,y,z)	(300,8800,500)	(15000, 13000,500)

IoD formation : five drones fly from start points to destination points as shown in Table 3.1.

Environment: four obstacles are assumed to be centered at (5000, 7000), (10000, 2500) (10000, 10000), (5000, 2000) in 15000 m by 15000 m environment ,as shown in Table 3.2.

Population size is 250 particles, maximum iteration is 200, the number of way points is 20, and the safety distance is set at 80 m.

The parameters setting of CIPSO are c_{max}=3.5, c_{min}=0.5, v_1=0.5, v_2=0.1, and other parameters are shown in Table 3.3

- Results and discussion

In this part, some performance metrics will be analyzed and compared for different versions of PSO. The results of simulation will be discussed and compared with standard PSO and CIPSO [29].

Table 3.2: Obstacles setting

Obstacle	Coordinate (x,y,z)	Radius (R)
Obstacle 1	5000, 7000 , 0	2000
Obstacle 2	10000, 2500, 0	1200
Obstacle 3	10000, 10000 , 0	1100
Obstacle 4	5000, 2000 , 0	800

Table 3.3: Parameters setting

PSO	ω_{max}	ω_{min}	c1	c2	ϵ_{max}	ϵ_{min}	V_{max}	μ
SPSO	0.9	0.4	2	2	-	-	0.3	-
CIPSO	0.9	0.4	-	-	-	-	-	4
IPSO	0.9	0.4	2.0	2.0	1.0	0.05	0.3	4

- IoD formation path planning

IoD formation includes several drones in which each one of them faces different environment constraints. Thus, evaluating the whole formation is more effective than single drone path planning. In this work, the IoD formation is evaluated using the proposed IPSO and compared with SPSO and CIPSO.

Fig 3.6.1, 3.3, and 3.4 show the formation paths in both two and three dimensional views in all algorithms. From figures, it is clearly seen that all three methods are able to generate feasible paths without any conflict with terrain obstacles.

Fig. 3.5 to Fig. 3.7 are the corresponding fitness value with iterations for IPSO, CIPSO, and SPSO, respectively. The fitness values presented in the figures are recorded every iteration. The figures illustrate that CIPSO shows lower fitness value than SPSO but still higher than IPSO. Besides, IPSO overcomes both SPSO and CIPSO.

The convergence speed is an important factor to evaluate the algorithm and it can be measured by a fitness value. IPSO shows faster convergence speed than both SPSO and CIPSO as shown in Fig. 3.5.

[htp]

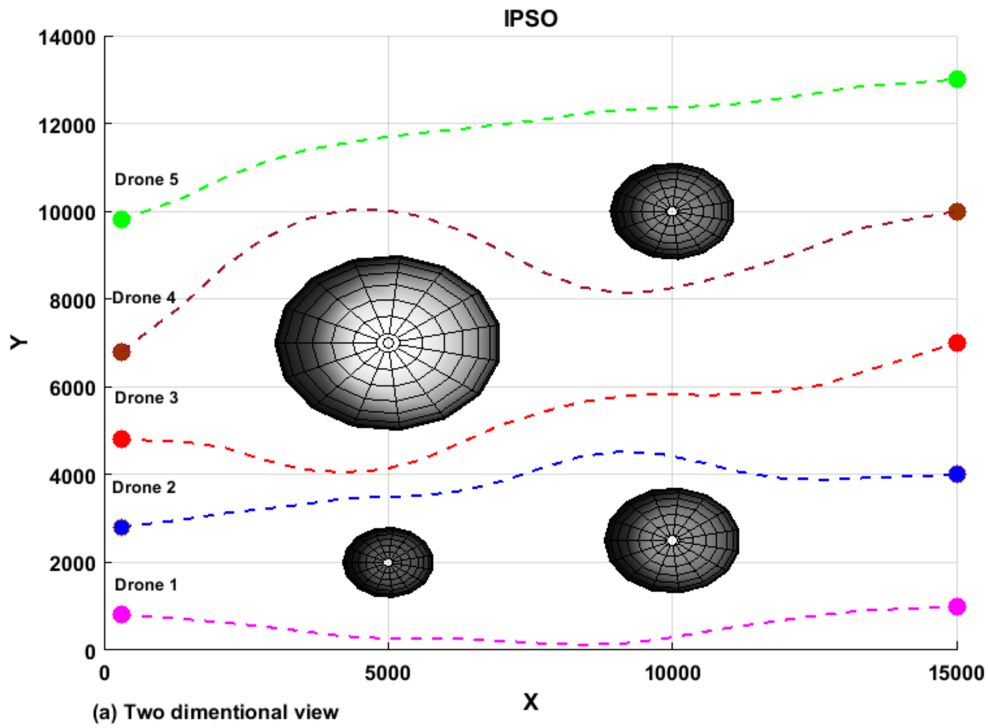

*

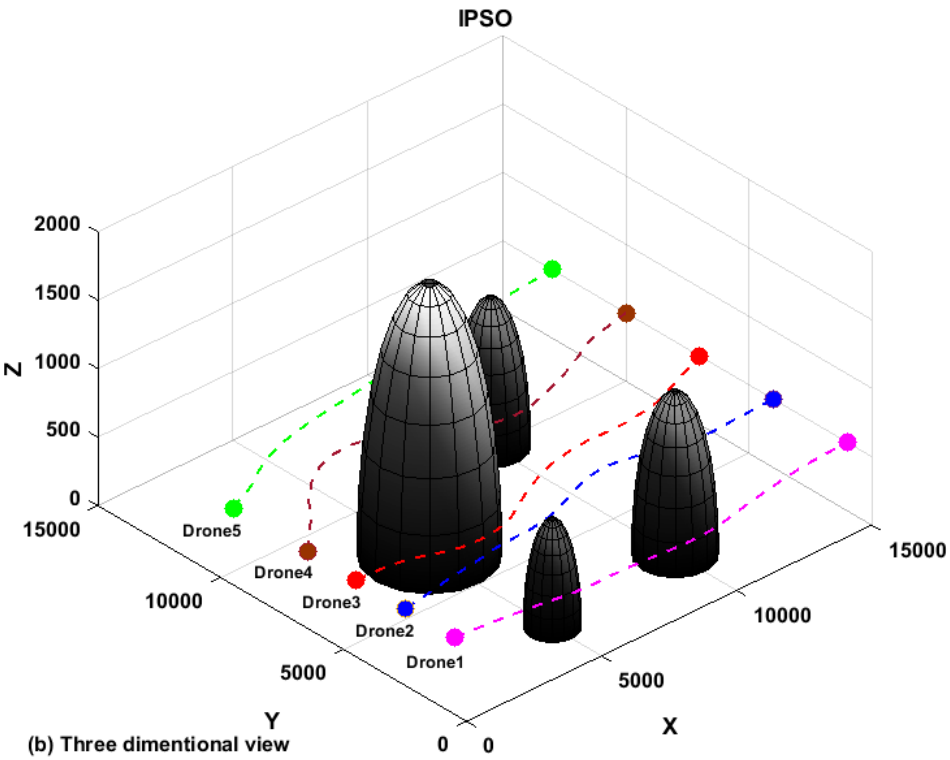

(b) Three dimentional view

*

- IoD paths optimality

To validate the effect of proposed method, we evaluate the average fitness value with iteration for the three mentioned methods. Moreover, the Average Fitness Value (AFV) is a measure of solution optimality which reflects the quality of solution. In path planning, AFV gives an indication of safety and cost effective path for drones in the flying environment.

For performance evaluation of proposed method, we carry out Monte Carlo simulation for 60 replications and AFV results are shown in Fig. 3.8 to Fig. 3.10.

Fig. 3.8 shows the average fitness value of 60 replications for IPSO for all drones. The figure exhibits different fitness for different drones. This is due to

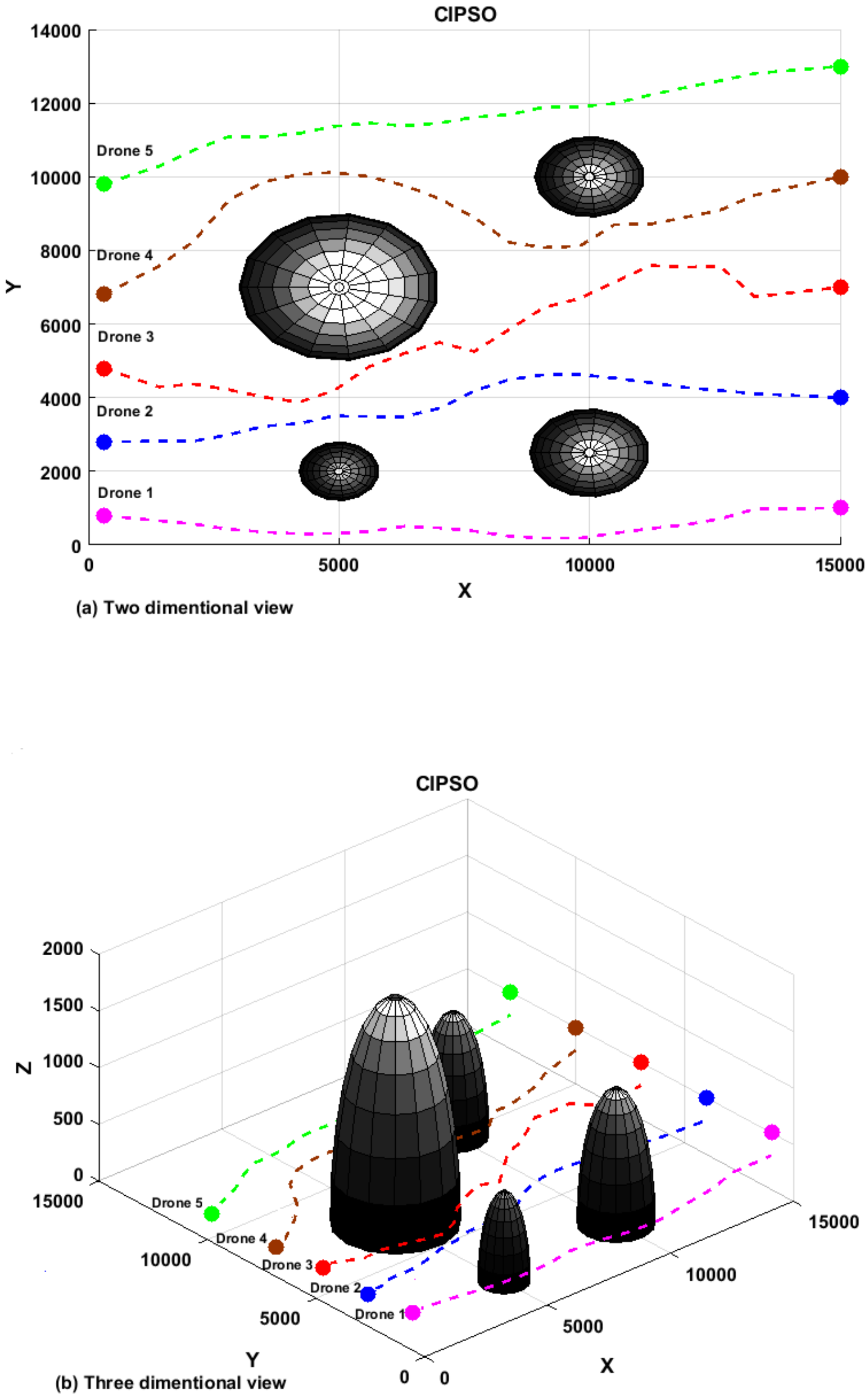

Figure 3.3: Two and three dimensional view for IoD path formation by CIPSO.

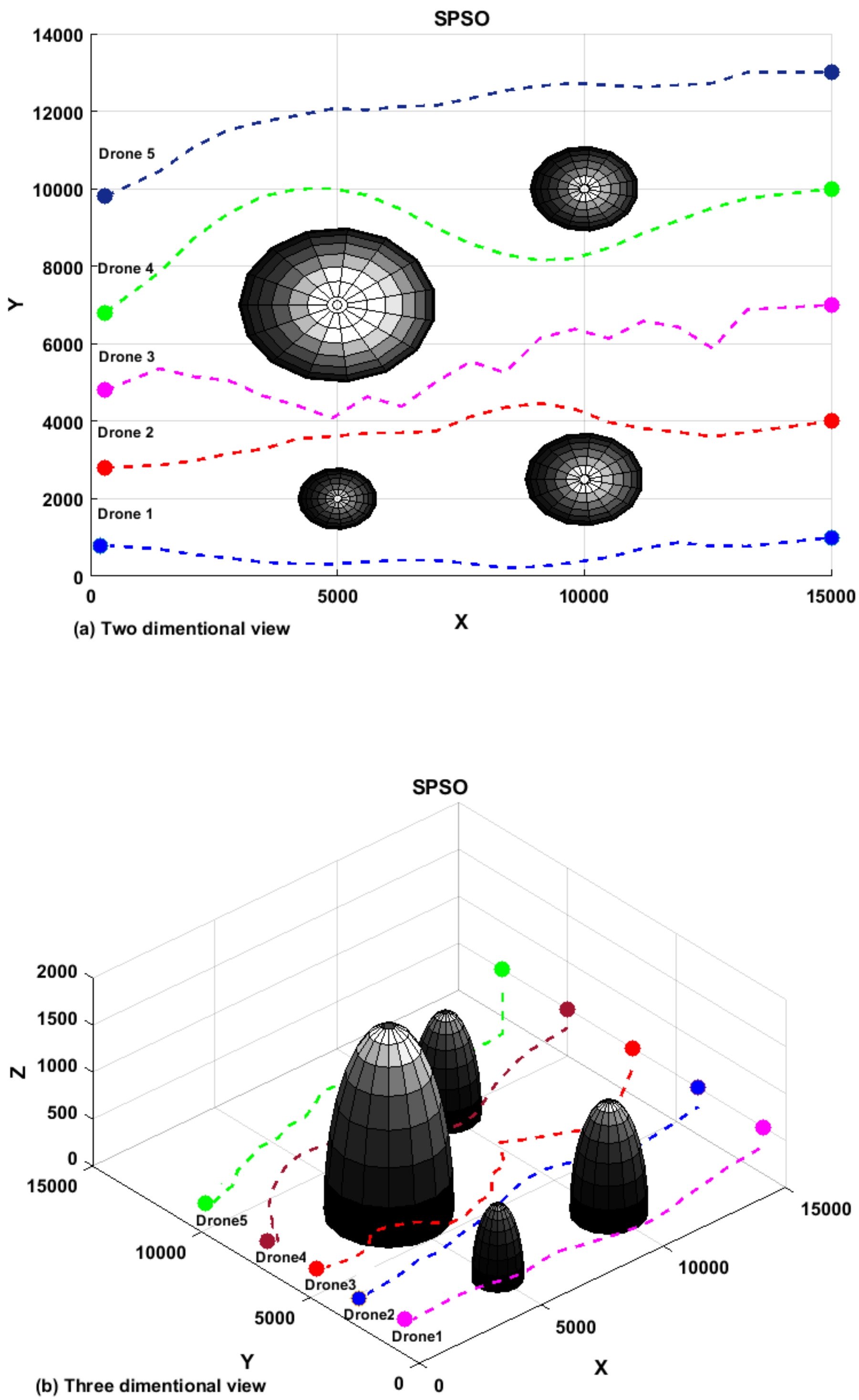

Figure 3.4: Two and three dimensional view for IoD path formation by SPSO.

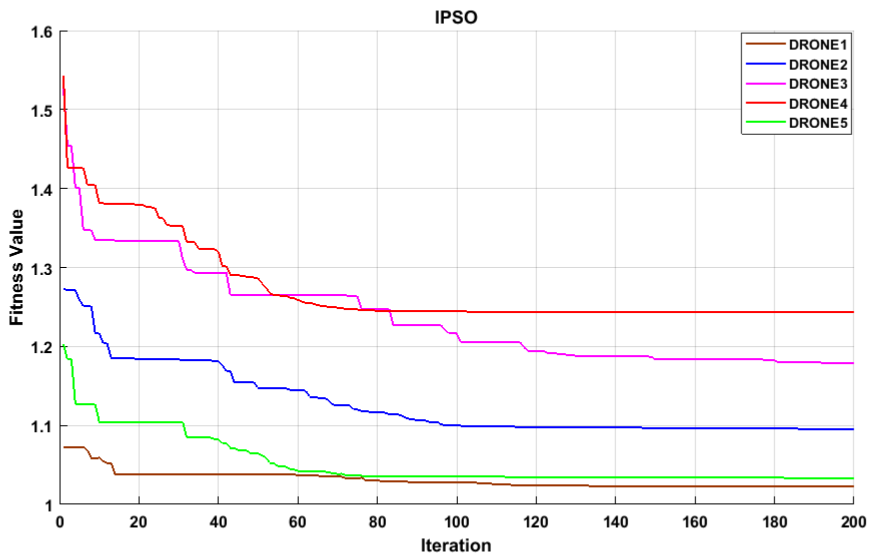

Figure 3.5: Fitness value for IoD formation by IPSO.

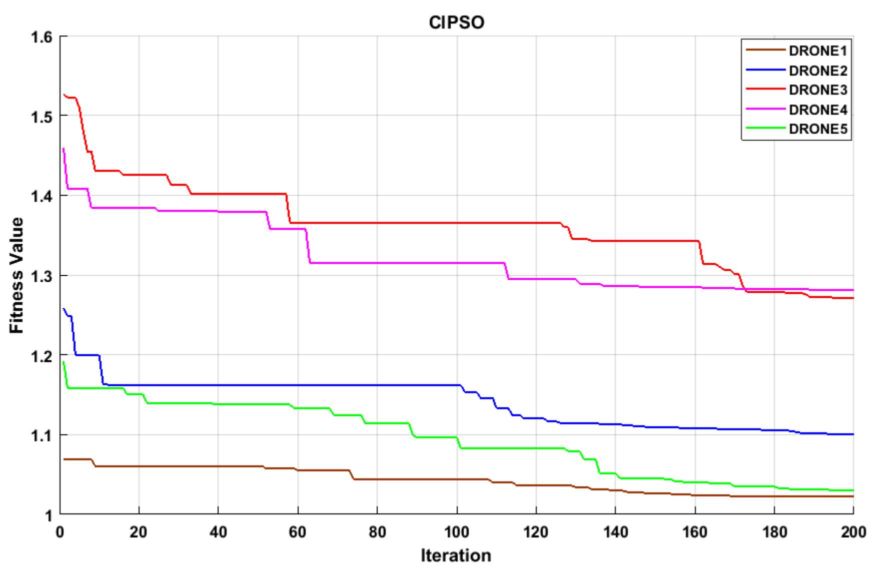

Figure 3.6: Fitness value for IoD formation by CIPSO.

different environment constraints. Drone 1 and 5 exhibit least fitness value because lower obstacles between start and destination point of path. Thus, drones can fly far from obstacles. On the other hand, the environment between start and end points of drones 2,3, and 4 is filled with obstacles and drones should avoid flying through obstacles that makes path longer and then higher cost of path (i.e., higher

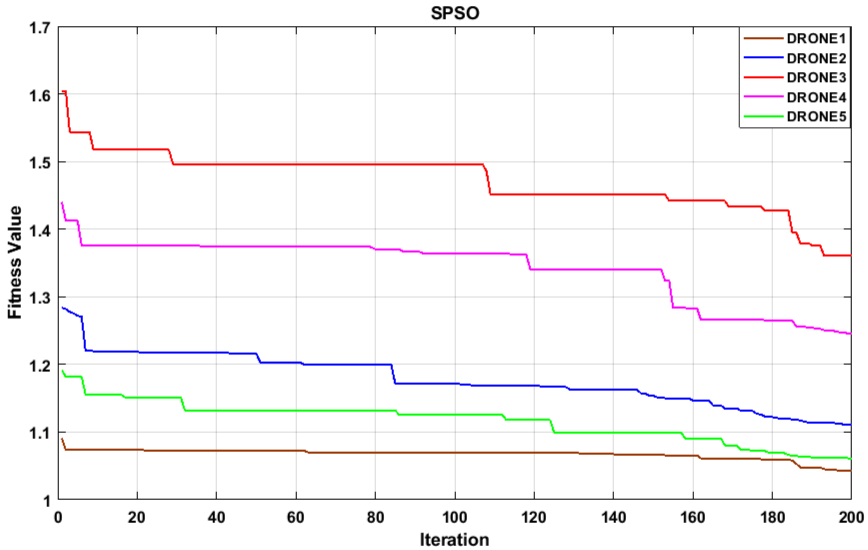

Figure 3.7: Fitness value for IoD formation by SPSO.

average fitness value).

The convergence speed is also a significant factor to show the effectiveness of the proposed algorithm. Fig. 3.8 demonstrates the convergence curve of IPSO. To clearly illustrate the evolution process, y-axis represents the average fitness value. It can be observed that IPSO shows faster convergence at early stage of process evolution which proves the ability of IPSO to generate more accurate and faster safety path.

For performance evaluation of the proposed method, we compare the results with both SPSO and CIPSO [29].

The results illustrate that the proposed method outperforms all other methods since it shows the least AFV while SPSO shows the highest fitness value. This is because SPSO suffers from sticking in local optima and premature convergence problem. The proposed method overcomes these problems by adaptive mutation of the solution that balances between local and global search by increasing the particle speed at the beginning of search (iteration) and reducing the speed at the end of iteration that leads to speed up the convergence. Additionally, if any particle becomes in active and can not improve the solution, it is replaced by fresh one that increases the diversity of search and pushes the solution toward global optima.

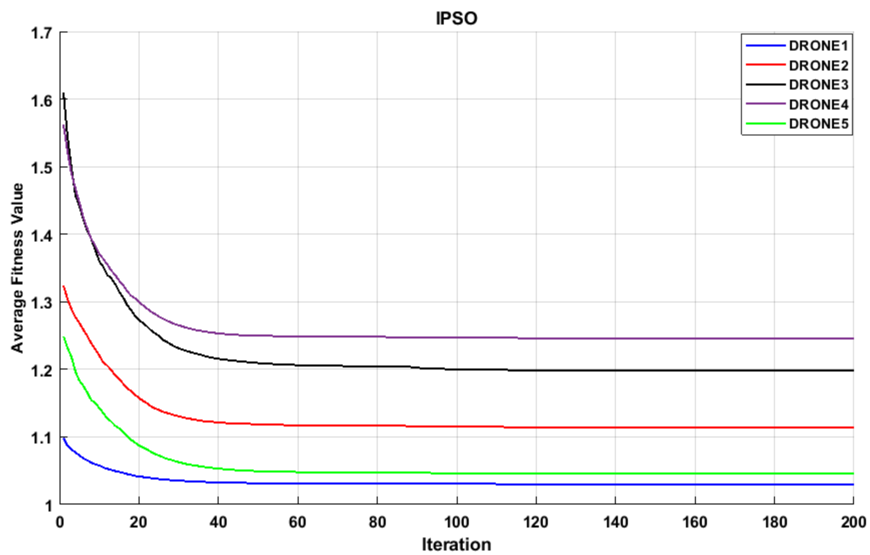

Figure 3.8: Average fitness value for IoD formation by IPSO.

- IoD formation performance

The evaluation of IoD formation is more effective because it reflects the overall formation of all members in IoD. The formation of IoD can be evaluated by obtaining the average fitness value of the whole formation which reflects the stability degree of IoD formation.

Again the average fitness value of the whole formation is obtained for 60 replications and the average fitness value of the formation for the three approaches are recorded in Table 3.4. The results show that the proposed method enhances

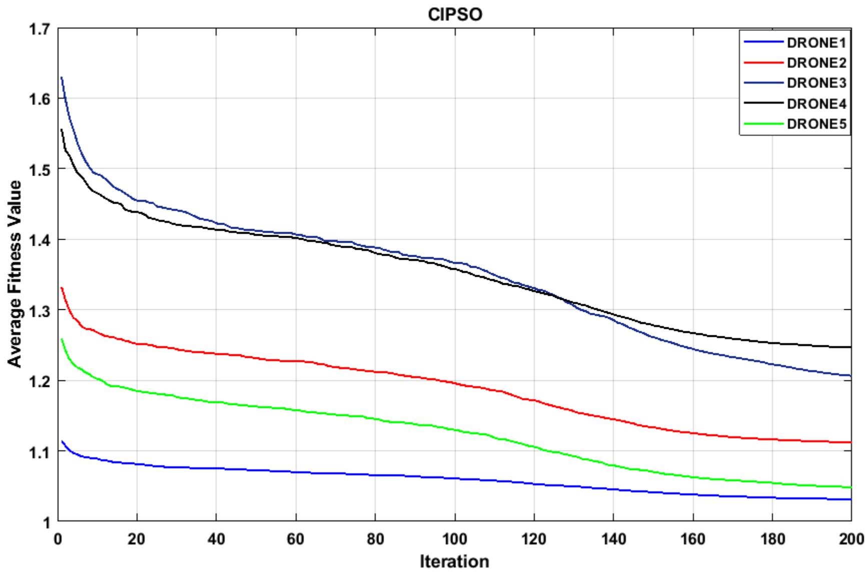

Figure 3.9: Average fitness value for IoD formation by CIPSO.

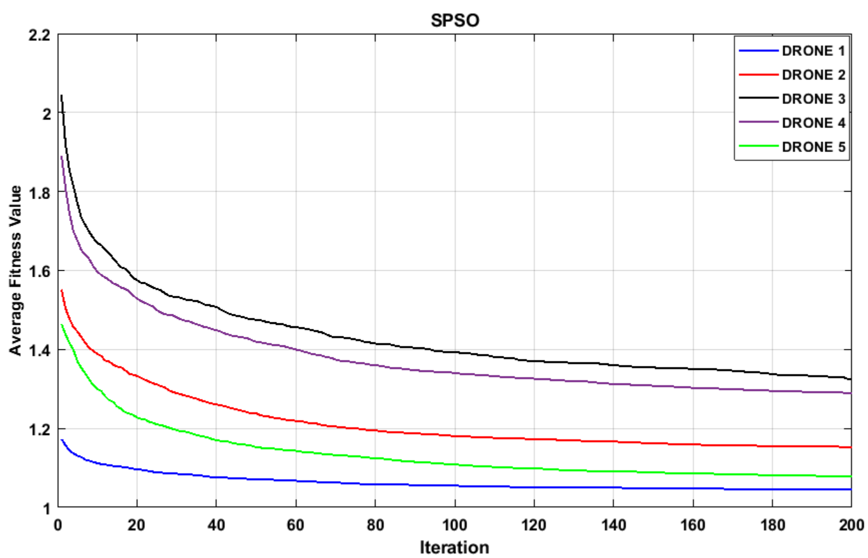

Figure 3.10: Average fitness value for IoD formation by SPSO.

the optimallity path generation by 14.65% compared with SPSO while the CIPSO enhancement is 7.31% compared with SPSO. The results show the advantage of proposed method on path generation.

- Accuracy of IoD path generation algorithm

Table 3.4: Average fitness value for all drones and formation

Drone	**Drone1**	**Drone2**	**Drone3**	**Drone4**	**Drone5**	**FAFV**	**%Imp**
IPSO	**1.024**	**1.091**	**1.22**	**1.22**	**1.0325**	**1.1175**	**14.65%**
CIPSO	**1.059**	**1.188**	**1.349**	**1.350**	**1.122**	**1.214**	**7.31%**
SPSO	**1.087**	**1.292**	**1.518**	**1.453**	**1.195**	**1.309**	**NA**

The accuracy of algorithm can be measured by its ability to generate success path. A failure rate which is defined as a number of trails in which algorithm fails to generate path without collision after last iteration, is utilized to measure the accuracy of the algorithm. To do so, Monte Carlo simulation for 60 replications is carried out and failure rate is calculated. Besides, zero failure rate indicates the highest accuracy algorithm.

The Table 3.5 depicts the average failure rate during Monte Carlo simulation using different algorithms (SPSO, CIPSO, and IPSO). It can be seen that IPSO yields the least failure rate of 0.8% which means that all paths of IoD formation are feasible and without collision. Furthermore, the second method (CIPSO) is the second best lower failure rate (2.5%), while SPSO shows the worst failure rate (14%). The gained improvement by proposed method is 94% compared with standard PSO while CIPSO achieves 82.12% improvement. Moreover, IPSO can guarantee a considerable improvement and achieve the highest accuracy in path generation.

- Running time comparison

Running time is also a significant factor to evaluate the performance of different algorithms. It plays an important role in path generation as well as collision avoidance response. In this work,the running time is measured for three methods and increasing time is recorded in Table 3.5. Besides, CIPSO needs internal loop for sorting and mutating the solution which in turn increases the time required to generate the paths. As a result, it suffers from longer running time. On the other hand, the proposed method checks and replaces the inactive particles. Therefore, it needs shorter time to generate the paths. What is more, the increasing time compared with SPSO is 9% for IPSO and 45% for CIPSO. The conclusion of this section is that the proposed method can generate the feasible paths for IoD formation faster and much better than other methods.

Table 3.5: Failure rate and simulation time

Method	failure rate	Improvement	Increasing Time
IPSO	**0.8%**	**94.2%**	**9%**
CIPSO	**2.5%**	**85.7%**	**45%**
SPSO	**14%**	**NA**	**NA**

- Effect of iterations on performance

The iterations number also impacts the performance of algorithm. To study the effect of number of iterations on algorithm performance, we study the average path length of all drones with respect to number of iterations. Path length is affected by number of iterations where the average path length becomes better as the number of iterations increases, as shown in Fig. 3.11. However, there is a specific iteration in which the path length is not enhanced after that iteration. It can be observed from figure that before iteration 80 is reached, the optimal solution is obtained and the stable of formation is achieved.

Besides the average path length with iteration comparison, we have compared

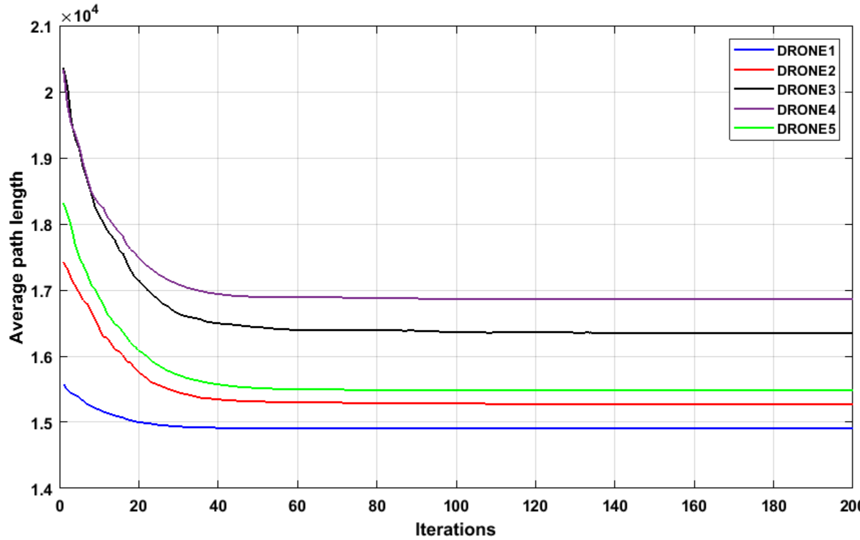

Figure 3.11: Average path length with iteration for the proposed algorithm.

the average path length with SPSO and CIPSO, and the results are illustrated in Fig. 3.12.

As can be observed in the figure, the proposed method outperforms other methods. The path length generated by proposed method is always shorter which proves the advantages of proposed method. The advantages of shorter path has affected the mission time of drones. The shorter path leads to shorter mission time and less energy consumption.

3.6.2 Variable Drones Altitudes

To further investigate the impact of proposed method on IoD formation path generation, we have carried out an extensive experiments in three dimensional environment in which drone can avoid collision horizontally or vertically. In this case, more freedom is given to generate safety paths which in turn reduces a failure rate of algorithm.

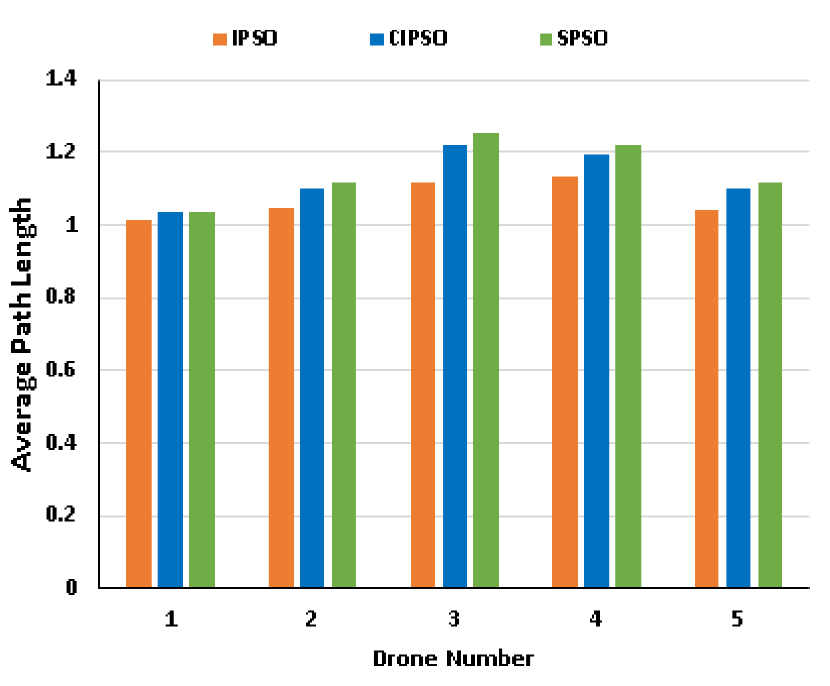

Figure 3.12: Average path length for different methods

The simulation results for different algorithms are given and the comparisons show the advantages and effectiveness of the proposed improvements.

Fig. 3.13 shows the obtained path length for different algorithms. In the figure, IPSO outperforms other methods and shows lower path length for all drones.

Fig. 3.14 to Fig. 3.16 illustrate the two and three dimensional paths for all algorithms. It can be observed that all algorithms guarantee feasible flying path without conflicting with obstacles. Besides, proposed method is able to generate smooth path for IoD formation and it shows lower fitness value and faster convergence rate where the optimal path is generated in the early stage of process operation as shown in Fig. 3.17. In the figure, the optimal path is generated before iteration 80.

Failure rate is also evaluated and it is 0.4%, 2%, 12% for IPSO, CIPSO, and SPSO,

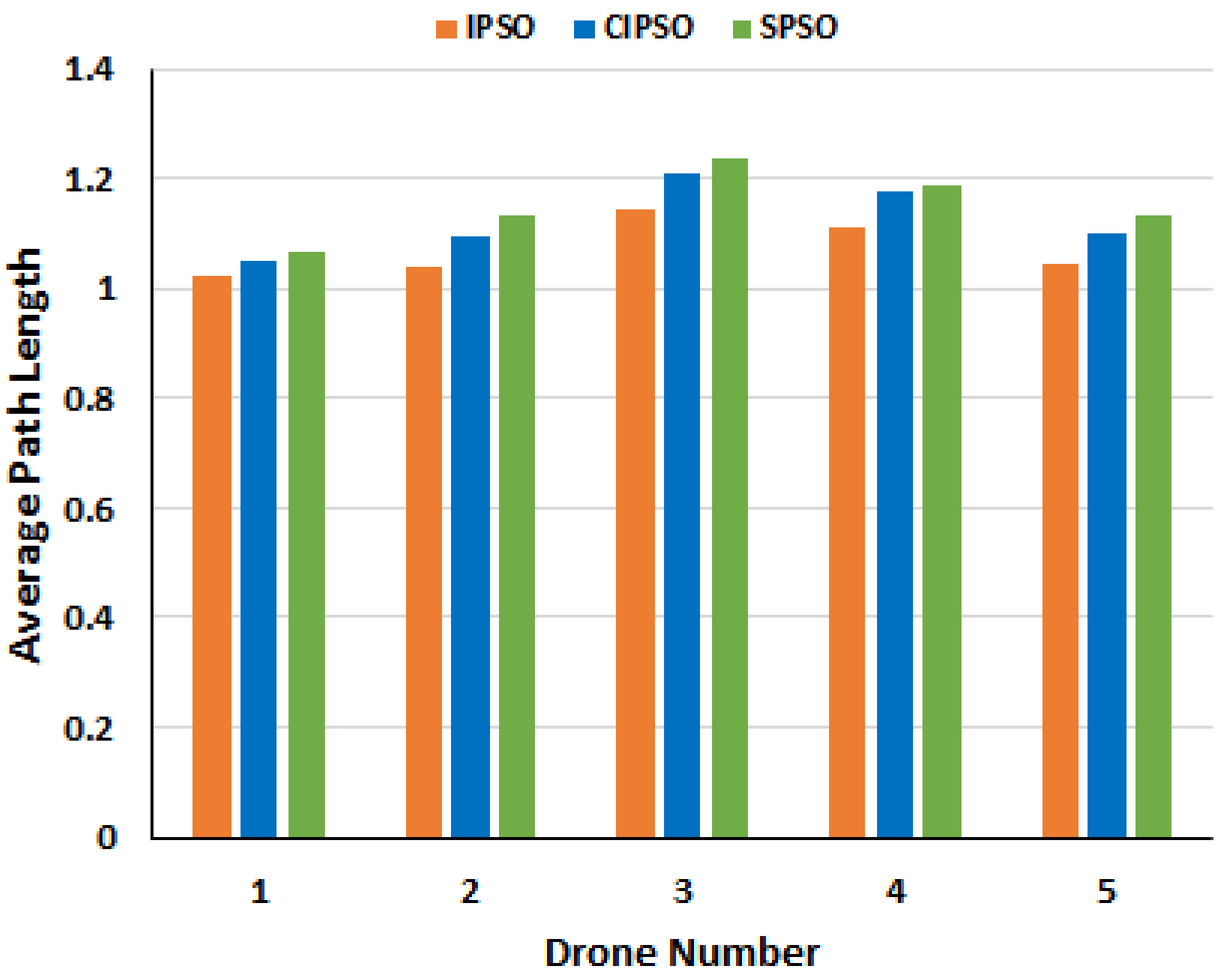

Figure 3.13: Average path length for different methods with variable drones altitudes.

respectively. The proposed method achieves over 96.67% improvement compared with SPSO.

3.6.3 Effect of Less Iteration on Performance

To further investigate the performance of the proposed method, we carry out simulation with less number of iterations. In this simulation, the number of iterations is reduced to 60 iterations and the other parameters are still the same. Moreover,

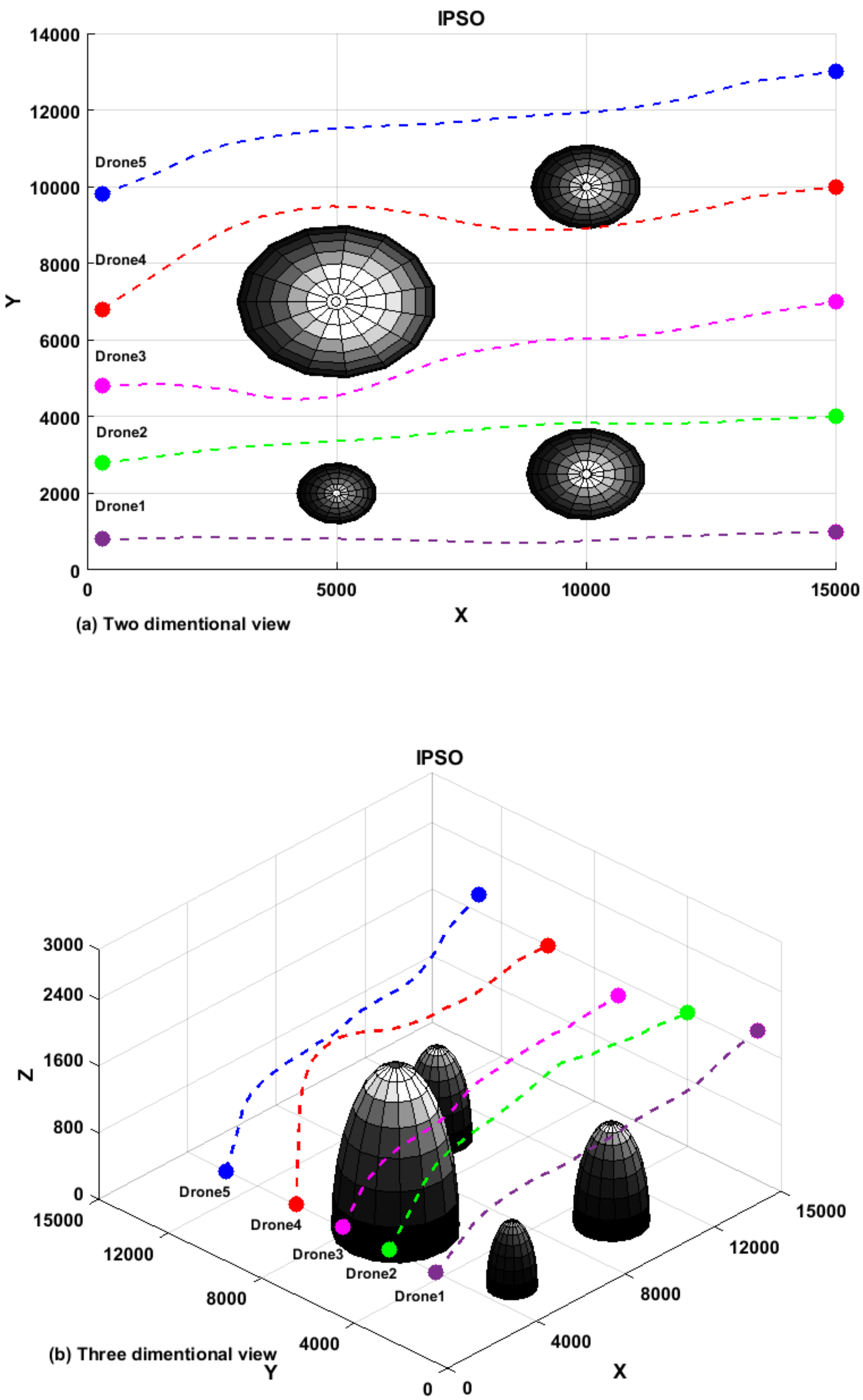

Figure 3.14: Two and three dimensional view for IoD path formation by IPSO with variable altitude.

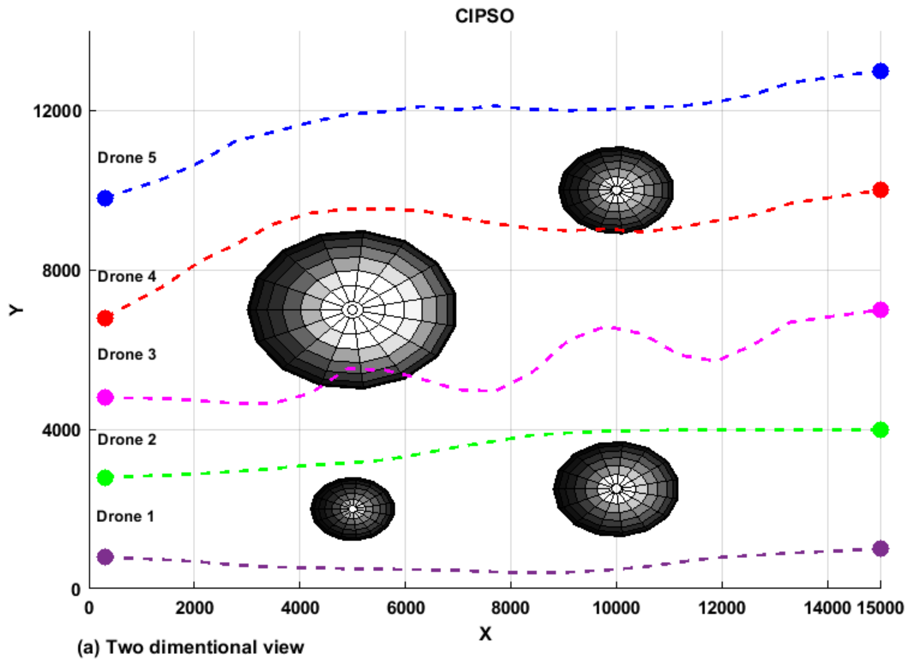

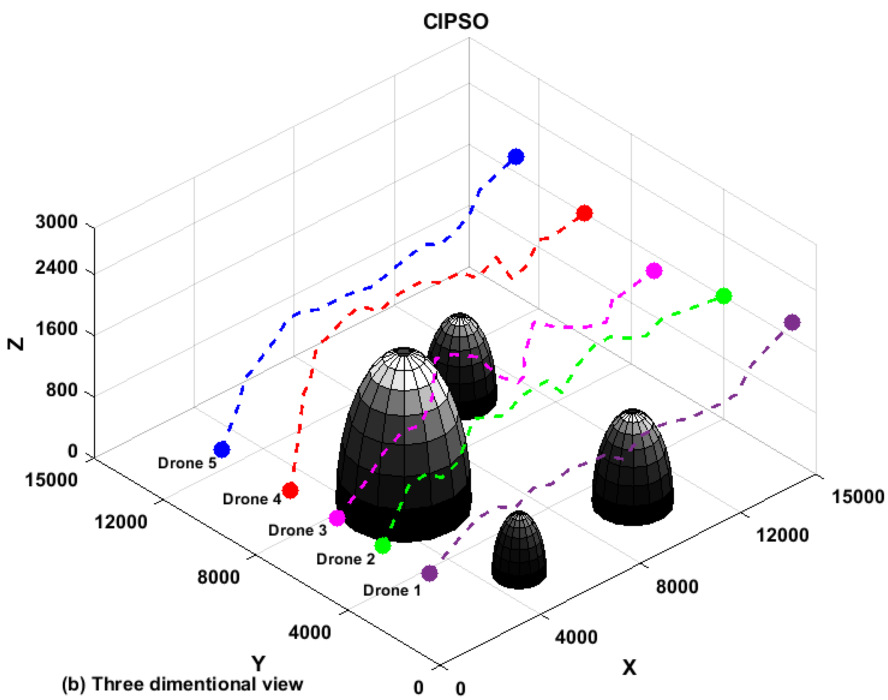

Figure 3.15: Two and three dimensional view for IoD path formation by CIPSO with variable altitude.

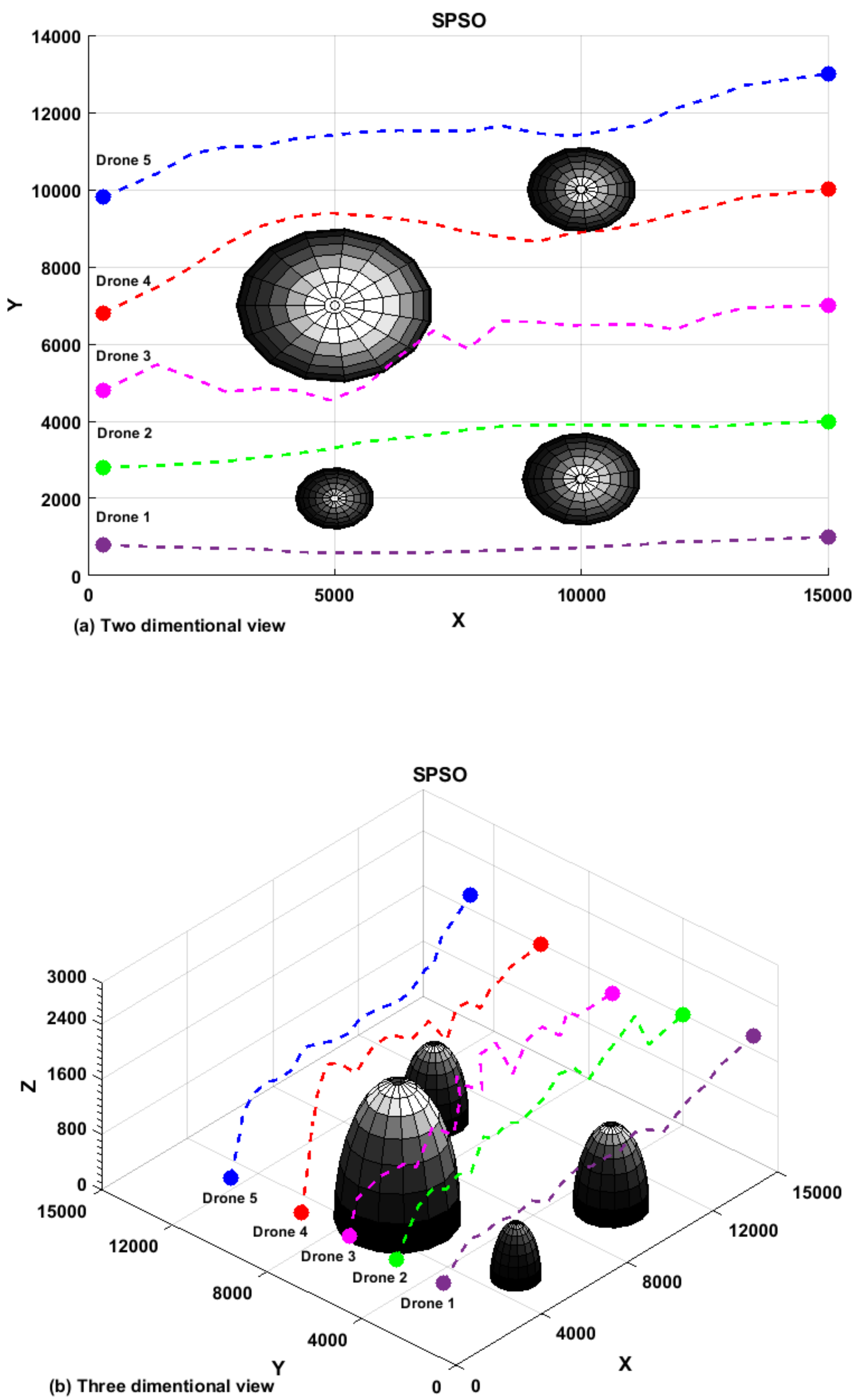

Figure 3.16: Two and three dimensional view for IoD path formation by SPSO with variable altitude.

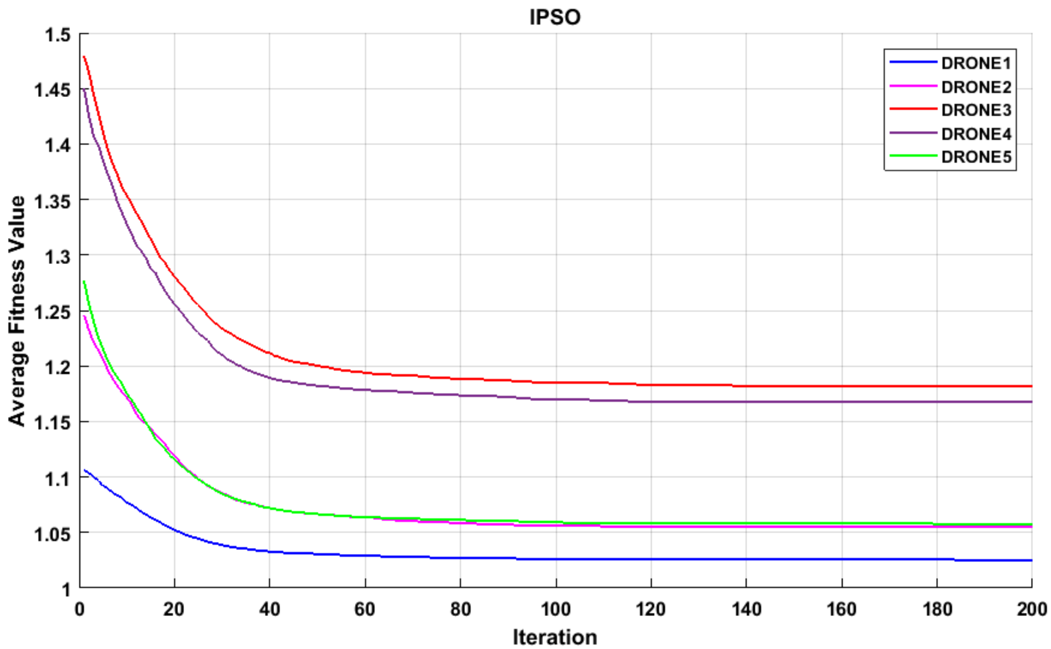

Figure 3.17: Three dimensional average fitness value for IoD formation by IPSO.

the average fitness value and failure rate are analyzed, and the results are illustrated in Fig. 3.18 and Fig. 3.19. It is straight forward observed that the fitness value is higher than that with large number of iterations.

It can be seen that IPSO exhibits better result and more accurate than SPSO. The convergence rate is still acceptable and the same trend with high number of iterations.

Failure rate is also discussed for both SPSO and IPSO. For low number of iterations, the failure rate increases significantly to greater than 90% in SPSO which means that SPSO is not able to generate IoD formation paths with small number of iterations. However, IPSO failure rate is 8% which proves the advantages of the proposed method. This is because in IPSO, evolution process linearly changes with iteration. The adaptive mutation of particle velocity which starts

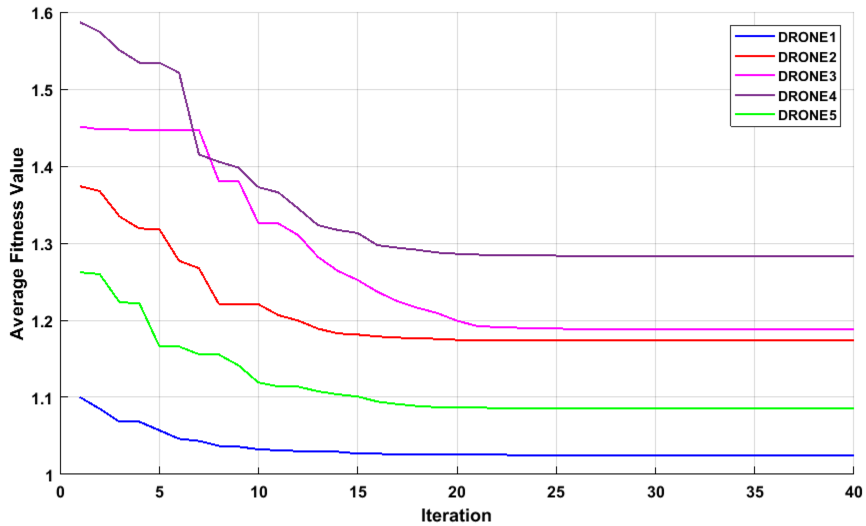

Figure 3.18: Average fitness value for IoD formation by IPSO with reduced maximum iteration.

with high value to achieve diversity and decreases linearly with iteration to small value at the end of iteration in which particles reach to the global solution. Thus, IPSO is able to generate safety paths with high probability to avoid collision with environment obstacles in short time.

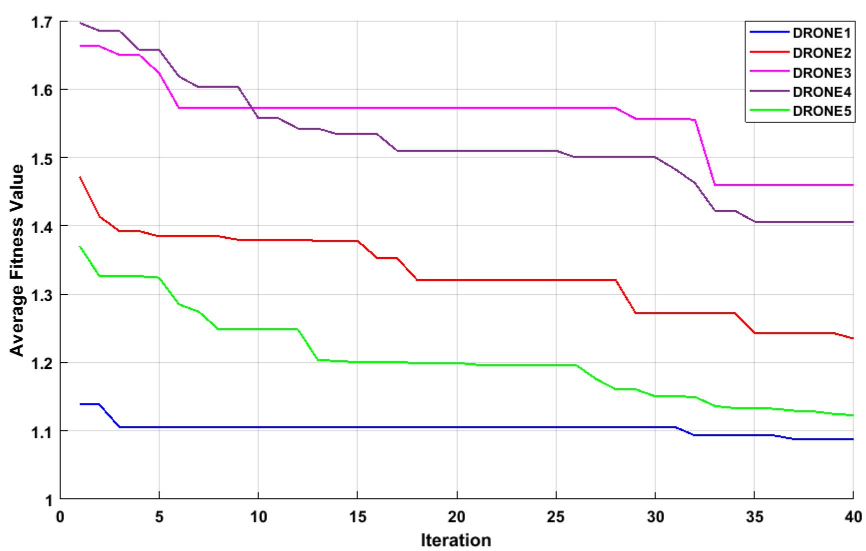

Figure 3.19: Average fitness value for IoD formation by SPSO with reduced maximum iteration.

3.7 Chapter Summary

The successful path planning for IoD swarm requires IoD nodes with the capability to adapt and configure themselves automatically to the surrounding environment without intervention of human. Due to the increasing number of nodes in IoD, the centralized systems are not practical. In this chapter, the new method for IoD formation path planning was proposed. The aim of improved particle swarm optimization (IPSO) is to increase the diversity capability of standard PSO. This study investigated the impact of optimization parameters on convergence speed. Moreover, the formation of IoD was evaluated and analyzed in two and thee dimensional space. For fair comparison, Monte Carlo simulation for IoD formation with five drones was conducted under different terrain constraints. The results were compared with standard PSO and CIPSO. The results demonstrated that the proposed method outperformed the other methods and provided fast and accurate IoD formation paths with obstacles and member collision avoidance.

CHAPTER 4

AN ENERGY EFFICIENT ONLINE COLLISION AVOIDANCE APPROACH

4.1 Chapter Motivation

Over the last few years, research in IoD formation has received significant attention in various complex applications. Therefore, for applications that require highly complex tasks, which individual drones can't perform effectively, IoD can be used to accomplish such tasks efficiently. On the other hand, the rapidly growing popularity of IoD for consumer applications dramatically increases the number of accidents involving drones. Thus, for drones to complete their missions, the prime concern is the mission's safety. Without preventing collision among drones and with obstacles, safety is not guaranteed. The main challenge in IoD formation is the need for an efficient and effective collision avoidance protocol in static and dynamic environments, which is very important in civilian and military applications.

In dynamic path planning, complete information about the environment may not be available ahead of time, so incomplete knowledge about dynamic obstacles is assumed. In this case, the obstacle has to be detected during the mission, which requires real-time path optimization or dynamic path planning in which a complete path is not available. But rather an optimal path information within the drone's field's of view. Moreover, in IoD, each drone has to be provided with an efficient mechanism to avoid the potential static and dynamic obstacles while continue planning its path. Besides, each member requires to maintain a specific minimum distance from other drones in the formation.

To avoid collision with nearby obstacles, the drones need to respond immediately as soon as obstacles are detected. Therefore, the drone should be endowed by fast convergence algorithm to fulfill this requirement.

Furthermore, in certain situations like an urban environment, the drones are tasked to fly through such an environment and must quickly navigate around considerable obstacles while avoiding the collision. Another example is in a forested environment in which the drone has to travel throughout the tree lines and has to avoid collisions. In such applications, the drone needs to be endowed by an efficient approach to respond quickly and avoid collision with nearby obstacles, while planning its flight path.

Despite the distinct features of UAVs and their increasing popularity, inherent limitations still hinder the full potential of their applications. The main limitation is the limited lifetime of on-board batteries which limits its flight time [14], [140]. As a result, most applications can not reach their full potentials. Moreover, for a long path where the drone needs to perform its mission in a large area, the energy consumption by UAV should be minimized to generate a safety path and reach its destination. To clarify the picture, if the energy of the UAV is improved, the UAV can accomplish more tasks in a shorter time. Conversely, if the drone is not endowed by an efficient energy mechanism, it needs to perform more recharge cycles which increases the mission time. For this reason, reducing the energy consumption during the drone mission is a key challenging problem.

Although the literature works have achieved an improvement on drone's collision avoidance and path planning, some works neglect IoD formation and consider only one drone. Additionally, they test their approaches using small number of obstacles in large environment dimension where the probability of collision is very small making their approaches suitable for applications in light environments and they are not guaranteed to work in dense environments. Moreover, most works consider only geometric constraints and neglect other drone's peculiar features such as energy consumption in IoD formation.

4.2 Chapter Contributions

To fill the above discussed gaps, this chapter developed an efficient energy-aware online dynamic and static obstacles collision avoidance algorithm for IoD formation which can operate within a radius detection range of drone online and in time. The proposed approach uses gradient optimization for fast and quick convergence. Unlike traditional collision avoidance algorithms that require prior knowledge about obstacles and their precise locations in advance, this work provides a novel algorithm where prior information about obstacles is not required. Instead, it receives instantaneous locations about detected obstacles and generates collision-free paths within the drone's detection range. The following points summarize the key contributions included in this chapter.

- The proposed approach aims to work online in a dense environment in which a drone flies through a narrow passage due to several static and dynamic obstacles filled the terrain. Therefore, the feasible paths from current locations for some drones in IoD formation might not be guaranteed especially in dense environment where obstacles fill the terrain.

- To guarantee feasible paths for all drones in situations where a desired collision-free path is not available within the drone's detection range, the Safety Ensure Approach (SEA) is proposed. It puts some drones in a hovering state for some time. Furthermore, the drone can backtrack when hovering in place is not possible. It is also noteworthy that, the proposed SEA allows a drone to fly vertically if hovering and backtracking are not possible to avoid crashing with nearby obstacles, which increases the ability to avoid collisions.

- The proposed mechanism provides an energy-efficient path generation to obtain a collision-free path with minimum energy requirement. To this end, the energy consumption is used as an objective to be achieved for IoD formation which guarantees collision-free trajectory with minimum energy consumption. Moreover, the algorithm is enabled only when obstacles are detected, which reduces the processing energy consumption during flight. Furthermore, it guarantees full paths for all drones in IoD in static obstacle environment. The algorithm is able to avoid the following collisions: (I). drone-to-drone (II). drone-to-static obstacles, and (III). drone-to-dynamic obstacles. More importantly, the proposed algorithm generates efficient drone trajectories and can be efficiently scaled up to a larger size.

This chapter is the result of a collaboration with Dr. Mohamed Deriche from Electrical Engineering Department, Prof. Ansar Ul-Haque Yasar from Transportation Research Institute, Hasselt University, Belgium. The work has been published in Ad Hoc Networks, 118, 102519, 2021.

4.3 Energy Model For Drone Path Planning

To cope with limited drone energy, the energy consumption is used as an objective to be minimized by an optimization approach during the planning of the path. To elaborate, in the drone field of view, the path, which minimizes energy consumption and avoids collision with obstacles, is selected. The energy is obtained for each generated segment, where the selected segment minimizes the total energy consumed in a whole mission. It has to be stressed that the best generated path is the path that requires minimum energy, and reduces the required energy to the destination. The algorithm is proposed to obtain the collision-free path that reduces energy consumption while satisfying all constraints.

We use the energy model for a quadrotor drone in [63]. This model is derived from real measurements and focuses on the impact of different factors on a drone's energy consumption. Different maneuvering activities like flying horizontally, flying vertically up and down, turning, and hovering are considered in the real experiments. Moreover, the energy consumption is obtained as a function of speed. They measure the power consumed (P) during such operations and the fitting curves are estimated and plotted in [63]. In path planning, we focus on the impact of movement (such as hovering, horizontal movement, and vertical movement) on energy consumption. Thus, the energy consumption for each operation is obtained in [63] as follows: The flying vertically up or climbing energy for Δh distance and with velocity v_{climb} is given by

$$E_{climb}(\Delta h) = P_{climb}\frac{\Delta h}{v_{climb}}. \tag{4.1}$$

The flying vertically down or descent energy for Δh distance and with velocity v_{desc} is given by

$$E_{desc}(\Delta h) = P_{desc}\frac{\Delta h}{v_{desc}}. \tag{4.2}$$

The hovering in place energy from time ***t1*** to time ***t2*** is given by

$$E_{hover} = P_{hover}(t2 - t1). \tag{4.3}$$

The flying horizontally is given as a function of velocity and can be given by

$$E_{horiz} = P_v \frac{d}{v}, \tag{4.4}$$

where d is the horizontal distance, and v is the horizontal speed. Therefore, the energy can be written as follow

$$E = E_{climb} + E_{desc} + E_{hover} + E_{horiz}. \tag{4.5}$$

According to the energy model, vertically flying (E_{climb}+E_{desc}) has a significant impact on energy consumption, while hovering and horizontally flying require less energy consumption than vertically flying.

In our energy model, the designed variables for hovering F_{hov}, flying horizontal F_{hor}, and flying vertical F_{fv} are used to trace the energy consumption by drone at each interval. For instance, if the drone decides to hover in place, then the designed variables $F_{hov} = 1$, $F_{hor} = 0$, and $F_{vf} = 0$, and the energy consumption required for the current segment will be the hovering energy. Besides, the energy path for each drone can be calculated by adding the segments' energy as follow.

$$Path_E = \sum_{i=1}^{M_s} SE_i + CSE, \tag{4.6}$$

where M_s is the number of planned segments proceed current segment, and SE_i is the energy of ith segment. To obtain the remained energy for each drone, an online calculation is performed as follow.

$$Rem_E = Total_E - Path_E, \tag{4.7}$$

The total energy of drone can be simply obtained as $Total_E = V_n * I_H * 3600 * P\%$, where P% is the maximum percentage of energy a drone can use (particularly 70%) to avoid battery or drone damage [63].

4.4 Energy-efficient IoD Path Planning Approach Description

To plan the path of IoD formation, some factors must be taken into accounts, such as terrain area, obstacles included in the terrain, and IoD formation. The mission environment may include obstacles such as mountains, buildings, radars, and other threats. Moreover, the IoD formation includes many drones flying in this environment. Thus, the IoD formation should be able to avoid colliding with these obstacles and with other drones in the formation. To do so, the path should be constrained to avoid all these threats and obstacles. On other words, the path should achieve the objectives and satisfy all constraints. In this chapter, we have modeled the path planning problem of IoD as an objective constrained optimization problem. The proposed approach guarantees safety paths for all drones with minimum energy consumption.

4.4.1 IoD Path Representation

The goal of using collision avoidance algorithms for path planning is to find a feasible path for a drone during its mission from the source to the destination in a complex environment. Lets the flight path be represented by finite positions $(P_1, P_2, P_3, ..., P_N)$. Then, the distance between two consecutive positions should be less than the sensing range of the drone. Each position P_i is represented by three-dimensional coordinates (x,y,z) as in [51]

$$(x, y, z)|x_{min} \leq x \leq x_{max}, y_{min} \leq y \leq y_{max}, z_{min} \leq z \leq z_{max}, \tag{4.8}$$

where $x_{min}, y_{min}, z_{min}$ are the lower bounds of the flying space, and $x_{max}, y_{max}, z_{max}$ are the upper bounds of the flying space.

Furthermore, in a dynamic environment, drones should respond quickly to avoid nearby obstacles. Thus, a simple and fast approach is needed to generate the path. In this work, we develop a fast and accurate approach for such purpose based on gradient optimization. Based on these considerations, quadratic Bezier curves are selected to represent the IoD paths due to their simplicity. To be more specific, the derivation of the quadratic Bezier curves can be computed at any location on the curve, which simplifies the constraints calculation. Additionally, quadratic Bezier curves have a fast curvature computation and state variables reduction, which makes flight constraint calculations straightforward. The Bezier curves (BZ) are defined as

$$BZ(t) = (1-t)^2 P_0 + 2(1-t)tP_1 + t^2 P_2, \tag{4.9}$$

where t $\in$ [0 1], and P_0, P_1, and P_2 are the points of Bezier curves, and $P_0 = (x_0, y_0)$ is the start point of a segment. The gradient of Bezier curves can be calculated as

$$\frac{\partial BZ}{\partial t} = 2(1-t)(P_1 - P_0) + 2t(P_2 - P_1). \tag{4.10}$$

4.4.2 Obstacle Model

In this subsection, the obstacle model including static and dynamic obstacles is presented. Furthermore, the space boundaries are assumed to be available in advance.

- Static obstacle model

In this model, the locations of obstacles are unknown in advance. Instead, the locations are available within the detection range. We model the obstacle in a 3D environment as a half-sphere as in [2]. Let SO is the static obstacle, Sx, Sy, Sz is its center coordination in 3D space, and Sr is its radius. Thus, it can be modeled as follow:

$$SO_k = (Sx_k, Sy_k, Sz_k, Sr_k), \tag{4.11}$$

where Sx_k, Sy_k, Sz_k are the three-dimensional coordinate of kth static obstacle and Sr_k is its corresponding radius. The coordinates are given by

$$Sx_k = Sr_k \cos(\theta)\sin(\phi) + Sx_{k0}, \tag{4.12}$$

$$Sy_k = Sr_k \sin(\theta)\sin(\phi) + Sy_{k0}, \tag{4.13}$$

$$Sz_k = Sr_k \cos(\phi) + Sz_{k0}, \tag{4.14}$$

where $Sx_{k0}, Sy_{k0}, Sz_{k0}$ is the center coordinate of kth static obstacle, $\theta \in [0\ 2\pi]$ and $\phi \in [0\ \frac{\pi}{2}]$

- Dynamic obstacle model

The dynamic obstacles are modeled as spheres moving in space. Let DO is the dynamic obstacle, Dx, Dy, Dz is its center coordination in 3D space, and Dr is its radius. Thus, the kth dynamic obstacle can be modeled as follow:

$$DO_k = (Dx_k, Dy_k, Dz_k, Dr_k), \tag{4.15}$$

where (Dx_k, Dy_k, Dz_k) is the three-dimensional coordinate of kth dynamic obstacle and can be calculated the same way as in Eq.4.12 to Eq.4.14, where $\phi \in [0\ \pi]$. The obstacle is moving with velocity

$$V_k = (Vx_k, Vy_k, Vz_k), \tag{4.16}$$

where Vx_k, Vy_k, Vz_k is the velocity of kth dynamic obstacle in x,y,z direction, respectively. Furthermore, the position of obstacle is updated while obstacle moving. The new position after $DurationTime$ can be obtained by

$$NewPos = OldPos + Velocity * DurationTime, \tag{4.17}$$

where $Velocity$ represents Vx, Vy, Vz. At any time, the new constraints are found so that the path is not colliding with obstacles.

4.4.3 Design of the Objective Function

In practice, the assigned missions to the drone are done with different objectives, which need to be optimized. The objective function is responsible for optimizing these objectives. Mathematically speaking, the generated value by objective function is either maximized or minimized by the optimization algorithm. In path planning, the objective function may include the length of the path, energy consumption, or elapsed time. In our work, the aim of the objective function is to minimize either the total path length or the energy required to complete the mission.

For instant, if the path is optimized for energy, the objective function will minimize the total energy consumed during flight by selecting the collision-free path which consumes minimum energy. It has to be stressed that the path with minimum length consumes minimum energy. Thus, we focus on energy objective path planning. In this subsection, we will explain those two objectives.

- Path length minimization

In some drone's missions, the longer path is not desirable because the drone is limited power and the longer path is power-consuming for a drone. Thus, the shortest path is preferable. Assuming SL, CS_l, and $LOLS$ are the segment's length, current segment length, and length of last segment, respectively. The following path length function (f_{pl}) used in [30] is used to evaluate the path length:

$$f_{pl} = \sum_{i=1}^{M_s} SL_i + CS_l + LOLS, \tag{4.18}$$

where Ms is the number of planned segments proceed current segment, SLi is the length of the i^{th} segment, and $LOLS$ is the shortest straight line segment between the end of the current segment and final destination and can be calculated by Euclidean distance from the current segment endpoint to the destination. Then the current segment is selected so that this quantity is minimized.

- Energy consumption minimization

The energy model described in section 4.4 can be used directly to measure the offline energy with predefined path generation in which a drone follows the generated path. However, in our dynamic path planning, the drone generates the collision-free path within its detection range online and on time. Our objective is to minimize the energy consumption by selecting the segment that minimizes the energy required to reach the destination. Thus, the best segment within the detection range not only the segment that consumes less energy but also the segment that requires minimum energy to reach the destination. For instant, the collision-free path is selected as an optimal path within the drone's detection range if it minimizes the energy consumed to reach the destination. The energy required to reach the destination is the energy of the current segment + energy required to reach the destination from the end waypoint of the current segment. To use the energy as an objective function to be minimized, the objective function is composed of two parts, i.e., energy of two paths. The first part calculates the optimized energy consumption for the current generated path (first path) and the second part calculates the energy consumption from the end waypoint of the current path to the destination (second path). For simplicity, the second path is a straight line obtained by Euclidean distance from the end waypoint of the first path to the destination. Therefore, the objective function is given by the following equation:

$$Obj\_Energy = CSE + Opt(Energytothedestination), \tag{4.19}$$

where CSE is the current segment energy which is the required energy by the collision-free path within the detection range of the drone and Opt(.) is the energy required to reach the destination when the drone flies at maximum speed to travel a minimum distance to the destination. The best path is the path that minimizes the objective function in eq.4.19.

It is noteworthy that the safety path is given the highest priority which means that the collision-free path is selected to be the new path of a drone even if the other non collision-free paths provide minimum path length or less energy consumption.

4.4.4 Design of Constraints

It is worth mentioning that constraints are used to ensure collision avoidance with other objects in the environment including dynamic and static obstacles in addition to other drones. In this subsection, we explain the constraints for obstacles and IoD formation.

- Obstacles constraints

The safe path of IoD formation does not go through obstacles. If even one point in the path goes through an obstacle, this path is penalized with high cost. In each interval, the distances from a drone path, including a drone size, and centers of obstacles within the detection range, are calculated. The satisfied constraints should be higher than the radius of the obstacles (i.e the uncertain boundary of obstacles). If the obstacles are outside the drone detection range, they are neglected. To design the obstacle constraint, the segment is divided into $\boldsymbol{n}$ points and the distances between each point of the segment to all detected obstacles are calculated. The constraints take the following form:

$$\sqrt{(x_i - x_{Oj})^2 + (y_i - y_{Oj})^2 + (z_i - z_{Oj})^2} \geq R_j, \tag{4.20}$$

where (x_i, y_i, z_i) are the points of the $path_i$, (x_{Oj},y_{Oj},z_{Oj}) and R$_j$ are the center and radius of $j^t h$ obstacle, respectively. For the dynamic obstacle, the new position of the obstacle is calculated by eq.4.17 and the constraints are calculated the same way as in static obstacles as soon as the obstacle is detected within the detection range.

- Drone member constraints

When the density of IoD formation increases, the drones get closer to each other, which increases the probability of drone collision. Therefore, drone collision avoidance should apply the drone member constraints during the trajectories planning for IoD formation. Thus, when IoD paths are generated, it is essential to test whether drones are getting too close while flying in their respective paths.

Assuming path_i is a path for drone_i and path_j are paths for other drones in the drone's field of view, i.e detection range. Then every point in path_i should be compared with every point of other paths (path_j) so that the path_i maintains sufficient space with other paths. To do so, a safety distance SDt should be maintained among drones. The safety distance among IoD members mainly depends on the maximum speed of drones, i.e., SP, wireless communication latency, and processing time [141]. Thus, the safety distance can be defined by

$$SD_t \geq SP * (processingtime + communicationtime). \tag{4.21}$$

Note that the safety distance should be greater than or equal to the minimum distance between drones. For example, if minimum distance is 5m and the obtained SD_t is less than minimum distance, SD_t will be set to 5m.

The required constraints to avoid collision among drones can be formulated as follow.

$$SD_t(i,j) \leq \sqrt{(x_i - x_j)^2 + (y_i - y_j)^2 + (z_i - z_j)^2}, \tag{4.22}$$

where (x_i, y_i, z_i) are the segment's points of path_i, (x_j, y_j, z_j) are the corresponding points in other paths in the drone's field of view.

4.5 System Model of Collision-Free Path Generation approach for IoD

In this section, the system model of the proposed approach is explained. The prior knowledge about obstacles is not required since the flight terrain is assumed to be unknown in advance. Thus, it does not need an offline path planning phase. The UAVs are taking off from starting locations and flying toward the destination locations without any interruption till the obstacles are detected. When obstacles are detected, the collision avoidance algorithm is triggered to avoid the detected obstacles.

The idea of the algorithm is to divide the total time into small intervals. At each interval, the path planning generator receives parameters and environmental constraints, and returns a feasible path, which is the best partial path in which objective function, i.e., reducing the path length or energy consumption, is achieved and constraints are satisfied. The system model block diagram of the proposed approach is illustrated in Fig. 4.1.

The main parts of the system model are the multipath generation module and collision avoidance algorithm module. The inputs of the model are the obstacle detection, IoD current locations, and objectives. The proposed approach undertakes to avoid collisions and obtain a collision-free trajectory within a field of detection range in an online manner. However, in dense environment in which obstacles fill the terrain, generating online free path might not be possible for some drones.

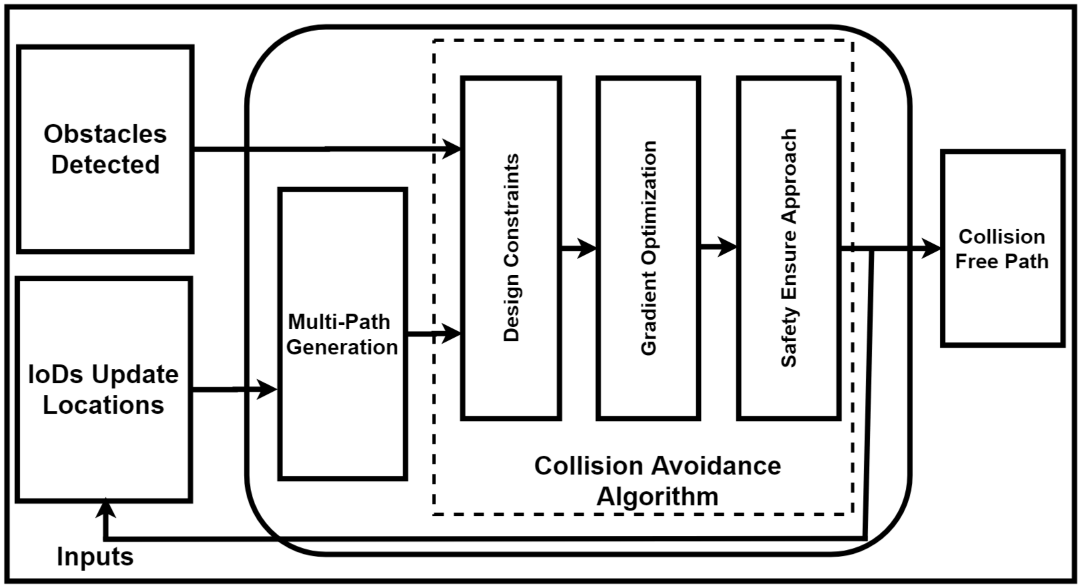

Figure 4.1: System model block diagram of proposed energy-efficient IoD static and dynamic collision avoidance approach.

In such scenarios, some drones are put in a hovering state till the danger of collision has gone. Furthermore, the proposed model might let some drones to temporarily backtrack and obtain more appropriate collision-free paths. If the backtracking might cause any potential collision or requires more energy than flying vertically, the drone is allowed to fly vertically. In other words, these extra features significantly increase the ability of drone to avoid any obstacle on its path. The main components of the proposed system model are described below.

4.5.1 Multipath Generation Module

In general, generating multiple paths increases the probability of drone safety because if one path lies in the way of obstacle, the others may be in different directions. On the other hand, as the number of paths increases, the time required to optimization them increases too. In our work, we generate up to 6 paths which are sufficient to generate safety paths and needs a short time to be optimized. The multipath generation module is responsible for generating multiple initial paths which will be optimized by gradient optimization. Generally speaking, at the beginning of each step, the multipath generation module receives the current position of drone as inputs and generates multiple segments toward the destination direction. Then these paths are optimized and the best one, which satisfies all constraints and achieves the objective, is selected as the new path of the drone. Finally, the drone follows this path and updates its current location using the GPS technique.

4.5.2 Collision Avoidance Algorithm Module

A collision avoidance module consists of three components, namely design constraint, gradient optimization, and safety ensure approach modules. When the obstacles are detected, the collision avoidance is invoked, which tries to avoid collisions with detected obstacles, and generates a collision-free trajectory for the drone online.

The design constraint module receives the initial generated paths and obtains the constraints required to avoid collisions. The obtained constraints include static, dynamic, and drone formation constraints. As soon as the constraints are obtained, the gradient optimization is called with initial generated paths, constraints, and objectives as inputs. Based on these inputs, the paths are optimized. The output of gradient optimization is the optimized paths with their corresponding flag that indicates if the path is collision-free or not. Now, the SEA module receives the output of gradient optimization and checks all the optimized paths. The paths that are not satisfying all constraints and achieving objective are excluded from collision-free paths. Then the best path is selected from the remained collision-free paths to be the new path of the drone.

The SEA composed of three approaches namely hovering, backtracking, and redirecting to z-direction, i.e., flying vertically, approach. If the path of drone is not clear, i.e., no available collision-free path, the hovering approach puts the drone in a hovering state for some time. If hovering, however, is not possible, the backtracking approach temporarily backtracks the drone to retreat and discover an alternative collision-free path. Moreover, in a dense environment, where several obstacles around drone exist and collisions may occur, backtracking may not be possible. In this case, the drone is redirected in z-direction and allowed to fly vertically and over the obstacle.

It has to be stressed that these approaches are ordered based on the required energy consumption. To clarify, as discussed in section 4.4, flying vertically requires higher energy than hovering and backtracking approach. Thus, to achieve an efficient energy saving, the hovering in place is enabled if the energy required is less than that in backtracking and flying vertically. To this end, an online energy calculation is performed and the energy-efficient approach is enabled. For example, if number of hoverings requires higher energy than flying vertically, then the flying vertically approach is enabled and the drone is enforced to fly in z-direction and bypass the obstacle instead of hovering. Besides, the backtracking is allowed only if hovering in place is not possible and the energy required by backtracking is still less than that in flying vertically. Finally, the new position of drone is updated using GPS which will be used as a starting location of the drone in the next step or interval. The optimization tool in this work is a matlab function SQP algorithm, which is considered to be the most reliable and consistent gradient algorithm [142], [143].

Algorithm 3 IoD path planning algorithm

INITIALIZATION:

initialize Xs ← start positions, Xd ← final positions,

max_velocity, min_velocity, Detection_Rang;

```
begin
    while IoD destinations are not met do
        Curent Locations ← Xs;
        Xn←Gen_Seg(Current locations);
        if Obstacles detected then
            Constraints←FindNewConstraints(Xn);
            Optimized_paths ← GradientBasedOptimize(Xs,Xn)
            if collision-free path not exist then
                if Hovering possible then
                    Enable hovering in place for some time
                    else if Backtracking possible then
                        Backtrack drone to search for an alternative path
                        else
                            Allow drone to fly vertically
                        end
                    end
                end
            end
        end
        if No obstacle detected then
            IoD_Constraints←FindNewConstraints(Xn);
            Optimize the generated paths for energy objective
        end
        Update IoD Current locations, Xs←IoD Current locations
    end
end
```

The pseudocode of the algorithm is presented in Algorithm 3. It starts with the initialization part, which is responsible for initializing all variables, such as starting locations (Xs) and final locations (Xd) of IoD formation, velocity constraints, which is the maximum velocity (max_velocity) and minimum velocity (min_velocity) of drone, and detection range (Detection_Rang). After that, the while loop starts by generating multiple paths starting from current positions (Xs). Moreover, at each interval, if the obstacles are detected, then the algorithm is enabled and static and dynamic obstacles locations are received from obstacles detection input. After the inputs have been received, the required constraints (static, dynamic, and IoD formation) for all drones are determined to avoid collision with detected obstacles and with other drones in the formation. If no obstacle is detected, only IoD formation constraint is obtained. According to these constraints, the optimized segments are generated using gradient optimization.

The gradient optimization approach receives the objective function, constraints, and the generated segments (Xn) by multipath generation module and returns the optimized segments with corresponding flags. The flag indicates if the optimized path is collision-free or not. The collision-free segment should achieve the objective and satisfy all constraints. Then the collision-free path with minimum energy consumption is selected as an optimal path. If the collision-free segment is not available, the drone is put in hover-in-place for some time, backtracked to discover alternative paths, or redirecting in z-direction as discussed above. The segment is then added to the full path.

To repeat steps, the current position of the drone is updated by GPS. Now, the

Xs receives the current positions to be used in the next step or interval. Then the steps are repeated till the drone reaches its destination land where the condition is met. Note that the gradient optimization approach calls the energy objective function for optimizing the generated paths. More importantly, if the collision-free path is not available, the SEA will generate the collision-free path with minimum energy consumption. Thus, the energy-aware is taken into account in all cases.

4.6 Simulation Results and Discussions

To evaluate the ability of the proposed approach in avoiding all obstacles with minimum energy consumption guaranteed, we carry out a simulation using Matlab tool with different static and dynamic obstacles. To show the effectiveness of our algorithm, various scenarios including environment with static obstacles only, dynamic obstacles only, and dense environment with static and dynamic obstacles, are simulated. The following collision avoidance scenarios, drone to static obstacles, drone to dynamic obstacles, and drone to drone; are also evaluated. For each scenario, we verify the safety distance required for avoiding collisions between drones, and then the minimum separation distances between drones and dynamic obstacles are recorded in dynamic obstacle and dense scenarios. Also, we study the impact of the environment on energy consumption for different environmental constraints. Moreover, the scalability is tested for energy consumption by increasing the number of drones in the formation to 10, 15, and 20 drones. Furthermore, we compare our results with the approach presented in [30]. The

Table 4.1: Drones Start and End Locations

Drones	Start Point (xs,ys,zs)	Destination Point (xd,yd,zd)
Drone 1	00, 00, 5	140, 020, 5
Drone 2	00, 030, 5	140, 060, 5
Drone 3	00, 060, 5	140, 100, 5
Drone 4	00, 090, 5	140, 120, 5
Drone 5	00, 110,5	140, 140, 5

simulation is run on intel Cori5 2430M CPU with 3 Giga Byte memory. In this section, the simulation parameters are explained and the results are discussed.

4.6.1 Parameters Setting

It is worth mentioning that the fast convergence feature of gradient optimization allows the proposed approach to accounts for the dense environment (numerous static and dynamic obstacles) such as the urban environment. In this case, the drone should traverse quickly around a large number of obstacles safely without collision. Thus, to account for high dense environment, the parameters are set as follows:

Environment: 20 and 50 static obstacles are distributed throughout 150 m by 150 m and 1500 m by 1500 m environment, respectively. Also, four dynamic obstacles are moving at random speeds in the opposite directions of drones' flying paths. Additionally, IoD formation includes five drones fly from start points to destination points as illustrated in Table 4.1. The max elevation for the drones is 10 meters. If the height of the obstacle is more than 10 meters, the drones will maneuver in the x-y coordinates.

It is worthy mentioning that the static obstacles are uniformly distributed throughout the area. Besides, the speeds and directions of movable obstacles are assumed to be known within drone's detection range and the aim of the proposed approach is to avoid colliding with these obstacles. In this work, we focus on collision avoidance. Thus, we assumed that there is no communication among drones, and other drones are considered as flying obstacles. Also, the drones are increased to 20 drones in 1500 m by 1500 m environment scenario. The minimum safety distance between drones is set at 5m, and the maximum speed of drones within the formation is 10m/s. Also, the movable obstacle velocity is between 1m/s to 10m/s.

4.6.2 Results and Discussions

In this subsection, different scenarios involving static obstacles, dynamic obstacles, and IoD formation collision avoidance with energy consumption consideration will be analyzed and the results of the simulation will be discussed.

- Energy optimization for IoD formation path planning

IoD formation includes several drones in which each one of them faces different environmental constraints. Thus, evaluating the whole formation is more effective than single drone path planning. The energy consumption is an important factor to evaluate the algorithm performance. It reflects the ability of the algorithm to generate a collision-free path with minimum energy consumption.

The drones fly from starting positions to the destinations and generate their trajectories with minimum energy consumption while avoiding colliding with obstacles and with other drones in the formation. The energy consumption is calculated for each generated path and the collision-free path with minimum energy is selected. Also, the total energy consumption is obtained for each drone as discussed above in section 4.5. We normalized the energy consumption by dividing the total energy consumption over the optimal energy when a drone follows the shortest path from starting location to the destination at its maximum speed. In the following scenarios, the static obstacles are randomly distributed throughout the environment in addition to four dynamic obstacles flying toward the staring locations of drones with random speed within a speed range. Three environment scenarios are simulated namely, static obstacles scenario, movable obstacles scenario, and both static and dynamic obstacles scenario, and the normalized average energy consumption of 30 replications during the mission for all drones are shown in Fig. 4.2 and 95% confidence intervals are illustrated in Table 4.2. Moreover, an online calculation of the remained energy for each drone is performed and the normalized remind energy results are illustrated in Fig. 4.3.

Table 4.2: Average normalized energy consumption confidence intervals of 30 runs for three environment scenarios: Static obstacle scenario, Dynamic obstacle scenario, and Static and Dynamic scenario.

Static Obstacles only	**Dynamic Obstacles only**	**Static and Dynamic Obstacles**
[1.13, 1.45]	[1.40, 1.45]	[1.36, 1.55]
[1.43, 1.65]	[1.53, 1.63]	[1.81, 2.16]
[1.32, 1.60]	[1.50, 1.59]	[1.56, 2.11]
[1.43, 1.58]	[1.48, 1.55]	[1.56, 1.72]
[1.35, 1.39]	[1.34, 1.37]	[1.37, 1.48]

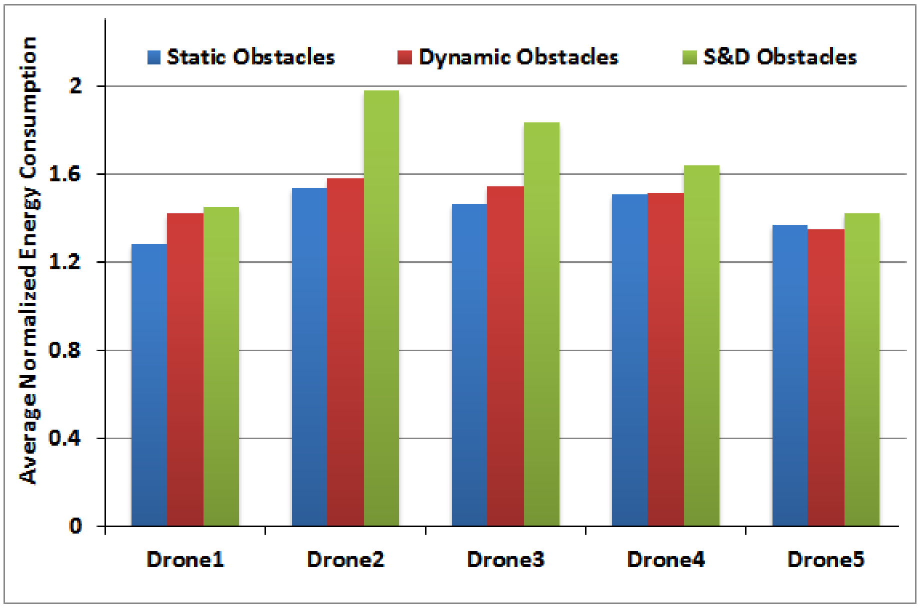

Figure 4.2: The average normalized energy consumption of 30 runs for IoD formation path planning for different obstacles: 20 static obstacles only, 4 dynamic obstacles only, and the dense environment with aforementioned static and dynamic obstacles.

Figures 4.2 and 4.3 illustrate different energy consumption for different drones. This is due to different environmental constraints. To clarify, drones 1 and 5 consume the least energy value due to a fewer number of obstacles between the start and destination points of their paths. Thus, the drones can bypass obstacles easily without needing to hover or fly vertically. On the other hand, the environment between the start and endpoints of drones 2, 3, and 4 is filled with obstacles and drones should use SEA to avoid flying through obstacles which in turn requires higher energy consumption. This is because they face dense obstacles and they need to hover, backtrack, or fly vertically to avoid crashing with them. It is noteworthy that the required energy in the static environment, i.e., static obstacles only, is less than that in the dynamic environment as shown in Fig. 4.2. This is because, in the static environment, the drone does not need to hover in place and rarely flies in z-direction while the drone requires higher energy in the dynamic environment due to movable obstacles that appear suddenly in the front of drone which needs to make an appropriate decision, i.e., hovering, backtracking, or flying vertically, to avoid crashing with them. For this reason, the remaining energy shown in Fig. 4.3 decreases at a higher rate in the third scenario where both static and dynamic obstacles exist in the environment.

The impact of environmental constraints on energy consumption increases as the number of obstacles included in the environment increases. Furthermore, the IoD formation constraints also affect the energy consumption for path generation. The drones are not allowed to fly to the same location at the same time to avoid IoD formation collision.

To assess the scalability of the proposed approach, we consider three scenarios with 10, 15, and 20 drones, respectively in the same environment. The average normalized energy consumption for the three scenarios per one drone is illustrated in Fig. 4.4 and Fig. 4.5. We can see that the IoD formation constraints have a significant effect on energy consumption for path generation. The drones are not allowed to fly to the same location at the same time to avoid the collision. As the number of drones increases, the distance between them decreases, which increases the possibility of collision. Since the drone needs to keep a safe distance to avoid the collision, they enable SEA to hover in place till the nearby drones get farther or fly in z-direction to avoid the collision, which leads to more energy consumption. Beyond 20 drones there will be collisions, long mission time and

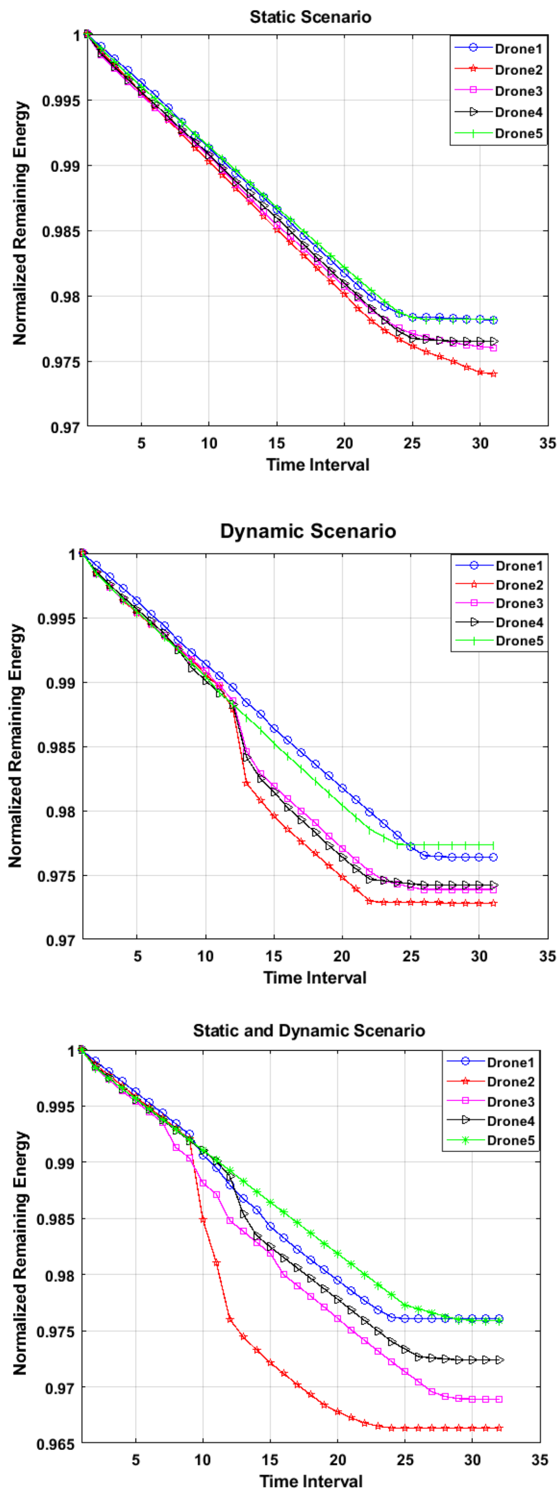

Figure 4.3: The average normalized remained energy consumption with respect to time intervals of 30 runs for IoD formation path planning for different obstacles scenarios: 20 static obstacles scenario, 4 dynamic obstacles scenario, and the dense environment with aforementioned static and dynamic obstacles.

frequent enabling of SEA which in turn degrade the system performance.

- IoD collision avoidance with static obstacles scenario

In this scenario, the terrain involves several random static obstacles. Additionally, within a detection range, the drone detects static obstacles and runs the collision avoidance algorithm to generate a feasible collision-free path, which achieves the objective and satisfies all constraints. With this in mind, the generated segment is added to a drone path meaning that the algorithm is able to generate the full path for IoD formation as illustrated in two and three-dimensional views in Fig. 4.6 and Fig. 4.7, respectively. It can be clearly seen that no collision is detected with static obstacles, and the drones are able to weave around obstacles. Also, no collision is detected among IoD nodes since the safety distance is maintained among IoD members meaning that the drones are able to perform collision avoidance with nearby obstacles and with other drones in the formation efficiently.

- IoD collision avoidance with dynamic obstacles scenario

The terrain in this scenario involves only dynamic obstacles moving throughout the environment. To evaluate the capability of the proposed algorithm to avoid colliding with moving obstacles, we show the planning progression through the obstacles field. It can be clearly observed from Fig. 4.8 that the UAVs are able to avoid collision with moving obstacles while flying toward their destinations. To elaborate, in the first frame of Fig. 4.8, drone 4 tries to avoid collision while flying toward the destination but unavoidable collision will happen because the obstacle

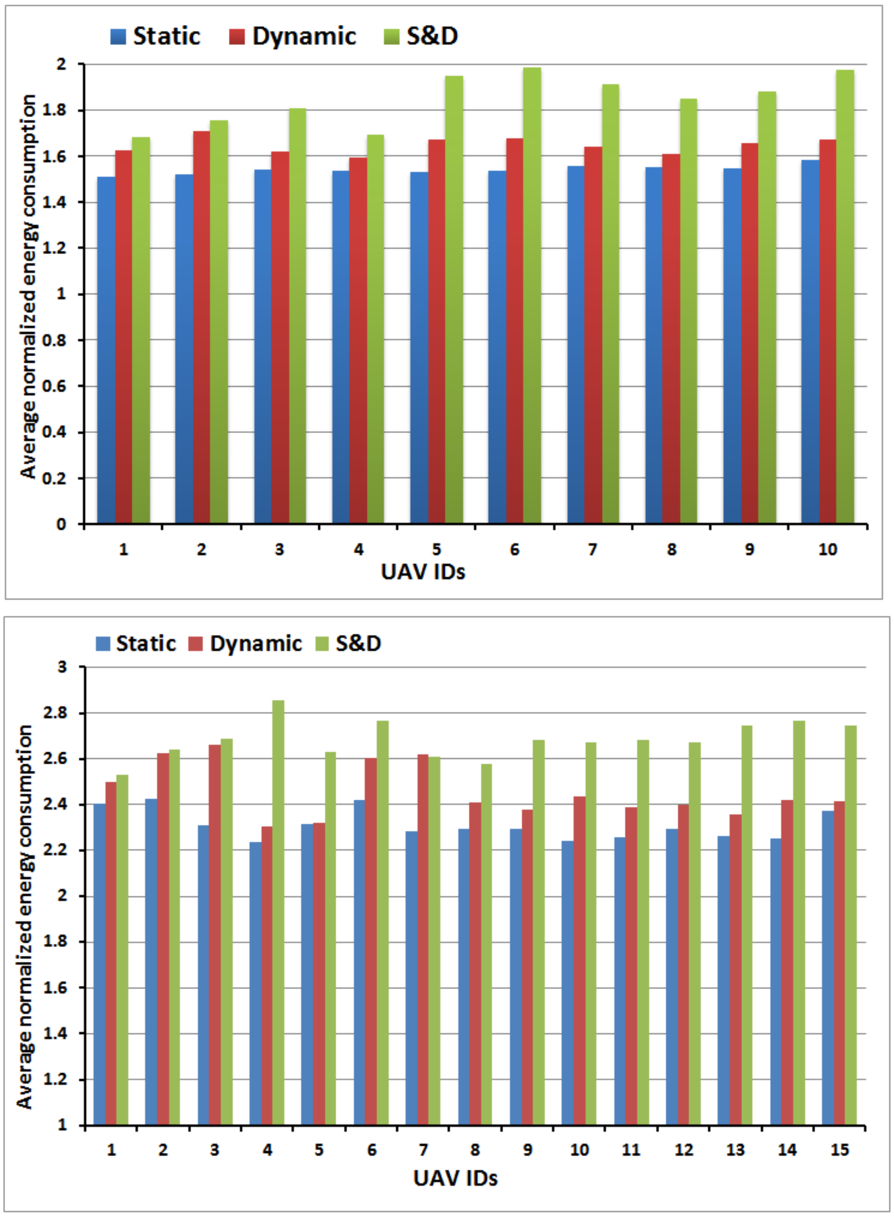

Figure 4.4: The average normalized energy consumption of 30 runs for IoD formation path planning for IoD sizes of 10 and 15 drones.

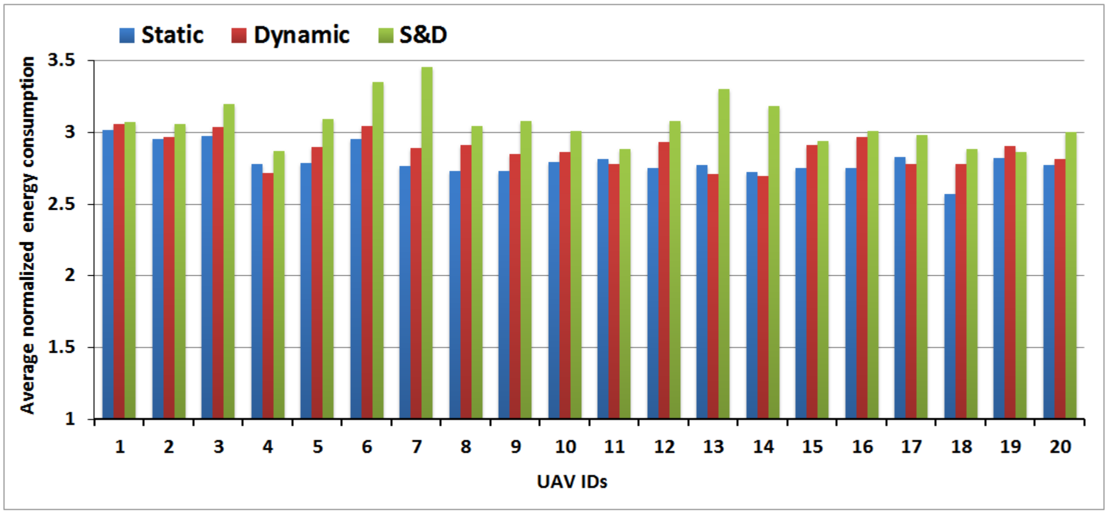

Figure 4.5: The average normalized energy consumption of 30 runs for 20 drones IoD formation path planning for different obstacles: scenario with 20 static obstacles, 4 dynamic obstacles only, and the dense environment with aforementioned static and dynamic obstacles.

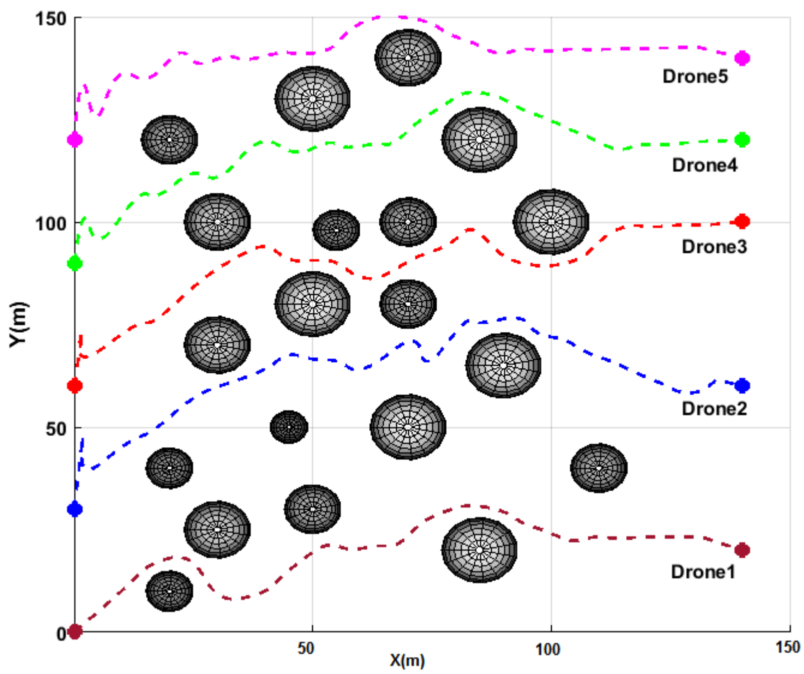

Figure 4.6: Two-dimensional view for IoD formation path planning with 20 static obstacles environment. The drones fly from the start positions to the destination positions while avoiding collisions with these static obstacles and with other drones.

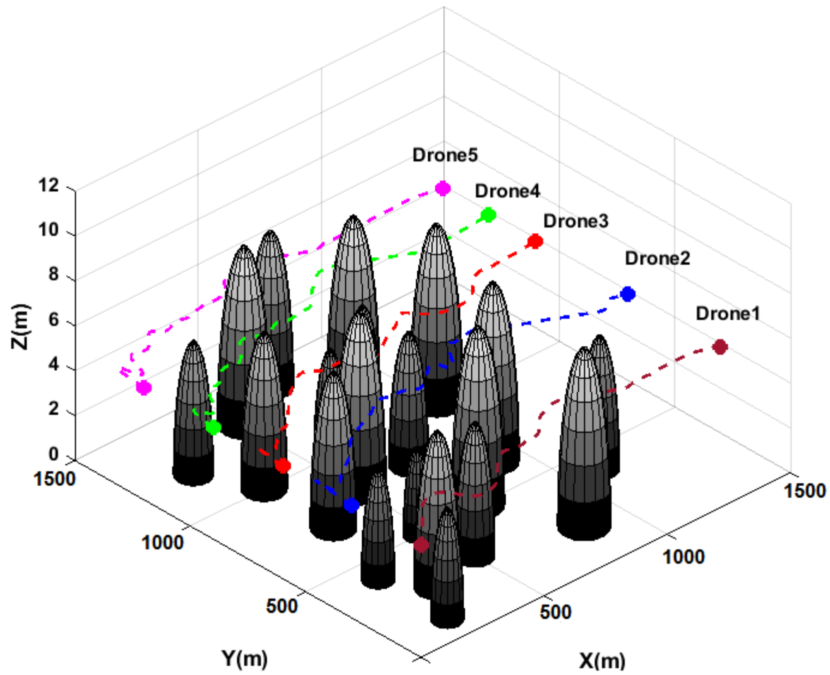

Figure 4.7: Three-dimensional view for IoD formation path planning with 20 static obstacles environment. The drones fly from start positions to the destination positions while avoiding collision with these static obstacles and with other drones.

moves toward drone 4 and backtracking may lead to a collision. Consequently, drone 4 flies vertically and over obstacle as illustrated in the fourth frame of Fig. 4.8 and Fig. 4.9, 3D view. Another example of avoiding collision is shown for drone 3 in the fifth and seventh frames of Fig. 4.8. In the fifth frame, the drone 3 can not find the collision-free path, and hovering in place is not possible due to potential collision. Then, it checks for possible backtracking, which is now possible, allowing the drone to retreat and discover an alternative collision-free path. Finally, all drones arrive at their destinations safely.

Also, we record the minimum distances between IoD formation and centers of obstacles for each segment of the path from starting point to ending point. The result is illustrated in Fig. 4.10. The results reveal that minimum separation

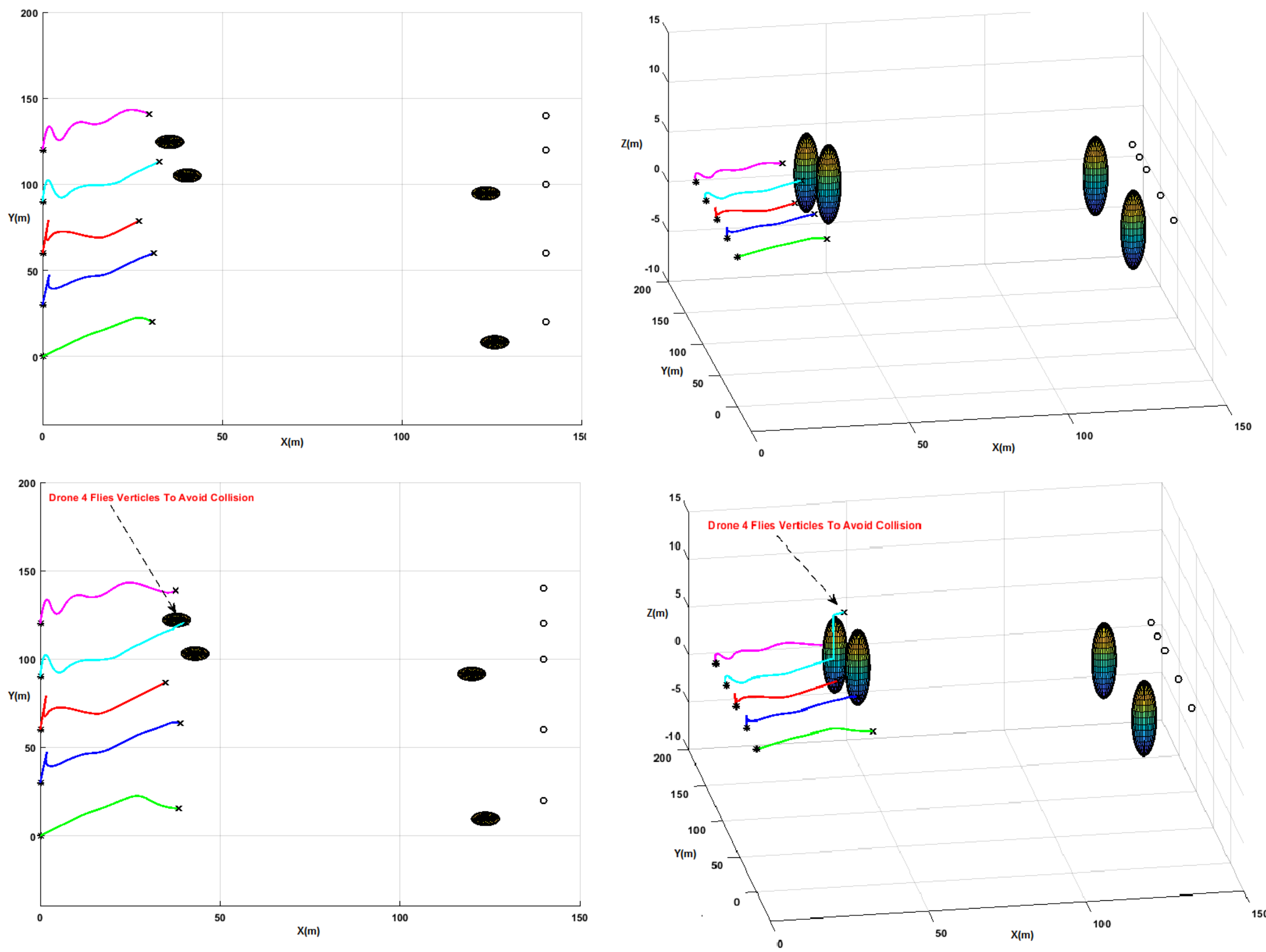

Figure 4.8: Two and three-dimensional views of IoD progression of five drones flying from start positions to destination positions in the dynamic environment including four dynamic obstacles moving in the opposite direction of drones' paths

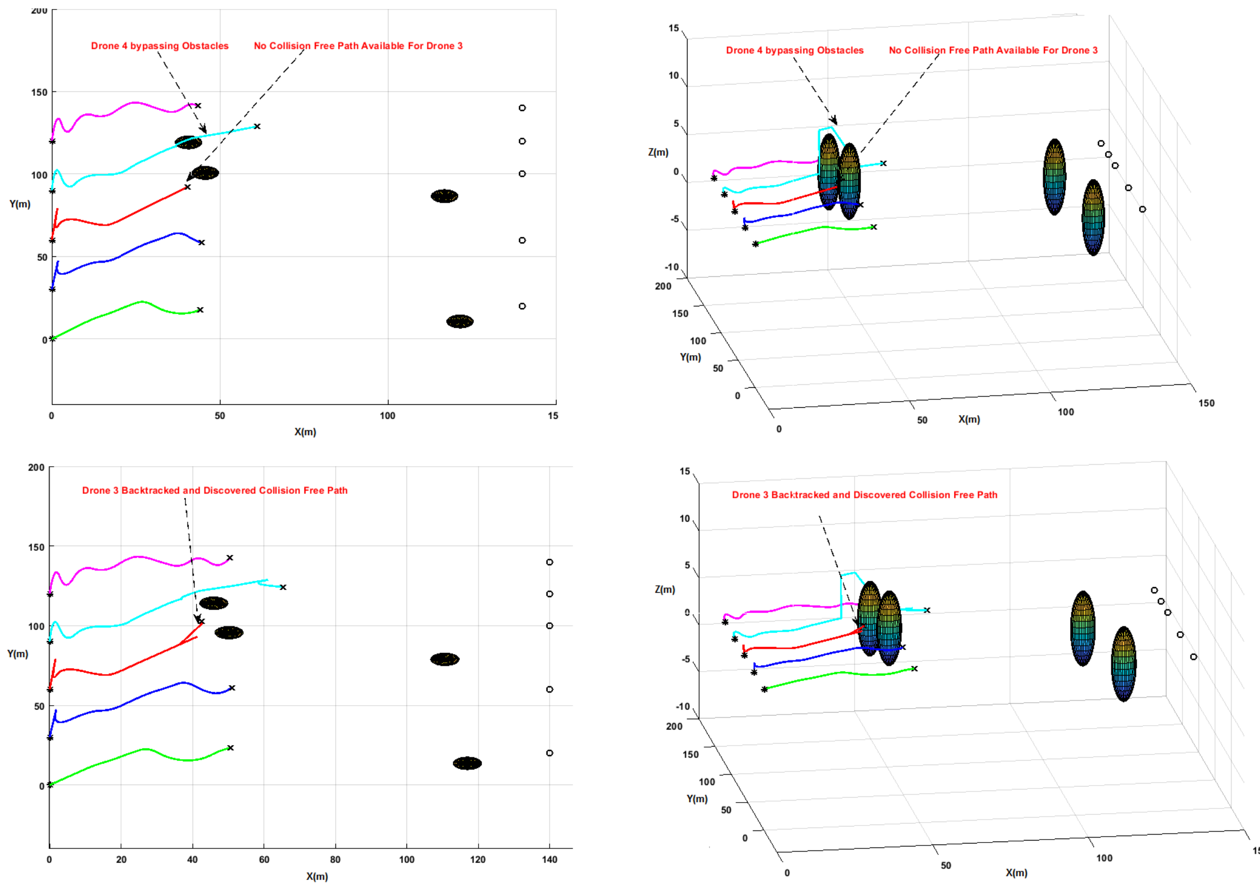

Figure 4.9: Two and three-dimensional views of IoD progression of five drones flying from start positions to destination positions in the dynamic environment including four dynamic obstacles moving in the opposite direction of drones' paths

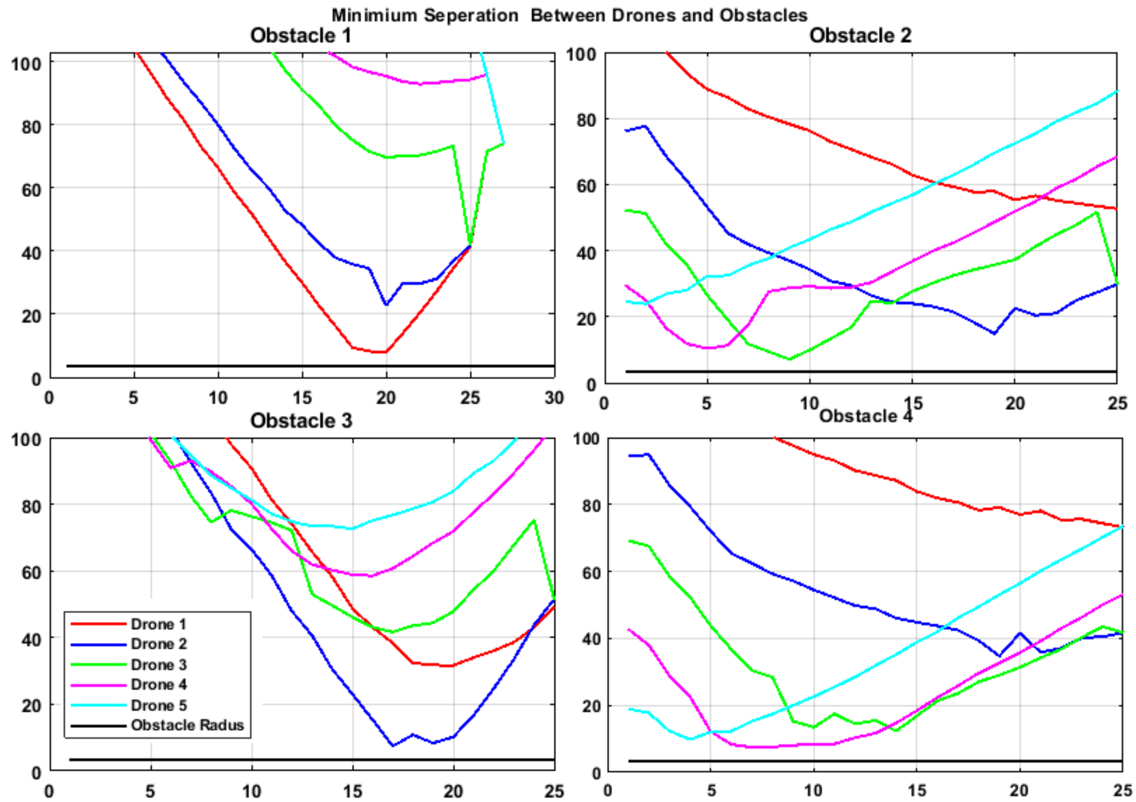

Figure 4.10: Dynamic environment scenario: Minimum separation distance in meter among five drones flying from start positions to destination positions and four dynamic obstacles moving in the opposite direction of drones' paths.

distances between any drone and centers of dynamic obstacles are greater than the radius of obstacles which clearly indicates that no collision is detected with dynamic obstacles. This demonstrates the importance of using SEA, i.e., hovering, backtracking, and vertically flying, in our technique to prevent any potential collision with obstacles.

- IoD collision avoidance with dense obstacles scenario

This scenario represents a dense environment, which involves several static and dynamic obstacles in addition to multiple drones flying throughout the environment. In this scenario, 20 static obstacles are distributed randomly throughout

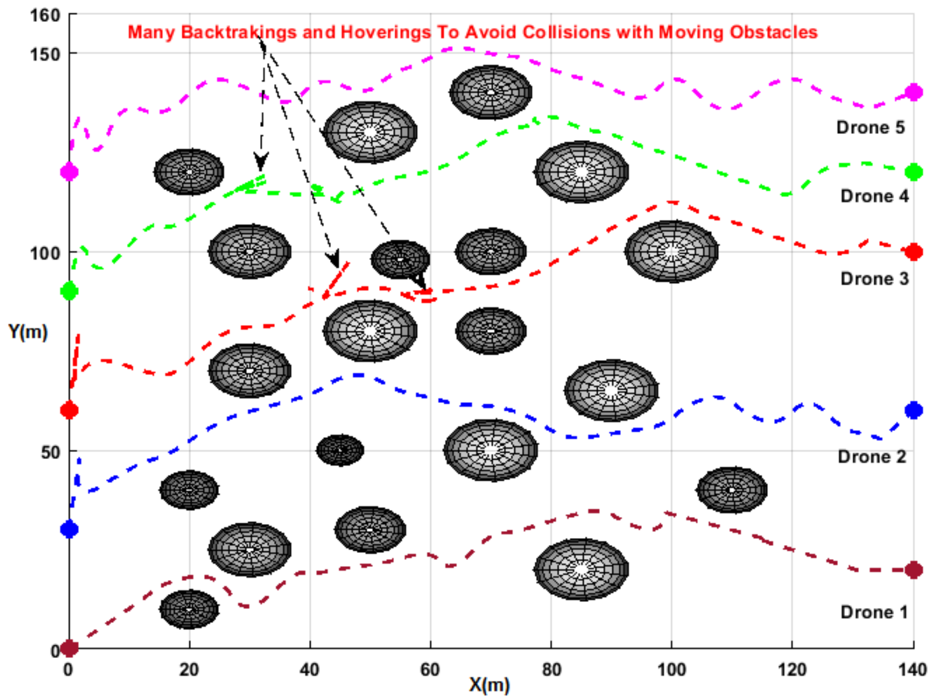

Figure 4.11: Two-dimensional view for IoD formation path planning with 20 static obstacles and four dynamic obstacles. The drones fly from the start positions to the destination positions while avoiding static and dynamic obstacles.

the environment. Also, four moving obstacles are moving in opposite directions of drones and with random velocities. The two and three-dimensional views depicted in Fig. 4.11 and Fig. 4.12 show the collision-free paths for all drones in IoD formation, i.e., no collision is detected with static obstacles and other drones. The drones maintain sufficient distance among members in the formation. Again the minimum separation distances between any drone and centers of dynamic obstacles highlighted in Fig. 4.13 confirm the ability of the proposed method in preventing crashes with moving obstacles. It can be observed from the results highlighted in Fig. 4.13 that the IoD formation maintains sufficient distances between any formation member and dynamic obstacles.

Turn now to progression planning to evaluate the capability of the proposed

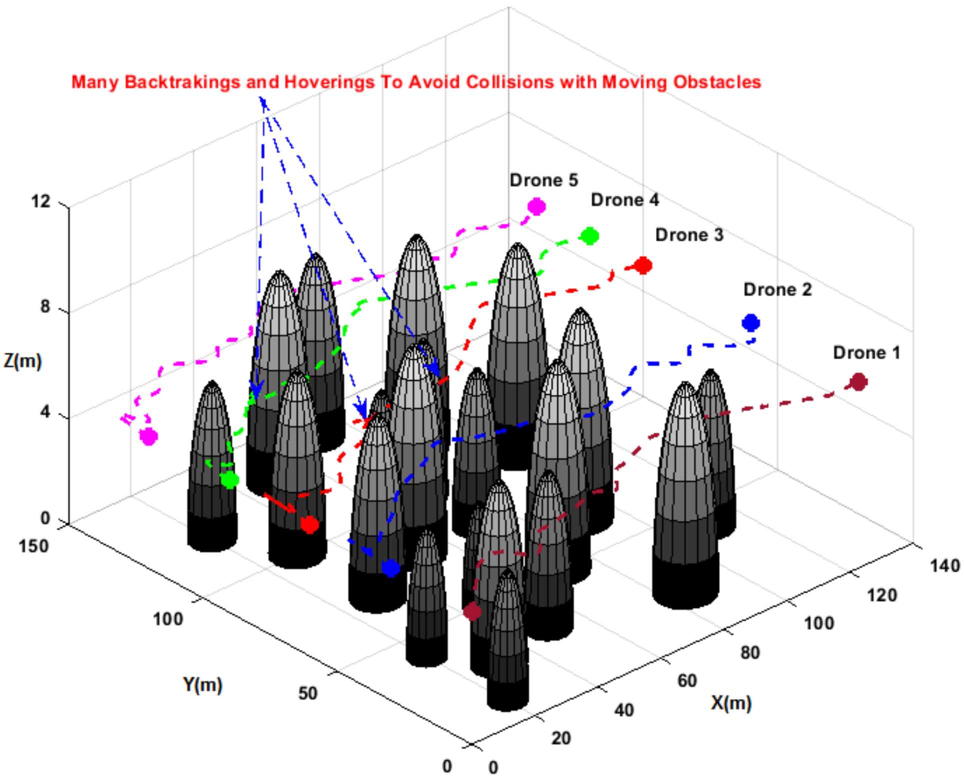

Figure 4.12: Three-dimensional view for IoD formation path planning with 20 static obstacles and 4 dynamic obstacles environment. The drones fly from the start positions to the destination positions while avoiding static and dynamic obstacles.

algorithm to avoid collision with moving obstacles. It can be clearly observed from Fig. 4.14 that the UAVs in IoD formation are able to avoid collision with moving obstacles while flying toward their destinations. To illustrate, in the second pair frame of Fig. 4.14, drone 4 tries to avoid collision while flying toward the destination but an unavoidable collision will happen. Drone 4 checks for hovering, but it can not hover in its place because a potential collision might happen in that position. Instead, it backtracks and hovers till the danger has gone as explained in the third and fourth pairs frames of Fig. 4.14. It has to be stressed that drone 4 performs online calculation of energy consumption and enables an appropriate

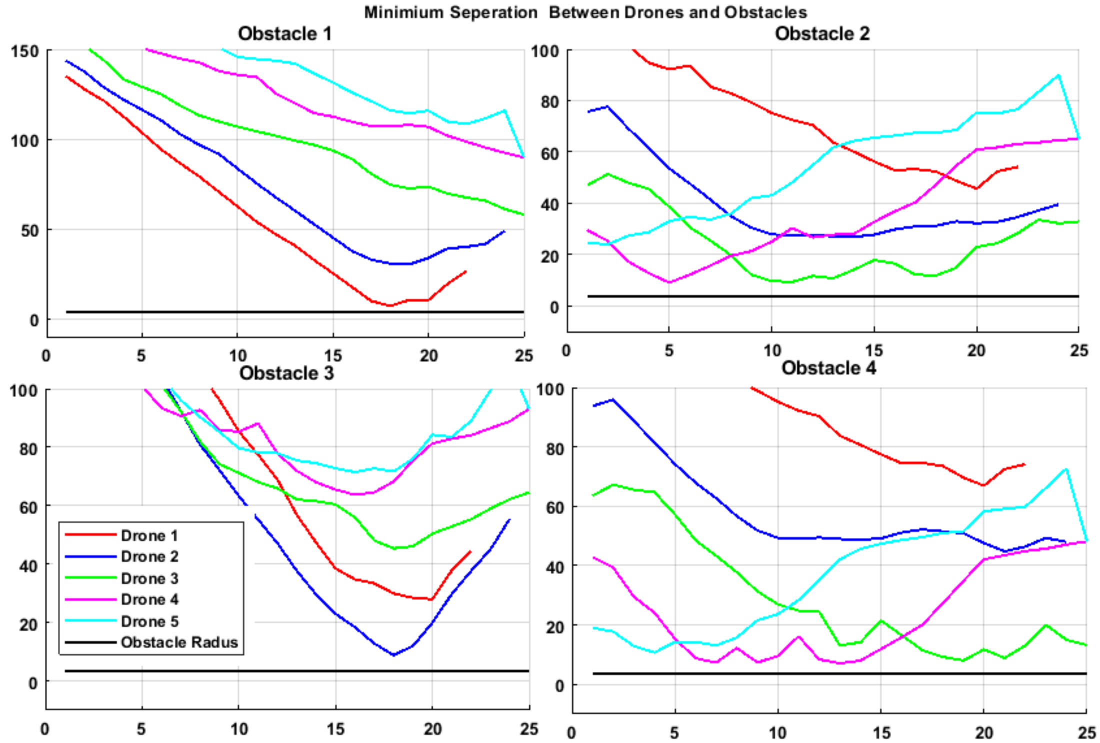

Figure 4.13: Dense environment scenario: Minimum separation distance in meter between any drone flying from the start position to the destination position and centers of four dynamic obstacles moving in the opposite direction of drones' paths.

ensure safety approach.

Another example of avoiding collision is shown for drone 3 in the fourth pairs frames of Fig. 4.14 and the first pairs frame of Fig. 4.15.

As can be observed from figures, the drone3 can not find the collision-free path and hovering in place is not possible due to potential collision. Then it checks for possible backtracking which is now possible, allowing the drone to retreat and discover an alternative minimum energy collision-free path. Note that drone 3 and drone 4 run several hovering and backtracking to avoid collision with obstacles. This reflects the ability of the proposed approach to work in a high density environment.

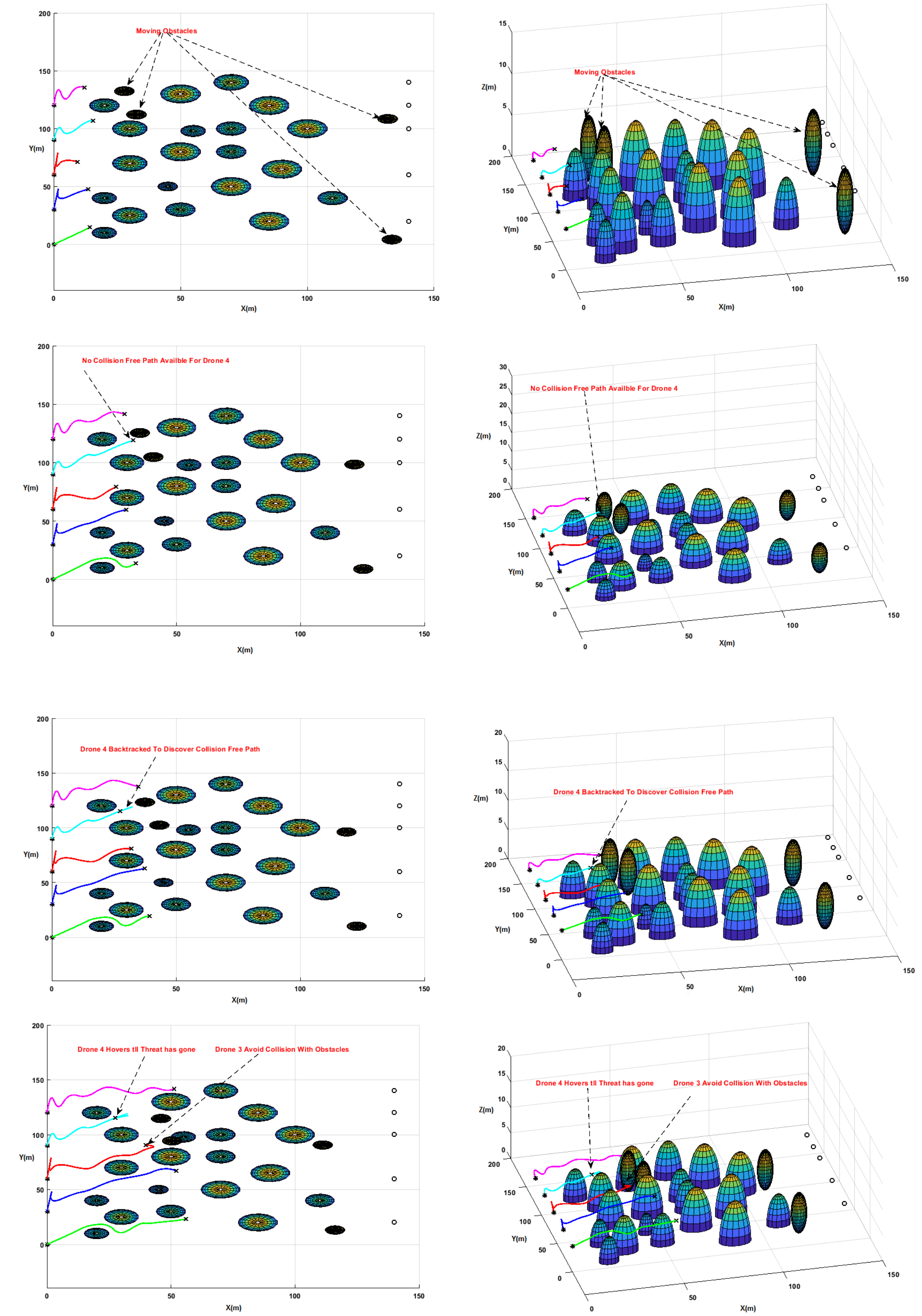

Figure 4.14: Two and three-dimensional views of IoD progression of five drones flying from start positions to destination positions in the dynamic environment including 20 static obstacles and four dynamic obstacles moving in the opposite direction of drones' paths

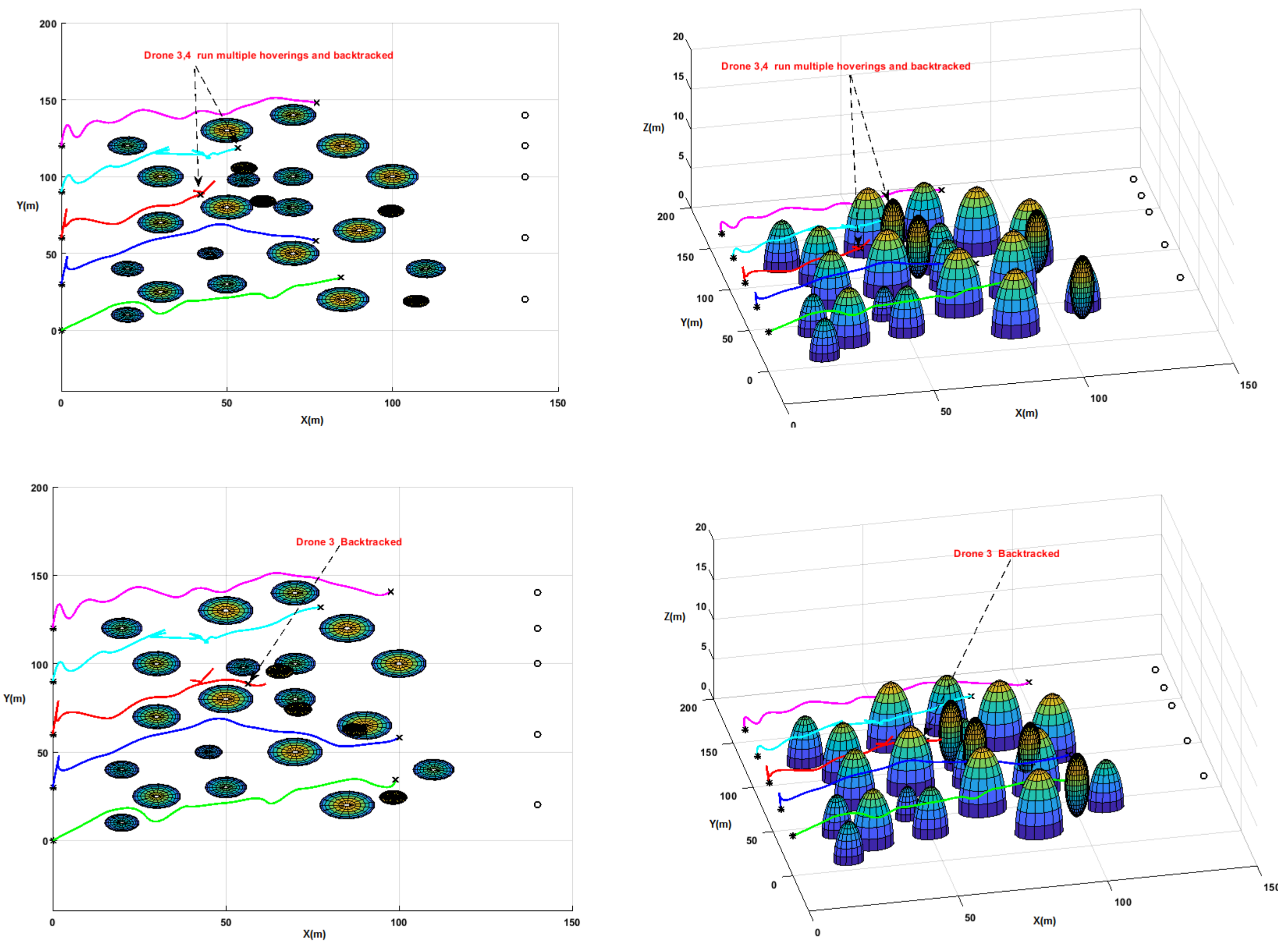

Figure 4.15: Two and three-dimensional views of IoD progression of five drones flying from start positions to destination positions in the dynamic environment including 20 static obstacles and four dynamic obstacles moving in the opposite direction of drones' paths.

To illustrate the ability of the proposed approach in dealing with a large scenario, we consider a large environment scenario (1500 m by 1500 m), where the IoD formation size is increased to 20 drones, static obstacles are increased to 50 static obstacles distributed throughout the environment, and 4 dynamic obstacles moving toward the start positions of drones. To show the ability of the proposed approach to generate a safety path for a large size of IoD formation, we record the minimum distances between IoD formation and centers of dynamic obstacles for each segment of the path from starting point to ending point. The minimum sufficient separation distances between any drone and centers of four dynamic obstacles are shown in frame 1 to frame 4 of Fig. 4.16. It is clearly seen that no collision is detected since the minimum sufficient separation distances between drones and centers of dynamic obstacles are larger than the obstacles' sizes. It is worth emphasizing once again that the safety is given the highest priority. More importantly, the energy objective function helps to select the collision-free path in the destination direction with minimum energy consumption. Thus, even for the large scenario, the proposed approach guarantees minimum energy consumption paths for all drones to reach their destinations safely.

Besides the above illustrations, we also compare the proposed approach with the work presented in [30]. The comparisons include three important parameter metrics for dynamic environment, namely, the Number of Collisions (NOCs), the time required to generate the segment within the drone's field of view, i.e., Duration Time (DT), and IoD formation. Furthermore, the comparison is conducted for 100 iterations and the maximum speed is set to 10 mps. It is worth

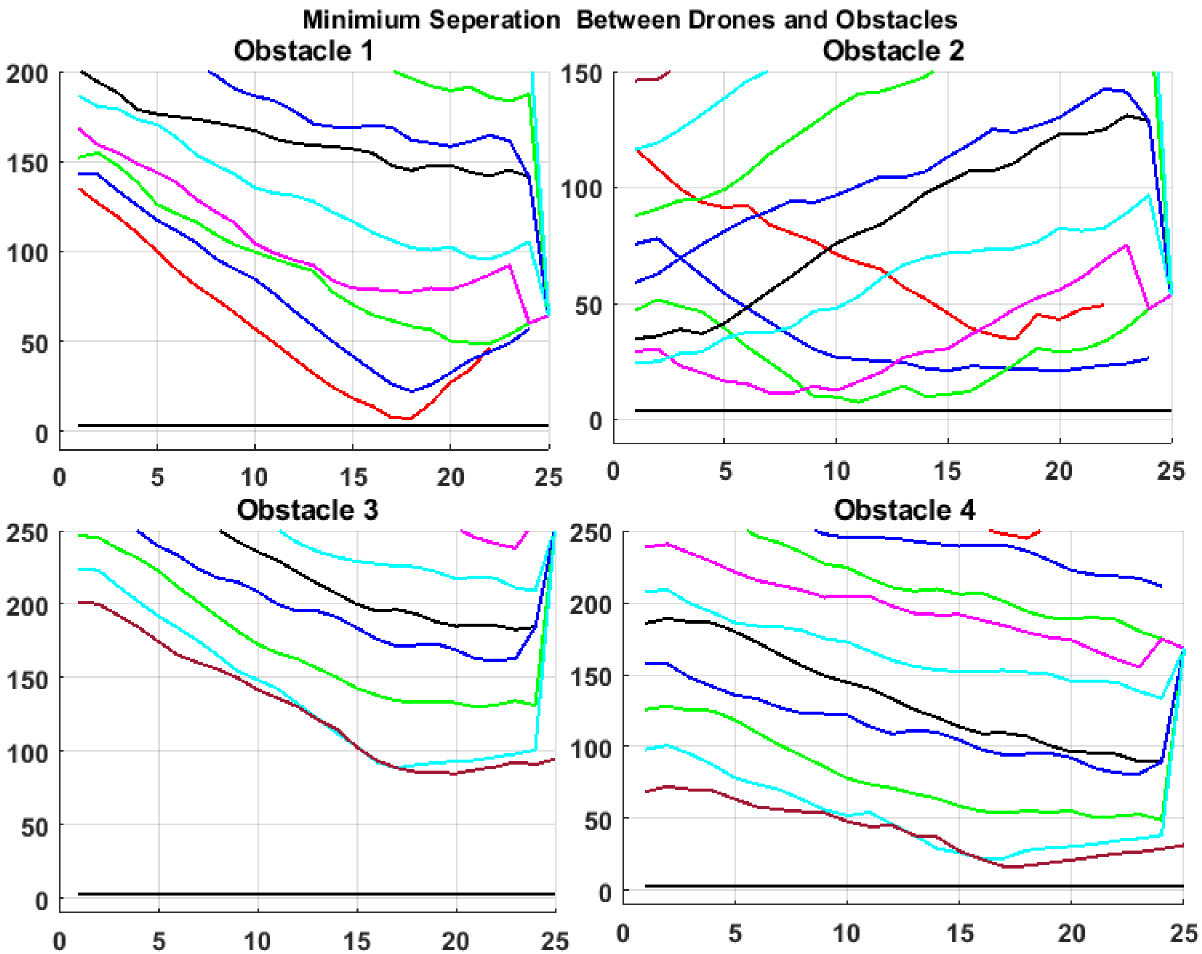

Figure 4.16: Large size environment scenario 1500 m by 1500 m: Minimum separation distance in meter between each drone flying from the start position to the destination position and centers of movable obstacles. The environment include 20 drones flying from the start position to their destination positions, 50 static obstacles, and four dynamic obstacles moving in the opposite direction of drones' paths.

Table 4.3: Comparison the results in static and dynamic environment scenarios including number of collisions, duration time to generate the partial path within drone's detection range, and IoD involved

Approach	Static Environment			Dense Environment		
	NoC	DT	IoD	NoC	DT	IoD
Proposed	00	288.16 ms	YES	00	447.4ms	YES
[30]	00	261.9 ms	NO	10	362.68ms	NO

emphasizing once again that, in the proposed algorithm, the mission's safety of IoD formation is given the highest priority of other objectives. For this reason, it does not produce the shortest path or shortest mission time. Instead, it produces collision-free paths with minimum energy. In this scenario, we consider a dense environment with static and dynamic obstacles involved.

Table 4.3 highlights the NoCs, duration time required to generate the segment within the drone's field of view (DT), and IoD formation. The second and fifth columns of Table 4.3 show the number of collisions in the static and dynamic environments, respectively. The results show that in static environment both algorithms are able to generate a safety path with zero collision while in the dense environment with static and dynamic obstacles involved, the number of collisions is zero, and ten for the proposed approach and the approach presented in [30], respectively. More importantly, the proposed algorithm outperforms the work presented in [30] in IoD formation scenario since it is able to perform drone to drone collision avoidance that provides the safety of IoD formation, while the work in [30] did not solve drone to drone collision avoidance. Finally, it is worth emphasizing that the proposed approach incurs overhead like increasing path length or elapsed time for a drone to accomplish its mission.

4.6.3 Effect of Obstacle Speed on Performance

To study the ability of the proposed algorithm to avoid collision with moving obstacles, the moving obstacles are simulated with different speed ranges. In this scenario, the obstacles are starting from drones destinations and moving toward the drones with the following speed ranges: [1-10] m/s, [11-20] m/s, [21-29] m/s, and $> = 30$ m/s. The result of this scenario is demonstrated in Fig. 4.17. It can be clearly observed that the algorithm can efficiently avoid collision with the moving obstacles when their speeds are in the range [1 10] m/s. This is due to sufficient distance between drone and obstacle, which offers higher freedom for a drone to move. For higher speed in the other ranges, the success rate decreases to 92.1% and 82.0% for speed range [11-20], and [21-29]m/s, respectively. Finally, if the obstacle speed is beyond 30 m/s, the collision avoidance is not guaranteed since the success rate drops down to 63.1%.

4.7 Chapter Summary

This chapter outlined an energy-efficient online collision-free trajectories generation for IoD formation with minimum energy consumption. It is worth mentioning that the successful path planning for IoD requires IoD nodes with the capability to adapt and configure themselves automatically to the surrounding environment without intervention of human. Due to the increasing number of nodes in IoD, the centralized systems are not practical. More importantly, inherent limitations still hinder the full potential of UAVs applications due to limited energy. The

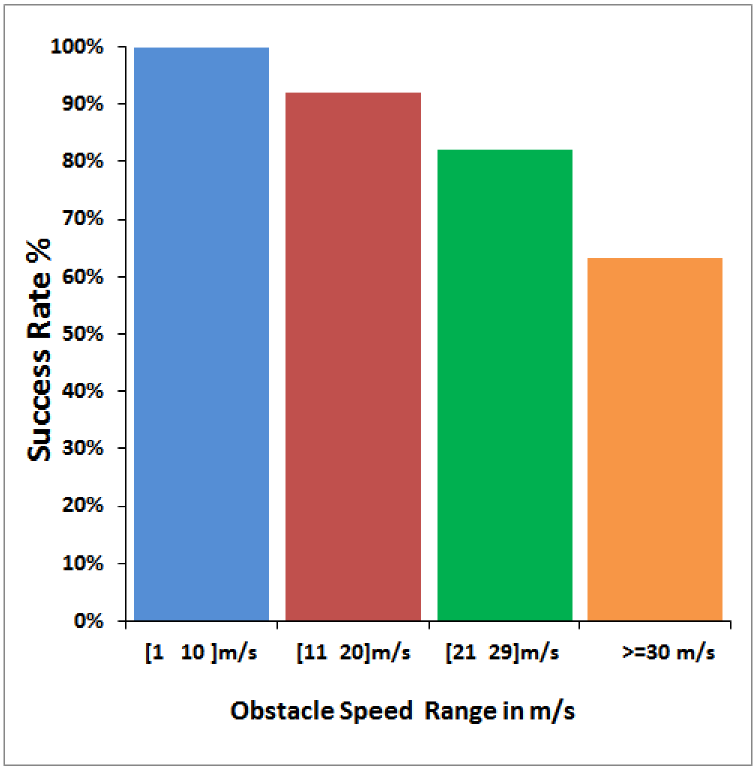

Figure 4.17: Success Rate with respect to obstacle speed: different ranges of obstacle's speed (1-10 m/s, 11-20 m/s, 21-29 m/s, and >=30 m/s) are implemented.

main limitation is the limited lifetime of on-board battery which limits its flight time. For drones to accomplish their task, an energy-efficient strategy is required. To accomplish path planning and optimize the energy consumption, a gradient optimization was used for fast and quick convergence. The proposed SEA allowed the drone to hover for some time, backtrack, or fly vertically to avoid any potential collision with energy-saving consideration. We also showed simulation based on Matlab implementation. The proposed mechanism provided fast and accurate IoD formation collision-free paths with minimum energy consumption. The energy consumption was evaluated for different environmental constraints. we compared our work with recent work where the results showed that our approach outperformed exist approach and confirmed the ability of the proposed approach to successfully generate a collision-free partial path within a drone's detection range, and full path with minimum energy consumed, which makes it appropriate for a high dense environment and even in applications with a high-risk collision with the obstacle of relative speed up to 10 m/s. Furthermore, it can generate safe and efficient energy consumed formation paths and scaled up to larger size problems.

CHAPTER 5

OPTIMAL DEPLOYMENT OF IOD FOR VANETS ASSISTANCE

5.1 Chapter Motivation

The IoD paradigm offers a significant feature which is its ability to have LOS connections toward the users due to drones' elevations. That is, when traditional ground networks are damaged, UAVs can support efficient and effective temporary communication networks. Unlike ground nodes that have to follow a specific route, the nodes in IoD can move freely in three-dimensional space and fly above high buildings which may obstruct the ground vehicle's communication. Thus, the LOS communication can be established effectively by adjusting the drones' altitudes and mitigating shadowing and signal blockage. Towards this end, dedicated UAVs are employed as aerial Access Points (APs), relays, RSUs, or BSs to provide wireless ground network communications, which is called UAV-assisted wireless communication. The UAV-assisted has become an alternative connection for ground vehicles and attracts the attention of extensive researchers.

Based on the above tremendous advantages of drone, V2V communication can be supported by IoD network when a direct multi-hop link between vehicles is not available. In this case, IoD can be utilized as a relay network to maintain the reliable wireless communication links between vehicles on the ground.

The interconnected nodes in the IoD network make it fault tolerance and robustness. It can be easily integrated with other networks and fast deployed in difficult conditions to provide the communication in which ground infrastructures get damaged or the manually deploying them are almost impossible. Coverage problems with ground vehicles have been examined extensively in the literature. Moreover, the harsh terrains can significantly limit the maneuverability of ground mobile vehicles. Generally speaking, two main factors affect the connectivity of IoD and ground network, namely LOS and the path loss. It has to stress that deploying IoD at high altitude enhances LOS condition but increases the distance between sender and receiver which in turn increases the path loss. To maintain the range of the received signal and achieve LOS condition, IoD positions should be optimized using an appropriate mechanism.

In conclusion, some previous works achieved improvements in ground network performance such as coverage, throughput, routing, and end to end delay. Other works focused on maximizing coverage area based on download facing camera.

Others achieved improvements in VANETs performance, but focus on routing protocols, or considered the static ground infrastructure. Generally, the full exploitation of superiority of drones to minimize isolated cars is omitted or neglected in the previous works.

5.2 Chapter Contributions

In this thesis, we propose implementing an optimization algorithm to obtain the optimal deployment of IoD in a dynamic vehicular communications environment. The adopted deployment of IoD at any instant of time allows providing communication between vehicles on the ground. We consider the coverage as the number of vehicles covered by the IoD network. Such an optimum deployment is determined by considering the current locations of ground vehicles and can be evaluated by considering the quality of the received signal at the receivers, i.e., vehicles on the ground.

The main contribution of this chapter is utilizing IoD as a relay network at optimum coverage base-on cars' locations using Received Signal Strength Indicator. In this chapter, the IPSO algorithm in chapter 3 is implemented to achieve the aforementioned objectives so that sufficient signal strength towards all isolated vehicles on the ground can be achieved by the IoD network to guarantee the best coverage at each specific time. Moreover, the connectivity of the IoD network is addressed by the proposed optimization approach where the objective function includes the connectivity to be achieved for a better solution. Furthermore, we design an IoDAV to boost the VANET communication performances. Based on the vehicles' distribution on the ground, the proposed approach dispatches the IoD nodes to the most appropriate locations in real-time. The main assumption is that a lack of infrastructures exists in the environment and the connectivity among vehicles is minimum. For example, in an urban area, the buildings may obstruct the line of sight and the connectivity among vehicles is lost. Besides, the movement of UAVs in IoD aims to explore the 3D space to offer connectivity to the ground vehicles.

The contributions included in this chapter can be summarized as follow

- A novel collaborative IoD architecture is proposed and integrated with VANETs. For a specific location, the demand for UAVs is evaluated using an optimization evaluation function to obtain the optimal deployment of IoD to assist the VANET.

- The population optimization scheme is designed to improve the proposed model. The optimization scheme has enabled the IoD nodes dispatching to the best service locations and maintains the connectivity constraint of the IoD network so that the efficiency of IoDAV approach is enhanced.

- Extensive simulation experiments are conducted to test the model performance, and evaluate the proposed model. The simulation results are discussed and analyzed in detail.

This chapter is the result of a collaboration with Dr. Ashraf Mahmoud from Computer Engineering Department, Muhammed Imran

from College of Applied Computer Science, King Saud University, and Muhammed Shoaib from College of Computer and Information Sciences, King Saud University. The work has been published in IEEE Access, 9, 61211-61223, 2021.

5.3 IoD-Assisted VANET Mechanism

As discussed in **Section 2.3**, the reviewed work related to VANET intended to enhance the performance of the VANET network, however, the UAV's mobility superiority was neglected. By controlling a few numbers of UAVs in a wide area, several infrastructures can be dispensed. Therefore, the VANET can be assisted by leveraging dynamic UAVs. As shown in Fig. 5.1, an IoD-Assisted-VANET model, consisting of the VANET network and IoD network, is proposed. The VANET network consists of terrestrial vehicles on the ground and their mobilities are restricted by predefined roads and traffic regulations. Additionally, the quality of communication is impacted by the surrounding environment. The IoD network, which is integrated with VANET, consists of UAVs swarm with wireless communication. The UAVs swarm are responsible for supporting the connectivity among vehicles. Thanks to their flexible mobility, they can be easily dispatched to the most appropriate locations where the relay is required among vehicles. Fig. 5.1 illustrates the effectiveness of the proposed IoDAV architecture in which the vehicles can not communicate directly within their communication range. The buildings are considered as obstacles and hinder the transmitted signal. Thus, UAV1 and UAV2 are dispatched to suitable positions, where vehicles are isolated by building and can neither communicate nor transmit data to infrastructure. The two UAVs act as a relay to create a connection among those separated vehicles.

It is noteworthy that the positions of UAVs are updating periodically based on the movement of ground vehicles and the state of received signal therein. The UAVs are first dispatched to the appropriate locations and then hover therein to provide communication among isolated vehicles. As the vehicles move, the distance between them increases and they might be isolated by obstacles lying between them, which in turn lose the connection. Then, the IoD's location is updated to connect the isolated vehicles.

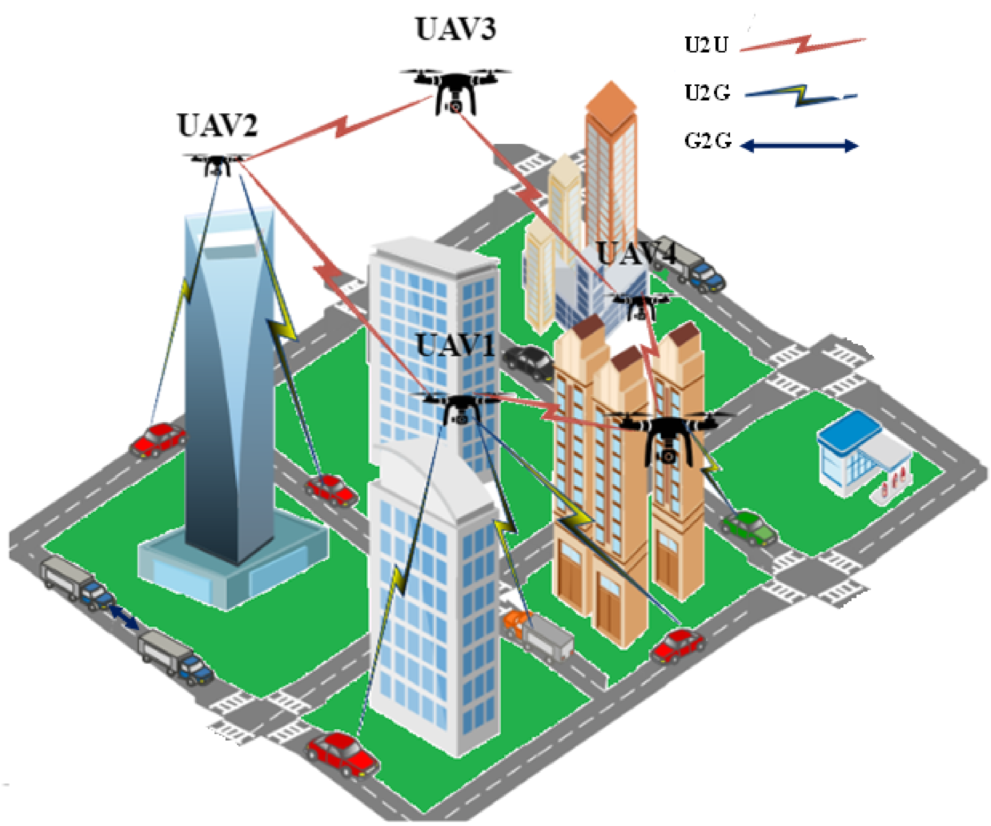

Figure 5.1: IoD-Assisted VANET Architecture

5.4 Optimal IoD Deployment

In this section, we will describe the formulation of IoD deployment. Particularly, we will explain how the optimization algorithm addresses the drone's positions as well as the optimization algorithm used.

5.4.1 Problem Formulation of IoD-Assisted VANET

The deployment of drones has been impacted by their coverage, which can be classified into static and dynamic coverage. In the former, the UAVs hover in the target region during the whole mission time. The complete design goal, such as maximizing the coverage area, has to be achieved in the deployment. In the letter, the UAVs keep changing their positions during the mission depending on the current locations of ground nodes. Besides, we focus on dynamic deployment with the aim of maximizing the coverage area in a 3D environment. To do so, we consider the scenario including many vehicles that follow specific paths on the existing region. Also, in the considered scenario, the area lacks sufficient infrastructures and the IoD will help to relay the information among vehicles. It is noteworthy that the locations of IoD nodes are changing throughout time depending on the locations of ground vehicles. At every time step, when the vehicles on the ground move, the new optimal locations of IoD have to be evaluated.

5.4.2 Optimization Problem

Our main objective is to obtain the best position of interconnected IoD network in a 3D space so that the transmitted signals from IoD nodes can be received by all isolated vehicles in the ground with sufficient power reception. Such dynamic deployment requires an efficient technique to dispatch the drones to the optimal locations. Furthermore, obtaining the best locations of IoD nodes by trying all possible locations in the space at each time step is an inefficient way. This is because it consumes a lot of resources and takes a lot of time which is considered as an NP-hard problem.

The sophisticated solution is to use a meta-heuristic algorithm where the optimal solution can be obtained without testing all possible values. Instead, the random position is generated and evaluated using the fitness function. Then the iterative manner is used to search for the best possible solution. Among those population-based, PSO, swarm intelligence algorithms, is one of the intelligent algorithms employed in the deployment problem. In this chapter, we consider the dynamic coverage using the improved version of intelligent optimization technique i.e., IPSO.

The RSSI metric in the received vehicles is utilized by the objective function to evaluate the generated positions and the best position of IoD nodes is selected. On the receiver side, the RSSI is selected and compared with the minimum threshold, defined in this chapter to be -86dBm (the threshold for successful packet delivery). Particularly, to achieve full coverage connectivity, the average RSSI should be greater than the minimum threshold. More importantly, the RSSI metric is utilized to calculate the number of covered vehicles in the ground by the IoD network. At each vehicle, we analyze the RSSI when the positions of IoD nodes are selected. Then the vehicle is counted to be covered if RSSI is greater than the minimum threshold. In the next section, the optimization algorithm utilized in our work is explained in detail.

5.5 Improved Particles Swarm Optimization for Coverage

To address the formulated problem, the IoDAV approach has to work in real-time. In this context, we propose an effective population scheme, IPSO, for IoDAV to design the feasible collaborative approach. The IoDAV dispatches multiple UAVs to different positions for optimal deployment. Obviously, this approach is designed to integrate the IoD network with the VANET network for assistant in infrastructure-less scenarios that need relay nodes for communication. IPSO is an enhanced version of traditional PSO. It avoids trapped in local optima and searches for the global optima in a more accurate and faster way. The enhancements are improving the initialization stage by using uniform initial distribution as in eq.5.1.

$$X_{n+1} = \mu X_n(1 - X_n), \tag{5.1}$$

where X_n represents the n^{th} chaotic variable, μ is a bifurcation coefficient. Then the velocity is updated using

$$\nu_{t+1} = \omega\nu_t + c_1r_1(pBest_t - x_t) + c_2r_2(gBest_t - x_t), \tag{5.2}$$

where c1, c2 are acceleration coefficients, r1, r2 are random variables, and ω is an inertia weight. The position of each particle is updated using

$$x(t+1) = x(t) + \epsilon\nu(t+1), \tag{5.3}$$

where ϵ selects how fast the particle moves. Furthermore, the parameters Inertia Weight (ω) and Epsilon(ϵ) are updated to balance global and local search using the following (5.4) and (5.5) equations, respectively.

$$\omega(t) = \omega_{min} + \frac{MaxIt - t}{MaxIt} * (\omega_{max} - \omega_{min}), \tag{5.4}$$

$$\epsilon = \epsilon_{max} - \frac{(\epsilon_{max} - \epsilon_{min})t}{MaxIt}, \tag{5.5}$$

where *MaxIt* is maximum simulation time and t is current simulation time, ω_{min}, ω_{max} are minimum and maximum value of inertia, respectively, ϵ_{max}, ϵ_{min} are constant value and $\epsilon_{max} > \epsilon_{min}$.

The inactive particles are replaced by new freshening particles to rich the diversification search of the algorithm.

The pseudo-code of IPSO for IoDAV is explained in the algorithm 4. The parameters of the algorithm such as acceleration coefficients c1 and c2 are initialized in the initialization part of the algorithm. The initialization part is also responsible to create the initial position and velocity of all particles. The algorithm receives parameters and environment constraints and returns the best locations of all UAVs that achieve the maximum coverage. For each iteration, the informant particles are assessed and the solution that achieves the best coverage is stored in LBest with the corresponding coverage and RSSI. The velocity and position of each solution are updated using eq.5.2 and eq.5.3, respectively. Then the fitness of generated solution is evaluated and compared with LBest solution. Moreover, the GBest is compared with LBest and the best overall solution is stored in GBest. Note that if two solutions achieve the same coverage, the solution with a higher average RSSI is selected as the best. Finally, the global solution that includes the best positions of IoD nodes with maximum coverage and RSSI is returned. It has to stress that the IoD is an interconnected network meaning that the GBest includes interconnected nodes of IoD.

Algorithm 4 IPSO algorithm for IoDAV

```
begin
    Input:
    Trail: Maximum Limit of trail, MaxIt: maximum iteration
    PSize: Population Size
    Bmin,Bmax : Environment Boundary
    Output: Best Positions and fitness of IoD nodes (GBest)
    INITIALIZATION:
    initialize c1, c2, PopSize
    begin
        for i = 1 : to PopSize do
            initialize position [Pos_i] with logistic map using Eq5.1, V_i = 0
            Fitness_i=Obj__Fun(Pos_i)
            if Fitness_i.Cov>GBest.Cov then
                GBest =Fitness_i
            end
            if (Fitness_i.Cov==GBest.Cov)∧(Fitness_i.RSSI>GBest.RSSI) then
                GBest =Fitness_i
            end
        end
        iter=0
        while Iter<Max_Iteration do
            Update ω by Eq5.4, ϵ by Eq5.5
            for i = 1 : to PopSize do
                Update the velocity V_i(t + 1) using Eq5.2, position Pos_i(t+1) using Eq5.3
                Fitness_i=Obj__Fun(Pos_i(t+1))
                if Fitness_i.Cov>LBest.Cov then
                    LBest= Fitness_i
                    if LBest.Cov>GBest.Cov then
                        GBest =LBest
                    end
                    if (LBest.Cov==GBest.Cov)∧(LBest.RSSI>GBest.RSSI) then
                        GBest=LBest
                    end
                    Clear trail of generated Particle
                else
                    Increment Particle trail (trail(i))
                end
            end
            for i = 1 : to PopSize do
                if trail(i)>limit then
                    Replace inactive particle by new fresh one,
                    Clear its trail
                end
            end
            Increment Iter
        end
        Repeat until ideal best is obtained or run out of time
    end
    RETURN (GBest)
end
```

5.6 Optimization Framework

The IoDAV aims to enhance the connectivity of infrastructure-less VANET network by optimally deploying the IoD network. To this end, the sophisticated approach based on a meta-heuristic algorithm is implemented to dispatch the IoD nodes to the optimal locations and maintain the connectivity of the IoD network. The proposed approach is implemented in the OMNET++ tool [144] and the framework is illustrated in Fig. 5.2. The new module is developed as an extension to the OMNET++ network simulator to implement the IPSO. The aim of this module is to optimally place IoD nodes so that the number of covered vehicles on the ground is maximized, i.e., dispatching the IoD nodes to the most appropriate locations, in addition to maintain the connectivity of the IoD network. Furthermore, the map is generated using the SUMO NetEdit tool and the traffic simulator SUMO [145] is utilized to mimic the movements of vehicles on the ground. Besides, the information of mobility from SUMO is polled at fixed intervals. Moreover, for more realistic vehicles communications, the Veins simulator [146] is used. Whenever the departure of a mobile node is simulated by SUMO, the dedicated simulation module is created by Veins in OMNeT++. Then, Veins updates the speed, position, and heading of the mobile node in the created module in OMNET++ as the mobile node moves in SUMO. Similarly, the OMNeT++ module is removed from the simulator when the mobile node arrives at its destination in SUMO. This way, the mobility of node in OMNeT++ is coupled to that in SUMO by Veins [147].

In light of the above illustration of the framework, the IoD deployment module receives the instantaneous locations of vehicles on the ground and dispatches IoD nodes to the most appropriate locations to maximize the number of covered vehicles and maintain the IoD network connectivity. The objective function of IPSO composes of two parts: the first part or objective includes the quality of the received signal at the receiver side, i.e., vehicles on the ground, which is obtained by path loss propagation model, and the coverage of ground vehicles, while the second part or objective maintains the connectivity of IoD nodes. The aim is to achieve those two objectives. The output of IPSO is the optimal positions of IoD nodes that maximize the number of covered vehicles by the interconnected IoD network.

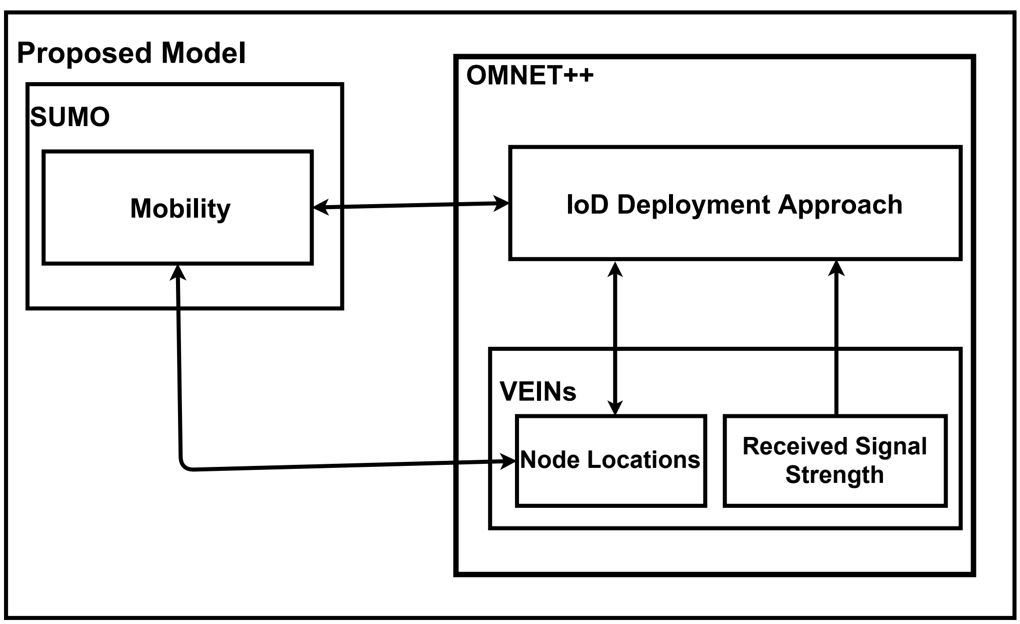

Figure 5.2: IoD-Assisted VANET framework in OMNET++ network simulator.

5.7 Simulation Results and Discussions

In this section, we show the effectiveness of the proposed IoDAV approach for achieving the optimal coverage in the dynamic environment. Throughout the obtained results, the influence of the IoD size and transmission power on the coverage and received signal strength are discussed. Moreover, the IoDAV is compared with standard VANET without IoD assisted, i.e., NIoD, and FIoD, to show why the VANET needs IoD rather than BS. Considering the aiming of the proposed scheme to improve the VANET connectivity, the performance metrics adopted in the simulation are the average coverage and average RSSI. Without loss of generality, the coverage is normalized to unity.

5.7.1 Parameters Setting

The simulation parameters used throughout this work are abstracted in Table 5.1. This chapter considers the Two-ray Ground Reflection propagation loss model provided by OMNET++ with α value of 2. In this propagation model, the ground reflection path, as well as the direct path, are taken into consideration for calculating the received power. So, an accurate calculation is given for the received power in this model. The approved amendment to the IEEE 802.11 standard (802.11p) implemented in Veins to add Wireless Access in Vehicular Environments (WAVE) is utilized. The setting parameters of the drone's communication network based on OMNET++ simulation tool are set as follows: The geographical range is 4000m x 4000m. The simulation area is generated by the SUMO NetEdit tool and the ve-

Table 5.1: Parameters setting

Parameter	Value
Geographical Range	4000m x 4000m
Propagation Model	Two-ray Ground Reflection
α value	2
IoD size	[2,4,6,8,10,12,14,16,18,20] UAVs
Drone's Altitude	100 m
Transmission Power	(20,30,40,50) mW
minPowerLevel	-86dBm
Transmission range	500 m
Antenna type	Directional antenna
MAC Protocol	IEEE 802.11p
Transmission Rate	6 Mbps
Antenna Gain	1 dBi
Optimization Approach	IPSO
Population Size	50
Maximum Iteration	50
Packet Size	1.4KB
Message Type	BSM
sending rate	1Hz
Update Interval	10 s
Simulation Time	400s

hicle movement is generated by the SUMO simulator. Moreover, the UDP packet is a Basic Safety Message (BSM) with a size of 1.4KB. The frequency band used is 5.9 GHz. The drones fly at 100m altitude. The simulation time is set to 400s, after which most of the vehicles in the ground reach their destinations, to test the behavior of the model. Moreover, the minimum threshold is defined to be -86dBm (the threshold for successful packet delivery). Each point in the figures represents the average of 10 replications of simulation. We implement two scenarios: sparse scenario (150 vehicles) and dense scenario (300 vehicles). We assume that the UAVs are senders and vehicles are receivers. The simulation is applied in 2D terrain, i.e., no obstacle is modeled. The drones fly at a fixed altitude, and thus, the problem has been simplified to 2D deployment problem. The IoD network is interconnected network. Finally, each drone is provided by GPS to properly obtain its location.

5.7.2 Impact of IoD Size on VANET Connectivity and RSSI

The IoD nodes have been deployed to provide wireless coverage to ground vehicles. The coverage is a percentage of connected vehicles and can be calculated by $V_C/\mathbf{V}$, where V_C is the connected vehicles, and $\mathbf{V}$ is the total vehicles on the ground. It can be replaced by isolated vehicles which is equal to $\mathbf{1\text{-}V}_C/V$. In this subsection, we will discuss the normalized coverage with respect to different IoD sizes in both sparse and dense scenarios.

The IoD sizes (different sets of UAVs in IoD) implemented are (2, 4, 6, 8, 10, 12, 14, 16, 18, and 20 UAVs) with transmission power of 50mW. The simulation result is illustrated in Fig. 5.3a.

We can observe from the figure that the IoD enhances the connectivity of the VANET network. This trend increases as the number of drones increases with the same transmission power used, demonstrating the size effect of the IoD network on coverage. However, increasing the IoD size might increase the interference and the probability of collision with adjacent drones. Besides, when the drones are too close to each other, they become redundant drones and play the same role. Thus, sufficient distances within their communication ranges should be maintained which is considered in the IoDAV approach. Furthermore, sufficient isolated vehicles appear due to their imbalance distribution and frequent movement.

In the dense scenario, the vehicles are close to each other and most vehicles can directly communicate within their communication range, demonstrating that the number of isolated vehicles appears with a low number and requires fewer IoD nodes to provide the connectivity among them, while in the sparse scenario, the vehicles are far from each other and number of isolated nodes appears with a high number and requires a higher number of IoD nodes for connecting them. This fact can be easily figured out in Fig. 5.3a. It can be seen that the maximum coverage is almost reached using 10 drones in the dense scenario and 16 drones in the sparse scenario.

To further evaluate the performance of the proposed IoDAV approach, we also discuss the impact of IoD size on RSSI at the receiver side, which is considered

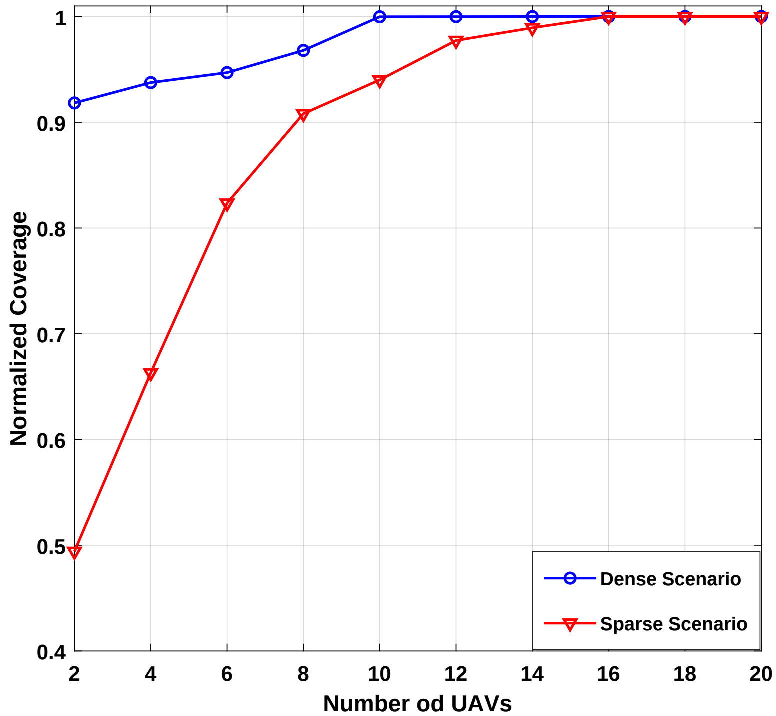

(a) Norm coverage

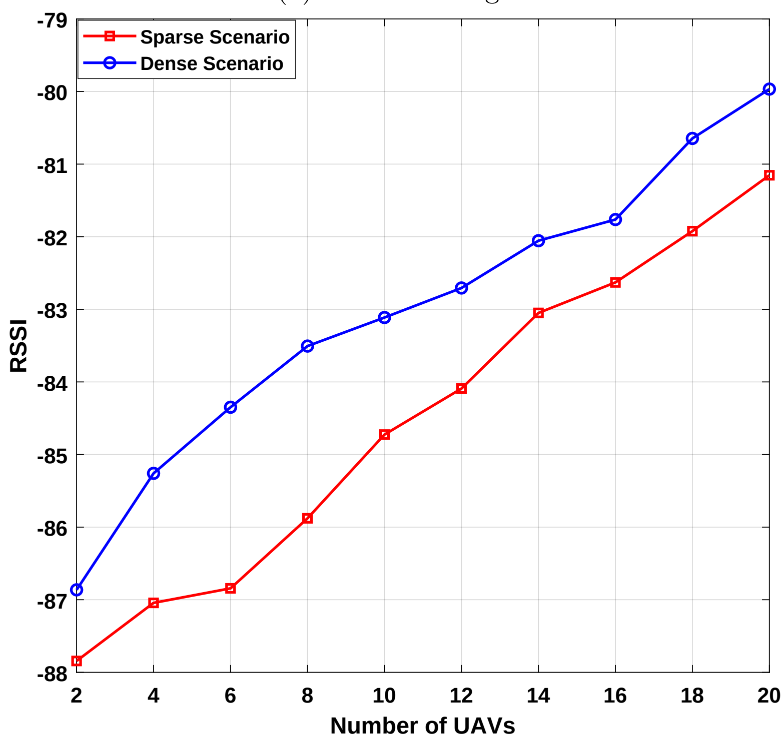

(b) Average RSSI

Figure 5.3: The average normalized coverage and RSSI for different IoD sizes in the IoDAV approach.

as an indicator of key performance. Particularly, RSSI is measured with respect to the simulation time and the average RSSI result is shown in Fig. 5.3b. The figure illustrates the average received signal quality at different receiver vehicles. It turns out that the quality of the received signal is lower in the beginning when only two UAVs are available, and it is improved as the IoD size increases. This advantage tends to grow higher in the dense scenario than in the sparse ones.

5.7.3 Impact of Transmitted Power on Coverage

To further investigate the effectiveness of the proposed IoDAV model, the impact of transmitter power on the total coverage is discussed, and the results of both scenarios are depicted in Fig. 5.4a and Fig. 5.4b, respectively.

The figures present the normalized coverage versus IoD size with different transmission power (20, 30, 40, and 50 mW) for both sparse and dense scenarios, respectively. As such, the impact of power transmission on coverage is examined where coverage is observed to improve continuously with increased transmission power as expected.

It is clear from the figures that the higher the transmitting power, the wider the range, which leads to covering a larger number of vehicles, that, in turn, improves the overall coverage. This tendency is evident in both scenarios. In the sparse scenario, we notice that the highest normalized coverage is provided by using 20 drones with the transmission power of 20 mW, 30 mW and 40 mW, reaches almost to 70%, 80%, and 93%, respectively, while it reaches to 100% in dense scenario using only 16 drones with a transmission power of 50 mW. We also note that 10 drones are sufficient to cover all isolated vehicles using a transmission power of 50 mW in the dense scenario, while the highest coverage achieved using the transmission power of 20 mW, 30 mW and 40 mW reaches almost to 94%, 95% and 95.9%, respectively.

For further investigating the effect of the transmitter power on improving coverage and reducing the number of drones required, we study the effect of the power transmission in the FIoD model and the results are shown in Fig. 5.5a, and Fig. 5.5b. The same tendency as in the IoDAV approach, but the improvement in FIoD is not significant as in IoDAV. The maximum normalized coverage that can be achieved is 80% and 94% in the sparse and dense scenarios, respectively. Comparison will be discussed in the forthcoming subsection. To sum up, the transmission power has a vital impact on improving the overall coverage as well as reducing the number of necessary drones.

5.7.4 Comparison with Other Schemes

We compare the proposed IoDAV approach against VANET without drone, i.e., NIoD and with FIoD. Furthermore, the performance metric which is the normalized overall coverage and RSSI are considered in the comparison.

To investigate the performance of the proposed IoDAV, we study the normalized overall coverage with respect to transmission power for 10 drones (sufficient number of drones to cover all vehicles by IoDAV in the dense scenario).

The results of the comparison are exhibited in Fig. 5.6a and Fig. 5.6b for sparse and dense scenarios, respectively. It can be easily shown that IoDAV

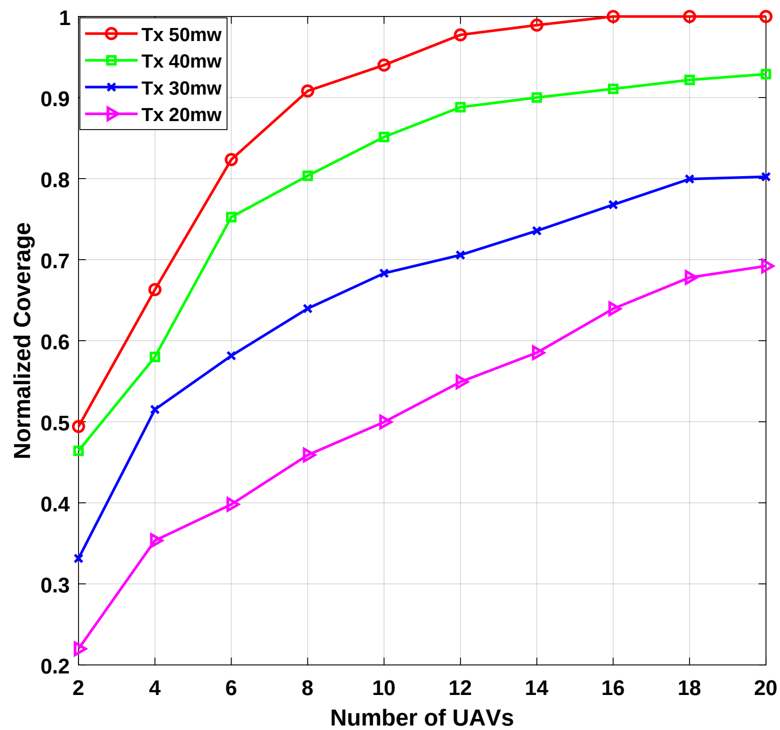

(a) Sparse scenario

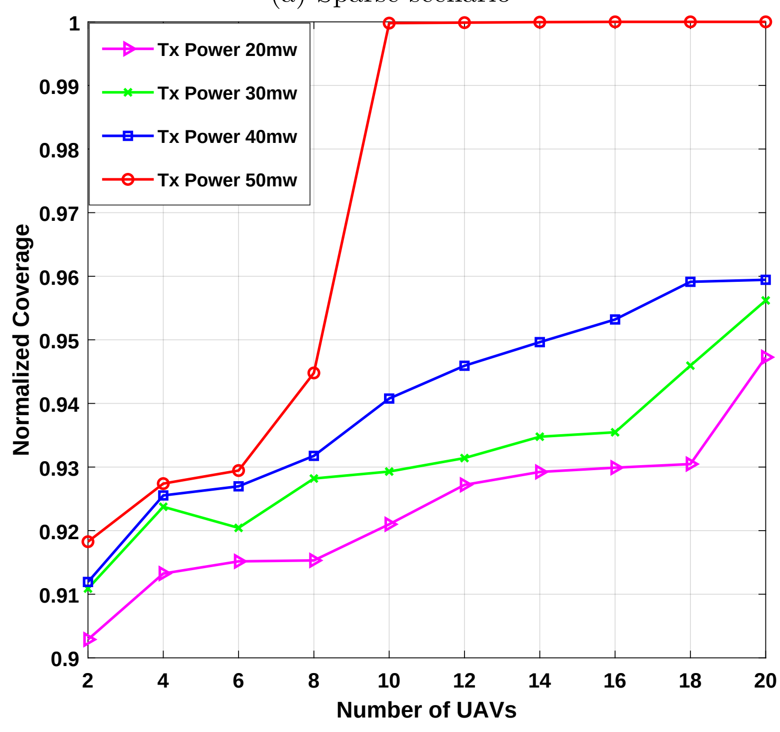

(b) Dense scenario

Figure 5.4: The average normalized coverage for different transmission power values with respect to different IoD sizes in the IoDAV scheme.

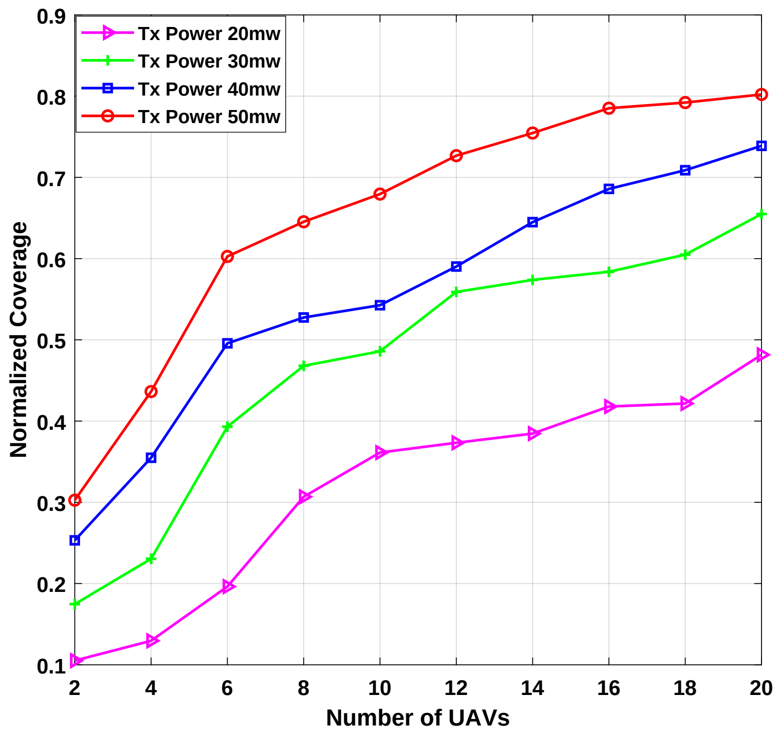

(a) Sparse scenario

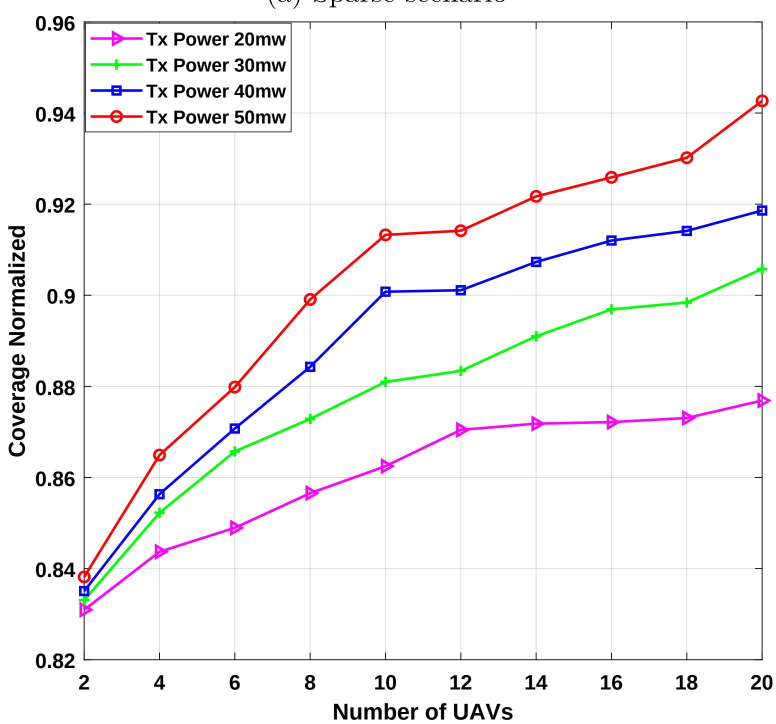

(b) Dense scenario

Figure 5.5: The average normalized coverage for different transmission power values with respect to a set of UAVs in the FIoD scheme.

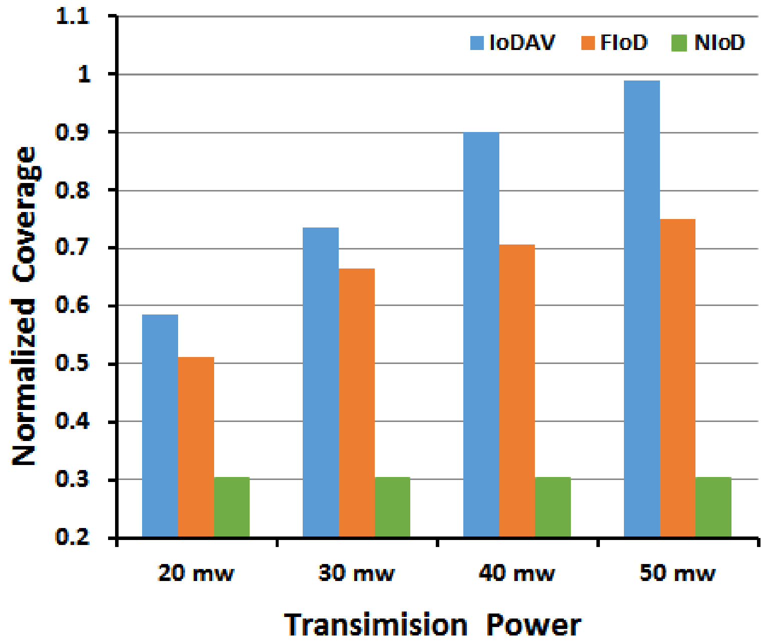

(a) Sparse scenario

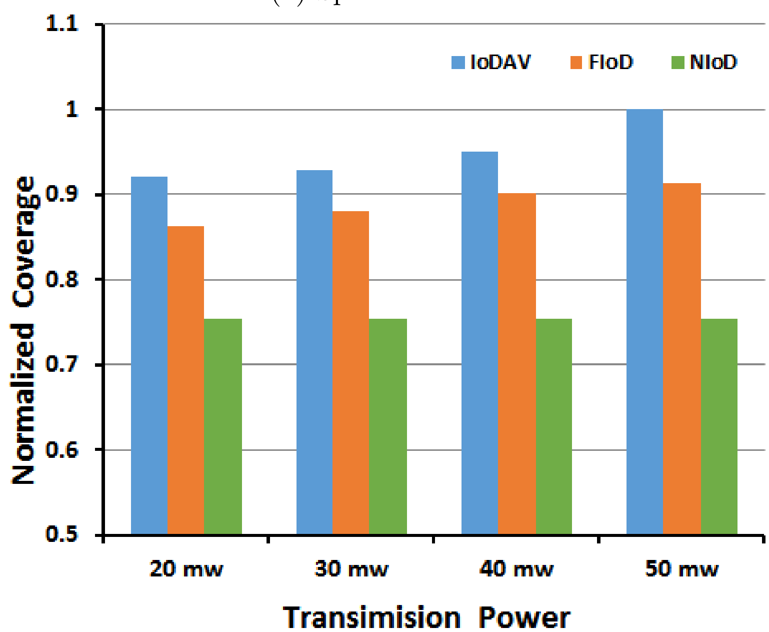

(b) Dense scenario

Figure 5.6: Average normalized coverage for different transmission power values in IoDAV, FIoD, and NIoD schemes.

achieves better coverage than other schemes. This is because, in the NIoD scheme, there is no infrastructure used to connect the isolated vehicles. Additionally, in FIoD, the drones are deployed only once and the movement of vehicles on the ground is neglected. Whereas the proposed IoDAV approach considers the vehicle's current position every 10 seconds to obtain the positions of IoD nodes. Thus, the UAVs in IoDAV adjust their locations based on the new locations of ground vehicles that allows the IoD nodes to follow the vehicles' movements on the ground and redeploys them accordingly. Besides, the IoDAV tries to keep the RSSI above the threshold value which is -86dBm and then number of covered vehicles is increased. Consequently, it provides a longer connectivity time.

We also compare the normalized coverage for a different set of UAVs (IoD size), and the results are shown in Fig. 5.7a and Fig. 5.7b for sparse and dense scenarios, respectively. It can be noticed that the coverage increases as IoD size increases with the same transmission power used, demonstrating the impact of IoD size on coverage. In the figure, the proposed IoDAV approach achieves better average coverage than other schemes with overall coverage improvements of 48.79% over NIoD and 36.6% over FIoD in the sparse scenario, while for the dense scenario the improvement is 12.9% over NIoD and 4.2% over FIoD. This means that in the dense scenario, the number of isolated vehicles is lower than that in the sparse scenario.

The experiment distribution results can be observed throughout the Box-plot in Fig. 5.8. As figure 5.8 illustrates, IoDAV plot-box indicators are higher than other schemes. The highest coverage achieved by IoDAV is 100% which represents superior to the upper bound of the other schemes. It also shows that NIoD and FIoD in the worst case are inefficient since the coverage is lower than 30% and

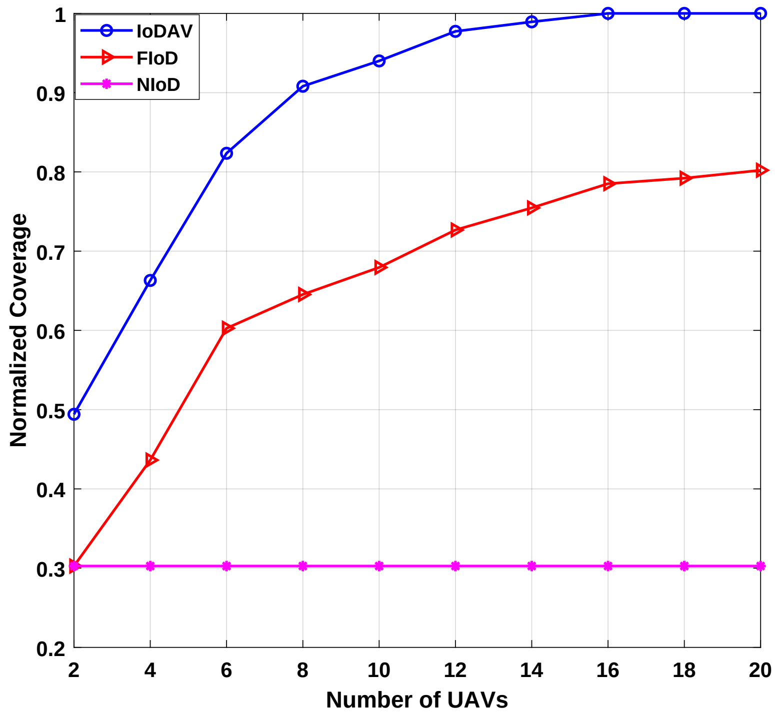

(a) Sparse scenario

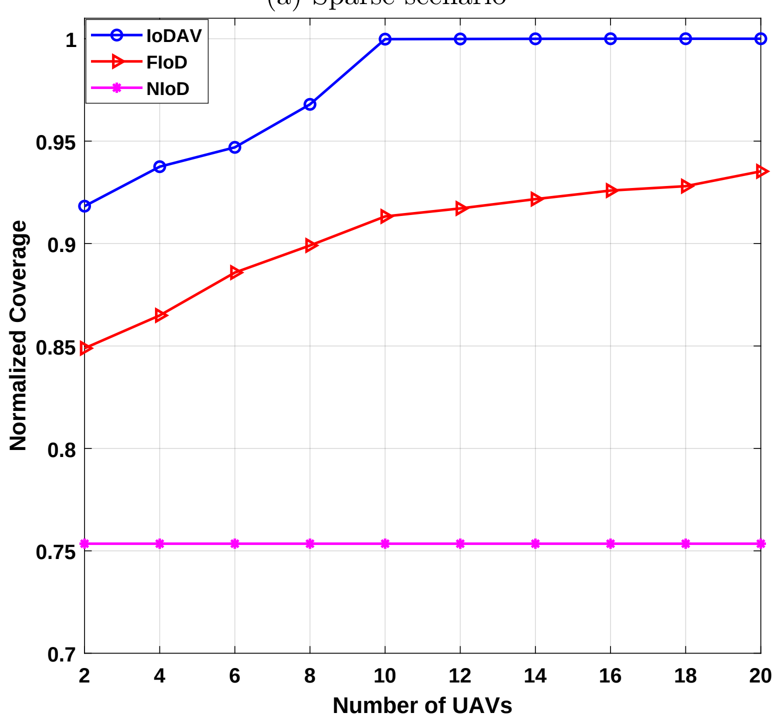

(b) Dense scenario

Figure 5.7: Average normalized coverage for different sets of UAVs in IoDAV, FIoD, and NIoD schemes.

51%, respectively, but still not higher than IoDAV. Moreover, half of IoDAV is higher than 90% which is higher than other schemes. It turns out that Box-plot shows the superiority of IoDAV to other approaches. IoDAV has great superiority in all indicators compared with other competitors.

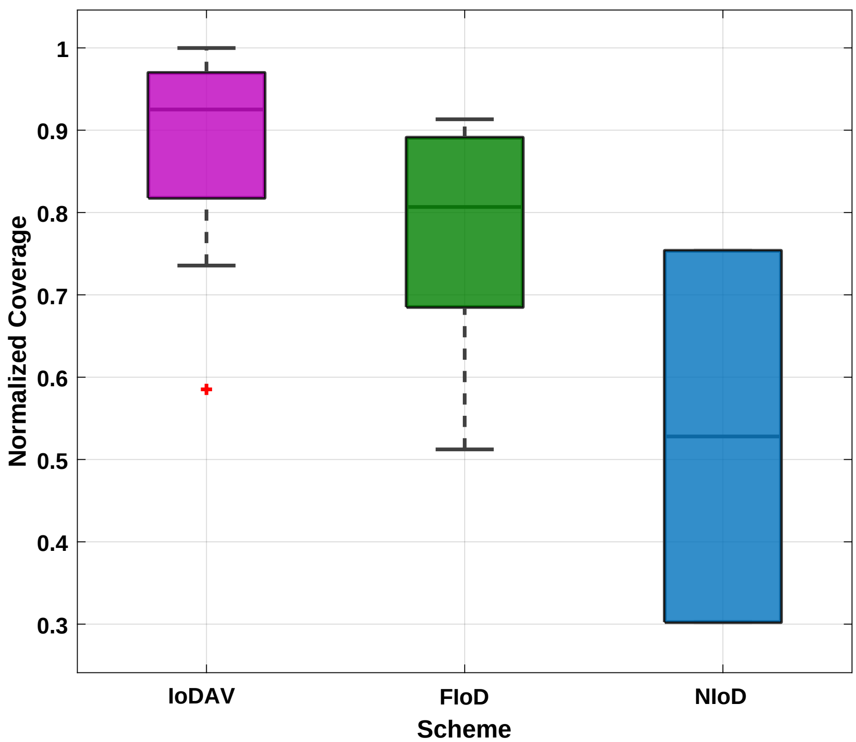

Figure 5.8: Box-plot of average normalized coverage in all scenarios for 10 UAVs in IoDAV, FIoD, and NIoD schemes.

To further investigate the performance of the proposed IoDAV deployment model, we discuss the impact of IoD size on RSSI at the receiver side, which is considered an indicator of key performance. Particularly, RSSI is measured with respect to the simulation time and the average RSSI for both FIoD and IoDAV are presented in Fig. 5.9a, and Fig. 5.9b for sparse and dense scenarios, respectively.

As discussed above, the positions of UAVs in FIoD are fixed, i.e., UAVs are hovering in their deploying places during the whole mission time, and neglect the movements of vehicles on the ground. Furthermore, the vehicles are moving, which implies that there are non-uniform densities of cars at a different time in the given region. Therefore, the whole region can't be covered with the available number of fixed drones and thus all vehicles can not be covered. As a result, the fixed UAVs become far from ground vehicles as they move which in turn reduces the RSSI while the dynamic IoD or IoDAV can cope with the updating of vehicles locations and then tries to keep the RSSI above threshold value which is -86dBm as exhibited in the figure. It turns out that the proposed IoDAV has the most consistent result.

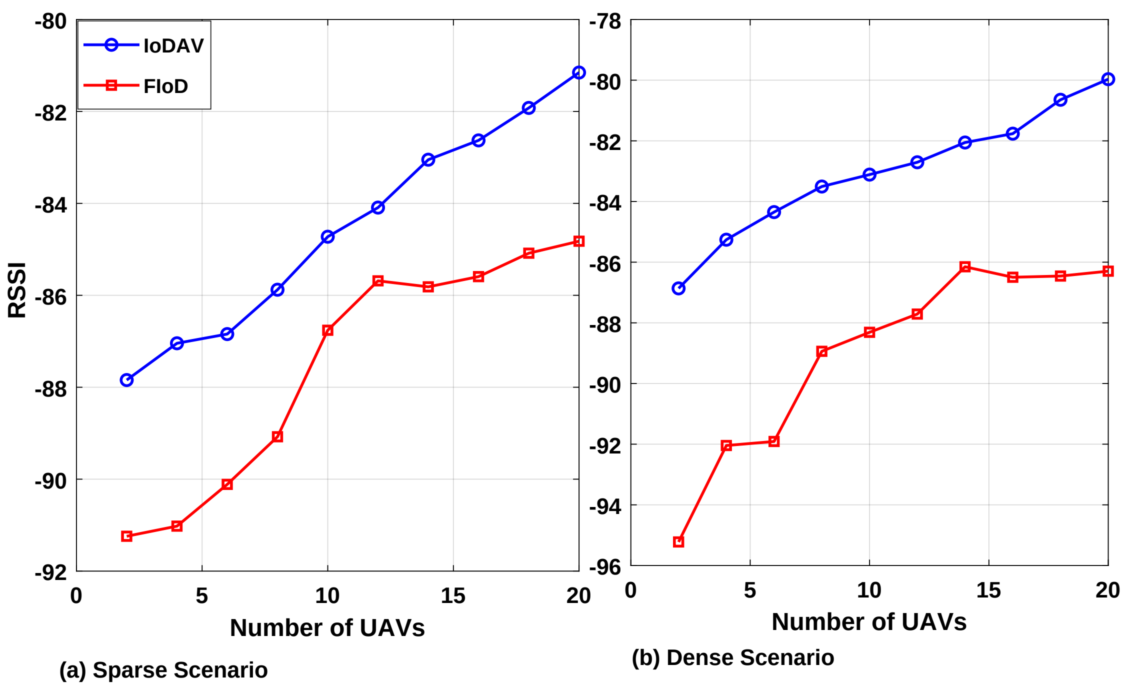

Figure 5.9: Average RSSI at the receiver for different sets of UAVs in IoDAV and FIoD schemes.

5.8 Chapter Summary

The successful IoD deployment on application area requires IoD nodes with the capability to adapt and configure themselves automatically and high level of coordination without intervention of human. Due to the increasing number of nodes in IoD, the centralized systems are not practical. This chapter developed a novel dynamic collaborative IoDAV model in which UAVs connected isolated vehicles on the ground with each other. We proposed an optimization approach, an improved version of particle swarm optimization, to optimally deploy IoD to provide communication among vehicles on the ground. Depending on the vehicles' locations at any instant, IoD nodes were deployed to provide the optimal connectivity for the isolated vehicles. Furthermore, the signal quality received at the car's receiver was utilized to assess the best IoD location to maximize connectivity. The RSSI was obtained via simulation by using the Two Ray Ground Reflection propagation model. Two scenarios were considered : sparse and dense scenarios. More importantly, the results were compared with the standard VANET and FIoD models. The results illustrated that the proposed IoDAV approach outperformed other schemes. This is because the dynamic model used in IoDAV could cope with a dynamic environment of ground vehicles and achieved better coverage than both standard VANET and FIoD models during the whole simulation time.

CHAPTER 6

3D IOD-TO-VEHICLES SIMULATION MODEL FOR IOD-ASSISTED VANET

6.1 Chapter Motivation

The deployment of the IoD network has been studied in the literature for coverage problems. However, such deployment has been hampered by underline challenges. Although deploying IoD at a high altitude provides a better LOS condition, the distance between the IoD network and vehicles on the ground increases which in turn increases the path loss. Besides, the terrain features have a significant impact on IoD-to-Vehicle (IoD2V) communication because the height of the terrain can act as an obstacle and causes signal attenuation. As a result, the IoD2V communication will experience the effect of multipath propagation. To assist the communication quality in the model involving IoD and vehicles, extensive simulation can be performed for scale analysis. In most existing works, the simulations are performed in a 2D environment, and the effect of terrain altitude on communication is neglected. In practice, the terrain is not perfectly flat as some roads encounter descent or ascent. To be more specific, some streets have been separated by hills lying between them, which may lead to different analysis results of VANETs communication due to neglecting such details.

To sum up, some previous works achieve enhancements in the performance of the VANET network such as routing, coverage area maximization, received signal strength, end-to-end delay, and throughput. Other works focus on VANETs communication enhancement. However, the simulation is performed in a 2D environment and neglects the effect of terrain profile on communication. Although fewer works consider the effect of terrain on communication, they neglect the IoD formation and focus on using only one UAV. In general, the superiority and flexibility of IoD formation are not fully exploited to improve the VANETs communication in 3D space.

6.2 Chapter Contributions

To address the challenges mentioned above, we propose an efficient IoD-assisted VANET approach in 3D space (3DIoDAV) to enhance the communication of vehicles on the ground. In doing so, the IoD nodes are optimally deployed to maximize the number of covered vehicles, i.e., reducing the number of isolated vehicles.

Moreover, the impact of terrain profile on communication has been addressed by proposing a 3D propagation model for IoD2V communication to assist the communication quality between IoD in air and cars on the ground. The proposed approach utilizes an optimization algorithm for deployment purposes. Towards this end, the optimal deployment of IoD nodes is obtained by the optimization algorithm implemented, i.e., IPSO. The proposed 3D propagation model is added to the objective function to evaluate the signal quality at receivers' sides, i.e., vehicles on the ground in which the effect of high-level terrain on communication is considered in calculating the received signal. As a result, the IoD nodes are dispatched to the most appropriate locations that minimize the impact of terrain obstacles on the transmitted signals and enhance the LOS condition between sender and receiver.

The main contribution of this work can be summarized as follows:

- A novel IoD2V communication model is proposed to characterize the 3D communication between the IoD network in the air and the VANETs network on the ground. The proposed model considers the terrain profile to detect the obstacles and evaluate the quality of the received signal accordingly.

- A novel 3D collaborative IoD architecture (3DIoDAV) is proposed to maximize the coverage area and enhance the quality of the received signal at a receiver side. The demand for drones is evaluated using an optimization evaluation function to optimally obtain the IoD deployment to assist the VANET.

- A population optimization scheme is utilized to dispatch the IoD nodes into the optimal locations in 3D space based on the locations of vehicles on the ground so that the connectivity of vehicles and received signal quality are improved. To achieve such objective, we implement IPSO so that adequate signal is guaranteed toward isolated vehicles. Besides, the proposed 3D propagation model is utilized by the objective function of IPSO so that the impact of terrain on communication is considered in the IoD deployment.

- The performance of the proposed IoD2V communication model, as well as the 3DIoDAV approach, are tested throughout simulation experiments.

This chapter is the result of a collaboration with Prof. Ansar Ul-Haque Yasar from Transportation Research Institute, Hasselt University, Belgium. The work has been accepted for publication in Sensors.

6.3 IoD-To-Vehicles communication model in 3D environment

The aim of the proposed IoD2V communication model is to support the communication among vehicles in an environment, where the infrastructures are limited and the terrain irregularities impacts the communication between nodes. In rural areas, the main challenge is the terrain profile, especially, if it includes hills or mountains that act as obstacles, and resulting in attenuation for the transmitted signal. Thus, obstacle detection is necessary to characterize the communication in such an environment. To do so, the terrain elevation is extracted where the high elevation of the terrain is acting as an obstruction to communication. In this section, the Digital Elevation Model and the 3D propagation model are explained in detail.

6.3.1 Digital Elevation Model (DEM)

The terrestrial surface information can be acquired thanks to satellite and radar technology advancement. These advancements allow generating a digital elevation model (DEM) at multiple temporal and spatial scales. The earth surface is presented by DEM and it is available to be downloaded from USGS. Furthermore, the DEM provides information about the surface of the earth and can be utilized to recognize the height of terrain above the level of the sea. The elevation of any point can be provided and obtained from different sources by USGS. One interesting source is documented based on Shuttle Radar Topology Mission (SRTM). In particular, a NASA DEM, which is collected from SRTM, is utilized [148]. In this model, the surface information of the earth is captured using a radar sensor from space. Various resolutions are supported which define the elevation accuracy.

- Structure of DEM file

The DEM file is in height format and named in the easting and northing format. The easting and northing mean the eastward and northward measure distance, respectively, when adapting the UTM system. The DEM covers one degree of latitude and longitude. Thus, the structure of the DEM file is a two-dimension array of cell points represented as grids. Besides, two resolutions are provided, namely 3-arc second and 1-arc second sampling. The elevation is extracted from the file by precisely selecting the suitable longitude and latitude into the right cell of the grid. The grids of 1-arc second sampling for obtaining the elevation data are illustrated in Fig. 6.1. The figure shows that the grid is composed of 3601 X 3601 cells and covers one degree of latitude and longitude. Each degree of latitude and longitude is represented by 3601 cells. Moreover, each cell index can be obtained by multiplying the fraction part of geographical coordinate by 3600, for an instant, 0.8 represents the 2880^{th} cell. In this chapter, we consider

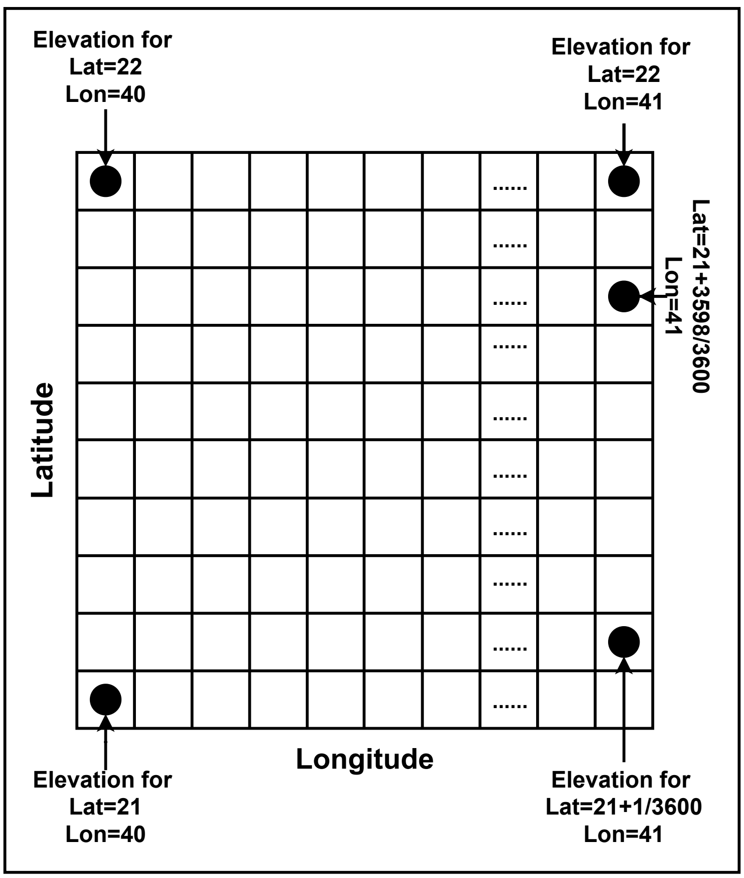

Figure 6.1: Digital Elevation Model (DEM) data structure.

a mountain terrain, ALHADA ROAD, KSA terrain, and the full 3D view of the terrain is represented and plotted using Matlab as shown in Fig. 6.2. The figure shows different heights, which results in elevation ranging from 758 m to 2608 m.

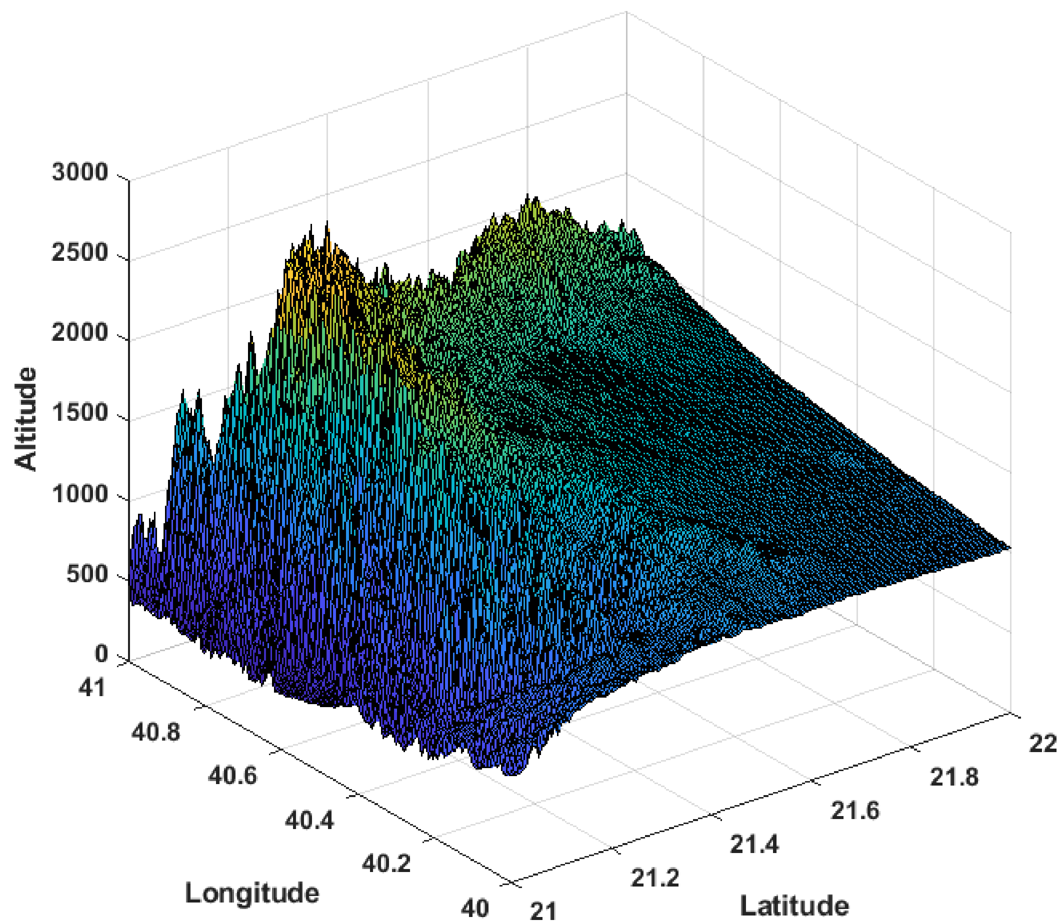

Figure 6.2: 3D view of Alhada Road in the DEM file.

- Elevation data extraction

In this part, we explain how to effectively extract the elevation data from DEM file. The data of DEM file cover a given latitude and longitude. However, the coordination used for location is in meters measurement. Compared with UTM system, the area provided by the DEM data provides a little tilled area. As illustrated in Fig. 6.1, the DEM file looks like a two-dimension array with a constant distance between consecutive points in both horizontal and vertical directions. Thus, the file contains N by N elevation points which can be extracted into N by N matrix. Each point represents the elevation on the z-axis. More importantly, the x-axis and y-axis can be omitted without losing the information of any given point. Towards this end, Matlab function ***geotiffread*** (DEMfile.tif) is utilized to extract the elevation of DEMfile.tif into two-dimension matrix. The function also provides information on latitude and longitude limits.

6.3.2 3D Propagation Model

In this subsection, we explain the propagation model utilized and show how to obtain the attenuation based on the elevation information extracted from the DEM file for a specific area. The quality of communication can be affected by high terrain that might obstruct the signal propagation. The Non-Line-Of-Sight (NLOS) conditions might occur due to the presence of mountains and hills, which reduce the power of the received signal or even block the signal. More importantly, the diffraction effect due to the high terrain deflects or bends the signal wave. To analyze the effect of diffraction, the obstacle can be approximated as a knife-edge. In this case, the knife-edge diffraction could attenuate the transmitted signal. To calculate the knife-edge effect, parameters such as the signal wavelength (λ), obstacle height above the LOS line between transmitter and receiver, and the distance between transmitter and receiver should be considered. Furthermore, the height of the obstacle above the LOS can be calculated by retrieving the elevation obstacle from the DEM file. That is, the LOS line between the sender and receiver can be obtained by considering the two points in 3D space. The first point is the sender position coordinate (xs, ys, zs) and the second point is the receiver position coordinate (xr, yr, zr). The prediction point can be determined and analyzed based on the number of slices that divide the LOS line. With this in mind, the inspection points divide the LOS into slices as shown in Fig. 6.3. According to these points, there is only one line passing through them. The LOS is divided into discrete points to detect the terrain obstructing the signal and acting as an obstacle. At each point, the prediction point coordination (xp, yp, zp) is obtained as in [93] using

$$xp = xs + \Delta(xr - xs), \tag{6.1}$$

$$yp = ys + \Delta(yr - ys), \tag{6.2}$$

$$zp = zs + \Delta(zr - zs), \tag{6.3}$$

where Δ is the fraction of the LOS line. It has to be stressed that the parameter Δ is selected so that the slices of the LOS line should not be higher or smaller than the DEM file resolution. After calculating the zp for each slice, the elevation of this position (Ep) is extracted using the DEM file, and compared with zp. The height of the obstacle above the LOS line is calculated using

$$hp = Ep - zp. \tag{6.4}$$

The obstacle is detected if the hp is positive meaning that the height of the obstacle is above the LOS line while the negative value of hp indicates that no obstacle is detected. In this chapter, we implement a single-knife edge propagation model to evaluate the signal attenuation.

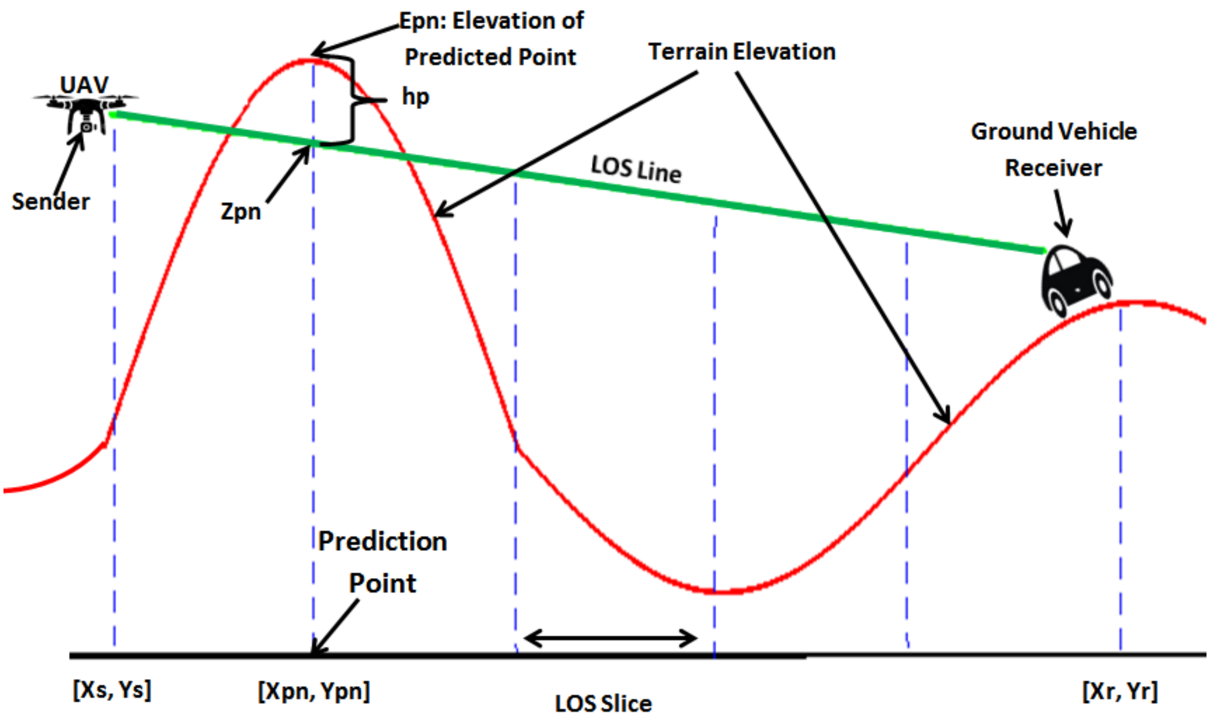

Figure 6.3: Dividing the LOS line between sender and receiver into a set of prediction points to detect the obstacles.

6.3.3 Single Knife Edge Propagation Model

In this model, after obtaining the obstacle height (hp), a Fresnel-Kirchhoff diffraction parameter (v_h) is evaluated. The diffraction parameter is a function of obstacle height, the distance between sender and obstacle (Ds), the distance between obstacle and receiver (Dr), and the wavelength of signal (λ). Hence, the diffraction parameter v_h can be calculated as in Lee [149] as follow:

$$v_h = hp\sqrt{\frac{2(Ds + Dr)}{\lambda DsDr}}. \tag{6.5}$$

Then the signal attenuation is calculated using Fresnel integral $\eta(v_h)$ as a function of v_h. The Fresnel integral is obtained as in Lee [149] as follow

$$\begin{aligned}
&\eta(v_h) = 0, v_h \leq -1,\\
&\eta(v_h) = 0.5 - 0.62v_h, -1 \leq v_h < 0,\\
&\eta(v_h) = 0.5e^{-0.95v_h}, 0 \leq v_h < 1,\\
&\eta(v_h) = 0.4 - \sqrt{0.1184 - (0.38 - 0.1v_h)^2}, 1 \leq v_h \leq 2.4,\\
&\eta(v_h) = \frac{0.225}{v_h}, v_h > 2.4
\end{aligned} \tag{6.6}$$

After obtaining Fresnel integral, the signal attenuation can be evaluated using the following formula (in dBm)

$$Atten = 20Log10(|\eta(v_h)|). \tag{6.7}$$

6.4 IoD-Assisted VANET Approach in 3D Terrain (3DIoDAV)

As highlighted in **Section2.4**, the previous works related to VANETs intended to improve the VANET network performance. However, the UAV's mobility superiority was neglected. Besides, the impact of terrain features on communication between IoD network and VANET network is also neglected. Integrating a few numbers of UAVs in a wide area with VANETs can dispense several infrastructures. Moreover, the terrain obstacles can be detected and included to consider the effect of terrain on communication. To this end, the proposed IoD2V communication model is utilized in IoD-assisted to properly calculate the signal attenuation due to terrain obstacles.

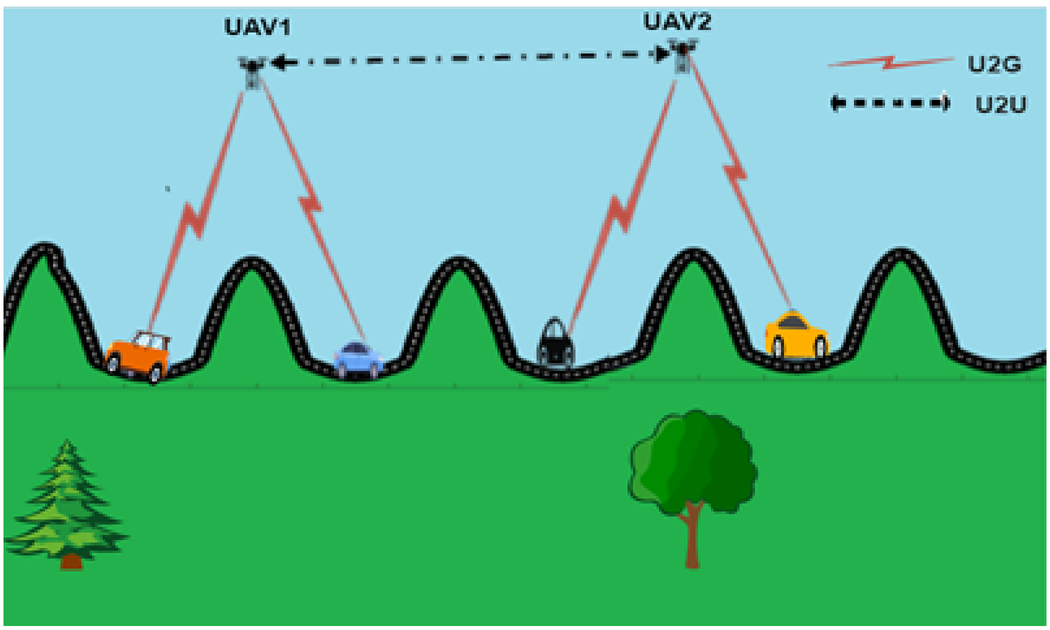

Figure 6.4: 3D-IoD-Assisted-VANET architecture.

As illustrated in Fig. 6.4, the proposed 3DIoDAV architecture is composed of the IoD network and VANET network. The mobility of vehicles in the VANET network is restricted by predefined paths. Additionally, the communication quality of vehicles is influenced by hills and mountains, which act as obstacles and might block the transmitted signal. The IoD network, consisting of UAVs swarm with wireless communication, is responsible to support communication between ground vehicles. Due to the flexibility and mobility of UAVs in the IoD network, they can be easily deployed to the optimal locations and act as a relay-assisted network. The proposed 3D propagation model for IoD2V communication is used to characterize the communication between IoD nodes and vehicles.

In Fig. 6.4, the effectiveness of the proposed architecture is illustrated in which the vehicles cannot communicate directly within their communication range. The hills and mountains obstruct the transmitted signal and act as obstacles. Thanks to the proposed 3DIoDAV, UAV1 and UAV2 are dispatched to suitable positions and act as relay nodes to provide communication between isolated vehicles. It is worth mentioning that the locations of drones are updated periodically based on the vehicles' locations on the ground and the received signal strength state therein. As the vehicles move, the distance between them increases and the obstacles lying in between might isolate them, and then losing the connection. The proposed approach aims to connect the isolated vehicles dynamically every time step.

6.5 Optimal IoD Deployment in 3D Terrain

This section describes how to optimize the IoD deployment in 3D space and the optimization approach used. In Chapter 5, the dynamic deployment of the IoD network is considered where the IoD nodes keep changing their positions dynamically based on the the locations of the vehicles on the ground. The aim is to maximize the coverage area and enhance the received signal at the receiver side. However, the effect of terrain obstacles is not considered. The main objective of this work is to obtain the best location of IoD nodes in a 3D environment where the effect of terrain obstacles is taken into account when deploying the IoD nodes. To this end, the proposed 3D propagation model for IoD2V communication is utilized to calculate the signal strength at the receiver side. More importantly, in the considered scenario, the lack of sufficient infrastructures is assumed and the IoD could help to relay the information among vehicles.

In the deployment problem, trying all possible positions in 3D space for obtaining the optimal positions is an inefficient way and consumes much time which is considered as NP-hard problem. A meta-heuristic algorithm is a sophisticated solution to addressed such problem where the optimal solution is obtained without trying all possible locations. Instead, the solution is randomly generated and evaluated by a fitness function every iteration and the best solution is obtained. In the proposed approach, we implement the improved version of particle swarm optimization (IPSO) presented in Chapter 3. The cost function is updated by including the proposed 3D propagation model to evaluate the solution. The objective function obtains the RSSI at the receiver side and evaluates the generated positions of IoD nodes. Moreover, the coverage is then found based on the RSSI obtained by comparing it with a minimum power level threshold which is defined in the proposed approach to be -89dBm (the threshold for successful packet delivery). Based on the value of RSSI, the number of covered vehicles is calculated where the vehicle is counted to be covered if its received signal is greater than the minimum power level threshold. The optimization algorithm utilized in this chapter is explained in detail in Chapter 5.

6.6 Optimization Framework

In this section, we will explain how to implement the proposed approach in a standard simulation tool. The aim of the proposed approach is to improve the VANETs network connectivity in 3D space by deploying the IoD nodes at optimal positions. Towards this end, the IPSO is implemented for dispatching the IoD nodes to the most appropriate locations. The proposed 3D propagation model is utilized in the objective function to evaluate the quality of a generated solution. It is worth emphasizing that the proposed approach is implemented as an extension to OMNET++ [144], Veins [146], and SUMO [145] by adding the 3D propagation model, where the physical layer is modified to simulate the effect of 3D wireless transmission. The main parameters that should be considered in the simulation are the terrain space, and nodes locations (longitudes, latitudes, and altitudes).

The framework of the proposed mechanism is illustrated in Fig. 6.5. The proposed 3D propagation model is composed of Elevation Estimation, Obstacle Detection, and Propagation model (Single Knife Edge) modules. The Elevation Estimation module is responsible to estimate the elevation of a given coordination. Moreover, the Obstacle Detection module receives the locations of senders and receivers and detects the obstacles lying between them. After detecting the obstacles and finding their heights, the module finds the maximum height and delivers it to the propagation model (Single Knife Edge) to calculate the signal attenuation. Fig. 6.5 shows how the parameters are implemented in Veins.

To obtain the optimal deployment of IoD network in 3D space for VANET assisted, the proposed approach works as follow. The elevation information of the terrain is extracted from the DEM file. The main challenge of using the whole digital elevation file is the longer simulation time. To optimize the simulation time, we use Matlab software function ***geotiffread*** to handle the geographical data. The function can read the downloaded DEMfile.tif and exports the limit of longitude and latitude as well as the elevation data of the terrain. The elevation data is exported as a 2D array that can be stored into a text file. To save computation time, the text file is stored locally in the OMNET++ simulator.

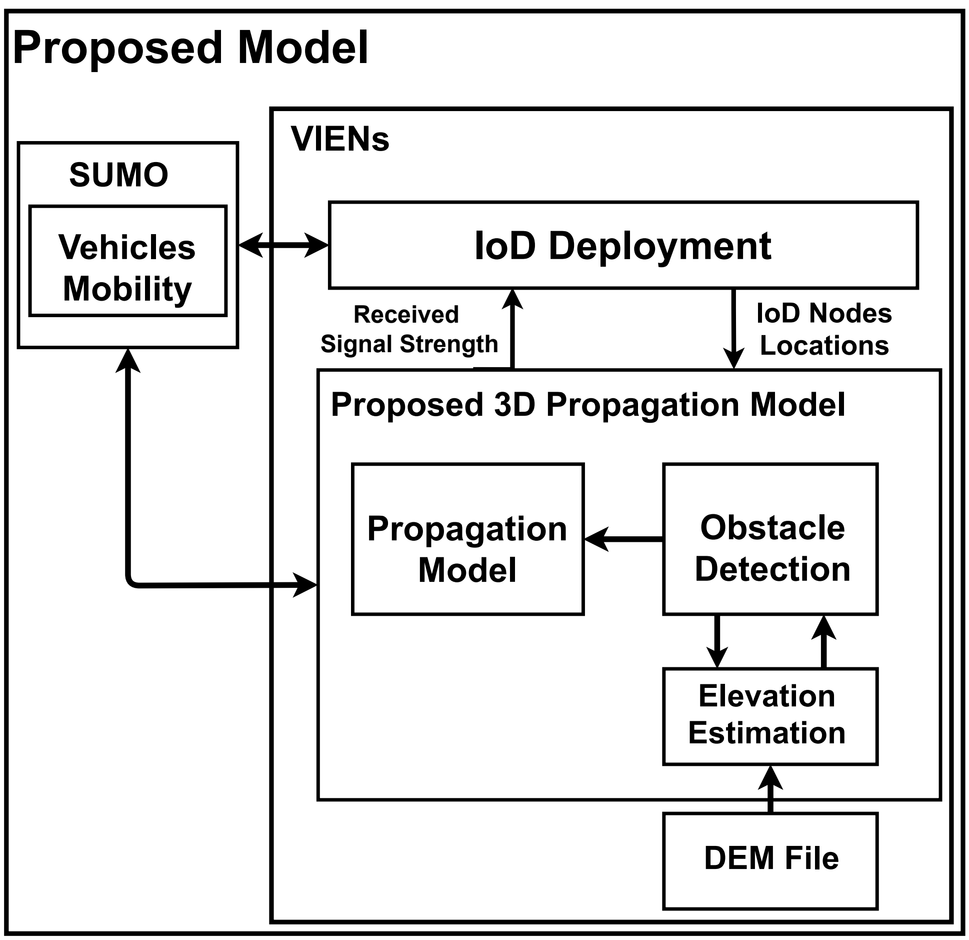

Figure 6.5: 3D-IoD-Assisted VANET framework.

Thanks to TraCI in SUMO, the exact geo coordinate positions of vehicles on the ground can be easily generated. Hence, the connecting of the Veins simulator with TraCI in SUMO allows obtaining the exact geo coordinate locations of vehicles according to the mobility of the vehicles. Then, the implemented Elevation Estimation module obtains the elevation of the transmitter and receiver. Moreover, the Obstacle Detection module detects the obstacles lying between transmitter and receiver. After that, the actual signal loss can be better determined by the propagation module using the single knife-edge diffraction model discussed above. Finally, the obtained signal strength is evaluated by the objective function of IPSO, and the optimal deployment of IoD nodes is obtained.

In the light of the above illustration, the IoD deployment gets the current locations of the cars on the ground and finds the most appropriate positions of IoD nodes to enhance the received signal strength and minimize the number of isolated vehicles, i.e., maximize the number of covered vehicles. The IPSO objective function evaluates the received signal quality at the receiver side which is obtained by the proposed 3D propagation model. The output of the IPSO algorithm is the IoD nodes' optimal locations so that the number of covered vehicles is maximized in 3D space.

6.7 Simulation Results and Discussion

In this section, we show the effectiveness of the proposed 3D propagation model to characterize the IoD2V communication, by illustrating the ability of the proposed 3D propagation model in detecting the obstacles lying between senders and receivers. This help to properly calculate the coverage as well as the quality of the received signal at a receiver side. We also illustrate the effectiveness of the 3DIoDAV approach to improve the performance of the VANET network by achieving the optimal coverage and maximum received signal strength. The influences of UAV's altitude, transmission power, and IoD size on coverage and RSSI are analyzed. The results are compared with the 2D model where only the free space propagation model is considered. We also compare results with IoDAV [28] to show the necessity of the proposed 3D propagation model for IoD2V communication to obtain more practical results.

Considering the goal of the proposed approach to produce more realistic results and improve the connectivity of VANET, the mean coverage and mean RSSI are the adopted performance metrics in the simulation. Without loss of generality, the coverage is normalized to unity.

6.7.1 Simulation Parameters Settings

To implement the proposed 3DIoDAV, the mountainous rural area of Alhada Road, Attaif, KSA is utilized as a simulation terrain. The map of the terrain has been imported from the Open Street Map (OSM) [150] to make the simulation more realistic. Besides, the elevation information of the terrain is obtained using SRTM DEM [148]. In such area, communication might be hindered due to the height of a terrain. The geographical area is 6000 m x 8000 m which is the limit of the exploration area. Furthermore, a Basic Safety Message (BSM) is a UDP packet with a size of 1.4KB. We have conducted two simulations. The first simulation

Table 6.1: Parameters setting.

Parameter	**Value**
Geographical Range	**6000 m x 8000 m**
Propagation Model	**3D Propagation Model**
Frequency	**5.9 GHz**
IoD size	**[1,2,3,4,5,6,7,8,9,10] UAVs**
minPowerLevel	**-89dBm**
Transmission range	500 m
Antenna type	Directional antenna
MAC Protocol	IEEE 802.11p
Transmission Rate	6 Mbps
Antenna Gain	1 dBi
Optimization Approach	**IPSO**
Population Size	**50**
Maximum Iteration	**50**
Packet Size	**1.4KB**
Message Type	**BSM**
sending rate	**1 Hz**
Update Interval	**10 s**
Simulation 1 Parameters Setting	
Deployment Altitude	**[30, 50, 100, 150, 200, 250, 300] m**
Transmission Power	**50 mW**
Simulation Time	**1040 s**
Simulation 2 Parameters Setting	
Deployment Altitude Range	**[50 m to 100 m] and [100 m to 150 m]**
Transmission Power	**[20, 40, 60, 80] mW**
Simulation Time	**600 s**

is to evaluate the proposed 3D propagation model, i.e., IoD2V communication model, and the second simulation is to show the effectiveness of the 3DIoDAV approach to achieve a VANET performance improvement. The time of simulation 1 and simulation 2 are limited to 1040s and 600s, respectively, after which most of the cars reach their destinations, to test the model's behavior. The parameters of simulations are abstracted in Table 6.1.

The IoD network is deployed to support the wireless connectivity of ground cars. The coverage is obtained as a percentage of connected cars to the total cars on the ground and can be obtained as in [28] by **Vcon/Vt**, where **Vcon** is the number of connected vehicles, and **Vt** is the total vehicles on the ground. We assume that the UAVs are senders and vehicles are receivers. Besides, in a free space model, we assumed a flat area where the main factor affecting the communication is the distance between a sender and receiver, and other factors are neglected. We also assumed that each UAV is provided by GPS to properly obtain its location.

6.7.2 Evaluation of The Proposed 3D Propagation Model for IoD2V Communication

The aim of this subsection is to validate the obtained results using the proposed framework that includes the 3D communication model with the results obtained from the 2D communication model in which the impact of the terrain is neglected. Since the main goal is to analyze the impact of the 3D communication model, we use the simplest diffraction model, namely a single knife-edge diffraction model. Besides, different IoD deployment altitudes are simulated.

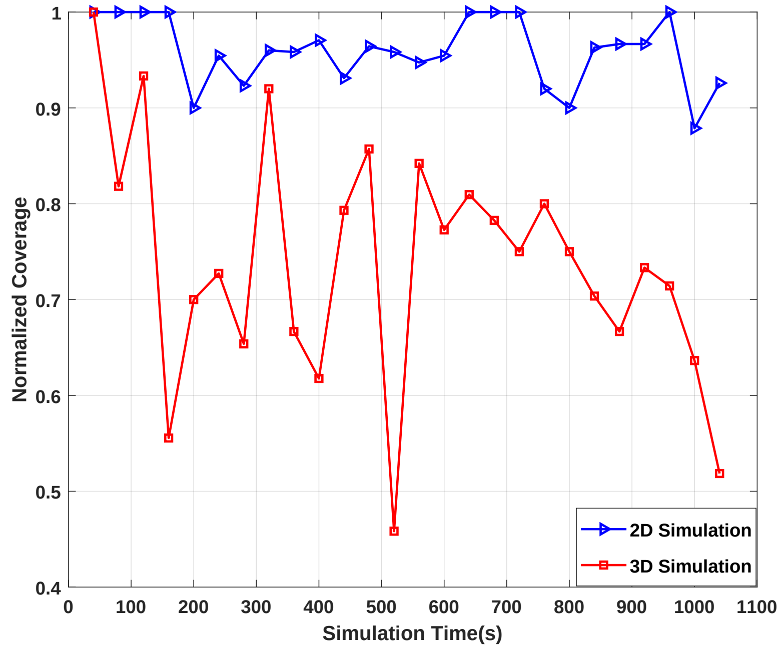

(a) 50 m deployment altitude

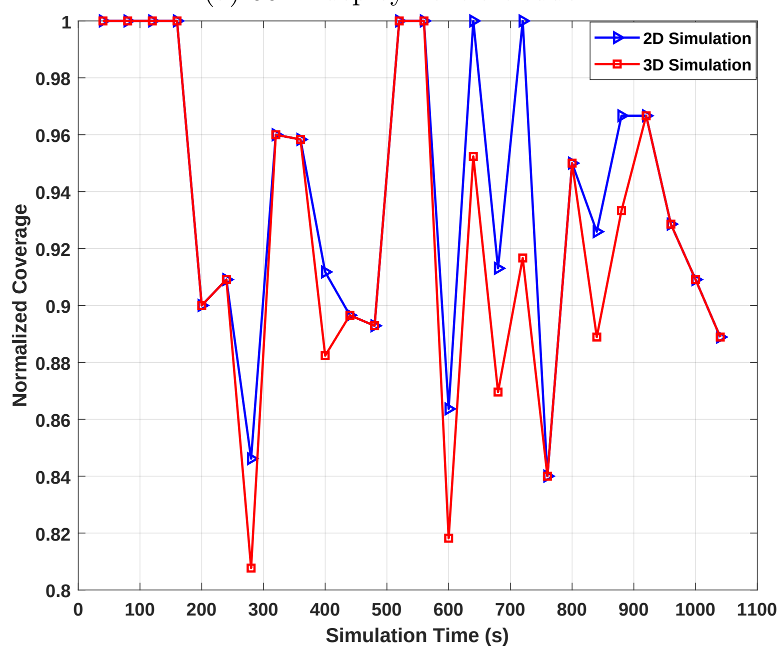

(b) 200 m deployment altitude

Figure 6.6: The average normalized coverage with respect to simulation time for two IoD deployment altitudes in 2D and the proposed 3D propagation models.

To asses the quality of the proposed communication model, we obtain the coverage with respect to a simulation time for two deployment altitudes of 50 m and 200 m with the same setting parameters. To have a better comparison, we compare the results with the 2D communication model, i.e., the effect of terrain elevation is neglected, using the same setting parameters. The results are illustrated in Fig. 6.6a and Fig. 6.6b.

It can be clearly seen that in the scenarios when the drones fly at 200 m altitudes, a LOS condition is attained in most cases and no noticeable difference is observed. A slight difference is observed at simulation times of 280s, 400s, and 600s as the proposed model shows lower coverage due to the terrain obstacles lying between some senders and receivers. The transmitted signal is completely obstructed to reach some vehicles that become isolated, and thus, reduce the coverage. Moving forward, in another scenario where the drones are optimally deployed at 50 m altitude, the impact of using the proposed model is noticeable. The elevation of the terrain obstructs the communication between IoD nodes and some vehicles on the ground, and then more vehicles cannot communicate. The results highlighted that only 77.4% of total vehicles are covered in the proposed model, while 96.5% of total vehicles are covered in the 2D propagation model which proves that the proposed communication model shows an acceptable level of realism due to considering the impact of terrain elevation on communication.

In 2D simulation, the main factor affects the communication is the distance between sender and receiver. Thus, flying at lower altitude reduces the path loss and enhances the RSSI, resulting in covering more vehicles and enhances the normalized coverage. Conversely, flying at higher altitude increases the path

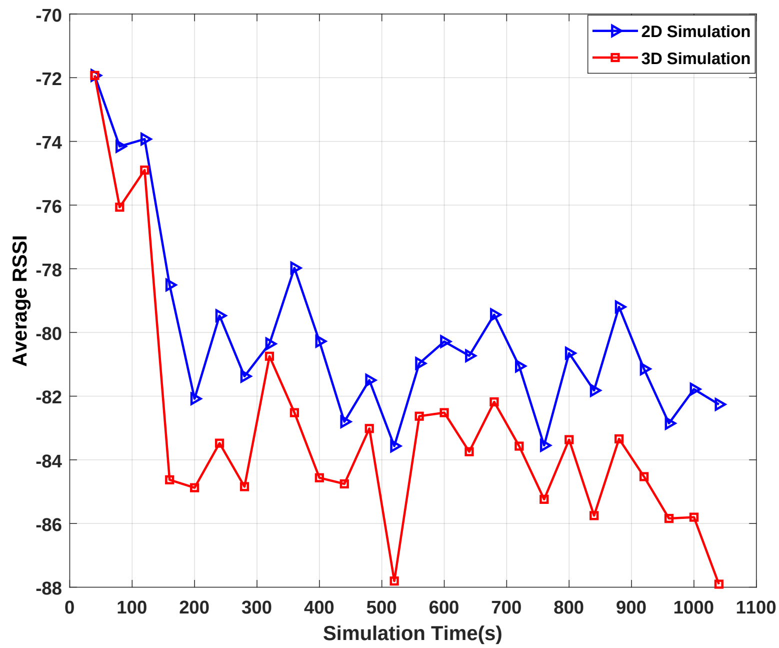

(a) 50 m deployment altitude

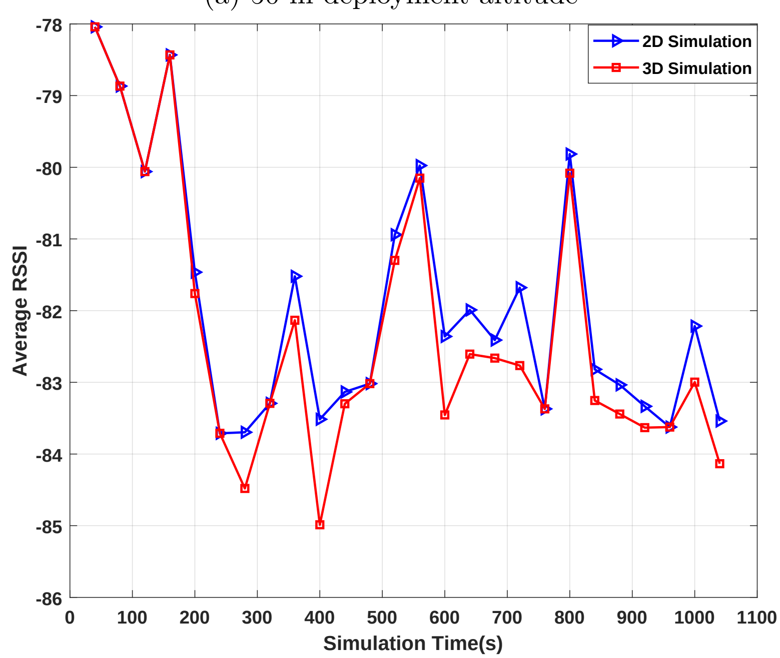

(b) 200 m deployment altitude

Figure 6.7: The average RSSI with respect to simulation time for two IoD deployment altitudes in 2D and proposed 3D propagation models.

loss and reduces the RSSI, resulting in lower vehicles covered and reduces the normalized coverage. While in 3D simulation model, two main factors affect the model, namely, the distance between sender and receiver and LOS communication to ground vehicles. There is an interesting trade off which is flying at lower altitude reduces path loss due to short distance versus reducing LOS communication to ground vehicles, resulting in covering fewer vehicles and therefore reduces the normalize coverage while flying at higher altitude increases path loss due to longer distance versus enhancing LOS communication to ground vehicles resulting in covering higher vehicles and therefore enhance the normalize coverage. This trade off is illustrated in Fig. 6.6 for different deployment altitudes. Note that, the lower deployment altitude is chosen to be 50 m where the transmitted signal is obstructed by obstacles between UAVs and vehicles while the higher deployment altitude is chosen to be 200 m in which the drone are flying above obstacles and can successfully establish the communication with ground vehicles. The idea is to demonstrate the capability of the proposed 3D propagation mode in detecting the terrain obstacles and properly calculates the received signal that reflects high level of realism results.

To further analyze the proposed 3D propagation model, the average RSSI is recorded and the results are exhibited in Fig. 6.7a and Fig. 6.7b for 50 m and 200 m altitudes, respectively. The figures include the results of the proposed communication model and the 2D propagation model. Fig. 6.7b shows the results of 200 m altitude that explains the reason why coverage is dropped at the 280s, 400s, and 600s. The simulation spots that at the same simulation time, there is a dropped in received signal strength where the lower value of RSSI is presented at 400s at about -85 dBm. At this simulation time, the signal is obstructed by higher terrain, resulting in high loss and lower covered vehicles. However, at other simulation times, the proposed communication model and the 2D communication model show similar results. On the other hand, for lower altitude deployment, i.e., 50 m deployment altitude, shown in Fig. 6.7a, the signal experiences NLOS condition in most cases. To elaborate, compared to the coverage results, the proposed communication model shows much lower RSSI at 520s simulation time. The average RSSI drops to about -88 dBm compared with the 2D communication model in which the average RSSI remains at -83.7 dBm. The results further confirm the significant impact of elevation on the signal path. At some locations, the terrain acts as an obstacle and obstructs a signal propagation.

For further evaluating the performance of the proposed communication model, we study the impact of IoD deployment altitudes on IoD2V communication. The IoD nodes are deployed at different altitudes (30m, 50m, 100m, 150m, 200m, 250m, and 300m) altitudes, and the average RSSI and normalized coverage are presented in Fig. 6.8a and Fig. 6.8b.

We can observe from the Fig. 6.8a and Fig. 6.8b that the deployment altitude has a vital impact on communication, where the VANET connectivity is enhanced as altitude deployment increases. This trend increases as the deployment altitude increases with the same transmission power until 250m deployment altitude where the highest coverage is observed (optimal altitude deployment). This is because the IoD nodes fly above high-level terrain where the LOS condition toward the ground vehicles is improved. The coverage starts decreasing as the deployment altitude increase after the optimal altitude. Although increasing the IoD deployment altitude after the optimal value will further improve the LOS condition and

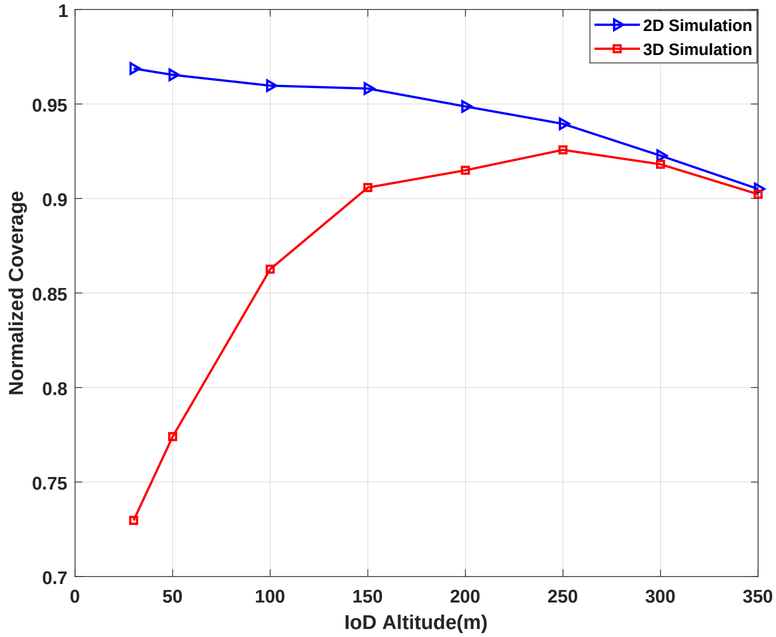

(a) Average Normalized Coverage

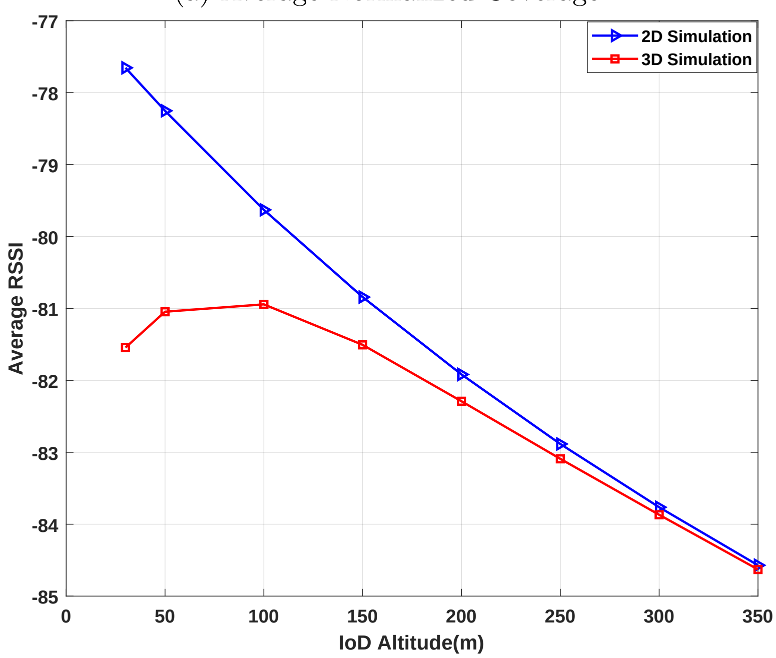

(b) Average RSSI

Figure 6.8: The average normalized coverage and RSSI for different IoD deployment altitudes.

minimize the impact of high-level terrain, it decreases the coverage and received signal quality. This is due to increasing the distance between IoD nodes and vehicles on the ground, which in turn increases the path loss. More importantly, the result shows that the proposed approach is able to find the optimal deployment altitude of IoD nodes to achieve the best performance (coverage and RSSI). It is worth mentioning that the optimal IoD deployment is obtained so as to maximize the coverage area and enhance the RSSI for such deployment. Thus, the RSSI at optimal deployment might not be the best RSSI value as illustrated in Fig. 6.8b. On the other hand, in the 2D propagation model, the main factor that affects the propagated signal is the distance between sender and receiver. Hence, the performance is degraded as the altitude of IoD deployment increases due to increasing the distance.

To further investigate the performance of the proposed 3D propagation model for IoD, we record the optimal locations of two deployed UAVs (IoD size) obtained by IPSO implementation throughout the simulation time, and connect them to create the optimal UAV paths generated by the 2D propagation model and the proposed 3D propagation model. The altitude deployment is set to be in the range [50 m to 200 m]. The result is illustrated in Fig. 6.9a where the trajectory of UAV in 2D and 3D space represents the best path to be followed to achieve the best coverage and received signal quality. The trajectories show how the dynamic deployment of UAVs should be to maximize the coverage and RSSI. It can be easily seen that the behavior of drones in 3D space differs from that in 2D space, i.e., neglecting the terrain elevation. This is due to the fact that the 3D propagation model considers the effect of terrain elevation on communication, and thus, the drones are dispatched to the most appropriate locations so as to improve the LOS condition and then increase the number of connected vehicles. Such dynamic

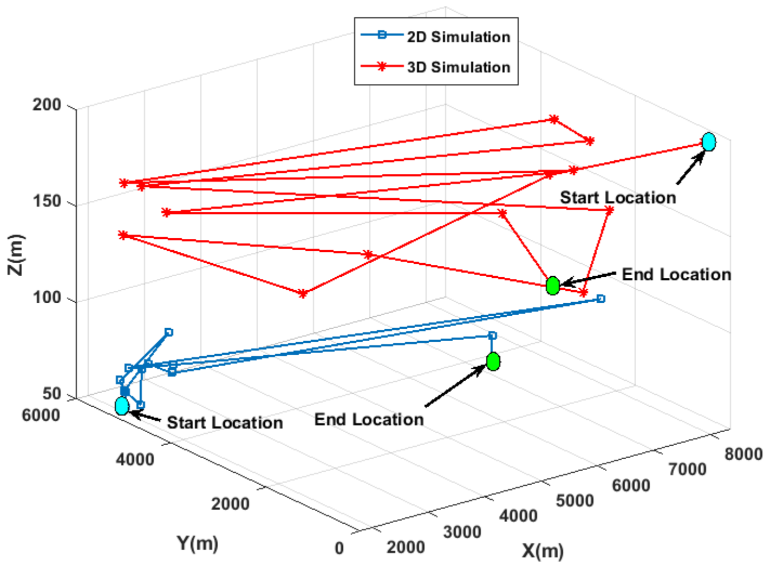

(a) UAV trajectories

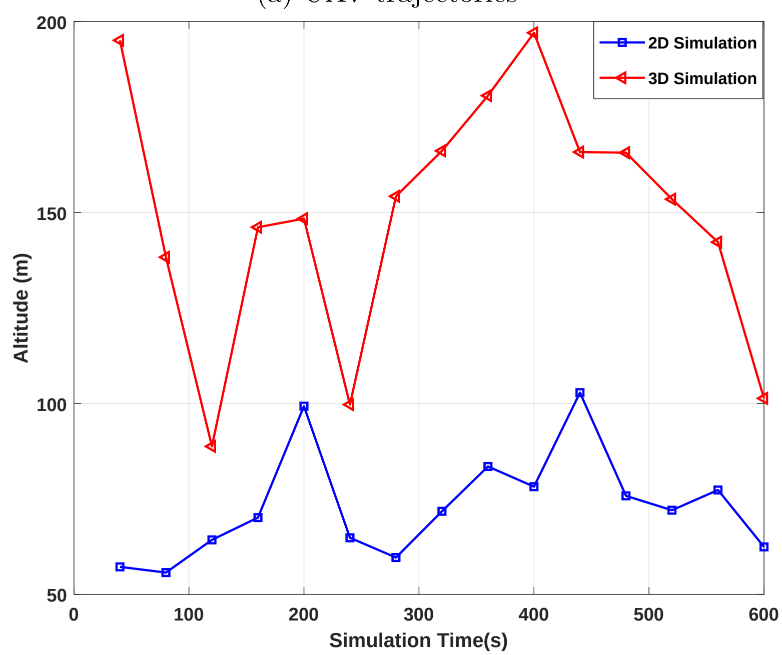

(b) Altitude variation

Figure 6.9: The trajectory of UAV and altitude variation in 2D propagation model and the proposed 3D propagation model.

movement of UAVs allows us to visualize the variation of the altitude throughout the simulation time in which the coverage is maximized and received signal quality is improved in both models as illustrated in Fig. 6.9b. This figure presents the

UAV altitudes for both propagation models after removing the terrain information from the 3D simulation. The results show that the drone tries to fly at a higher altitude in the 3D propagation model than that in the 2D propagation model. This occurs because, in the 3D model, the UAV altitude is constantly adjusted so that the signal quality toward ground vehicles is enhanced while avoiding NLOS conditions caused by terrain elevation between UAV and ground vehicles. The irregular terrain that acts as an obstacle enforces the UAV to fly at a high altitude to ensure good communication while in the 2D model, the terrain elevation is neglected, and therefore, the UAV can fly at a low altitude for better performance.

6.7.3 Three Dimension IoD-Assisted-VANET (3DIoDAV) Performance

In this subsection, we will study the effect of IoD size and transmitted power on VANETs connectivity and RSSI.

- Analyze the effect of IoD size on VANET connectivity and RSSI

In this part, the average normalized coverage and average RSSI are discussed with two altitude ranges, i.e., two scenarios. Besides, different IoD sizes are implemented with 80 mW transmission power. The results are illustrated in Fig. 6.10a for altitude range [50 m to 100 m] and altitude range [100 m to 150 m], respectively.

It is worth noting that the VANET connectivity is enhanced when integrated with IoD. This fact is illustrated in the Fig. 6.10a. As the IoD size increases, this trend increases with the same power transmission, demonstrating the impact of IoD size on the coverage. However, increasing the size of IoD might increase the interference and the probability of collision with other drones. Additionally, the drones that are close to each other play the same role and become redundant drones. For this reason, adequate distance should separate drones within their communication ranges, which is considered in this thesis.

When drones fly at low altitude, the propagated signal experiences a NLOS condition due to the terrain elevation. Generally speaking, using IoD2V communication has been influenced by two main factors, namely LOS condition and path loss. That is, deploying the IoD network at a low altitude decreases the distance between IoD and vehicles, which decreases the path loss but it reduces the probability of LOS condition. On the other hand, deploying IoD nodes at high altitudes increases the probability of LOS condition, however, it increases the distance between IoD nodes and vehicles on the ground, which in turn increases the path loss.

In the 3D propagation model where the terrain elevation is considered, deploying IoD at low altitude might increase the path loss and the IoD2V communication might be hindered by terrain elevations. Consequently, a sufficient number of isolated vehicles appears. This fact can be easily figured out in Fig. 6.10a where the average coverage is enhanced in the altitude range [100 m to 150 m] more than that in the altitude range [50 m to to 100 m]. Moreover, the IoD size also has a vital impact on VANET connectivity and received signal strength. It can be observed that the coverage is improved as the IoD size increases, and the maximum

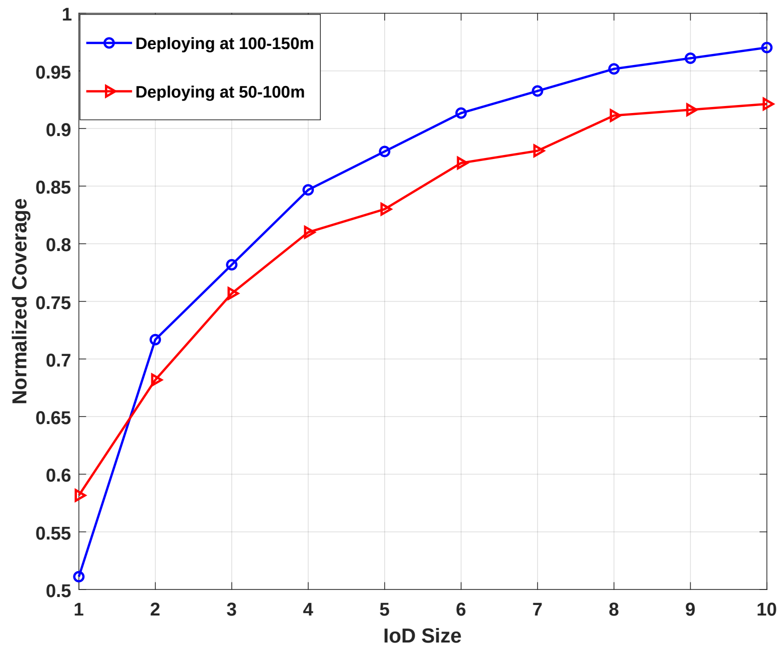

(a) Normalized Coverage

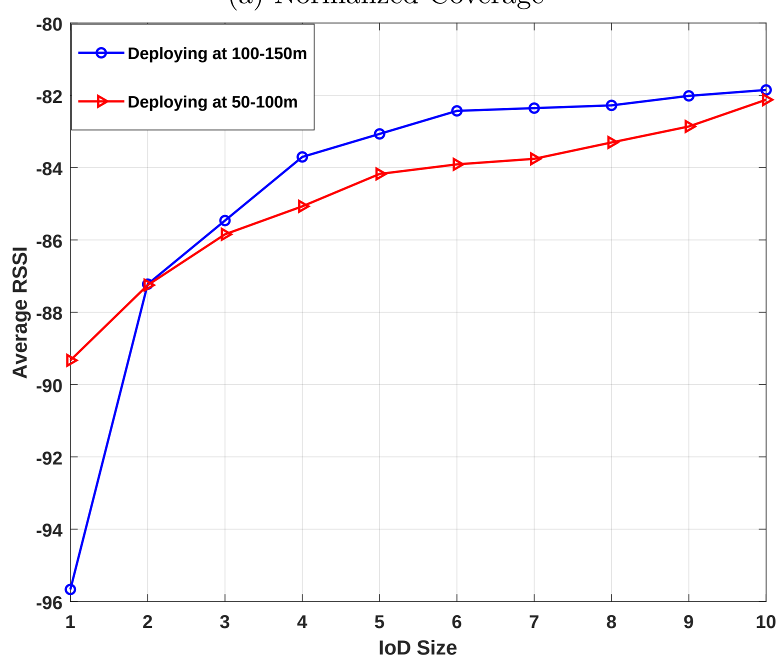

(b) Average RSSI

Figure 6.10: The average normalized coverage and RSSI for different IoD sizes in 3DIoDAV.

coverage can be reached using 10 drones in both scenarios.

For further evaluating the proposed IoD-assisted VANET performance in 3D space, the impact of IoD size on RSSI is discussed. Particularly, the RSSI is measured with respect to simulation time, and the average RSSI with respect to IoD size is illustrated in Fig. 6.10b. This figure reveals that the quality of the received signal is low at the beginning where the target area is covered by only one UAV and it is enhanced as the number of UAVs increases. This advantage tends to grow higher in the altitude range [100 m to 150 m] more than that in the altitude range [50 m to 100 m]. This is because when UAVs fly at higher altitudes, the impact of terrain on IoD2V communication decreases, which improves the LOS condition.

- Impact of transmission power on coverage and RSSI

For further investigating the effectiveness of the proposed IoD-assisted VANET in a 3D environment, we discuss the impact of power transmitted on the total coverage, i.e., average normalized coverage. The results are depicted in Fig. 6.11a and Fig. 6.11b for both scenarios.

Fig. 6.11a illustrates the normalized coverage w.r.t IoD size with different power transmission (20 mW, 40 mW, 60 mW, and 80 mW) for both altitude ranges scenarios. As such, the effect of power transmission on average normalized coverage is examined, where the average normalized coverage is noticed to enhance continuously with the increase of power transmission as expected. This intuitive proportional relationship is attributed to the fact that the higher the power transmission, the wider the coverage range and the larger the number of covered vehicles, which leads to improving the overall coverage. This tendency

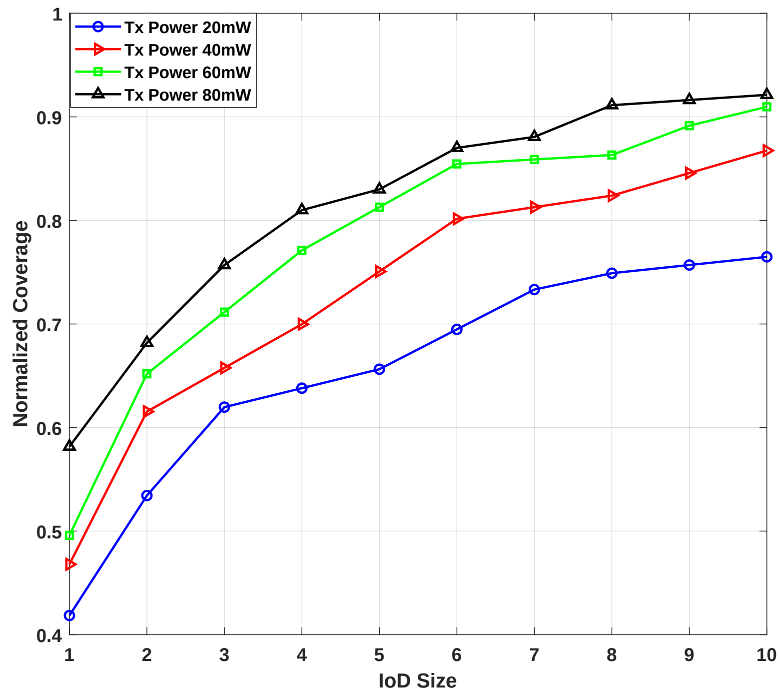

(a) 50 m to 100 m Altitude

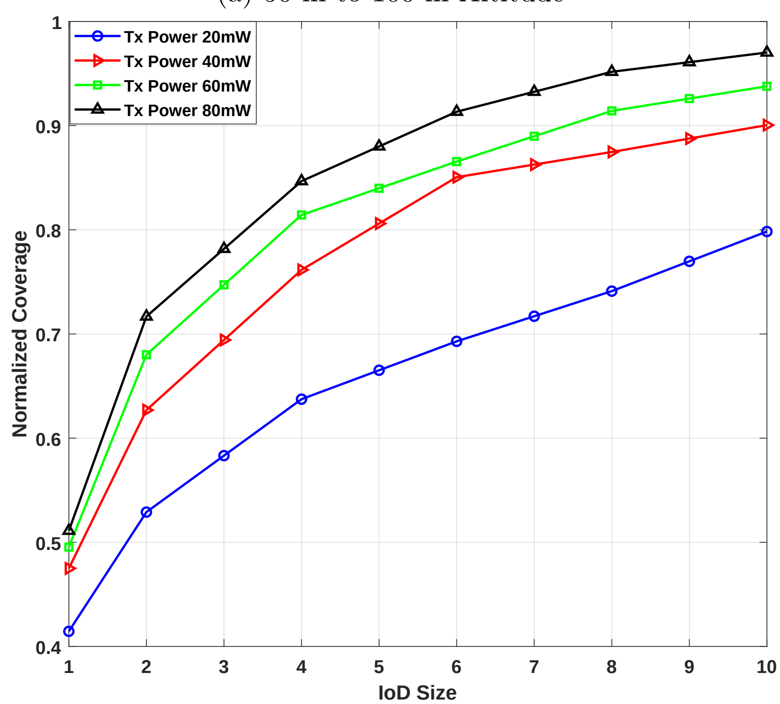

(b) 100 m to 150 m Altitude

Figure 6.11: The average normalized coverage for different transmission power values with respect to different IoD sizes in 3DIoDAV.

is evident in both scenarios and the highest normalized coverage can be achieved in scenario1 (altitude deployment range 50m to 100m) by using 10 UAVs with a power transmission of 20 mW, 40 mW, 60 mW, and 80 mW, reaches to 76.4%, 86.2%, 92.0%, and 92.2%, respectively, while it reaches to 79.8%, 90%, 93.7%, and 99.1% in scenario2 (altitude deployment range 100 m to 150 m) using 10 UAVs. We observe that 10 UAVs can cover 99.1% of isolated vehicles using power transmission of 80 mW in scenario2, while in scenario 1, the highest coverage achieved is 92%. Besides, the transmitted power has a vital impact on improving the received signal quality, where the RSSI is observed to improve as the power of transmitted signal increases as shown in Fig. 6.12a and Fig. 6.12b for both altitude range scenarios. To sum up, the power transmission has a significant impact on improving the VANETs performance.

6.7.4 Comparison with Other Approaches

In order to validate the proposed 3DIoDAV, i.e., 3D communication model is used in IoDAV, and show a better comparison, we compare the proposed 3DIoDAV against the 2D communication model and IoDAV [28]. Besides, in the comparison, we consider the average normalized coverage and RSSI as performance metrics. The comparison includes average normalized coverage and RSSI with respect to IoD size for 80 mW transmission power. We also show the effect of transmission power on coverage for 10 drones in the comparison.

Fig. 6.13a and Fig. 6.13b compare the normalized coverage using 3DIoDAV, 2D, and IoDAV approaches for both scenarios, i.e., two deployment altitudes.

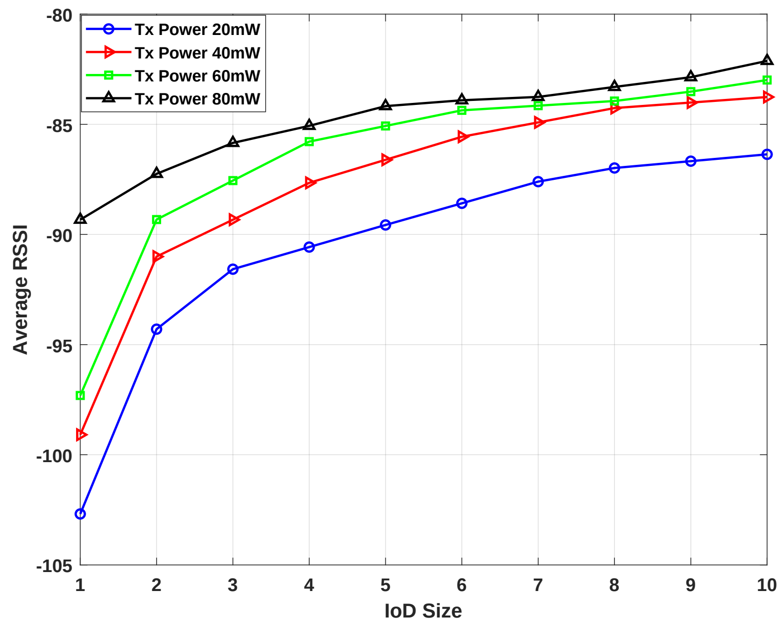

(a) 50 m to 100 m Altitude

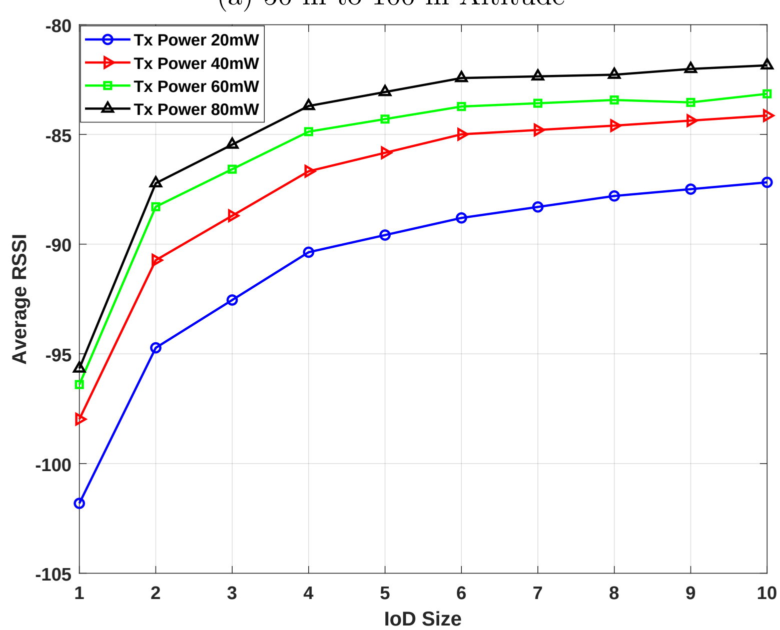

(b) 100 m to 150 m Altitude

Figure 6.12: The average RSSI for different transmission power values with respect to different IoD sizes in 3DIoDAV.

Additionally, the average RSSI are illustrated in Fig. 6.14a and Fig. 6.14b for both scenarios (altitude range1 and altitude range2), respectively. These figures show that the IoD size has a significant impact on performance where the average

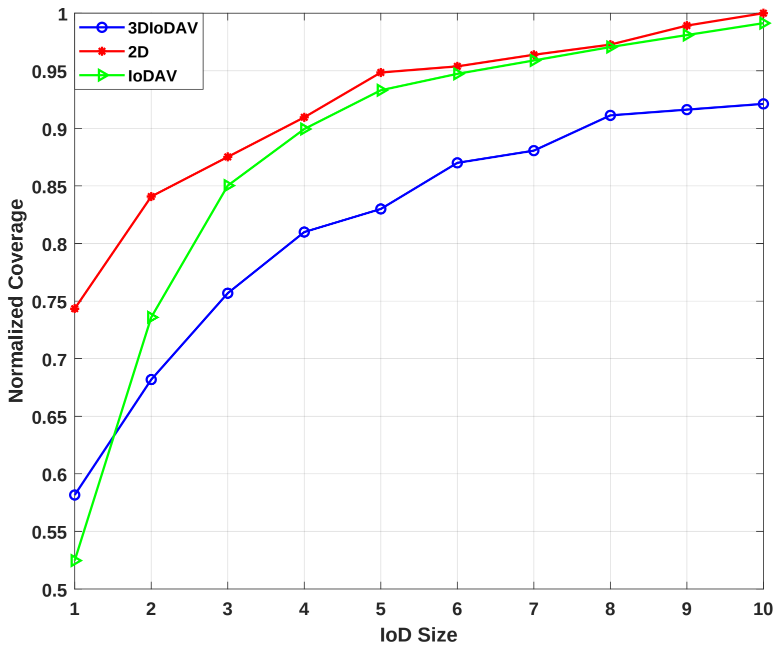

(a) 50 m to 100 m Altitude

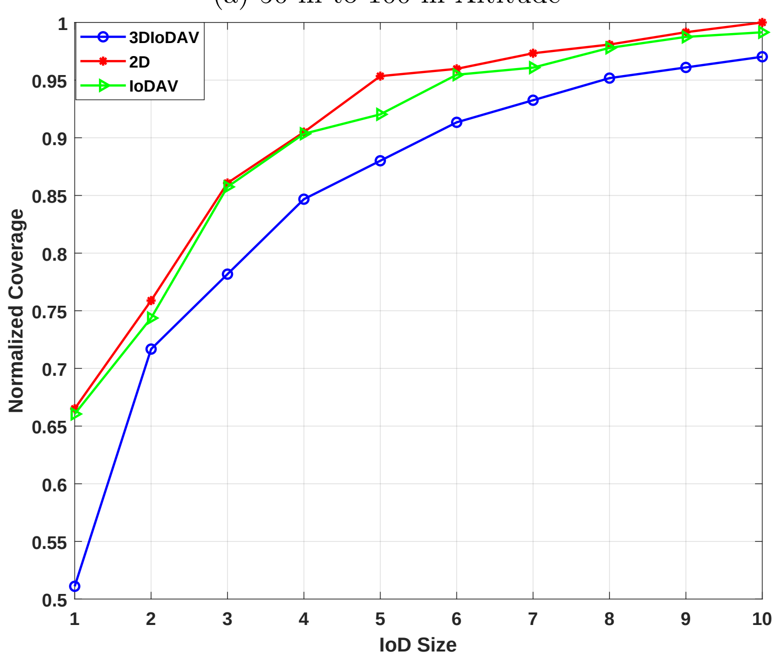

(b) 100 m to 150 m Altitude

Figure 6.13: Average normalized coverage for different IoD sizes in 3DIoDAV, 2D, and IoDAV approaches.

normalized coverage increases as IoD size increases. This tendency is evident in both scenarios. The results reveal that the proposed 3DIoDAV shows lower coverage and lower RSSI than other approaches. This is because the proposed

3DIoDAV approach considers the impact of terrain elevation on communication that is neglected in other approaches. Thus, it reflects more level of reality result than other approaches. It is observed that the coverage and RSSI are improved as altitude increases for the proposed 3DIoDAV. This can be clearly observed in scenario 2, i.e., altitude range [100 m to 150 m]. This is because when the drone flies at high altitude, the LOS condition is improved, which in turns improves the communication between IoD and vehicles. To sum up the observations highlighted in Fig. 6.14a and Fig. 6.14b, we plot the average normalized coverage and average RSSI as a function of power transmission for 10 IoD size in Fig. 6.15a and Fig. 6.15b for both scenarios.

Although the 2D propagation model and IoDAV approaches achieve better coverage and better RSSI than the proposed approach, they do not reflect the real results due to neglecting the impact of terrain elevation on communication, i.e., flat terrain is assumed. The lower coverage and RSSI shown by the proposed approach in Fig. 6.15a and 6.15b demonstrate the significant impact of terrain elevation on signal propagation, which should not be neglected. The results also demonstrate the ability of the proposed 3DIoDAV to detect the terrain obstacles and dispatch the IoD nodes to the most appropriate locations that minimize the effect of terrain elevation on communication.

Finally, to show the ability of the proposed approach to dispatch the IoD nodes to the most appropriate locations, we run the 2D simulation model and obtain the optimal locations and then evaluate the 2D optimal locations (2D deployment based) using 3DIoDAV approach. The result is compared with optimal locations

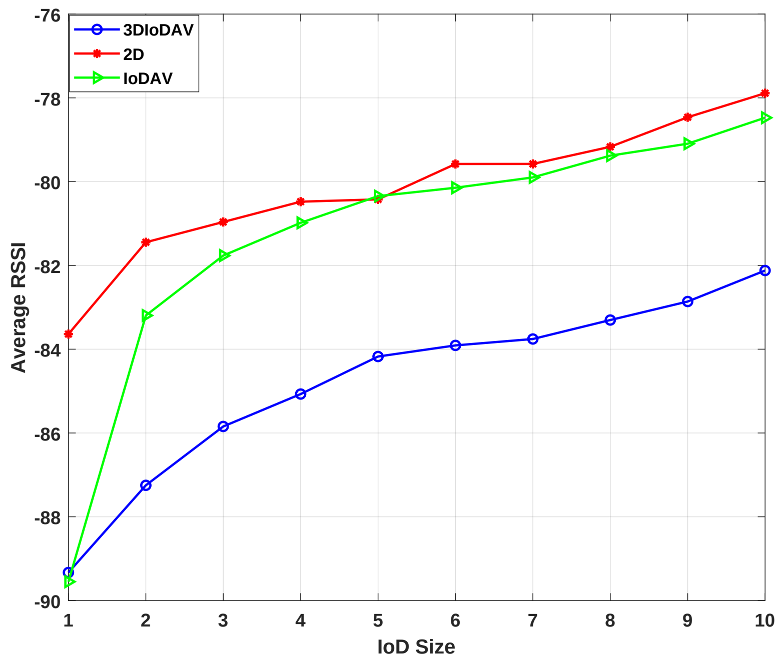

(a) 50 m to 100 m Altitude

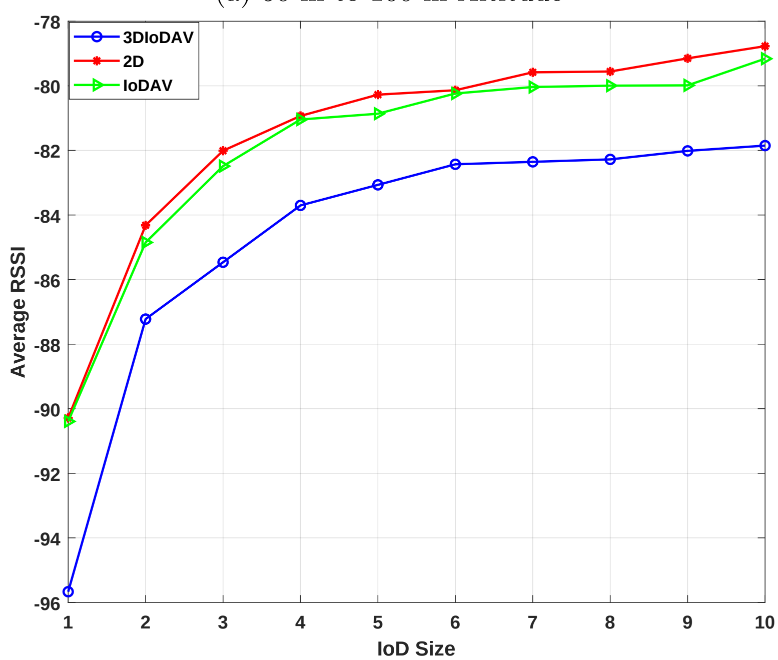

(b) 100 m to 150 m Altitude

Figure 6.14: Average RSSI for different set of UAVs in the three approaches.

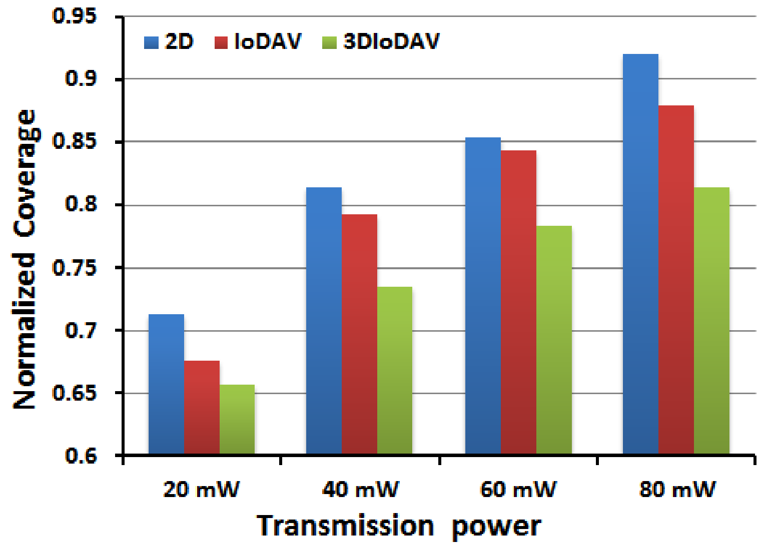

(a) 50 m to 100 m Altitude

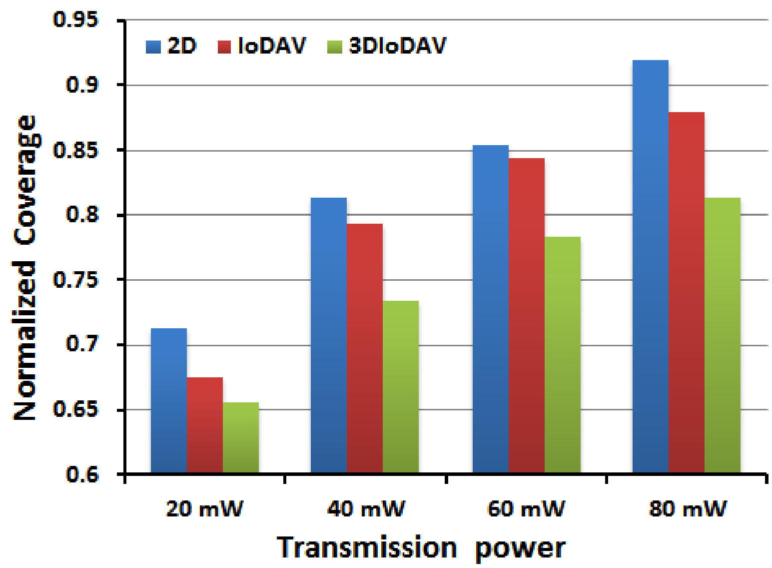

(b) 100 m to 150 m Altitude

Figure 6.15: Average normalized coverage in the three approaches for different transmission power values for 10 UAVs.

obtained by 3DIoDAV approach (3D deployment based).

The results are illustrated in Fig. 6.16a and Fig. 6.16b for normalized coverage and RSSI, respectively. It can be observed that the locations obtained by the proposed 3DIoDAV approach provide higher coverage and better RSSI than that obtained

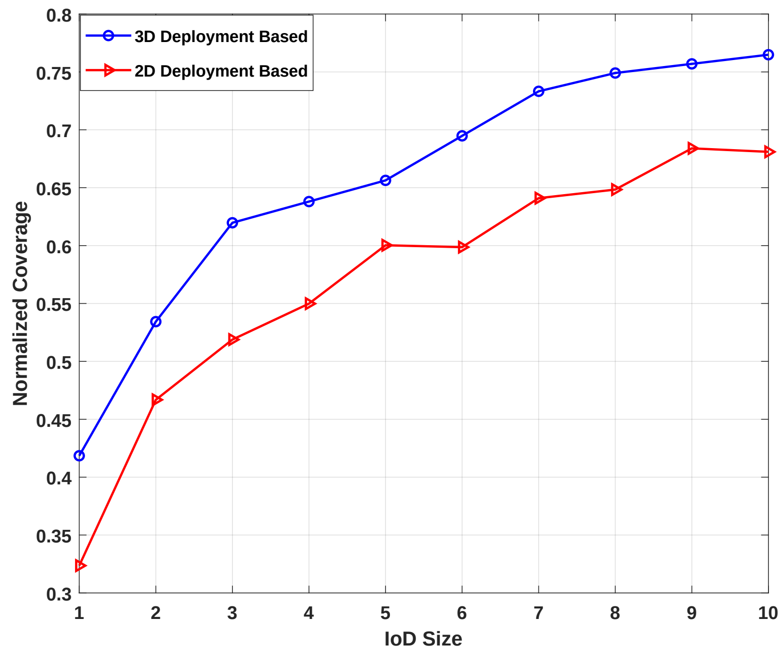

(a) Normalized coverage

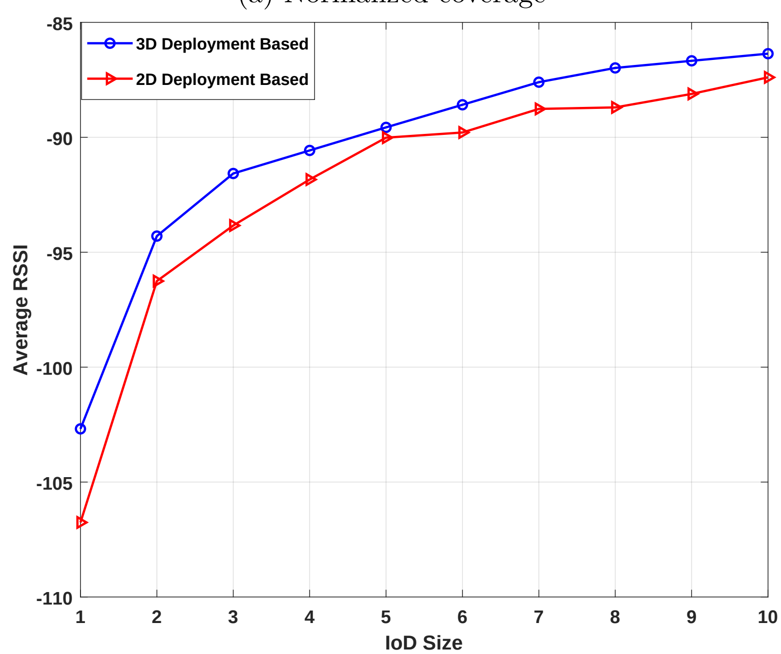

(b) Average RSSI

Figure 6.16: Two and three dimensional IoD deployment evaluated by 3DIoDAV for different sets of UAVs (a) Normalized coverage, (b) Average RSSI.

by the 2D propagation model, demonstrating the ability of the proposed 3DIoDAV to dispatch the IoD nodes to the most appropriate locations that improve the VANET performance.

6.8 Chapter Summary

In this chapter, we developed a novel 3D propagation model for IoD2V communication that considered the terrain elevation information in the communication of IoD in the air and vehicles on the ground. The proposed 3D propagation model was evaluated throughout the simulation and compared against the 2D propagation model approach. The results showed a significant impact of terrain information on communication. Specifically, the proposed 3DIoDAV had the ability to detect the terrain obstacles and properly evaluated the received signal quality. Moreover, we utilized the proposed 3D propagation model in the IoDAV approach to develop a novel 3DIoDAV approach in which the IoD network improved the VANETs connectivity. We also proposed using of an optimization approach, namely IPSO, for optimally deploying the IoD network so as to maximize the coverage area and enhance the received signal quality. More importantly, the proposed 3DIoDAV was compared with the 2D and IoDAV approaches. The comparison results illustrated that the proposed 3DIoDAV approach was able to retrieve the terrain information and considered it in the communication of IoD in the air and vehicles on the ground, which provided a high level of realism results.

CHAPTER 7

MATHEMATICAL MODEL FOR COVERAGE PATH PLANNING BASED ON MILP FORMULATION

7.1 Chapter Motivation

The terrain coverage is one of the most essential tasks of drones, which has been engaged in many applications, such as disaster management, photography, and intelligent agriculture [9], [23]. In such applications, planning an efficient flight path is a critical issue due to limited onboard battery-powered that limits the flight time of a drone. The determination of a trajectory that covers the whole region by passing through all points of the area of interest (AOI) while avoiding obstacles is called coverage path planning (CPP) [10]. The goal of the CPP mechanism is to seek an optimal collision-free flight path so that full coverage of a given region is guaranteed under specific constraint conditions, which is considered as a complicated global optimum problem. The quality of area coverage alone is not the exact metric for achieving high-quality missions. Instead, several operational objective goals, constraints, and restrictions have to be jointly optimized. The constraints and objectives are the two aspects that underpin any mission planning. The overall outputs quality from a mission mainly depends on optimizing final planning to account for both constraints and objectives. These constraints and objectives are required in mission planning for deriving a detailed agenda for a drone in terms of how it should be traveling through an ROI.

Despite UAVs' ample applications, the onboard energy has fundamentally limited the UAV performance and endurance, which is practically finite. Several works in the literature have presented area coverage using a single UAV, whereby a simple task is done by only one autonomous UAV in small areas such as room cleaning. However, in outdoor like broader area coverage, a UAV may not complete the mission due to battery drainage, and it should stop for refueling. For this reason, the best coverage trajectory for UAV should be obtained such that the energy cost is reduced as much as possible when the optimal coverage path is obtained. Hence, energy-efficient system coverage path planning for maximizing the coverage of a target region is of paramount importance.

Several applications have outgrown the capability of a single drone. Thus, coverage efficiency has been improved by deploying multiple UAVs. This is because multi-UAV provides more significant advantages over a single UAV in CPP robustness enhancing and operational time minimization [106]. Furthermore, in large-scale real-time and distributed collaborative systems, there is an increasing tendency to adopt multiple UAVs for detecting or searching missions. For example but not limited, in an agriculture domain, multiple UAVs cooperate, monitoring the weed, vegetation growth terraces, and states in forests. It is noteworthy mentioning that adapting multiple UAVs has dramatically improved the overall performance and energy conservation. It can be employed when the region size is too large to be covered by a single UAV, thus, significantly reducing the completion time.

Although adapting the swarm of drones in coverage path planning achieves flexibility enhancement and cost reduction in practical applications development, carrying out their path planning in a complex and large-scale environment increases the complexity of collaborative control and decision-making systems [24]. Such strategies have a significant impact on coverage problem efficiency because generating trajectories require several constraints and high levels of coordination, which are highly dependent on the positions of UAVs.

For handling multiple constraints, many approaches in the literature have formulated the CPP problem based on mixed-integer linear programming (MILP) [151]–[153]. Exact optimization approaches, such as dynamic programming, branch-and-bound, and constraint satisfaction, have been used to solve the problem via a MILP formulation for optimality using standard solvers in [151], [152]. Nevertheless, they are computationally intensive or intractable with hard constraints. Besides, for large-scale problem size, the exact solver fails to obtain the optimal path in a reasonable time.

7.2 Chapter Contribution

To handle the issues discussed above in a tractable manner, we propose a coverage path planning algorithm that aims to achieve full coverage of the ROI. To this end, in a large-scale problem size in which the exact solution fails to find a solution in a reasonable time, a heuristic approach is implemented to address a large-scale problem in a reasonable time. Most research has focused on obtaining the shortest path coverage and neglected the energy consumption, which depends mainly on acceleration, deceleration, distance, and speed of the drone. To fill this gap, a more accurate model with energy consumption constraints is provided to calculate the energy-efficient optimization trajectory. The problem is formulated as a MILP based optimization problem. The proposed approach composes of two phases. In the first phase, the AOI is decomposed into small cells, where the centers of these cells are known as Point of Interests (POIs) or waypoints. The cells that constitute the ROI, are covered in the second phase when a UAV passes through their centers. The contribution of this chapter can be summarized as follows:

- We develop an optimization formulation of single and multi-UAVs coverage path planning. Mixed-integer linear programming is used to formulate the CPP problem as a minimization problem, where the energy consumption is used as the objective to be minimized. The proposed approach can reduce energy consumption which in turn reduces the required number of drones to cover the ROI. Since the turns have a significant effect on energy conservation, the number of turns is included in the objective function to be minimized.

- The collision avoidance mechanism is proposed to avoid collision with terrain obstacles by designing the required constraints in the proposed formulation. As a result, the proposed CPP approach not only determines the optimal flight path for UAVs but also avoids collision with region obstacles that guarantee to complete the task safely. The proposed CPP problem is solved using the exact approach, i.e., CPLEX solver, and a heuristic approach, i.e., simulated annealing and greedy approaches. The results are analyzed and compared.

- The proposed approach considers small and large ROI, and uses single and multiple drones. In a single UAV scenario, the proposed approach provides multiple trips for a large regional area. Particularly, if the energy of the UAV is not sufficient to cover the whole region, the UAV is allowed to return to the depot and recharges its battery to start the next trip till completing the coverage mission. For multiple UAVs, the proposed approach provides a decomposition mechanism to decompose the region into subregions and allocate the subregions to the available UAVs. The region allocation aims to balance the energy consumption and reduce the completion time. The subregions are created to minimize the overall energy consumption for coverage.

For UAV safety, the proposed CPP approach provides an energy calculation or constraint so that the drone can safely return to the depot for recharging.

7.3 Energy Model For UAV Coverage Path Planning

In spite of the significant features of UAVs, the full potential of their applications is still hindered. The limited lifetime of drones due to onboard battery-powered is considered the main limitation [7], [154], which causes incomplete missions in some applications. The coverage path planning mission should be done with minimum energy consumption to cope with such limitations. In this chapter, the CPP problem is formulated and optimized as a minimization problem. The objective function involves energy consumption which is minimized by the optimization approach. That is, the optimal coverage path is selected to fully cover the target area with minimum energy consumption.

It has to be stressed once again that the number of turns has a significant impact on energy consumption. Hence, to further optimize the coverage path, the number of turns is included in the objective function to be reduced. Moreover, the CPP approach is proposed to determine the collision-free path that guarantees to cover the target region with minimum energy and safely returns to the depot.

The energy model for a quadrotor drone in [63] is utilized in our work to calculate the energy consumption during a drone flight mission. The energy model was derived from real measurements, and the effect of different factors on energy consumption is studied. The real experiments considered different maneuvering activities like flying vertically up and down, flying horizontally, hovering, and turning. The energy consumption was obtained as a function of speed. The power consumption (P) was measured during such operations, and the fitting curves were estimated and plotted in [63]. In path planning, we focus on the impact of movement (such as hovering, horizontal movement, vertical movement, and turning) on energy consumption. Thus, the energy consumption for each operation is obtained in [63]. The energy can be written as follow

$$E = E_{climb} + E_{desc} + E_{hover} + E_{horiz} + E_{turn}. \tag{7.1}$$

The power and the time needed during rotations were measured. The angular speed turn was assumed to be w_{turn} (2.1 rad/s) and the corresponding power P_{turn} (225 W/s) which is considered to be constant during rotations. Then, the energy required to cover an angle θ can be computed as

$$E_{turn} = P_{turn} \frac{\Delta\theta}{w_{turn}}. \tag{7.2}$$

Other terms are explained in details in Section 4.3.

7.4 Energy-efficient UAVs Coverage Path Planning Approach Description

The coverage path planning algorithm needs to find the optimal coverage path from a base station, i.e., depot, covering the target region and then returning to the depot. To do so, we divide the coverage path planning into two stages. In the first stage, the ROI is decomposed into small cells, which need to be surveyed by UAV. Then the problem is formulated and solved using both exact and heuristic solvers in the second stage. The proposed coverage path planning framework is shown in Fig. 7.1 and illustrated in algorithm 5.

The proposed approach first decomposes the target region into cells, called PoIs, based on the drone camera footprint. Then, the path is planned in the coverage path planning stage, i.e., second stage, where the problem is formulated based on MILP and solved by both exact and heuristic approaches. Due to the complexity of the exact solver, the maximum CPU time is set to a reasonable time, and the best solution of all (exact and heuristic) is selected. The output of the algorithm is a collision-free path that guarantees covering the target region. In algorithm 5, the proposed approach consists of many parts. It starts with the initialization part that receives the region boundaries and uses a decomposition strategy to generate the waypoints to be covered by the drone. The energy matrix is also obtained in this stage. The second stage, as shown in Fig. 7.1, then formulates the problem as MILP formulation and solves the problem using exact and heuristic approaches. The best solution of exact and heuristic is selected as the optimal solution. The proposed strategy can reduce the energy consumption required to fully cover the ROI as much as possible. This section will explain the parts of the proposed approach in detail.

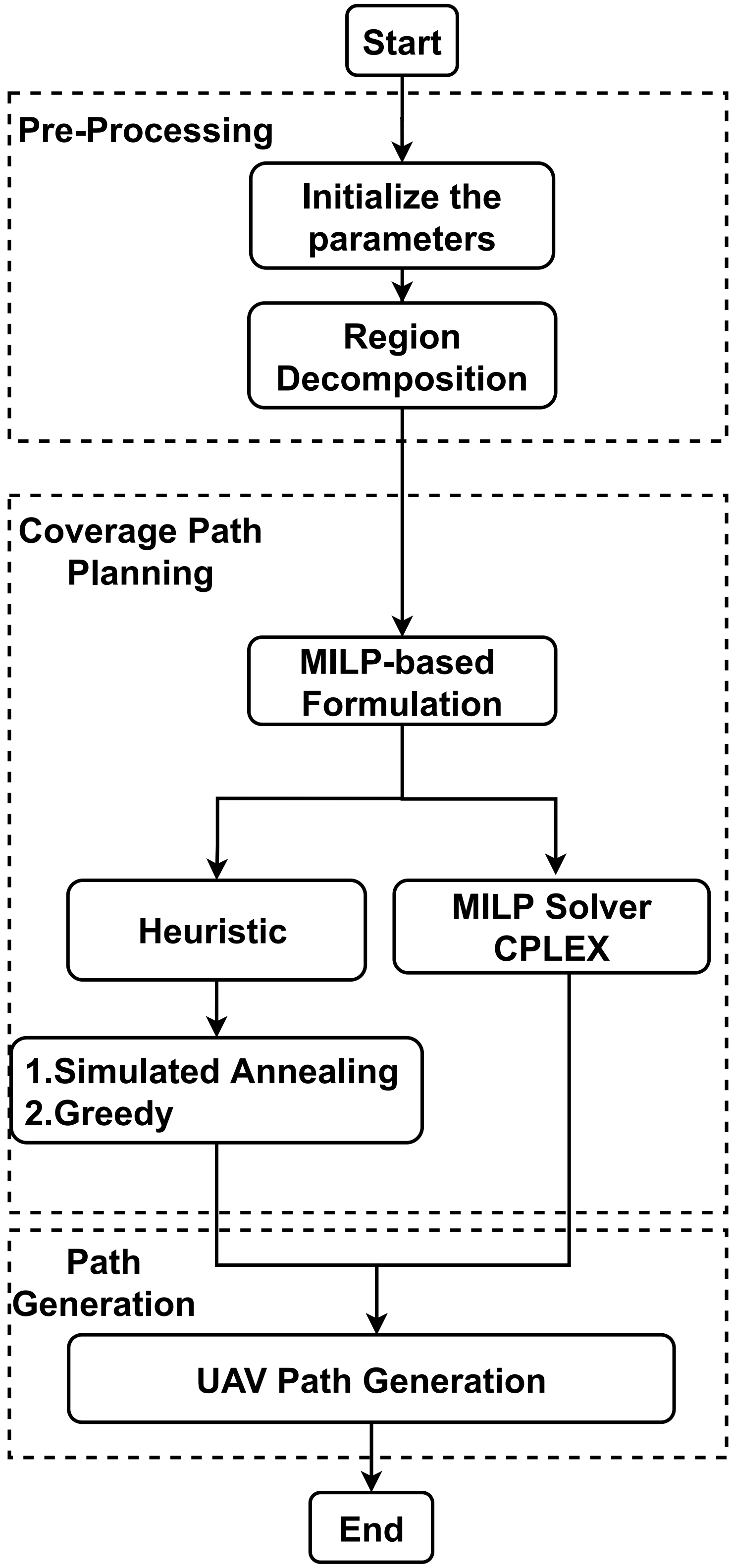

Figure 7.1: Two phases Energy-Efficient coverage path planning approach.

Algorithm 5 Energy-Efficient for UAVs CPP Algorithm

Input:

Region (R), Obstacles(Obs)

Output: Optimal CPP path

INITIALIZATION:

RD← Decompose(R,Obs), PoI(1:length(RD)).WP←RD;

EMatrix← Calculate the energy matrix

Formulation← Formulate the problem based on MILP.

NoD← Number of available UAVs

begin

  if $NoD > 1$ **then**

    SubReg ← RegionAllocation(PoI)

    Exact_*Solution* ←

    CPLEXSolver(SubReg, Formulation, E_{Matrix})

    SA_*Solution* ← SA(SubReg, E_{Matrix})

    Greedy_*Solution* ← Greedy(SubReg, E_{Matrix})

  else

    Exact_*Solution* ← CPLEXSolver(RD,Formulation,E_{Matrix})

    SA_*Solution* ← SA(RD,E_{Matrix})

    Greedy_*Solution* ← Greedy(RD,E_{Matrix})

  end

  Optimal solution ← Best(Exact, heuristics)

  Return optimal solution

end

7.4.1 Region Decomposition

To achieve better coverage, the ROI is decomposed into cells. The cell size is determined by UAV's camera footprint and can be fully covered when a UAV is passing through its center, as illustrated in Fig. 7.2.

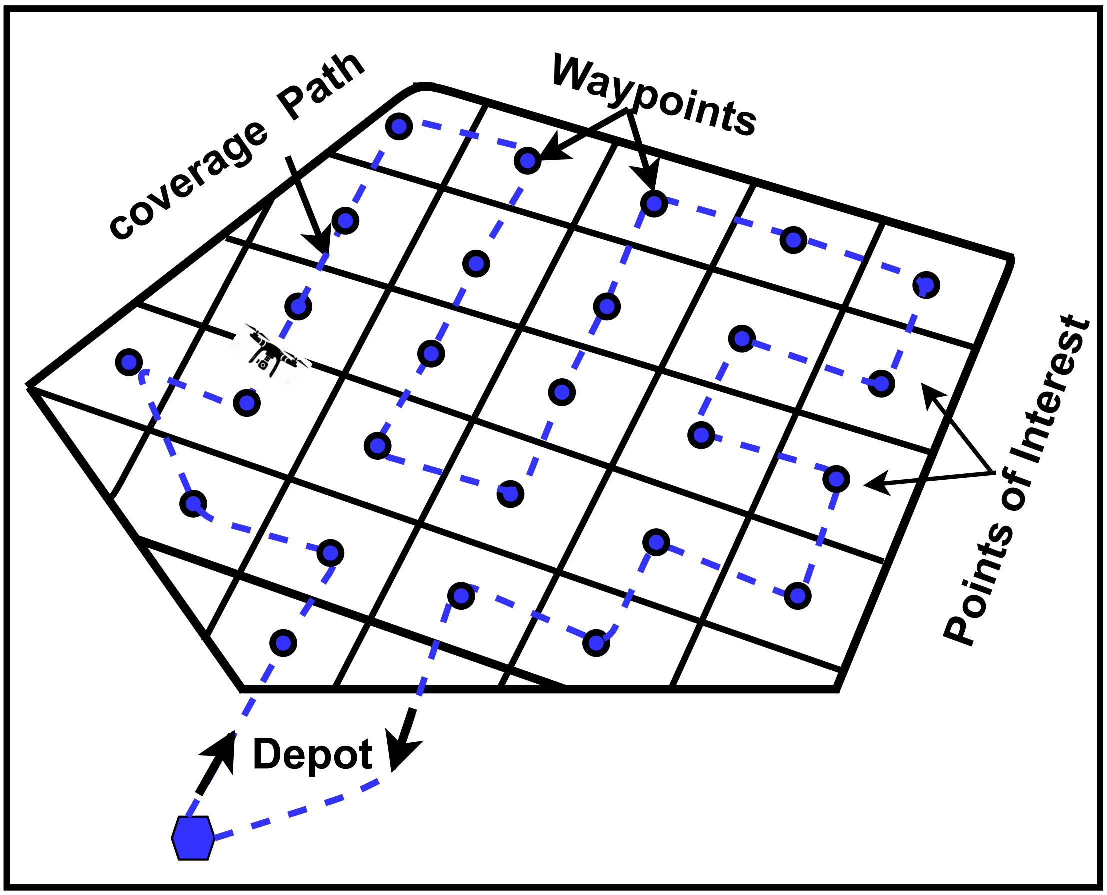

Figure 7.2: Region decomposed and covered by covering a set of waypoints and returning to the depot.

7.4.2 Problem Description and Formulation

Given an ROI, depot, and UAVs, the aim is to minimize the energy consumption and maximize the coverage region simultaneously. The output of the proposed path planning algorithm is the optimal collision-free flight path with minimum energy consumption for all drones with the following requirements: UAVs can refuel at a depot, i.e., base station. Moreover, the UAVs take off and land at the depot. To this end, the following assumptions are made.

- The flight trajectory for UAV is planned in a static manner. In other words, the path of a UAV is planned in advance, i.e., before the beginning of a mission.

- The drone is equipped with a download-facing camera with its coverage capacity known in advance.

- The drone flies at a fixed altitude, and thus, the problem has been simplified to 2D CPP problem.

- The ROI can be any shape, squire, circle, polygon, etc.

The objective is to fully cover the ROI with minimum energy consumption. Hence the objective function is a minimization problem. Moreover, the decision variables are inspired by the classical MILP formulation.

Let N is a number of positions or waypoints (1 - depot, 2,..., N) in the ROI that are required to be covered by N_d drones, d_{ij} is a distance from $position_i$ to $position_j$, E_u is the available energy of each UAV u, Eij is the energy consumed to fly from $position_i$ to $position_j$, OCij is the cost due to terrain obstacles and can be formulated as follow

$$OC_{ij} = \begin{cases} inf & \text{if the path from position}_i \text{ to position}_j \text{ goes through obstacle} \\ 0 & Otherwise. \end{cases}$$

The decision variable x_{uij} can be represented as follow:

$$x_{uij} = \begin{cases} 1 & \text{if a drone u flies from position}_i \text{ to } position_j \\ 0 & Otherwise. \end{cases}$$

The objective of these constraints is to generate a collision-free path so that the ROI is fully covered with minimum energy consumption. Thus, the objective function considers both coverage and drone's safety mission, i.e., collision avoidance with terrain obstacles.

With this definition, the formulations of MILP are listed bellow. The objective function is a minimization problem and can be formulated as

$$min\ \Gamma = \sum_{i=1}^{N} \sum_{j=1}^{N} (E_{ij} * x_{uij} + OC_{ij} * x_{uij}), u \in [1, N_d]. \tag{7.3}$$

Subject to the following constraints:

$$\sum_{j=1}^{N} x_{uij} = 1 \quad \forall i = 2, ..., N, \forall u = 1, ..., N_d. \tag{7.4}$$

$$\sum_{j=1}^{N} x_{u1j} = \sum_{j=2}^{N} x_{uj1} = u, \quad \forall u = 1, ..., N_d. \tag{7.5}$$

$$\sum_{j=1}^{N} E_{ij} - \sum_{j=1}^{N} E_{ji} = 0, \forall i = 2, ..., N. \tag{7.6}$$

$$\sum_{i=1}^{N} \sum_{j=1}^{N} E_{ij} * x_{uij} \leq E_u. \tag{7.7}$$

$$0 < E_{ij} * x_{uij} + E_{j1} \leq E_u \forall i, j = 1, ..., N, u = 1, ..., N_d. \tag{7.8}$$

$$\sum_{u=1}^{N_d} \sum_{j=1}^{N} x_{uij} = 1 \quad \forall i = 1, ..., N. \tag{7.9}$$

$$x_{uij} \in [0, 1] \forall i, j = 1, ..., N. \tag{7.10}$$

The objective function in Eq.(7.3) minimizes the total traveling energy consumption across all waypoints inside the ROI. The first part of the objective function is energy calculation for traveling across all waypoints while the second part adds a penalty, i.e., cost, if the path from $waypoint_i$ to $waypoint_j$ is passing through an obstacle that prevents collision with terrain obstacles. The constraint in Eq.(7.4) indicates that each position is preceded and preceded by exactly one another position except the depot. The constraint in Eq.(7.5) indicates that each UAV departs from the depot and returns to the depot, i.e., the initial location of the drone or base station. Eq.(7.6) presents the constraint that flying from $waypoint_i$ to $waypoint_j$ or from $waypoint_j$ to $waypoint_i$ consumes the same energy. The constraint presented in Eq.(7.7) indicates that the required energy to accomplish the trip by drone **u** should be less than the available energy of the drone. For large regions in which the available energy of the drone is not sufficient to cover the region, the drone will return to the base station for recharging and complete region coverage. The constraint in Eq.(7.8) explains that the drone cannot fly from $waypoint_i$ to $waypoint_j$ unless its available energy to travel from *waypoint*i to $waypoint_j$ and from $waypoint_j$ to the depot is sufficient. This constraint guarantees a safe return to the depot. For multi-UAV, constraint in Eq.(7.9) ensures that only one UAV flies from $waypoint_i$ to $waypoint_j$ and only once. Finally, Eq.(7.10) shows that x_{uij} is a binary variable.

7.4.3 Sub Region Allocation to Multiple UAVs

In multiple UAVs, the large region is decomposed depending on the available number of drones. This step aims to prevent drones from intra-collision and balance the energy consumption for different drones. To do so, the region is decomposed into M cells, which are grouped into N groups, i.e., N sub-regions, where the number of sub-regions is equal to the number of drones. The allocation algorithm is illustrated in algorithm 6. The algorithm receives the PoI and the available number of drones. Without loss of generality, the sub-regions or groups are created as follow:

$$SubRegion_i = [M/N * (i-1) + 1 \ to \ M/N * i]. \tag{7.11}$$

To elaborate, assume that two available UAVs cover a region. The whole region is divided into two groups that are determined with different colors, as illustrated in Fig. 7.3.

For further optimizing the energy consumption, we further optimize the assigned group to UAVs. To clarify, the waypoints in different positions are swapped and the crossover between different groups is done so that the overall energy cost is minimized as explained in algorithm6 (Optimize(SubR)).

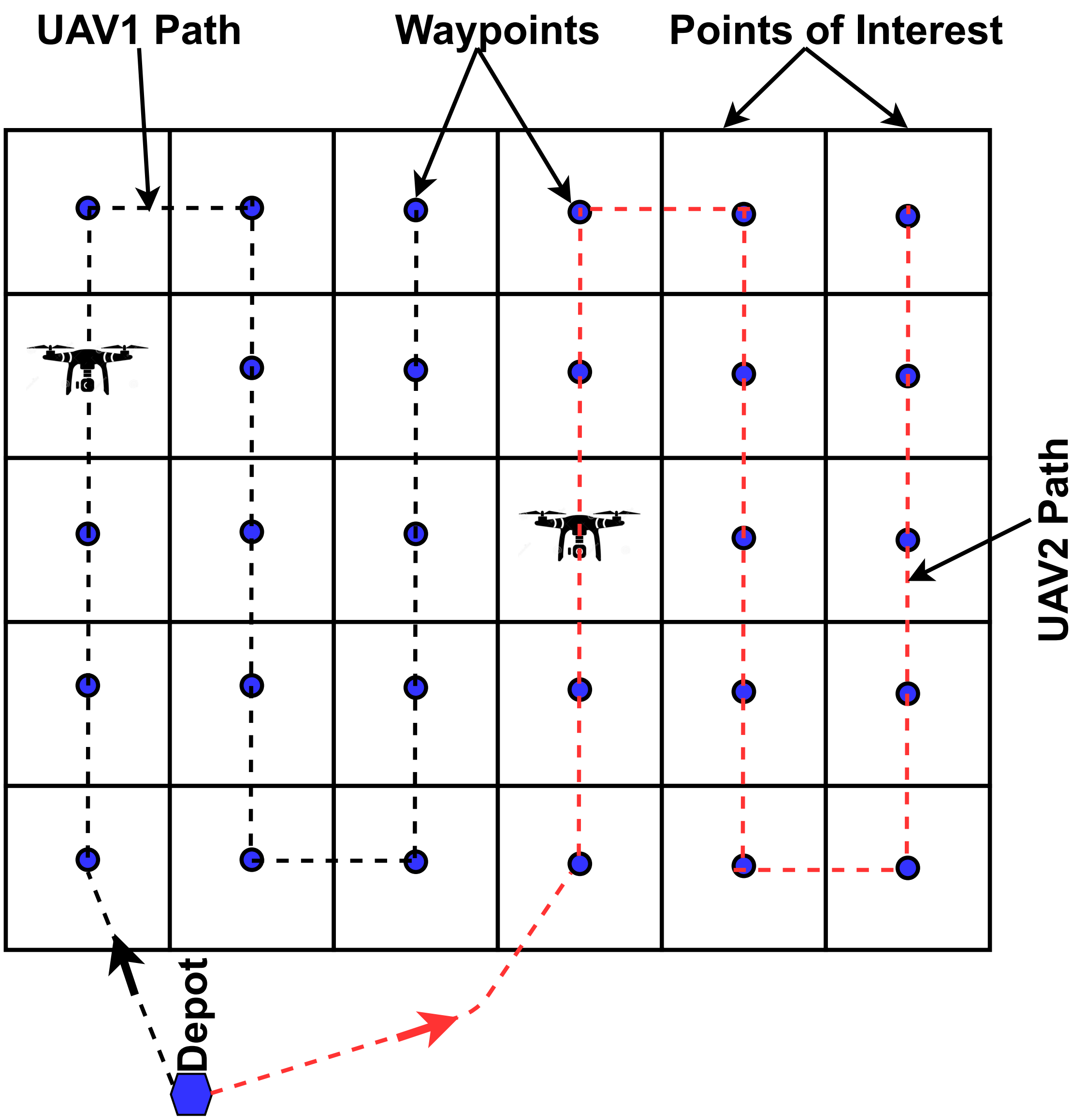

Figure 7.3: Region decomposed and allocated among two UAVs starting from the same depot.

Algorithm 6 sub-region Allocation Algorithm

Input:

UAVs (NoD), PoI

Output: optimal CPP path for all UAVs

begin

INITIALIZATION:

M ← size(PoI)

U ← NoD;

SR ← M/U;

// Assign Subregions to UAVs

for $u \leftarrow 1$ **to** U **do**

Indx← [(u-1)*SR+1 u*SR]

SubR(u)←PoI(Indx)

end

OpUAVsPath=Optimize(SubR)

Return OpUAVsPath

end

7.5 Heuristic Optimization Solution

The problem formulation of the proposed coverage path planning approach is similar to Vehicle Routing Problem (VRP) which is an NP-Hard problem. The aim is to fully cover the ROI by passing through all waypoints, and minimizing energy consumption.

The exact solution will achieve the best trajectory for drones by completely exploring the solution space if no time limit is set. For small-scale problems, the solution can be obtained within acceptable time consumption. Unfortunately, the solution space is significantly exploding for large-scale and complex system problems, resulting in an inefficient application of such formulation due to the required time consumption. Therefore, the linear programming-based formulation efficiency is unacceptable, especially in large-scale cooperative real path planning. To handle this issue in a tractable manner, we propose implementing simulated annealing [110] and greedy search [155]. This section, will explain these meta-heuristic approaches to solve the formulated CPP problem.

7.5.1 Simulated Annealing Solution for Coverage Path Planning Problem

One approximation approach for solving the large-scale coverage path planning is simulated annealing. The SA [156]–[158] is a single-solution meta-heuristic based on the concept of the neighborhood to improve the quality of the current solution. The SA, inspired by physical annealing process used in metallurgy, begins the search with a single initial solution. Then, the initial solution is updated through a series of modifications depending on its neighborhood. The purpose of these local changes is to explore the neighborhood of the solution to gradually improve its quality during the iterations. The quality of the final solution especially depends on the modifications made by the neighborhood operators. The pseudo-code of the algorithm is shown in algorithm 7.

The SA starts with an initial part that is responsible for initializing the algorithm's parameters such as initial temperature, stop temperature, and damping rate of the temperature. The initialization part is also responsible to create the initial path, i.e., sequence of waypoints to be followed. It receives parameters and constraints and the best path that achieves the full coverage of ROI with minimum energy consumption is returned. For each iteration, a new solution, i.e., path, is generated from the current solution neighborhood, and the feasibility of the new solution is checked for ensuring that no constraint is violated. Then, the feasible solution is assessed by the objective function and the best solution so far will be stored with the corresponding fitness, i.e., energy consumption. Otherwise, the feasible solution will be accepted as a new solution with probability P, called acceptance probability function, which can be calculated as :

$$P = \begin{cases} 1 & \text{if the cost of current solution} < = \text{minCost}, \\ e^{-\delta/T} & \text{if the cost of current solution} > \text{minCost}, \end{cases}$$

where δ is the difference between the fitness value of the current solution and the best solution. The current solution can be accepted if $p = 1$, i.e., $\delta < 1$, or the random number generated (r_n) is less than P. Note that the objective function receives the path and calculates the energy required by the drone to follow that path.

It has to be stressed that the orders of two cells' positions is randomly exchanged to generate a new solution. Then the transition will occur if the quality of the current solution, i.e., the energy consumption of the new path, is better than the best solution. In the Metropolis criterion, the iteration process is controlled by the temperature T, which controls the whole algorithm. Once all iterations finish, the current temperature is gradually reduced. In this stage, the current temperature is multiplied by the cooling rate to obtain the next temperature (T=T*r) and the iteration starts again. This process is terminated when the temperature reaches stop temperature criteria and the best path so far for UAV is returned.

Algorithm 7 Simulated Annealing algorithm

```
Input :Waypoints←XY-Coordinate, Em←Energy matrix
Output : Optimal solution
INITIALIZATION:
T ← initial temperature
r ← Temperature damping rate
Ts ← Stop temperature
Model ←CreateModel(Waypoints, Em)
InitialRoute ←Generate initialroute(model)
Path ← InitialRoute
begin
    Cost← Obj-Func(path, model)
    MinCost← Cost
    MinPath← Path
    Max_It: maximum iteration
    while T ≥ Ts do
        Iter←1
        while Iter <= Max_It do
            Newpath←Neighbor(Path)
            NewCost←Obj-Func(Newpath, model)
            δ←NewCost-Cost
            if δ < 0 then
                Cost← NewCost
                Path ← Newpath
            else
                P ← e^−δ/T
                if r_n < P then
                    Cost← NewCost
                    Path← Newpath
                end
            end
            Iter← Iter+1
        end
        if Cost < MinCost then
            MinCost← Cost
            MinPath← Path
        end
        T←T*r
    end
    Return Optimal solution
end
```

7.5.2 Greedy Approach Solution for CPP

The greedy algorithm is an iterative heuristic that obtains a local optimum at each iteration. It is used to address optimization problems, where a solution is constructed through a sequence of available choices. At every step, once the choice is made, subsequent steps are not changed [159]. The global optimum solution is not always obtained. Instead, an optimal local solution is obtained in less time. The process of calculating the minimum energy consumption in greedy is the same as simulated annealing without making mutation, inversion, and temperature damping. For this reason, it cannot always find a globally optimal solution. The greedy algorithm is easy to implement due to its simplicity and it is generally faster. However, finding the globally optimal solution is not guaranteed due to the short-term solution [160]. The pseudo-code of the greedy algorithm for CPP is explained in algorithm 8.

Algorithm 8 Greedy algorithm

Input :

Waypoints← XY-Coordinate, Em←Energy matrix

Output : Optimal Path

INITIALIZATION:

Model ←CreateModel(Waypoints, Em)

InitialRoute ←Generate_initialroute(model)

Path ← InitialRoute

begin

Cost← Obj-Func(path, model)

MinCost← Cost

MinPath← Path

Max_It: maximum iteration

Iter←1

while *Iter <= Max_It* **do**

Newpath←Neighbor(Path)

NewCost←Obj-Func(Newpath, model)

δ←NewCost-Cost

if $\delta < 0$ **then**

MinCost← NewCost

MinPath ← Newpath

end

Iter←Iter+1

end

end

7.6 Simulation Results and Discussions

In this section, the correctness and efficiency of the proposed approach are verified. The exact solution is compared against heuristic approaches, i.e., SA and greedy. The comparison includes execution time and energy consumption, important metrics in coverage path planning, for a different number of waypoints.

7.6.1 Execution Time Evaluation

To investigate the ability of the three methods used in the proposed approach in finding the optimal solution of the coverage path planning problem, the execution time that represents a key factor for evaluating the performance, is tested. The average execution time for 10 replications is illustrated in Fig. 7.4.

It can be observed that the execution time of the three methods goes up simultaneously as the ROI size increases, demonstrating the effect of problem size on execution time. It is worth emphasizing that the greedy obtains a locally optimal solution by looking for the best solution to find a globally optimal solution. Consequently, it needs a shorter time to generate the solution. On the other hand, the exact solution obtains the best solution for drones by thoroughly exploring the solution space.

For small-scale problems, the exact solution can be obtained within acceptable time consumption, while in large-scale and complex system problems, the solution space is significantly exploding, resulting in an inefficient application of such formulation due to the required time consumption. This fact is depicted in Fig. 7.4.

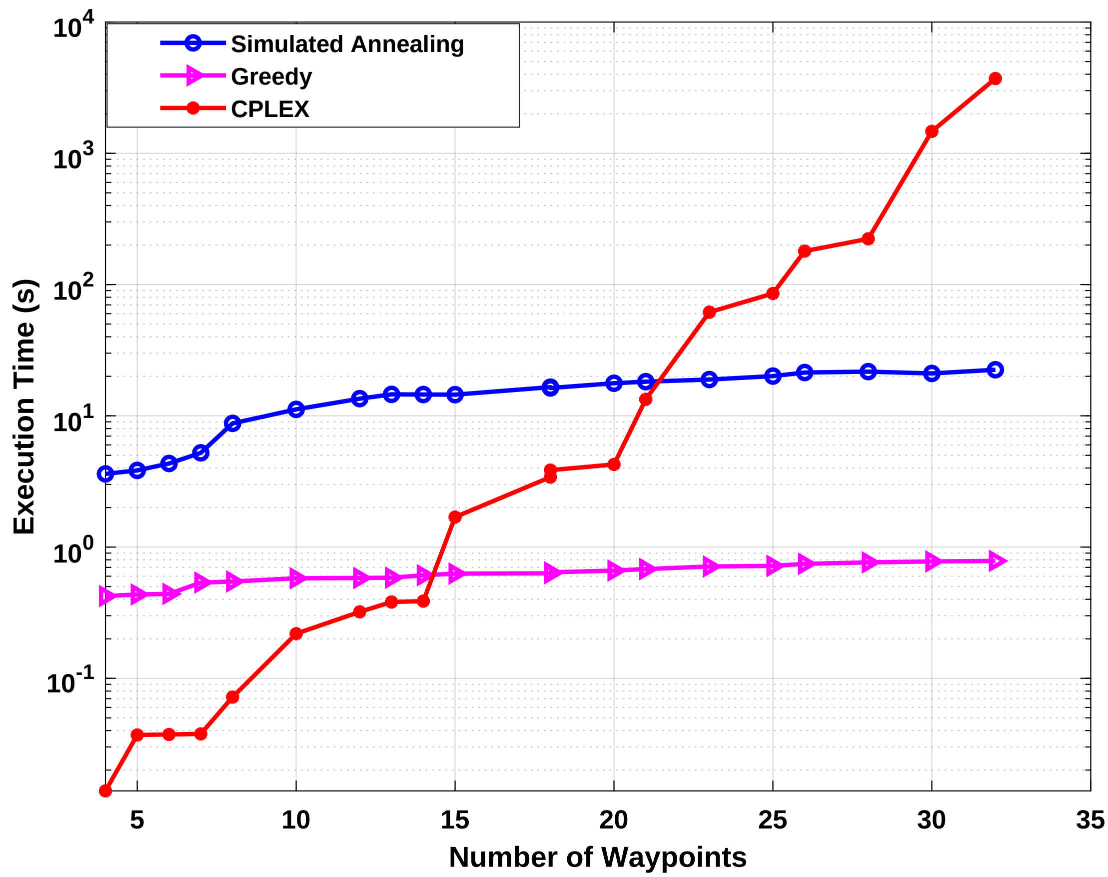

Figure 7.4: The average execution time with respect to number of waypoints for the three approaches, SA, greedy, and CPLEX solver.

As the number of waypoints increases, this trend increases, demonstrating the impact of problem size on the execution time of exact solution. When the number of waypoints exceeded 30, the execution time of the CPLEX solver is significantly increasing, while the execution time shown by SA and greedy are around 25 s and 0.8 s, respectively. When the region size is enlarged, the proposed exact solution model is unable to provide a solution. However, the heuristic approaches obtain the results within reasonable computation times. The results show the ability of the proposed approach in obtaining the solution for different problem sizes by an appropriate solver.

7.6.2 Energy Consumption Evaluation

Energy consumption is recognized as an essential metric for evaluating the performance of algorithms. It reflects the ability of the proposed approach to generate an efficient collision-free path. The drone flies from the depot covering every waypoint and returns. The visited sequence of waypoints is selected so that the overall energy consumption is minimized while avoiding obstacles' collision and intra-swarm collision (in the case of multi-UAVs). The average energy consumption of 10 replications is shown in Fig. 7.5. The energy consumption of the three methods goes up simultaneously with an increase in the number of waypoints, i.e., region size, demonstrating the effect of problem size on energy consumption. From Fig. 7.5, we can observe that the proposed approach shows lower energy consumption by CPLEX solver than heuristic, while greedy shows the highest energy consumption. This gap increases as the number of waypoints increases. The reason is that the greedy obtains a locally optimal solution by looking for the best solution to find a global optimal solution, and due to the short-term solution, it generates a poorer solution and does not guarantee to find the globally optimal solution. The CPLEX solver will achieve the best solution for drones by completely exploring the solution space. However, for large-scale and complex system problems, the solution space is significantly exploding, resulting in inefficient application due to the required time consumption as discussed before.

For further analyzing the optimal solution of the proposed model, the optimality gaps between CPLEX solver and heuristics are calculated and the results

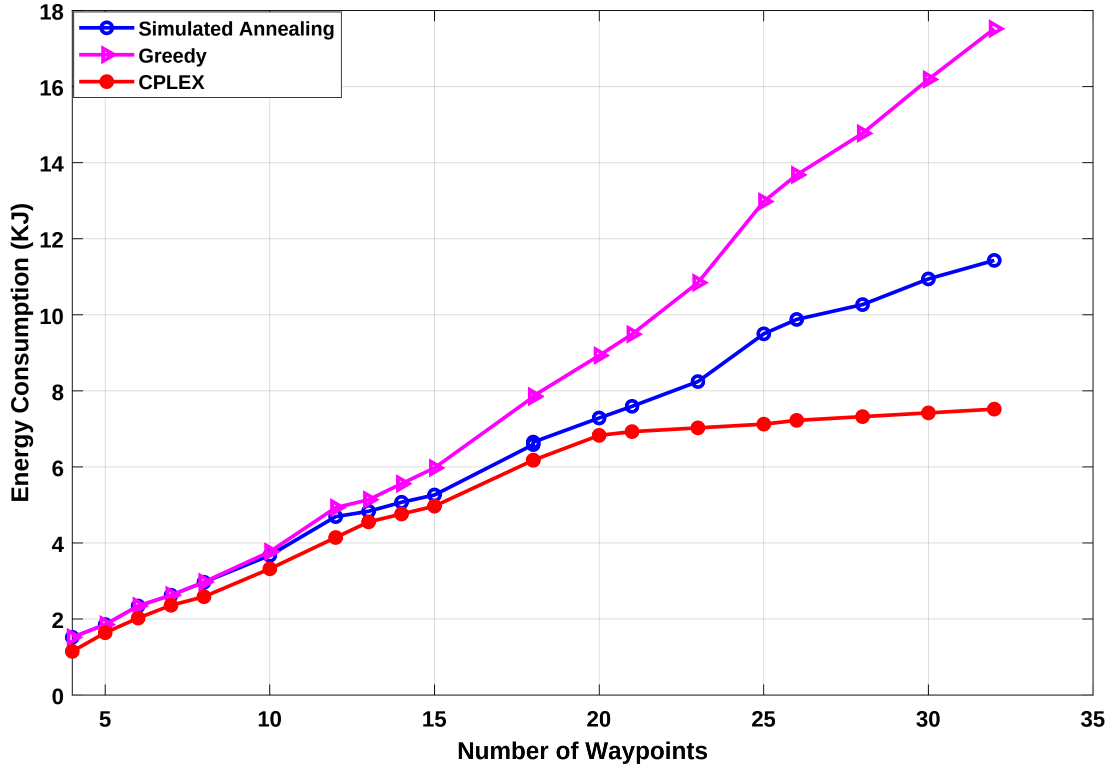

Figure 7.5: The average energy consumption with respect to number of waypoints for the three strategies, SA, greedy, and CPLEX solver.

are recorded in table 7.1. Gap% represents the gap between CPLEX solver and heuristic approaches, respectively, and can be obtained by

$$SA_{Gap} = \frac{SA_{En} - CPLEX_{En}}{CPLEX_{En}} * 100. \tag{7.12}$$

$$Greedy_{Gap} = \frac{Greedy_{En} - CPLEX_{En}}{CPLEX_{En}} * 100. \tag{7.13}$$

Owing to the complexity of the CPLEX solver, i.e., exact solution model, the maximum CPU time is set to 3,600 s. The average optimal solutions of 10, 20, 30, 40, and 50 waypoints are shown. Both greedy and SA could achieve the optimal solutions in a significantly shorter time than the CPLEX solver. For large scenarios, i.e., >30 waypoints, the CPLEX solver cannot solve for optimality in reasonable time while heuristic approaches yield a solution with a gap of (44.8707% and 51.308%) for SA and (3.45% and 18.97%), for greedy. The percentage gap shows that in a small number of waypoints, i.e., small region, the CPLEX solver achieves a better solution than heuristics. The negative sign of Gap% indicates poor solution by CPLEX solver, when the number of waypoints exceeded 30 waypoints.

To further illustrate the impact of execution time on the quality of energy consumption, we plot the energy consumption with respect to number of waypoints, 10 to 50 waypoints, and the result is highlighted in Fig. 7.6. The result emphasizes that the CPLEX fails to obtain the optimal solution in a reasonable time for the large-scale problem. It also shows the advantage of heuristic approaches in solving large-scale problems in a shorter time.

Table 7.1: Energy consumption statistic (in joule) of the three approaches when the number of waypoints increases from 10 to 50.

Energy Consumption				**Gap%**	
WP	CPLEX solver	SA	Greedy	SA	Greedy
10	3320.9	3673.633	3769.768	9.61	13.51
20	6829.37	7286.015	8929.121	6.68	30.74
30	11061.58	11430.86	17521.43	3.34	58.39
40	25874.82	14264.6	24981.7	-44.87	-3.45
50	35200.95	17693.87	28894.24	-51.30	-18.97

7.6.3 Collision Avoidance Evaluation

In this subsection, the terrain involves two static obstacles. The proposed approach generates a feasible collision-free path, which achieves the objective and satisfies all constraints. The generated collision-free path covers the whole region

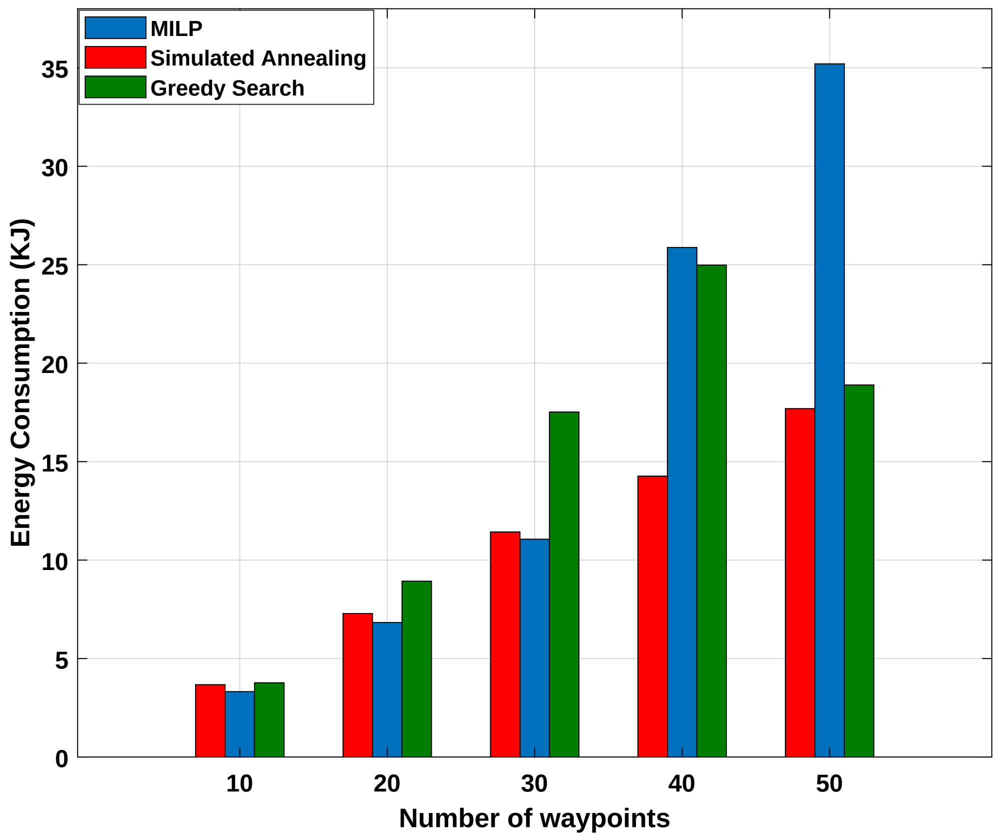

Figure 7.6: The energy consumption with respect to number of five region sizes, 10 to 50 waypoints, for the three approaches, SA, greedy, and CPLEX solver.

with minimum energy consumption, as illustrated in two-dimensional views in Fig. 7.7. It can be clearly seen that no collision is detected with static obstacles in all approaches, and the drones can weave around obstacles efficiently.

It is worth noting that considering the collision avoidance with obstacles impacts the drone's energy consumption and might increase the number of turns to avoid colliding with terrain obstacles. This fact can be easily seen in Fig. 7.8. The figure shows the energy consumption for different waypoints with and without collision avoidance considerations. The drone needs more energy to avoid colliding with obstacles which basically reflects more practical results.

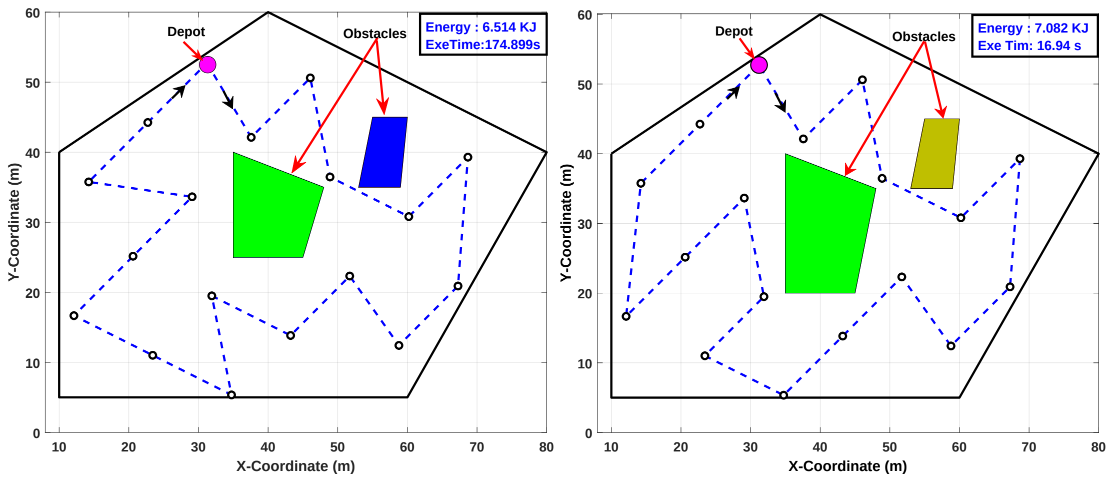

(a) CPLEX solver collision-free path (b) Simulated annealing collision-free path

Figure 7.7: Two-dimensional view for coverage path planning with 2 static obstacles environment. The drone flies from the depot, covering the region, and returns to the depot position while avoiding collisions with these static obstacles.

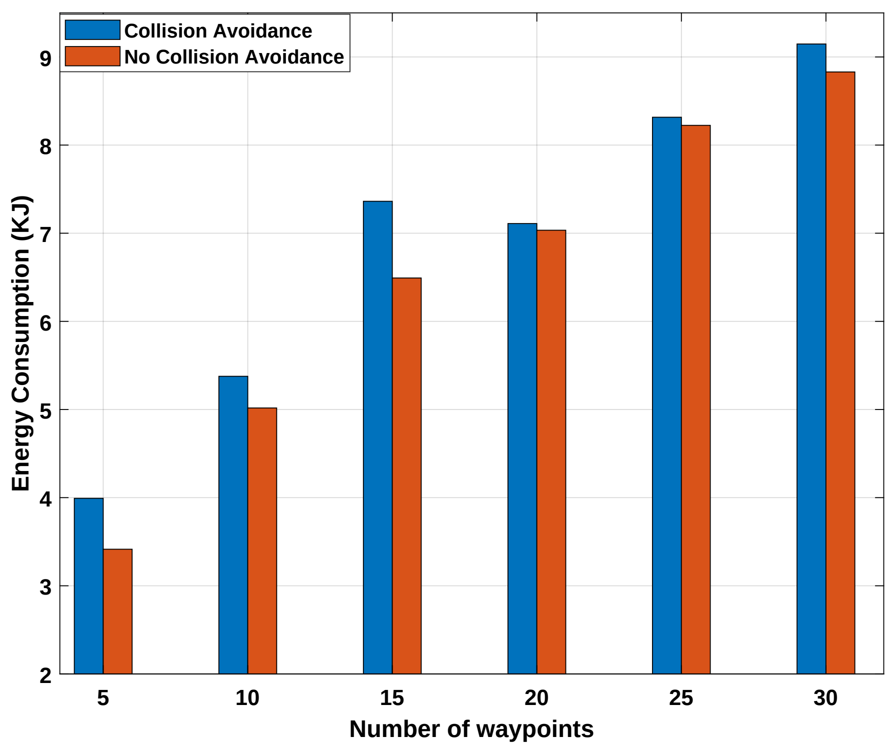

Figure 7.8: The energy consumption with respect to five region size, 10 to 50 waypoints, with and without considering the effect of obstacles on energy.

7.6.4 Effect of Sub Region Allocation Optimizing on Performance

To further analyze the effectiveness of the proposed region allocation approach on energy conservation, we discuss the impact of region allocation on reducing the energy consumption to cover the ROI. The optimal solutions of different region sizes are obtained and recorded in table 7.2. where the percentage of the average improvement gap of the proposed region allocation is calculated.

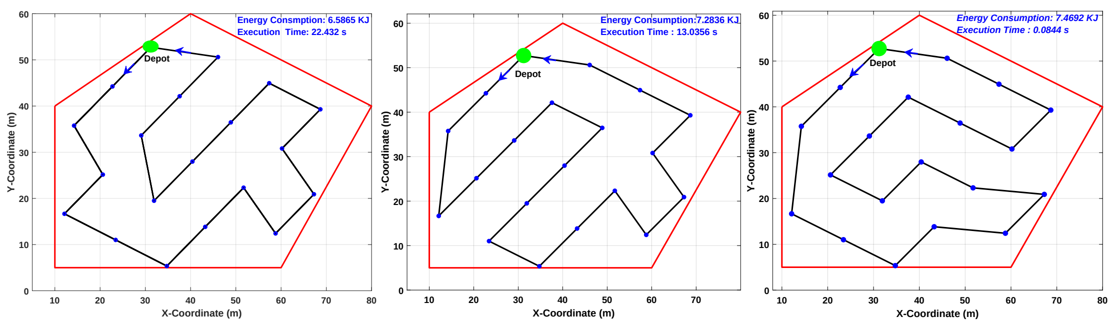

(a) CPLEX solver coverage path (b) Simulated annealing coverage path (c) Greedy coverage path

Figure 7.9: Two-dimensional view for coverage path planning for the three approaches, SA, greedy, and CPLEX solver. The drone flies from the depot, covering the region, and returns to the depot position.

7.6.5 Trajectory Optimization of UAV in Small and Large Region

To show the performance of the proposed approach in addressing small and large region areas, different scenarios involving single UAV and multi-UAV with the small and large region are presented.

Table 7.2: The improvement gap percentage statistic of region allocation optimization approach for different region sizes.

Region Area (m2)	**No RA Optimization**	**RA Optimization**	**Improvement Gap %**
7168	19807.65263	19481.0597	1.648822
9072	24844.04037	24396.02768	1.8033
11200	29556.10933	28690.02266	2.930314
13552	35392.05027	34085.57421	3.691439
16128	42681.06277	41132.89634	3.627291
18928	49012.12125	48129.767	1.800278
21952	57948.43785	56950.48396	1.722141
25200	65112.06962	65101.67432	0.015965
28672	74981.2094	73353.79255	2.170433
32368	86464.31403	83104.89846	3.88532
36288	94563.97185	94120.23399	0.469246

- Single UAV coverage path planning performance evaluation.

  In this scenario, the drone is flying from the depot (we consider the starting waypoint of the coverage path as the depot), covering all waypoints, and then returns to the depot, i.e., the region is covered in one trip, as illustrated in Fig. 7.9. The figure shows the coverage path planning for the three approaches used in the proposed algorithm, where 20 waypoints are covered. As discussed in section 7.3, the number of turns has a significant effect on energy consumption due to deceleration and acceleration operation to take a turn that consumes significant energy. It can be shown in Fig. 7.9 that the SA trajectory requires less energy consumption than greedy but is still greater than the CPLEX solver, which shows the lowest energy consumption. On the other hand, greedy approach shows the fastest execution time while the CPLEX solver shows the slowest execution time. If the region cannot be completely covered by one trip due to insufficient energy, the drone needs to return to the base station or depot and recharges its battery to continue covering the region. To do so, we provide a remaining energy calculation that guarantees the safety of the drone to come back to the base station. The remind energy is calculated as follows: the drone is allowed to fly from $position_i$ to $position_j$ if its available energy is sufficient to fly from $position_i$ to $position_j$ and from $position_j$ to the depot. This constraint is formulated in Eq.(7.8), and it allows generating the safety path with minimum energy consumption, as shown in Fig. 7.10. The UAV needs two trips to cover the region. Thus, the proposed approach generates two paths for two trips. It is noteworthy that the proposed algorithm avoids previously explored covered waypoints, as illustrated in Fig. 7.10. In this figure, the returning path is also exploited to scan the waypoints in the path toward the depot. The offline failsafe measure is proposed to verify if the UAV has sufficient energy to execute the mission.

- Multi-UAV coverage path planning performance evaluation.

  In this scenario, three UAVs are assumed to be available. Thus, the ROI is divided into three parts, and each drone is tasked to cover a set of waypoints as explained above in section 7.4.3. The multi-UAVs can be employed when the region size is too large and can not be covered by a single UAV. Thus, the region is split into sub-region that are assigned among UAVs. The paths generation is shown in Fig. 7.11. It can be clearly seen that inter-collision is addressed, and the successful collision-free paths are generated for all UAVs.

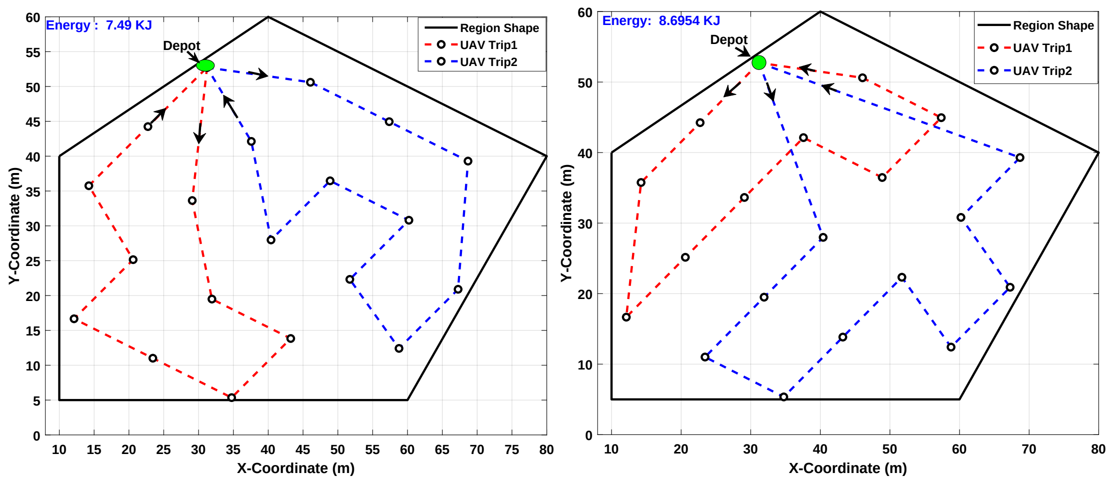

(a) CPLEX solver multi trips coverage paths

(b) Simulated annealing multi trips coverage paths

Figure 7.10: Two-dimensional view for multiple trips coverage path planning when available energy consumption of drone is not sufficient to cover the region by one trip.

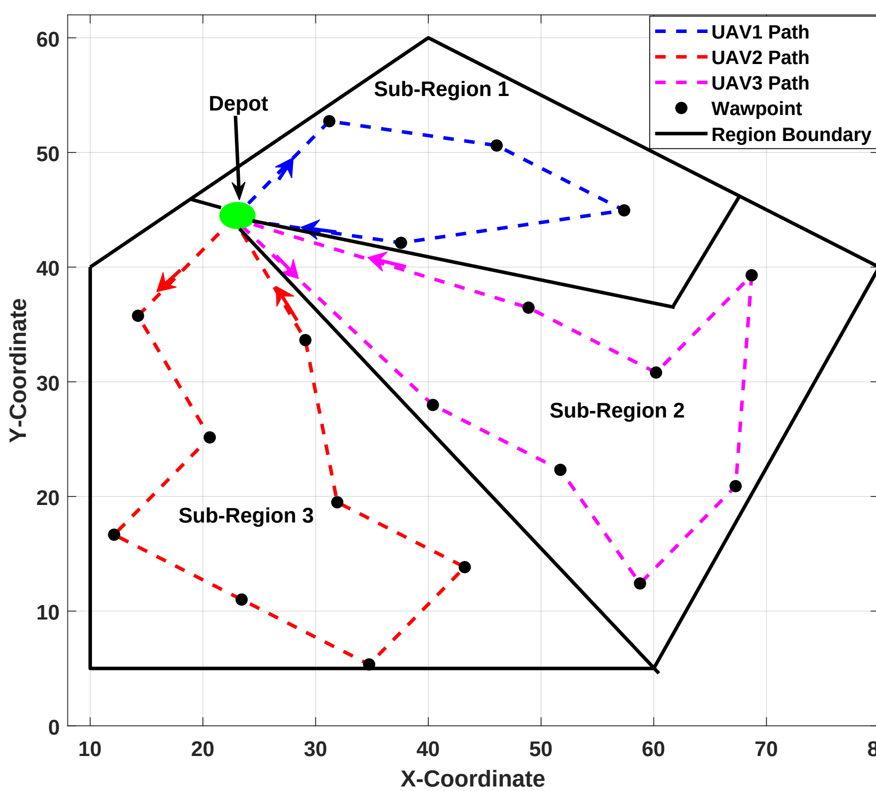

Figure 7.11: Two-dimensional view of coverage path planning for three UAVs.

7.7 Chapter Summary

In this chapter, an energy-efficient coverage path planning approach that considered different region sizes was developed. The exact formulation was proposed based on mixed integer linear programming to seek the optimal trajectories for drones so that the generated path minimized the energy consumption and satisfied all constraints during the mission. The energy consumption model was based on acceleration, deceleration, turning, and hovering. The proposed approach was able to optimally decompose the region considering single and multiple drones. The proposed sub-region allocation strategy contributed in reducing energy consumption. The MILP-based formulation was solved using CPLEX solver and heuristic approaches, i.e., SA and greedy. Several scenarios were studied to verify the correctness of the proposed approach. The results showed that in small problem sizes, both exact and heuristic approaches were able to generate collision-free paths for UAVs. Additionally, the CPLEX solver outperformed the heuristic approaches in small-scale problems. However, in large-scale problems, the CPLEX failed to generate the optimal solution in a tractable time. The results showed that simulated annealing with energy optimization used less energy consumption than the greedy mechanism. Furthermore, the results illustrated that the energy conservation was more prominent as the region size increased.

CHAPTER 8

IOD ROUTING PROTOCOLS

8.1 Introduction And Motivation

The UAVs network can perform highly complex tasks that are beyond a single UAV capability [2], [7], [161]. Thus, it has attracted great attention from researchers due to the convenience and safety which would be acquired when applied in the reality. It can be used in the transportation system to reduce the number of accidents and consequently decreases the number of death in the passenger and drivers. Furthermore, vehicles, drones, and roadside units can disseminate information to identify the danger place on the road in addition to improving traffic management efficiency. Besides, wireless communication among multi-UAVs is necessary for proper collaboration and cooperation among UAVs. The drone communication network is an extension of a mobile ad hoc network with its own network features. The terrain limits the nodes in MANET while the drones in the flying network have not been affected by the interference of terrain when moving in the air. Additionally, the speed of drones in the air is higher than the nodes in MANET and the topology is changing extremely [5], [28], [131], [162]–[164]. The communication is performed either directly with the nodes in the range or by using multi-hop, in which the intermediate nodes forward the packet to the destination [165]–[167].

To exchange packets in the UAV network, routing protocols are essential and play a significant role to enable reliable UAV-to-UAV communications for the UAV network. However, developing these protocols in highly dynamic topology changes becomes a challenge. The extreme change in topology causes intermittent disconnection of the network. The restriction range between the drones and the base station is another challenge. Hence, dynamic topology, and high mobility of drones make the development of a routing protocol to ensure reliable communication is difficult to achieve in UAV network [25]–[27]. On the other hand, the UAV network shares many similarities with the traditional ad hoc network. Therefore, traditional routing protocols can be utilized as the basis to provide UAV swarm communication.

In the flying network, the drones can be utilized as transmission nodes, receiving nodes, and forwarding nodes at the same time. Moreover, the multi-hop path transmission is established in this network where the topology changes very frequently due to the high mobility of the nodes which affects the flying network communication and makes the maintenance of routing difficult. Furthermore, the drone to drone communication requires a routing protocol to provide an efficient and reliable data transmission [168]–[172]. In this chapter, three routing protocols, named AODV, OLSR, and DSDV will be analyzed and compared using testing parameters such as throughout, end-to-end delay, and packet delivery ratio.

8.2 Communication Architecture of UAV Network

In the UAV network, nodes are generally mobile and can move in three dimensions. Point to Point (P2P) Communication can usually be achieved between nodes only if the nodes are close to each other, i.e., at closed proximity with each other. However, Multi-Point Relay (MPR) technique is usually utilized if the nodes are far away from each other, where the intermediate nodes act as forwarding nodes. Each UAV can act as a transmitter, receiver, and relay node. However, the node's communication is exposed to different constraints, such as permanent network fragmentation, packet losses, and sudden disconnections. Thus, to cope well with the frequent topology change, UAVs cooperate and organize themselves as a relay network [173].

The communication architecture of the cellular and centralized network is improved using a swarm of drones. In the following subsections, we explain the UAV-to-UAV communication and UAV-to-Ground communication in detail.

8.2.1 UAV-to-UAV (U2U) Communication

UAVs are communicating directly with each other to satisfy the needs of different missions. The communication is conducted by frequently exchanging data packets with other UAVs in the transmission ranges. The nodes that are out of transmission range run multi-hop communication over other UAVs. The multi-hop communication extends a coverage of specific area of interest. Since the UAVs

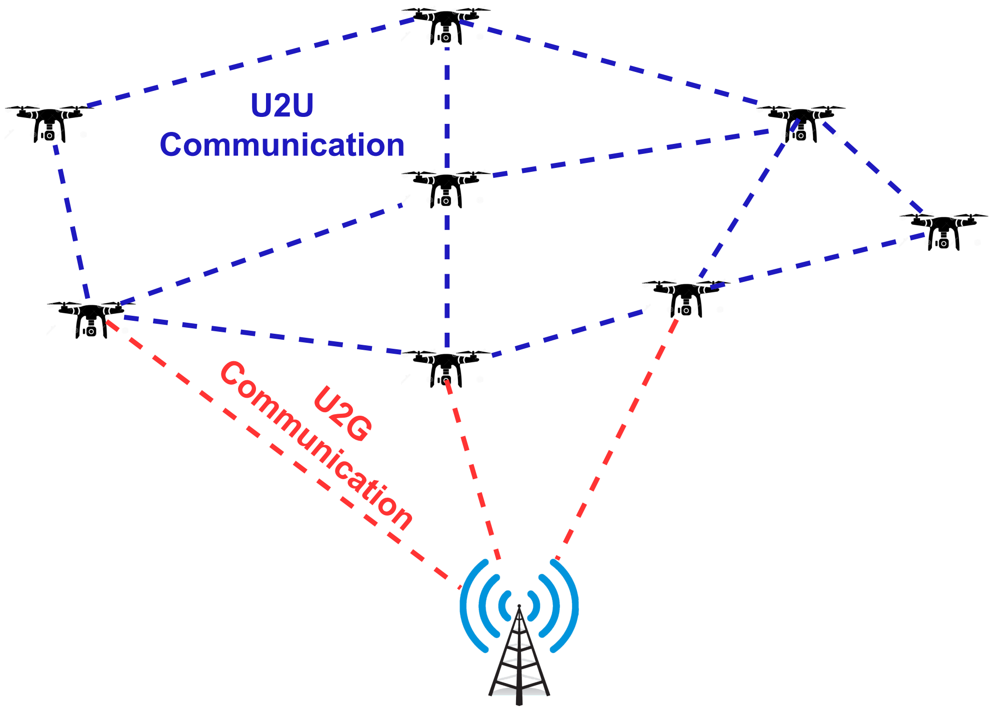

Figure 8.1: Communication Architecture of UAV Network.

are deployed in the air, where no obstacles exist between UAVs, the probability of line-of-sight (LOS) increases and becomes predominant in U2U communications. Nevertheless, the LOS is not guaranteed in a rural area where buildings or hills act as obstacles and block the transmitted signal [28], [174].

8.2.2 UAV-to-Ground (U2G) Communication

For better control of flying UAVs, infrastructures in the form of ground base station are fixed on the ground in order to exchange critical control and command messages [175]. In addition, ground BSs are also used to link different groups of UAVs between each other. Generally, there are specific UAVs that are able to communicate with ground BSs in order to decrease the congestion of the network and to enhance throughput and connectivity. Flying UAVs at high altitudes improve LOS conditions in U2G links. Reversely, at low altitudes flying, LOS is not ensured with ground users due to the existing obstacles on the ground which cause the phenomenons of diffraction and reflection [176].

Several advantages are provided by FANET: a rapid coverage of the large area is enabled, and the scalability is guaranteed by drones mobility, multi-hop communication provides efficient reuse of bandwidth, and the decentralized approach improves the reliability. Thus, if one drone fails, the whole network has not been affected [132].

8.3 Routing Protocols

To disseminate the information in the UAV network, UAVs should relay the traffic to the destination. For doing so, the route between nodes should be established in the fly. Due to the UAVs' dynamic nature and highly mobile, a routing protocol is responsible to adapt the requirements changing of the UAV network. Among many challenging issues, one fundamental problem highlighted by [177] is that currently, the FANET routing protocols are at least in the development stages. Due to this limitation, currently, the existing routing protocols used in MANET can be adapted to meet the FANET requirements [178]. They can be mainly classified into two types named topology-based and location-based. The topology-based can be divided into proactive and reactive routing protocols.

In proactive routing protocols, a fresh routing table is maintained beforehand and the routing table is distributed periodically throughout the network. DSDV and OLSR are from this category. Unlike proactive protocols, reactive protocols establish the route on-demand between nodes when they need to communicate. To do so, the network is flooded by route request packet and the route is established. DSR and AODV are two types of this category. In this subsection, the description of AODV, OLSR, and DSDV routing protocols is presented.

8.3.1 Adhoc On Demand Distance Vector Routing Protocol (AODV)

It is a well-known reactive routing protocol [179] used in both MANET, VANET, and FANET networks. In AODV routing, when the source initiates, the route from source to the destination is determined and kept till the source no longer needs it. The processes to discover the target node start by broadcasting a Route Request (RREQ) packet by the source node. The intermediate nodes forward RREQ and use source information for updating themselves. When the RREQ packet reaches the destination, a route reply (RREP) packet is returned back to the source. Furthermore, the RREP packet contains the number of hops required to reach the destination. If the route is invalid, a route error packet (RERR) message is created to inform the source node which in turn initiates a route discovery again by a source. Additionally, the route to the destination is recorded by all intermediate nodes to be used in future communication. Besides, a link failure is detected by periodically sending a hello message. AODV suffers from a latency issue due to searching for a new destination.

8.3.2 Optimized Link State Routing (OLSR)

This routing algorithm is one of the proactive routing protocols used in ad hoc network [180] where the path to the destination is computed in advance for sending the data. Besides, OLSR uses the GPS information of the nodes for taking route decisions. The expected transmission count (ETX) is evaluated by considering the corresponding speeds of two nodes to enhance the routing decision. Thus, all nodes provide fresh information about the state of the network to each other. To do so, each node relays the control packet systematically to maintain the connection route to any other node. The neighbor list is created by sharing information about its direct links only with some neighbors by periodically exchanging a hello message and topology control packet among neighbors. The significant factor that affects the OLSR performance is the multipoint relay (MPR) which is selected by the sender node and covers two hops neighbors. Moreover, MPR nodes are the only nodes responsible to forward updating information during the flooding process. [132], [181], [182].

8.3.3 Destination-Sequenced Distance-Vector Protocol (DSDV)

DSDV is a proactive routing protocol [183] and it has been specially designed for mobile networks. It is based on the classic idea of Bellman-Ford's distributed algorithm. This protocol works as follows: Each node maintains a routing table that contains all possible destinations, the number of hops required to reach the destination, and the sequence number which corresponds to a destination node. In order to maintain the consistency of the routing tables in a rapidly varying topology, each node of the network periodically transmits its routing table to its direct neighbors. The node can also transmit its routing table if the content of the message undergoes significant changes compared to the last content sent. Moreover, updating the routing table can be done in two ways: a complete update and an incremental update.

In the complete update, the node transmits the entire routing table to the neighbors, whereas in an incremental update, only the entries which have undergone a change compared to the last update, are sent which reduces the number of packets transmitted.

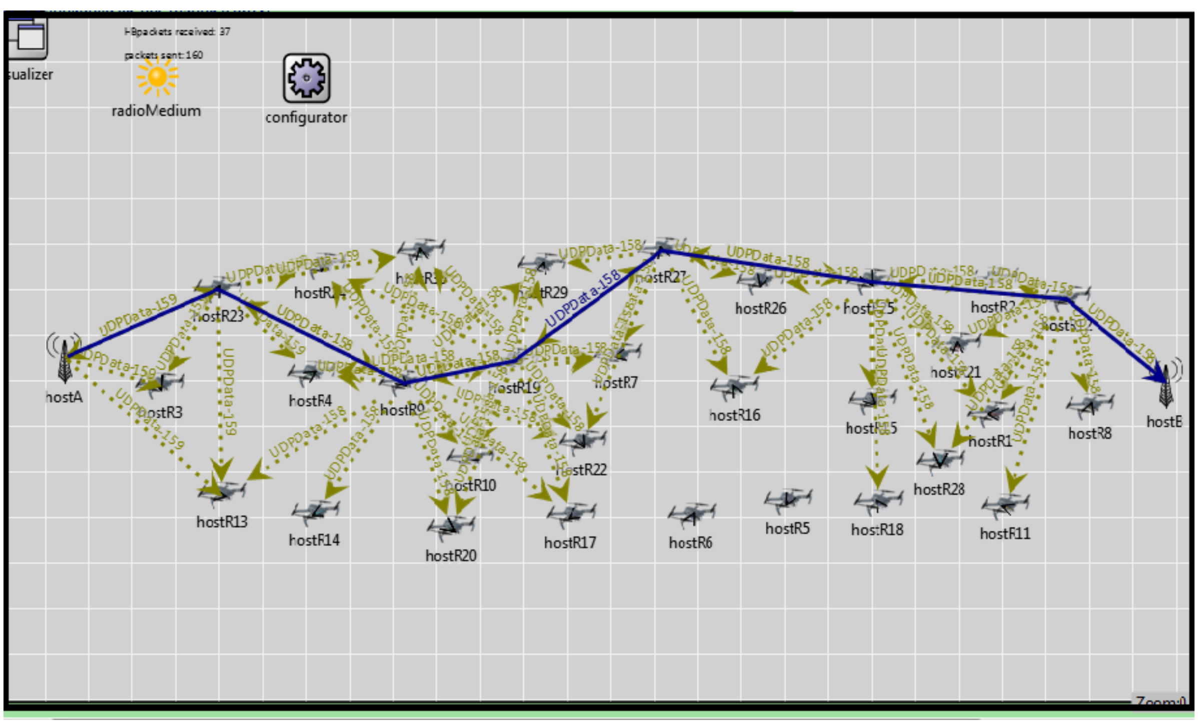

Figure 8.2: Snapshot of UAVs relay network.

Table 8.1: Parameters setting

Parameter	Value
Geographical Range	3500 m x 1500 m
Network Size	10, 20, 30, 40
Mobility Model	Linear Mobility with random start angle
Drone's Speed(mps)	0, 5, 10, 15, 20, 25, 30
Drone's Altitude	100 m
Communication Range	500 m
Routing Protocol	AODV, OLSR, DSDV
Data Rate	54Mbps
Simulation Time	100 s

8.4 Simulation Results and analysis

To evaluate the performance of the three routing protocols (AODV OLSR, and DSDV), we carry out a simulation using the Omnet++ tool with different performance metrics. To show the performance of those routing protocols in flying networks, various scenarios including different network sizes and different speeds of the nodes, are tested and compared.

The flying network acts as a relay network between sender and receiver as shown in the Fig. 8.2. The simulation is run on intel Cori5 2430M CPU with 3 GigaByte memory. In this section, the simulation of DSDV, OLSR, and AODV will be illustrated.

8.4.1 Parameters Setting

Without loss of generality, the setting parameters of the drone's communication network based on the Omnet++ simulation tool are set as follows.

The geographical range is 3500 m x 1500 m. The mobility model used is a linear mobility model with random starting angles. The communication data rate is 54Mbps. The network sizes are 10, 20, 30, and 40 drones respectively. The speed of drones is set to 0 mps, 5 mps, 10 mps, 15 mps, 20 mps, 25 mps, and 30 mps. The routing protocols evaluated are AODV, OLSR, and DSDV. The parameters setting are shown in Table 8.1.

8.4.2 Performance Metrics

In this subsection, we will explain the performance metrics utilized in this work to evaluate the UAV network routing protocols.

- Average End-to-End delay (E2ED)

The E2ED represents the average necessary time required for the packet to reach the destination. It includes queuing at interface MAC, buffering during the route discovery process, propagation time, and transmission time. The average E2ED is calculated over all iterations or runs by.

$$Avg\_E2ED = \frac{1}{m}\sum_{i=1}^{m}\frac{\sum_{j=1}^{n}(Tr(P_j) - Ts(P_j))}{n}, \tag{8.1}$$

where $\mathrm{Tr}(\mathrm{P}_j)$ is a received time of packet_j, $\mathrm{Ts}(\mathrm{P}_j)$ is a transmission time of packet_j, n is the number of packets received during run_i, and m is the number of runs. The lower value of this metric, the better the performance.

- Average Packet Delivery Ratio (PDR)

The average PDR illustrates the ratio between the number of successfully received packets by the destination and the total packets sent by the source node.

The average PDR is calculated over all iterations or runs by

$$Avg\_PDR = \frac{1}{m} \sum_{i=1}^{m} \frac{PcktRcvd_i}{PcktSnt_i}, \tag{8.2}$$

where $\mathrm{PcktRcvd}_i$ is the number of packets received by the destination in iteration i, $\mathrm{PcktSnt}_i$ is the total packets sent by the source node in iteration i, and m is the number of iterations. The higher the value of a packet delivery ratio, the better the performance.

Average throughput

The throughput, measured in bit per second(bps), is defined as the total packets successfully received by the destination divided by the simulation time. The average throughput is calculated over all iterations or runs as follow.

$$Avg\_Throughput = \frac{1}{m} \sum_{i=1}^{m} \frac{Pckt_i}{ST}, \tag{8.3}$$

where Pckt_i is the total packets received by the destination in iteration i, ST is a simulation time, and m is the number of runs or iterations. The higher the value of this metric, the better the performance.

8.4.3 Results and Discussions

In this subsection, different scenarios involving PDR, Throughput, and E2ED with different speeds of nodes and different network sizes will be analyzed and the results of the simulation will be discussed.

In all scenarios, the sender and receiver are 3400m away from each other. The drone network is utilized as a relay network to forward the sent packets from the

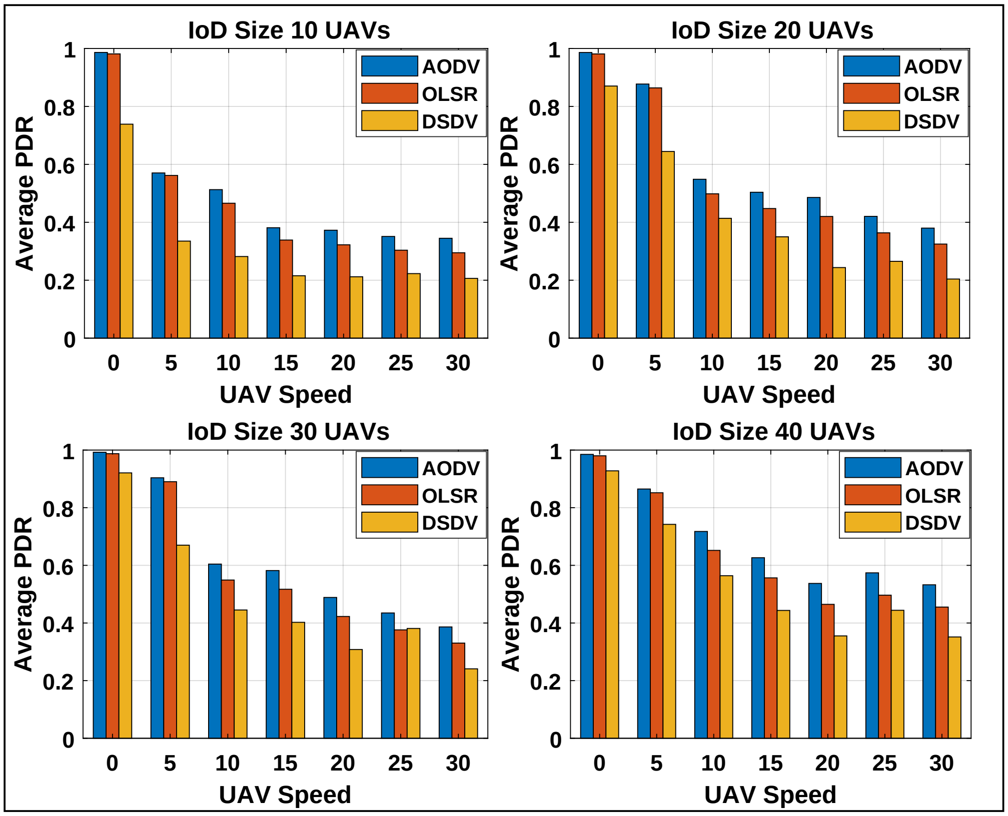

Figure 8.3: The mean packet delivery ratio for AODV, OLSR, and DSDV routing protocols.

sender to the receiver.

- Packet delivery ratio analysis

The PDR is a metric used to measure the network connectivity where the high value of the packet delivery ratio reflects the network connectivity. Fig. 8.3 exhibits the average PDR with respect to nodes speed for different network sizes(10,20,30,40) nodes. As can be seen from the figure, the speed of drones affects the network connectivity. The network disconnection increases as the speed increases which reduces the number of received packets, i.e, increases the number of drop packets, which in turn reduces the PDR.

Another factor affecting the PDR in UAV networks is the network size or the number of nodes in the network. The higher the number of nodes, the higher chance to find a route to the destination. This is due to the limited communication range of UAVs. In the sparse network where there are fewer available UAVs, the UAVs get far from each other and become out of their communication ranges which reduces the chance to find the route to the destination. For this reason, the PDR improves as the network size increases. This trend is exhibited in Fig. 8.3 for the three routing protocols. It is worthy to show that both reactive and proactive routing protocols behave similarly when speed and network size change. However, AODV outperforms OLSR and DSDV in PDR especially when the speed of nodes increases. The PDR in DSDV decreases significantly as the speed of drones increases. This is because when the node's speed increases the network topology change at a higher value which leads to increasing the link failure.

- End-to-End delay analysis

The average End-to-End delay (E2ED) with respect to the node speed for different network sizes is illustrated in Fig. 8.4. As the node's speed increases, the end-to-end delay time in OLSR and DSDV routing increases slightly whereas end-to-end delay increases significantly as the node speed increases in ADOV. Thus, in the case of the end-to-end delay, OLSR performs better than the AODV routing protocol, and DSDV shows the minimum end-to-end delay.

This is because the routing information is not reused in AODV and it needs to start the route discovery whenever the source node wants to transmit. Also, due to the high mobility of the nodes, when the route replay packet reaches to sender, the node closed to a receiver node has already moved away.

On the other hand, in table-driven protocols, the update route is given in the routing table. Therefore, they don't face longer setup time. Fig. 8.4 shows

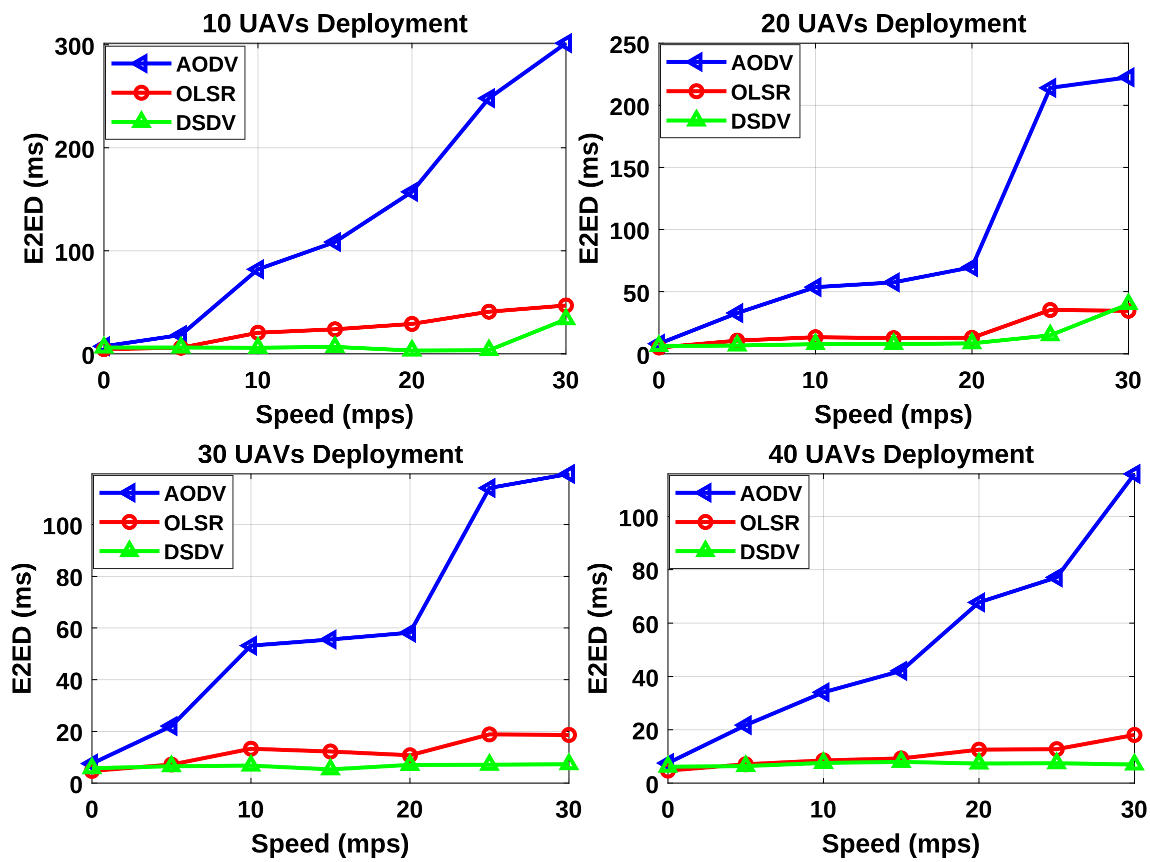

Figure 8.4: Average end-to-end delay for different routing protocols.

different network sizes (10, 20, 30, 40) UAVs which have a vital effect on end-to-end delay where the end-to-end delay improves more in the dense network than that in a sparse one. This is because the higher the number of nodes, the higher chance to find a route to the destination. This is due to the limited communication range of UAVs. In the sparse network where there are fewer available UAVs, the UAVs get far from each other and become out of their communication ranges which reduces the chance to find the route to the destination. For this reason, the

E2ED improves as the network size increases. In short, for high topology change, AODV exhibits poor end-to-end delay compared with OLSR and DSDV routing protocols.

- Throughput analysis

As illustrated in Fig. 8.5, in the static network, i.e., nodes' speed is 0, the average throughput of OLSR is higher than that of AODV and DSDV. As the speed of the node increases, the average throughput degrades in the three routing protocols, demonstrating the impact of node speed on the average throughput. Therefore,

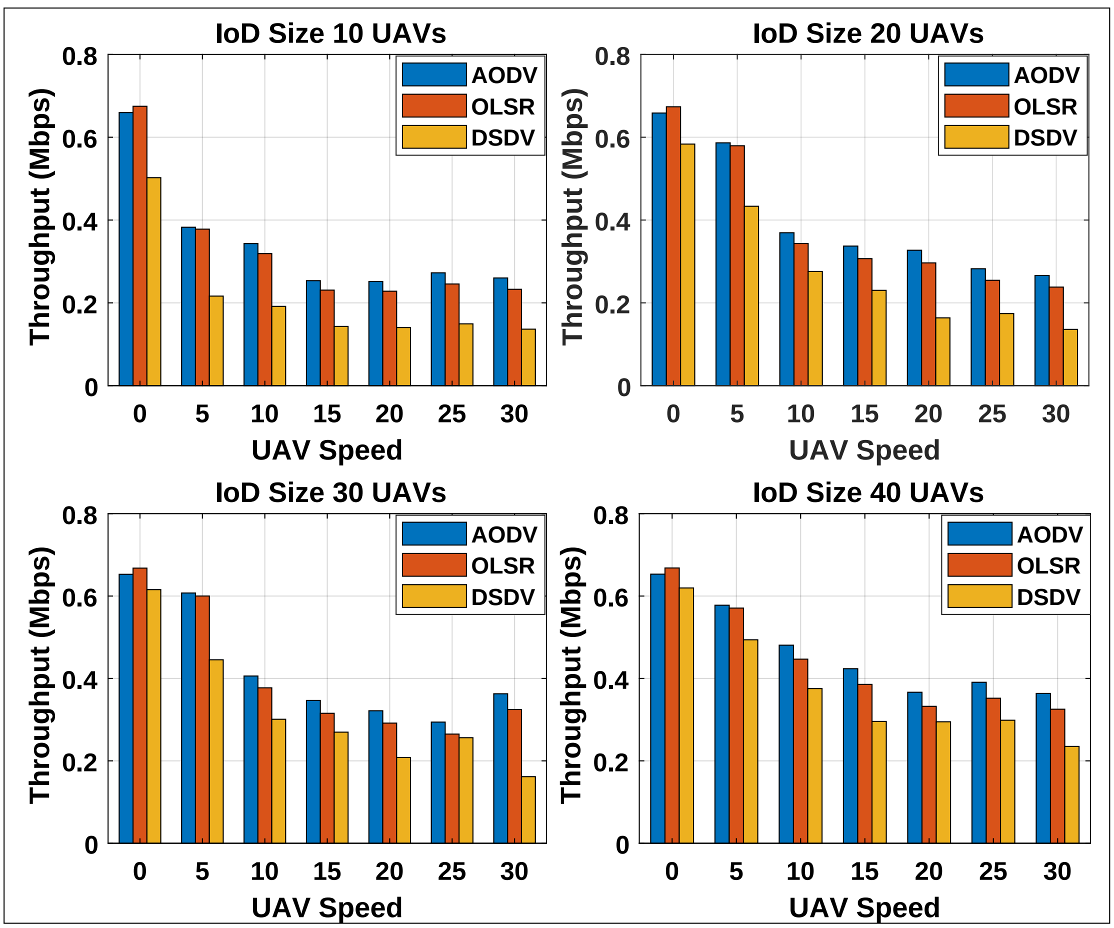

Figure 8.5: The mean throughput for AODV, OLSR, and DSDV routing protocols.

in the case of the average throughput, AODV performs better than other routing protocols. The higher the speed of the nodes, the more frequent network disconnection and the lower number of packets received by the destination during the simulation time. However, AODV provides the best throughput at high nodes' speed due to the reactive nature to the topology change.

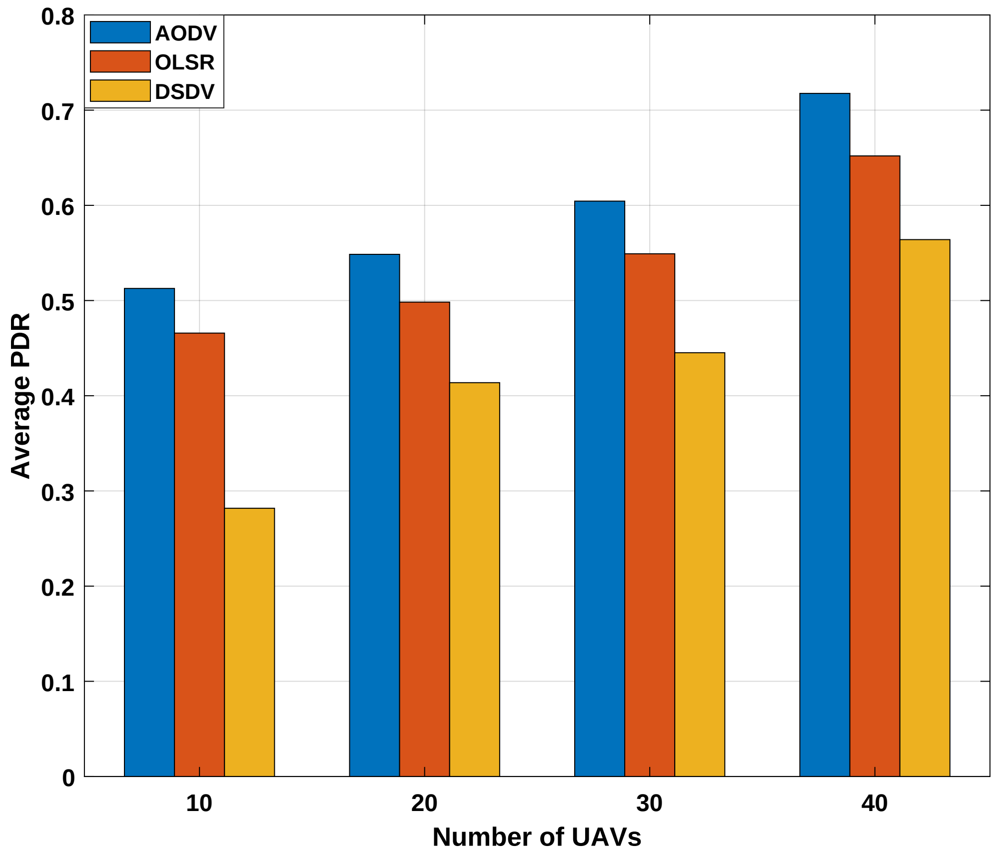

Figure 8.6: Average packet delivery ratio with speed of 30 mps for the AODV, OLSR, and DSDV routing protocols.

- Effect of network size on performance at high nodes' speed

The network size has an important impact on UAV network performance. In this subsection, the network size changes from 10 to 40 nodes in a step of 10. Also, the speed of nodes is set to 30 mps. The PDR, E2ED, and throughput are studied for AODV, OLSR, and DSDV.

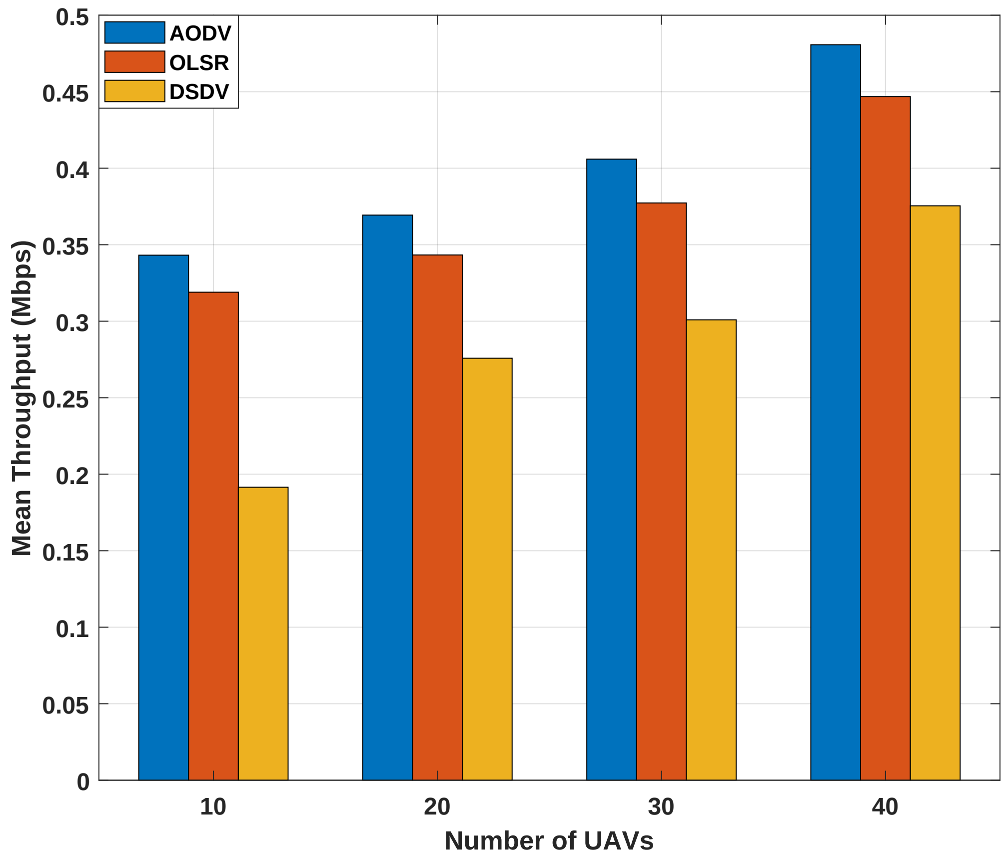

Figure 8.7: Average throughput with speed of 30 mps forthe AODV, OLSR, and DSDV routing protocols.

For a small network size (10 nodes), the chance of discovering a path to the destination is very low and the network suffers from frequent disconnections especially at the high speed of nodes.

As the network size increases, the chance of finding the path to the destination is improved and the performance metrics of networks like PDR and throughput are enhanced as shown in Fig. 8.6 and 8.7, respectively.

The figures also show that AODV outperforms OLSR and DSDV in both PDR and throughput.

According to the network delay, it can be seen from Fig. 8.8 that the average end-to-end delay enhances as the network size increases in all routing protocols.

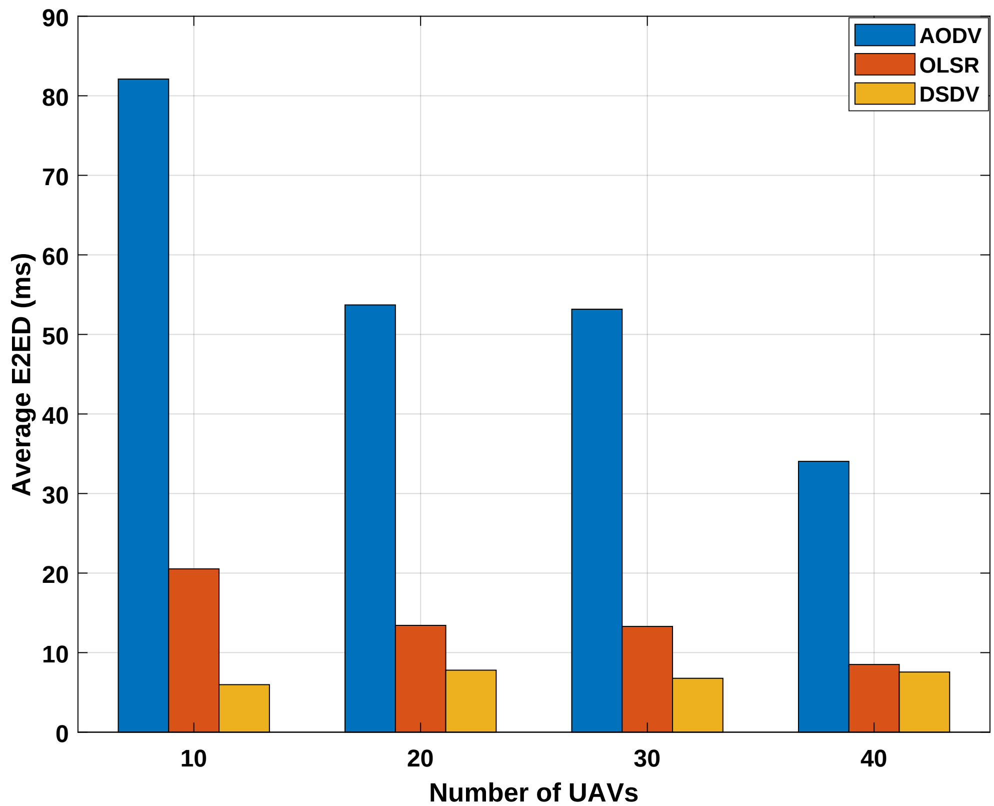

Figure 8.8: Average end-to-end delay with speed of 30 mps for the AODV, OLSR, and DSDV routing protocols.

This is because increasing the number of nodes in the network provides a high chance to find the route to the destination which reduces the time to discover the route. However, DSDV exhibits the lowest end-to-end delay.

8.5 Chapter Summary

In this chapter, we analyzed the performance of AODV, OLSR, and DSDV routing protocols in terms of average packet delivery ratio, end-to-end delay, and throughput. The results revealed that DSDV is not appropriate for high dynamic networks like drone networks since the packet delivery ratio is significantly decreased as the speed of drones increases. The results also showed that the OLSR routing algorithm is not suitable for highly-dynamic and low-density networks like UAV networks. Despite these limitations, proactive algorithms offer fast connections among drones. This is due to the availability of routing information in the routing table when needed. Thus, the data traffic is sent with no delay when the sender needs to send its data. The reactive routing protocol, AODV, outperformed both OLSR and DSDV in terms of packet delivery ratio and throughput. This can be concluded from the reactive nature with topology changes. On the other hand, AODV suffers from a high end-to-end delay. We can conclude that no routing protocols achieved optimal performance. Thus, the suitable routing protocol can be selected according to the required performance. However, AODV routing protocol seems to be the most appropriate routing protocol for dynamic topology change like UAVs network adopted in this thesis due to its reactive nature to dynamic topology change.

CHAPTER 9

CONCLUSION AND FUTURE WORK

Intelligent Transportation Systems (ITS) have gained broad-spectrum attention as a leading technology to exploit the smart devices involved in the transportation object that improves transportation systems. The importance of the ITS lies in many factors, such as increasing the global population, globalization, and modernization, which lead to high demands for vehicle transportation. The development of ITS is a cornerstone in the designing and implementation of smart cities. The goal of ITS is to automate the interactions between infrastructure and vehicles for competence in vehicular communication, comfort, and accomplishing high levels of safety measures. In this final chapter, the relevant contributions are summarized, an outlook on potential future work is sketched out, and the publications emanating from this thesis are listed

9.1 Thesis Conclusions

To foster the adaptation of the existing collision avoidance and deployment of drones in intelligent transportation systems, this thesis makes the following contributions.

9.1.1 Energy-efficient static and dynamic collision avoidance

Two approaches are proposed for collision avoidance. The first approach is to deal with static collision avoidance, and presented in chapter 3. The aim is to enhance the optimality and rapidity of three dimensional IoDs path generation by improving the particle swarm optimization (PSO) algorithm. The results exhibit significant improvement in convergence speed as well as an optimal solution, which proves the ability of the proposed method to generate a safety path for IoDs formation without collision with terrain obstacle and among drones. It also presents thorough analysis considering the optimality and rapidity of IPSO in generating collision-free paths for IoDs.

To tackle the challenging of dynamic collision avoidance and energy limitation, this thesis proposes an online Energy-efficient static and dynamic collision avoidance approach presented in chapter 4. The proposed approach aims to work online in a dense environment in which a drone flies through a narrow passage due to several static and dynamic obstacles filled the terrain. Therefore, the feasible paths from current locations for all drones in IoD formation are not always guaranteed. To guarantee a feasible paths for all drones in the formation, the proposed approach puts some drones in a hovering state for some time. Furthermore, the drone can backtrack when hovering in place is not possible. It is worth mentioning that, the drone is allowed to fly vertically if hovering and backtracking are not possible to avoid crashing with nearby obstacles, which increases the ability to avoid collisions. It also provides an energy-efficient path generation to obtain a collision-free path with minimum energy requirement. The algorithm is able to avoid the following collisions:

- Drone-to-drone collision avoidance.
- Drone-to-static obstacles collision avoidance.
- Drone-to-dynamic obstacles collision avoidance.

The proposed approach is implemented using matlab software.

9.1.2 2D Collaborative IoD-Assisted VANETs (IoDAV)

The dynamic deployment of drones for VANET assistant is presented in chapter 5. The aim is to dynamically dispatching the IoD, used as a relay network, at optimum coverage base-on cars' locations using RSSI. In this work, the IPSO algorithm presented in chapter in 3 is implemented to achieve the aforementioned objectives so that sufficient signal strength towards all isolated vehicles on the ground can be achieved by the IoD network to guarantee the best coverage at each specific time. Moreover, the connectivity of the IoD network is addressed by the proposed optimization approach where the objective function includes the connectivity to be achieved for a better solution. Based on the vehicles' distribution on the ground, the proposed approach dispatches the IoD nodes to the most appropriate locations in real-time. The main assumption is that lack of infrastructures exists in the environment and the connectivity among vehicles is minimum. For example in urban area, the buildings may obstruct the line of sight and the connectivity among vehicles is lost. Besides, the movement of UAVs in IoD aims to explore the 3D space to offer the connectivity to the ground vehicles. The SUMO, VIENS, in OMNET++ network simulator are utilized to implement the proposed approach. Besides, the IoDAV is compared against VANET without drone, i.e, No IoD and with static deployment IoD, i.e., FIoD. The IoDAV outperforms NIoD and FIoD in terms of normalized overall coverage and average RSSI.

9.1.3 3D Collaborative IoD-Assisted VANETs (3DIoDAV)

The terrain obstacles have a significant impact on Air-to-ground communication, where the terrain obstacles might block the transmitted signal. For practical result, the terrain elevation should be considered when calculating the received signal strength. Therefore, this thesis proposes 3DIoDAV that is presented in chapter 6. The aim is to enhance the communication of vehicles on the ground and reduce the impact of terrain obstacles on communication. In doing so, the 3D propagation model for IoD2V communication to assist the communication quality between IoD in air and cars on the ground is proposed and used in IoD assisted VANETs. Towards this end, the optimal deployment of IoD nodes is obtained by the optimization algorithm implemented, i.e., IPSO. The proposed 3D propagation model is added to the objective function to evaluate the signal quality at receivers ‘sides, i.e., vehicles on the ground in which the effect of high-level terrain on communication is considered in calculating the received signal. As a result, the IoD nodes are dispatched to the most appropriate locations that minimize the impact of terrain obstacles on the transmitted signals and enhance the LOS condition between sender and receiver. The proposed approach is implemented using SUMO and VIENS in OMNET++ network simulator. The effect of the terrain is considered by extracting the elevation information of the terrain from the Digital Elevation Model (DEM) file and use it in calculating the received signal strength. Besides, the 3DIoDAV is compared against free-space pathloss model and IoDAV model. The results show the ability of 3DIoDAV to detect the terrain obstacles and properly evaluated the received signal quality. Besides, the 3DIoDAV approach can retrieve the terrain information and considers it in the communication of IoD in the air and vehicles on the ground, which provides a high level of realism results.

9.1.4 Energy-efficient Collision-free Coverage Path Planning

The key aim is to develop a mathematical model for path planning and coverage based on MILP formulation, and compare it with heuristic approach for different problem sizes. An optimization formulation of single and multi-UAVs collision-free coverage path planning is derived. To do so,the MILP is used to formulate the CPP problem as a minimization problem, where the energy consumption is used as the objective to be minimized. The proposed approach is capable of reducing energy consumption which in turn reduces the required number of drones to cover the ROI.

9.1.5 IoD Routing Protocols

Exploring different routing protocols for IoD. In the light of collision-free path planning and IoD deployment for VANET assistant, the drone speed does not exceed 10 m/s to efficiently generate collision-free path planning. As a result, AODV has been seen to be the most appropriate routing protocol for IoD.

9.2 Future Work

- Since the convergence speed as well as solution optimality presented in Chapter 3 are enhanced, in the future work, we will focus on using IPSO to plan IoD paths in a dynamic environment which includes unexpected obstacles (i.e movable obstacles) where the movable obstacles need to be avoided on time.

- IoDAV approach presented in Chapter 5 will be extended to include the influence of other propagation models such as Nakagami Fading on communication.

- The proposed model presented in Chapter 6 can be extended for future work by considering the buildings as obstacles, where signal attenuation will be investigated.

REFERENCES

[1] I. Yaqoob, L. U. Khan, S. M. A. Kazmi, M. Imran, N. Guizani, and C. S. Hong, "Autonomous driving cars in smart cities: Recent advances, requirements, and challenges," *IEEE Network*, vol. 34, no. 1, pp. 174–181, 2020.

[2] G. Ahmed, T. Sheltami, A. Mahmoud, and A. Yasar, "Iod swarms collision avoidance via improved particle swarm optimization," *Transportation Research Part A: Policy and Practice*, vol. 142, pp. 260–278, 2020.

[3] N. Lin, L. Fu, L. Zhao, G. Min, A. Al-Dubai, and H. Gacanin, "A novel multimodal collaborative drone-assisted vanet networking model," *IEEE Transactions on Wireless Communications*, 2020.

[4] W. H. O. D. of Violence, I. Prevention, W. H. O. Violence, I. Prevention, and W. H. Organization, *Global status report on road safety: time for action.* World Health Organization, 2009.

[5] L. Hota, B. P. Nayak, A. Kumar, B. Sahoo, G. Ali *et al.*, "A performance analysis of vanets propagation models and routing protocols," *Sustainability*, vol. 14, no. 3, p. 1379, 2022.

[6] E. Hossain, G. Chow, V. C. Leung, R. D. McLeod, J. Mišić, V. W. Wong, and O. Yang, "Vehicular telematics over heterogeneous wireless networks: A survey," *Computer communications*, vol. 33, no. 7, pp. 775–793, 2010.

[7] G. Ahmed, T. Sheltami, M. Deriche, and A. Yasar, "An energy efficient iod static and dynamic collision avoidance approach based on gradient optimization," *Ad Hoc Networks*, vol. 118, p. 102519, 2021.

[8] T. Xu, S. Zhang, Z. Jiang, Z. Liu, and H. Cheng, "Collision avoidance of high-speed obstacles for mobile robots via maximum-speed aware velocity obstacle method," *IEEE Access*, vol. 8, pp. 138 493–138 507, 2020.

[9] S. W. Cho, H. J. Park, H. Lee, D. H. Shim, and S.-Y. Kim, "Coverage path planning for multiple unmanned aerial vehicles in maritime search and rescue operations," *Computers & Industrial Engineering*, vol. 161, p. 107612, 2021.

[10] C. S. Tan, R. Mohd-Mokhtar, and M. R. Arshad, "A comprehensive review of coverage path planning in robotics using classical and heuristic algorithms," *IEEE Access*, 2021.

[11] A. Ashraf, A. Majd, and E. Troubitsyna, "Online path generation and navigation for swarms of uavs," *Scientific Programming*, vol. 2020, 2020.

[12] R. Battulwar, G. Winkelmaier, J. Valencia, M. Z. Naghadehi, B. Peik, B. Abbasi, B. Parvin, and J. Sattarvand, "A practical methodology for generating high-resolution 3d models of open-pit slopes using uavs: Flight

path planning and optimization," *Remote Sensing*, vol. 12, no. 14, p. 2283, 2020.

[13] J. N. Yasin, S. A. S. Mohamed, M.-H. Haghbayan, J. Heikkonen, H. Tenhunen, M. M. Yasin, and J. Plosila, "Energy-efficient formation morphing for collision avoidance in a swarm of drones," *IEEE Access*, vol. 8, pp. 170 681–170 695, 2020.

[14] M. Li, N. Cheng, J. Gao, Y. Wang, L. Zhao, and X. Shen, "Energy-efficient uav-assisted mobile edge computing: Resource allocation and trajectory optimization," *IEEE Transactions on Vehicular Technology*, vol. 69, no. 3, pp. 3424–3438, 2020.

[15] S. Al-Sultan, M. M. Al-Doori, A. H. Al-Bayatti, and H. Zedan, "A comprehensive survey on vehicular ad hoc network," *Journal of network and computer applications*, vol. 37, pp. 380–392, 2014.

[16] K. Zheng, Q. Zheng, P. Chatzimisios, W. Xiang, and Y. Zhou, "Heterogeneous vehicular networking: A survey on architecture, challenges, and solutions," *IEEE communications surveys & tutorials*, vol. 17, no. 4, pp. 2377–2396, 2015.

[17] N. B. Truong, G. M. Lee, and Y. Ghamri-Doudane, "Software defined networking-based vehicular adhoc network with fog computing," in *2015 IFIP/IEEE International Symposium on Integrated Network Management (IM).* Ieee, 2015, pp. 1202–1207.

[18] A. Manzoor, T. N. Dang, and C. S. Hong, “Uav trajectory design for uav-2-gv communication in vanets,” in *2021 International Conference on Information Networking (ICOIN)*. IEEE, 2021, pp. 219–224.

[19] L. Xu, X. Zhou, M. A. Khan, X. Li, V. G. Menon, and X. Yu, “Communication quality prediction for internet of vehicle (iov) networks: An elman approach,” *IEEE Transactions on Intelligent Transportation Systems*, 2021.

[20] S. Zhu, G. Lin, D. Zhao, N. Cheng, Q. Zhang, and X. Lang, “Learning-based computation offloading approaches in uavs-assisted edge computing,” *IEEE Transactions on Vehicular Technology*, vol. 70, no. 1, pp. 928 – 944, Jan. 2021.

[21] G. Raja, S. Anbalagan, A. G. Subramaniyan, M. S. Selvakumar, A. K. Bashir, and S. Mumtaz, “Efficient and secured swarm pattern multi-uav communication,” *IEEE Transactions on Vehicular Technology*, 2021.

[22] G.-W. Yang and S. Zhang, “A dual-band shared-aperture antenna with wide-angle scanning capability for mobile system applications,” *IEEE Transactions on Vehicular Technology*, vol. 70, no. 5, pp. 4088–4097, 2021.

[23] A. G. Melo, M. F. Pinto, A. L. Marcato, L. M. Honório, and F. O. Coelho, “Dynamic optimization and heuristics based online coverage path planning in 3d environment for uavs,” *Sensors*, vol. 21, no. 4, p. 1108, 2021.

[24] I. Maza and A. Ollero, "Multiple uav cooperative searching operation using polygon area decomposition and efficient coverage algorithms," in *Distributed Autonomous Robotic Systems 6*. Springer, 2007, pp. 221–230.

[25] O. K. Sahingoz, "Mobile networking with uavs: Opportunities and challenges," in *2013 International Conference on Unmanned Aircraft Systems (ICUAS)*. IEEE, 2013, pp. 933–941.

[26] K. Zhang, W. Zhang, and J.-Z. Zeng, "Preliminary study of routing and date integrity in mobile ad hoc uav network," in *2008 International Conference on Apperceiving Computing and Intelligence Analysis*. IEEE, 2008, pp. 347–350.

[27] W. Wu, F. Zhou, B. Wang, Q. Wu, C. Dong, and R. Q. Hu, "Unmanned aerial vehicle swarm-enabled edge computing: Potentials, promising technologies, and challenges," *arXiv preprint arXiv:2201.08517*, 2022.

[28] G. A. Ahmed, T. R. Sheltami, A. S. Mahmoud, M. Imran, and M. Shoaib, "A novel collaborative iod-assisted vanet approach for coverage area maximization," *IEEE Access*, vol. 9, pp. 61 211–61 223, 2021.

[29] S. Shao, Y. Peng, C. He, and Y. Du, "Efficient path planning for uav formation via comprehensively improved particle swarm optimization," *ISA transactions*, 2019.

[30] B. T. Ingersoll, J. K. Ingersoll, P. DeFranco, and A. Ning, "Uav path-planning using bezier curves and a receding horizon approach," in *Aiaa modeling and simulation technologies conference*, 2016, p. 3675.

[31] P. Yao, H. Wang, and Z. Su, "Cooperative path planning with applications to target tracking and obstacle avoidance for multi-uavs," *Aerospace Science and Technology*, vol. 54, pp. 10–22, 2016.

[32] Y. Chen, J. Yu, X. Su, and G. Luo, "Path planning for multi-uav formation," *Journal of Intelligent & Robotic Systems*, vol. 77, no. 1, pp. 229–246, 2015.

[33] Y.-b. Chen, G.-c. Luo, Y.-s. Mei, J.-q. Yu, and X.-l. Su, "Uav path planning using artificial potential field method updated by optimal control theory," *International Journal of Systems Science*, vol. 47, no. 6, pp. 1407–1420, 2016.

[34] Y. V. Pehlivanoglu, "A new vibrational genetic algorithm enhanced with a voronoi diagram for path planning of autonomous uav," *Aerospace Science and Technology*, vol. 16, no. 1, pp. 47–55, 2012.

[35] S. Bayili and F. Polat, "Limited-damage a*: A path search algorithm that considers damage as a feasibility criterion," *Knowledge-Based Systems*, vol. 24, no. 4, pp. 501–512, 2011.

[36] M. Baumann, S. Léonard, E. A. Croft, and J. J. Little, "Path planning for improved visibility using a probabilistic road map," *IEEE Transactions on Robotics*, vol. 26, no. 1, pp. 195–200, 2010.

[37] M. A. Brubaker, A. Geiger, and R. Urtasun, "Map-based probabilistic visual self-localization," *IEEE transactions on pattern analysis and machine intelligence*, vol. 38, no. 4, pp. 652–665, 2015.

[38] M. Kothari and I. Postlethwaite, "A probabilistically robust path planning algorithm for uavs using rapidly-exploring random trees," *Journal of Intelligent & Robotic Systems*, vol. 71, no. 2, pp. 231–253, 2013.

[39] C.-b. Moon and W. Chung, "Kinodynamic planner dual-tree rrt (dt-rrt) for two-wheeled mobile robots using the rapidly exploring random tree," *IEEE Transactions on industrial electronics*, vol. 62, no. 2, pp. 1080–1090, 2014.

[40] H. Ma, S. Shen, M. Yu, Z. Yang, M. Fei, and H. Zhou, "Multi-population techniques in nature inspired optimization algorithms: a comprehensive survey," *Swarm and evolutionary computation*, vol. 44, pp. 365–387, 2019.

[41] Y. Zhao, Z. Zheng, and Y. Liu, "Survey on computational-intelligence-based uav path planning," *Knowledge-Based Systems*, vol. 158, pp. 54–64, 2018.

[42] M. Dileep, S. Kamath, and V. G. Nair, "Particle swarm optimization applied to ascent phase launch vehicle trajectory optimization problem," *Procedia Computer Science*, vol. 54, pp. 516–522, 2015.

[43] A. Rahimi, K. Dev Kumar, and H. Alighanbari, "Particle swarm optimization applied to spacecraft reentry trajectory," *Journal of Guidance, Control, and Dynamics*, vol. 36, no. 1, pp. 307–310, 2013.

[44] D. E. Kirk, *Optimal control theory: an introduction.* Courier Corporation, 2004.

[45] J. N. Yasin, S. A. Mohamed, M.-H. Haghbayan, J. Heikkonen, H. Tenhunen, and J. Plosila, "Navigation of autonomous swarm of drones using translational coordinates," in *International Conference on Practical Applications of Agents and Multi-Agent Systems.* Springer, 2020, pp. 353–362.

[46] X. Xia, Y. Xing, B. Wei, Y. Zhang, X. Li, X. Deng, and L. Gui, "A fitness-based multi-role particle swarm optimization," *Swarm and evolutionary computation*, vol. 44, pp. 349–364, 2019.

[47] A. Lin, W. Sun, H. Yu, G. Wu, and H. Tang, "Global genetic learning particle swarm optimization with diversity enhancement by ring topology," *Swarm and evolutionary computation*, vol. 44, pp. 571–583, 2019.

[48] A. Gopal, M. M. Sultani, and J. C. Bansal, "On stability analysis of particle swarm optimization algorithm," *Arabian Journal for Science and Engineering*, pp. 1–10, 2019.

[49] C. Gao, Z. Zhen, and H. Gong, "A self-organized search and attack algorithm for multiple unmanned aerial vehicles," *Aerospace Science and Technology*, vol. 54, pp. 229–240, 2016.

[50] I. Fister, I. Fister Jr, X.-S. Yang, and J. Brest, "A comprehensive review of firefly algorithms," *Swarm and Evolutionary Computation*, vol. 13, pp. 34–46, 2013.

[51] Y. Liu, X. Zhang, X. Guan, and D. Delahaye, “Adaptive sensitivity decision based path planning algorithm for unmanned aerial vehicle with improved particle swarm optimization,” *Aerospace Science and Technology*, vol. 58, pp. 92–102, 2016.

[52] D. Tian and Z. Shi, “Mpso: Modified particle swarm optimization and its applications,” *Swarm and evolutionary computation*, vol. 41, pp. 49–68, 2018.

[53] L. N. N. T. Ha, D. H. P. Bui, S. K. Hong *et al.*, “Nonlinear control for autonomous trajectory tracking while considering collision avoidance of uavs based on geometric relations,” *Energies*, vol. 12, no. 8, p. 1551, 2019.

[54] Z. Lin, L. Castano, E. Mortimer, and H. Xu, “Fast 3d collision avoidance algorithm for fixed wing uas,” *Journal of Intelligent & Robotic Systems*, vol. 97, no. 3, pp. 577–604, 2020.

[55] A. E. Oguz and E. Duymaz, “Artificial potantial field based autonomus uav fligh in dynamic environment,” in *16th AIAA Aviation Technology, Integration, and Operations Conference*, 2016, p. 3454.

[56] C. Y. Kim, Y. H. Kim, and W.-S. Ra, “Modified 1d virtual force field approach to moving obstacle avoidance for autonomous ground vehicles,” *Journal of Electrical Engineering & Technology*, vol. 14, no. 3, pp. 1367–1374, 2019.

[57] D. Choi, K. Lee, and D. Kim, "Enhanced potential field-based collision avoidance for unmanned aerial vehicles in a dynamic environment," in *AIAA Scitech 2020 Forum*, 2020, p. 0487.

[58] Y. Watanabe, A. Calise, and E. Johnson, "Vision-based obstacle avoidance for uavs," in *AIAA guidance, navigation and control conference and exhibit*, 2007, p. 6829.

[59] S. Biswas, S. G. Anavatti, and M. A. Garratt, "A particle swarm optimization based path planning method for autonomous systems in unknown terrain," in *2019 IEEE International Conference on Industry 4.0, Artificial Intelligence, and Communications Technology (IAICT)*. IEEE, 2019, pp. 57–63.

[60] P. Sujit and R. Beard, "Multiple uav path planning using anytime algorithms," in *2009 American control conference*. IEEE, 2009, pp. 2978–2983.

[61] S. Pérez-Carabaza, J. Scherer, B. Rinner, J. A. López-Orozco, and E. Besada-Portas, "Uav trajectory optimization for minimum time search with communication constraints and collision avoidance," *Engineering Applications of Artificial Intelligence*, vol. 85, pp. 357–371, 2019.

[62] D. M. Vijayakumari, S. Kim, J. Suk, and H. Mo, "Receding-horizon trajectory planning for multiple uavs using particle swarm optimization," in *AIAA Scitech 2019 Forum*, 2019, p. 1165.

[63] C. Di Franco and G. Buttazzo, “Coverage path planning for uavs photogrammetry with energy and resolution constraints,” *Journal of Intelligent & Robotic Systems*, vol. 83, no. 3-4, pp. 445–462, 2016.

[64] T. M. Cabreira, P. R. Ferreira, C. Di Franco, and G. C. Buttazzo, “Grid-based coverage path planning with minimum energy over irregular-shaped areas with uavs,” in *2019 International Conference on Unmanned Aircraft Systems (ICUAS)*. IEEE, 2019, pp. 758–767.

[65] F. Leo, E. Ferrari, C. Baccelliere, J. Zarate, H. Shea, E. Cocchi, A. Waszkielewicz, and L. Brayda, “Enhancing general spatial skills of young visually impaired people with a programmable distance discrimination training: a case control study,” *Journal of neuroengineering and rehabilitation*, vol. 16, no. 1, pp. 1–16, 2019.

[66] W. Rafique, L. Qi, I. Yaqoob, M. Imran, R. U. Rasool, and W. Dou, “Complementing iot services through software defined networking and edge computing: A comprehensive survey,” *IEEE Communications Surveys Tutorials*, vol. 22, no. 3, pp. 1761–1804, 2020.

[67] Y. Liu, H.-N. Dai, Q. Wang, M. K. Shukla, and M. Imran, “Unmanned aerial vehicle for internet of everything: Opportunities and challenges,” *Computer Communications*, vol. 155, pp. 66–83, 2020. [Online]. Available: https://www.sciencedirect.com/science/article/pii/S0140366419318754

[68] M. Younis and K. Akkaya, "Strategies and techniques for node placement in wireless sensor networks: A survey," *Ad Hoc Networks*, vol. 6, no. 4, pp. 621–655, 2008.

[69] Y. Shi, Y. T. Hou, and A. Efrat, "Algorithm design for base station placement problems in sensor networks," in *Proceedings of the 3rd international conference on Quality of service in heterogeneous wired/wireless networks*, 2006, pp. 13–es.

[70] J. Lee and C. M. Kim, "A roadside unit placement scheme for vehicular telematics networks," in *Advances in computer science and information technology.* Springer, 2010, pp. 196–202.

[71] O. Trullols, M. Fiore, C. Casetti, C.-F. Chiasserini, and J. B. Ordinas, "Planning roadside infrastructure for information dissemination in intelligent transportation systems," *Computer Communications*, vol. 33, no. 4, pp. 432–442, 2010.

[72] B. Aslam, F. Amjad, and C. C. Zou, "Optimal roadside units placement in urban areas for vehicular networks," in *2012 IEEE Symposium on Computers and Communications (ISCC).* IEEE, 2012, pp. 000 423–000 429.

[73] Y. Liu, H.-N. Dai, H. Wang, M. Imran, X. Wang, and M. Shoaib, "Uav-enabled data acquisition scheme with directional wireless energy transfer for internet of things," *Computer Communications*, vol. 155,

pp. 184–196, 2020. [Online]. Available: https://www.sciencedirect.com/science/article/pii/S0140366419304852

[74] M. Mozaffari, W. Saad, M. Bennis, and M. Debbah, "Efficient deployment of multiple unmanned aerial vehicles for optimal wireless coverage," *IEEE Communications Letters*, vol. 20, no. 8, pp. 1647–1650, 2016.

[75] I. A. Nemer, T. R. Sheltami, and A. S. Mahmoud, "A game theoretic approach of deployment a multiple uavs for optimal coverage," *Transportation Research Part A: Policy and Practice*, vol. 140, pp. 215–230, 2020.

[76] S. Yan, M. Peng, and X. Cao, "A game theory approach for joint access selection and resource allocation in uav assisted iot communication networks," *IEEE Internet of Things Journal*, vol. 6, no. 2, pp. 1663–1674, Oct. 2018.

[77] B. Jiang, J. Yang, H. Xu, H. Song, and G. Zheng, "Multimedia data throughput maximization in internet-of-things system based on optimization of cache-enabled uav," *IEEE Internet of Things Journal*, vol. 6, no. 2, pp. 3525–3532, Dec. 2018.

[78] H. Shakhatreh, A. Khreishah, A. Alsarhan, I. Khalil, A. Sawalmeh, and N. S. Othman, "Efficient 3d placement of a uav using particle swarm optimization," in *2017 8th International Conference on Information and Communication Systems (ICICS)*. IEEE, 2017, pp. 258–263.

[79] X. He, W. Yu, H. Xu, J. Lin, X. Yang, C. Lu, and X. Fu, "Towards 3d deployment of uav base stations in uneven terrain," in *2018 27th International*

Conference on Computer Communication and Networks (ICCCN). IEEE, 2018, pp. 1–9.

[80] E. Tuba, R. Capor-Hrosik, A. Alihodzic, and M. Tuba, "Drone placement for optimal coverage by brain storm optimization algorithm," in *International Conference on Health Information Science*. Springer, 2017, pp. 167–176.

[81] S. Sabino and A. Grilo, "Topology control of unmanned aerial vehicle (uav) mesh networks: A multi-objective evolutionary algorithm approach," in *Proceedings of the 4th ACM Workshop on Micro Aerial Vehicle Networks, Systems, and Applications*, 2018, pp. 45–50.

[82] Q. Yang and S.-J. Yoo, "Optimal uav path planning: Sensing data acquisition over iot sensor networks using multi-objective bio-inspired algorithms," *IEEE Access*, vol. 6, pp. 13 671–13 684, 2018.

[83] M. Gupta and S. Varma, "Optimal placement of uavs of an aerial mesh network in an emergency situation," *Journal of Ambient Intelligence and Humanized Computing*, vol. 12, no. 1, pp. 343–358, Jan. 2021.

[84] C. Sommer, D. Eckhoff, R. German, and F. Dressler, "A computationally inexpensive empirical model of ieee 802.11 p radio shadowing in urban environments," in *2011 Eighth international conference on wireless on-demand network systems and services*. IEEE, 2011, pp. 84–90.

[85] P. Pourbaba, K. S. Manosha, S. Ali, and N. Rajatheva, "Full-duplex uav relay positioning for vehicular communications with underlay v2v links,"

in *2019 IEEE 89th Vehicular Technology Conference (VTC2019-Spring)*. IEEE, 2019, pp. 1–6.

[86] O. S. Oubbati, N. Chaib, A. Lakas, P. Lorenz, and A. Rachedi, "Uav-assisted supporting services connectivity in urban vanets," *IEEE Transactions on Vehicular Technology*, vol. 68, no. 4, pp. 3944–3951, 2019.

[87] O. S. Oubbati, A. Lakas, P. Lorenz, M. Atiquzzaman, and A. Jamalipour, "Leveraging communicating uavs for emergency vehicle guidance in urban areas," *IEEE Transactions on Emerging Topics in Computing*, 2019.

[88] X. Wang, L. Fu, Y. Zhang, X. Gan, and X. Wang, "Vdnet: an infrastructure-less uav-assisted sparse vanet system with vehicle location prediction," *Wireless Communications and Mobile Computing*, vol. 16, no. 17, pp. 2991–3003, 2016.

[89] X. Lin, V. Yajnanarayana, S. D. Muruganathan, S. Gao, H. Asplund, H.-L. Maattanen, M. Bergstrom, S. Euler, and Y.-P. E. Wang, "The sky is not the limit: Lte for unmanned aerial vehicles," *IEEE Communications Magazine*, vol. 56, no. 4, pp. 204–210, 2018.

[90] O. S. Oubbati, A. Lakas, M. Güneş, F. Zhou, and M. B. Yagoubi, "Uav-assisted reactive routing for urban vanets," in *Proceedings of the Symposium on Applied Computing*, 2017, pp. 651–653.

[91] H. Seliem, R. Shahidi, M. H. Ahmed, and M. S. Shehata, "Drone-based highway-vanet and das service," *IEEE Access*, vol. 6, pp. 20 125–20 137, 2018.

[92] O. S. Oubbati, A. Lakas, F. Zhou, M. Güneş, N. Lagraa, and M. B. Yagoubi, "Intelligent uav-assisted routing protocol for urban vanets," *Computer communications*, vol. 107, pp. 93–111, 2017.

[93] S. A. Hadiwardoyo, C. T. Calafate, J.-C. Cano, Y. Ji, E. Hernández-Orallo, and P. Manzoni, "3d simulation modeling of uav-to-car communications," *Ieee Access*, vol. 7, pp. 8808–8823, 2018.

[94] S. A. Hadiwardoyo, C. T. Calafate, J.-C. Cano, K. Krinkin, D. Klionskiy, E. Hernández-Orallo, and P. Manzoni, "optimizing uav-to-car communications in 3d environments through dynamic uav positioning," in *2019 IEEE/ACM 23rd International Symposium on Distributed Simulation and Real Time Applications (DS-RT)*. IEEE, 2019, pp. 1–8.

[95] H.-Y. Lin, C.-W. Yao, K.-S. Cheng *et al.*, "Topological map construction and scene recognition for vehicle localization," *Autonomous Robots*, vol. 42, no. 1, pp. 65–81, 2018.

[96] A. Ghaddar, A. Merei, and E. Natalizio, "Pps: Energy-aware grid-based coverage path planning for uavs using area partitioning in the presence of nfzs," *Sensors*, vol. 20, no. 13, p. 3742, 2020.

[97] R. I. da Silva and M. A. Nascimento, "On best drone tour plans for data collection in wireless sensor network," in *Proceedings of the 31st annual ACM symposium on applied computing*, 2016, pp. 703–708.

[98] E. Galceran and M. Carreras, "A survey on coverage path planning for robotics," *Robotics and Autonomous systems*, vol. 61, no. 12, pp. 1258–1276, 2013.

[99] C. Di Franco and G. Buttazzo, "Energy-aware coverage path planning of uavs," in *2015 IEEE international conference on autonomous robot systems and competitions*. IEEE, 2015, pp. 111–117.

[100] A. Király and J. Abonyi, "Redesign of the supply of mobile mechanics based on a novel genetic optimization algorithm using google maps api," *Engineering Applications of Artificial Intelligence*, vol. 38, pp. 122–130, 2015.

[101] A. Ghaddar and A. Merei, "Eaoa: Energy-aware grid-based 3d-obstacle avoidance in coverage path planning for uavs," *Future Internet*, vol. 12, no. 2, p. 29, 2020.

[102] J. Valente, A. Barrientos Cruz, J. d. Cerro Giner, and D. Sanz Muñoz, "A waypoint-based mission planner for a farmland coverage with an aerial robot-a precision farming tool," 2011.

[103] A. Ghaddar and A. Merei, "Energy-aware grid based coverage path planning for uavs," in *Proceedings of the Thirteenth International Conference on*

Sensor Technologies and Applications SENSORCOMM, Nice, France, 2019, pp. 27–31.

[104] I. Shnaps and E. Rimon, "Online coverage of planar environments by a battery powered autonomous mobile robot," *IEEE Transactions on Automation Science and engineering*, vol. 13, no. 2, pp. 425–436, 2016.

[105] R. J. Afonso, M. R. Maximo, and R. K. Galvão, "Task allocation and trajectory planning for multiple agents in the presence of obstacle and connectivity constraints with mixed-integer linear programming," *International Journal of Robust and Nonlinear Control*, vol. 30, no. 14, pp. 5464–5491, 2020.

[106] Y. Zuo, R. Tharmarasa, R. Jassemi-Zargani, N. Kashyap, J. Thiyagalingam, and T. T. Kirubarajan, "Milp formulation for aircraft path planning in persistent surveillance," *IEEE Transactions on Aerospace and Electronic Systems*, vol. 56, no. 5, pp. 3796–3811, 2020.

[107] G. Wang, Q. Li, and L. Guo, "Multiple uavs routes planning based on particle swarm optimization algorithm," in *2010 2nd International Symposium on Information Engineering and Electronic Commerce.* IEEE, 2010, pp. 1–5.

[108] H. Tong *et al.*, "Path planning of uav based on voronoi diagram and dpso," *Procedia Engineering*, vol. 29, pp. 4198–4203, 2012.

[109] W. Zheng, L. Qiaoqiao, T. Hongtao, and L. Jianxun, "Multiple task planning based on ts algorithm for multiple heterogeneous unmanned aerial ve-

hicles," in *Proceedings of 2014 IEEE Chinese Guidance, Navigation and Control Conference.* IEEE, 2014, pp. 630–635.

[110] T. Turker, O. K. Sahingoz, and G. Yilmaz, "2d path planning for uavs in radar threatening environment using simulated annealing algorithm," in *2015 International Conference on Unmanned Aircraft Systems (ICUAS).* IEEE, 2015, pp. 56–61.

[111] V. Roberge, M. Tarbouchi, and G. Labonté, "Comparison of parallel genetic algorithm and particle swarm optimization for real-time uav path planning," *IEEE Transactions on industrial informatics*, vol. 9, no. 1, pp. 132–141, 2012.

[112] A. Sonmez, E. Kocyigit, and E. Kugu, "Optimal path planning for uavs using genetic algorithm," in *2015 International Conference on Unmanned Aircraft Systems (ICUAS).* IEEE, 2015, pp. 50–55.

[113] R. Shivgan and Z. Dong, "Energy-efficient drone coverage path planning using genetic algorithm," in *2020 IEEE 21st International Conference on High Performance Switching and Routing (HPSR).* IEEE, 2020, pp. 1–6.

[114] C. Zhao, Y. Liu, and J. Zhao, "Path planning method of uav area coverage searching based on pega," *Science and Technology Review*, vol. 32, no. 22, pp. 85–90, 2014.

[115] I. A. Hameed, "Intelligent coverage path planning for agricultural robots and autonomous machines on three-dimensional terrain," *Journal of Intelligent & Robotic Systems*, vol. 74, no. 3, pp. 965–983, 2014.

[116] X. Hu and Z. Lin, "Coverage path planning of penaeus vannamei feeding based on global and multiple local areas," in *International Conference on Data Service*. Springer, 2019, pp. 687–697.

[117] J. Kennedy, "The particle swarm: social adaptation of knowledge," in *Proceedings of 1997 IEEE International Conference on Evolutionary Computation (ICEC'97)*. IEEE, 1997, pp. 303–308.

[118] T.-K. Lee, S.-H. Baek, Y.-H. Choi, and S.-Y. Oh, "Smooth coverage path planning and control of mobile robots based on high-resolution grid map representation," *Robotics and Autonomous Systems*, vol. 59, no. 10, pp. 801–812, 2011.

[119] T. K. Priyambodo, D. Wijayanto, and M. S. Gitakarma, "Performance optimization of manet networks through routing protocol analysis," *Computers*, vol. 10, no. 1, p. 2, 2021.

[120] A. Guillen-Perez, A.-M. Montoya, J.-C. Sanchez-Aarnoutse, and M.-D. Cano, "A comparative performance evaluation of routing protocols for flying ad-hoc networks in real conditions," *Applied Sciences*, vol. 11, no. 10, p. 4363, 2021.

[121] N. I. Shuhaimi, N. L. Ashmadi, E. Abdullah, R. Mohamad, and S. Y. Mohamad, "Performance analysis of radio propagation models in vanet application," in *2021 IEEE 11th IEEE Symposium on Computer Applications & Industrial Electronics (ISCAIE)*. IEEE, 2021, pp. 372–377.

[122] A. Hinds, M. Ngulube, S. Zhu, and H. Al-Aqrabi, "A review of routing protocols for mobile ad-hoc networks (manet)," *International journal of information and education technology*, vol. 3, no. 1, p. 1, 2013.

[123] E. P. de Freitas, T. Heimfarth, F. R. Wagner, C. E. Pereira, and T. Larsson, "Exploring geographic context awareness for data dissemination on mobile ad hoc networks," *Ad hoc networks*, vol. 11, no. 6, pp. 1746–1764, 2013.

[124] S. Arvind Narayan, R. Rajashekar Reddy, and J. Femilda Josephin, "Secured congestion control in vanet using greedy perimeter stateless routing (gpsr)," in *Artificial Intelligence and Evolutionary Computations in Engineering Systems*. Springer, 2020, pp. 683–700.

[125] L. Wu and X. Wang, "Performance analysis of cbrp, aodv and dsr routing protocols in vanets based on idm-im," in *International Conference on Communicatins and Networking in China*. Springer, 2017, pp. 33–40.

[126] P. Sarao, P. Sindhu, and V. Navakishor, "Analysis of routing protocols based on network parameters in wanet," *Int. J. Comput. Sci. Eng*, vol. 6, no. 6, pp. 8–13, 2018.

[127] S. Sarkar, "Reliable and energy-aware routing in mobile ad-hoc networks," *International Journal of Wireless and Mobile Computing*, vol. 16, no. 2, pp. 117–127, 2019.

[128] O. G. Prakasi and P. Varalakshmi, "Decision tree based routing protocol (dtrp) for reliable path in manet," *Wireless Personal Communications*, vol. 109, no. 1, pp. 257–270, 2019.

[129] G. Sallam and A. Mahmoud, "Performance evaluation of olsr and aodv in vanet cloud computing using fading model with sumo and ns3," in *2015 International Conference on Cloud Computing (ICCC)*. IEEE, 2015, pp. 1–5.

[130] J. Jiang and G. Han, "Routing protocols for unmanned aerial vehicles," *IEEE Communications Magazine*, vol. 56, no. 1, pp. 58–63, 2018.

[131] X. Tan, Z. Zuo, S. Su, X. Guo, X. Sun, and D. Jiang, "Performance analysis of routing protocols for uav communication networks," *IEEE Access*, 2020.

[132] A. V. Leonov and G. A. Litvinov, "Applying aodv and olsr routing protocols to air-to-air scenario in flying ad hoc networks formed by mini-uavs," in *2018 Systems of Signals Generating and Processing in the Field of on Board Communications*. IEEE, 2018, pp. 1–10.

[133] P. Xie, "An enhanced olsr routing protocol based on node link expiration time and residual energy in ocean fanets," in *2018 24th Asia-Pacific Conference on Communications (APCC)*. IEEE, 2018, pp. 598–603.

[134] P. Yang, K. Tang, J. A. Lozano, and X. Cao, "Path planning for single unmanned aerial vehicle by separately evolving waypoints," *IEEE Transactions on Robotics*, vol. 31, no. 5, pp. 1130–1146, 2015.

[135] C. Huang and J. Fei, "Uav path planning based on particle swarm optimization with global best path competition," *International Journal of Pattern Recognition and Artificial Intelligence*, vol. 32, no. 06, p. 1859008, 2018.

[136] E. W. Weisstein, "Hemisphere," 2002.

[137] J. Gou, Y.-X. Lei, W.-P. Guo, C. Wang, Y.-Q. Cai, and W. Luo, "A novel improved particle swarm optimization algorithm based on individual difference evolution," *Applied Soft Computing*, vol. 57, pp. 468–481, 2017.

[138] S. Luke, "1 essentials of metaheuristicsl," 1.

[139] K. Salah, "On the deployment of voip in ethernet networks: methodology and case study," *Computer Communications*, vol. 29, no. 8, pp. 1039–1054, 2006.

[140] X. Ji, X. Meng, A. Wang, Q. Hua, F. Wang, R. Chen, J. Zhang, and D. Fang, "E2pp: An energy-efficient path planning method for uav-assisted data collection," *Security and Communication Networks*, vol. 2020, 2020.

[141] B. J. O. de Souza, "An approach for movement coordination of swarms of unmanned aerial vehicles using mobile networks," Ph.D. dissertation, Master's thesis, Pontifical Catholic University of Rio de Janeiro, 2015.

[142] Z. Liu, A. C. Reynolds *et al.*, "A sequential-quadratic-programming-filter algorithm with a modified stochastic gradient for robust life-cycle optimization problems with nonlinear state constraints," *SPE Journal*, 2020.

[143] Z. Zheng, Y. Wang, F. Xie, and C. Li, "Entry optimization computation using simplex algorithm reference trajectory programming," in *Proceedings. The 2009 International Symposium on Computer Science and Computational Technology (ISCSCI 2009).* Citeseer, 2009, p. 120.

[144] A. Varga and R. Hornig, "An overview of the omnet++ simulation environment," in *Proceedings of the 1st international conference on Simulation tools and techniques for communications, networks and systems & workshops.* ICST (Institute for Computer Sciences, Social-Informatics and ..., 2008, p. 60.

[145] D. Krajzewicz, J. Erdmann, M. Behrisch, and L. Bieker, "Recent development and applications of sumo-simulation of urban mobility," *International journal on advances in systems and measurements*, vol. 5, no. 3&4, 2012.

[146] C. Sommer, R. German, and F. Dressler, "Bidirectionally coupled network and road traffic simulation for improved ivc analysis," *IEEE Transactions on mobile computing*, vol. 10, no. 1, pp. 3–15, 2010.

[147] C. Sommer, D. Eckhoff, A. Brummer, D. S. Buse, F. Hagenauer, S. Joerer, and M. Segata, "Veins: The open source vehicular network simulation

framework," in *Recent Advances in Network Simulation.* Springer, 2019, pp. 215–252.

[148] M. Drusch, U. Del Bello, S. Carlier, O. Colin, V. Fernandez, F. Gascon, B. Hoersch, C. Isola, P. Laberinti, P. Martimort *et al.*, "Sentinel-2: Esa's optical high-resolution mission for gmes operational services," *Remote sensing of Environment*, vol. 120, pp. 25–36, 2012.

[149] W. C. Lee, *Mobile communications engineering: theory and applications.* McGraw-Hill Education, 1998.

[150] M. Haklay and P. Weber, "Openstreetmap: User-generated street maps," *IEEE Pervasive computing*, vol. 7, no. 4, pp. 12–18, 2008.

[151] B. Alidaee, H. Wang, and F. Landram, "A note on integer programming formulations of the real-time optimal scheduling and flight path selection of uavs," *IEEE transactions on control systems technology*, vol. 17, no. 4, pp. 839–843, 2009.

[152] N. Nigam, S. Bieniawski, I. Kroo, and J. Vian, "Control of multiple uavs for persistent surveillance: Algorithm and flight test results," *IEEE Transactions on Control Systems Technology*, vol. 20, no. 5, pp. 1236–1251, 2011.

[153] B. D. Song, J. Kim, and J. R. Morrison, "Rolling horizon path planning of an autonomous system of uavs for persistent cooperative service: Milp formulation and efficient heuristics," *Journal of Intelligent & Robotic Systems*, vol. 84, no. 1-4, pp. 241–258, 2016.

[154] C.-M. Tseng, C.-K. Chau, K. Elbassioni, and M. Khonji, "Autonomous recharging and flight mission planning for battery-operated autonomous drones," *arXiv preprint arXiv:1703.10049*, 2017.

[155] T. A. Feo and M. G. Resende, "Greedy randomized adaptive search procedures," *Journal of global optimization*, vol. 6, no. 2, pp. 109–133, 1995.

[156] N. Metropolis, A. W. Rosenbluth, M. N. Rosenbluth, A. H. Teller, and E. Teller, "Equation of state calculations by fast computing machines," *The journal of chemical physics*, vol. 21, no. 6, pp. 1087–1092, 1953.

[157] S. Kirkpatrick, C. D. Gelatt, and M. P. Vecchi, "Optimization by simulated annealing," *science*, vol. 220, no. 4598, pp. 671–680, 1983.

[158] R. W. Eglese, "Simulated annealing: a tool for operational research," *European journal of operational research*, vol. 46, no. 3, pp. 271–281, 1990.

[159] Y. Wu and J. Wang, *Algorithm Design Practice for Collegiate Programming Contests and Education*. CRC Press, 2018.

[160] P. Joshi, *Artificial intelligence with python*. Packt Publishing Ltd, 2017.

[161] M. Y. Arafat and S. Moh, "Routing protocols for unmanned aerial vehicle networks: A survey," *IEEE Access*, vol. 7, pp. 99 694–99 720, 2019.

[162] R. A. Nazib and S. Moh, "Routing protocols for unmanned aerial vehicle-aided vehicular ad hoc networks: A survey," *IEEE Access*, vol. 8, pp. 77 535–77 560, 2020.

[163] M. Y. Arafat, M. A. Habib, and S. Moh, "Routing protocols for uav-aided wireless sensor networks," *Applied Sciences*, vol. 10, no. 12, p. 4077, 2020.

[164] M. Polese, F. Chiariotti, E. Bonetto, F. Rigotto, A. Zanella, and M. Zorzi, "A survey on recent advances in transport layer protocols," *IEEE Communications Surveys & Tutorials*, vol. 21, no. 4, pp. 3584–3608, 2019.

[165] D. S. Lakew, U. Sa'ad, N.-N. Dao, W. Na, and S. Cho, "Routing in flying ad hoc networks: A comprehensive survey," *IEEE Communications Surveys & Tutorials*, vol. 22, no. 2, pp. 1071–1120, 2020.

[166] C. Pu, "Link-quality and traffic-load aware routing for uav ad hoc networks," in *2018 IEEE 4th international conference on collaboration and Internet computing (CIC)*. IEEE, 2018, pp. 71–79.

[167] C. Li, L. Zheng, W. Xie, and P. Yang, "Ad hoc network routing protocol based on location and neighbor sensing," in *2018 IEEE international conference on computer and communication engineering technology (CCET)*. IEEE, 2018, pp. 1–5.

[168] M. F. Sohail, C. Y. Leow, and S. Won, "Non-orthogonal multiple access for unmanned aerial vehicle assisted communication," *IEEE Access*, vol. 6, pp. 22 716–22 727, 2018.

[169] A. M. Hayajneh, S. A. R. Zaidi, D. C. McLernon, M. Di Renzo, and M. Ghogho, "Performance analysis of uav enabled disaster recovery net-

works: A stochastic geometric framework based on cluster processes," *IEEE Access*, vol. 6, pp. 26 215–26 230, 2018.

[170] H. H. Choi, S. H. Nam, and T. Shon, "Two tier search scheme using micro uav swarm," *Wireless Personal Communications*, vol. 93, no. 2, pp. 349–363, 2017.

[171] F. Liang, J. Nguyen, W. Gao, W. G. Hatcher, and W. Yu, "Towards uav assisted multi-path data streaming in mobile ad-hoc networks," in *2018 International Conference on Computing, Networking and Communications (ICNC)*. IEEE, 2018, pp. 599–603.

[172] A. H. Wheeb, R. Nordin, A. Samah, M. H. Alsharif, M. A. Khan *et al.*, "Topology-based routing protocols and mobility models for flying ad hoc networks: A contemporary review and future research directions," *Drones*, vol. 6, no. 1, p. 9, 2022.

[173] M. Tanveer, A. Alkhayyat, A. Naushad, N. Kumar, A. G. Alharbi *et al.*, "Ruam-iod: A robust user authentication mechanism for the internet of drones," *IEEE Access*, 2022.

[174] M. Mozaffari, W. Saad, M. Bennis, Y.-H. Nam, and M. Debbah, "A tutorial on uavs for wireless networks: Applications, challenges, and open problems," *IEEE communications surveys & tutorials*, vol. 21, no. 3, pp. 2334–2360, 2019.

[175] A. Orsino, A. Ometov, G. Fodor, D. Moltchanov, L. Militano, S. Andreev, O. N. Yilmaz, T. Tirronen, J. Torsner, G. Araniti *et al.*, "Effects of heterogeneous mobility on d2d-and drone-assisted mission-critical mtc in 5g," *IEEE Communications Magazine*, vol. 55, no. 2, pp. 79–87, 2017.

[176] A. A. Khuwaja, Y. Chen, N. Zhao, M.-S. Alouini, and P. Dobbins, "A survey of channel modeling for uav communications," *IEEE Communications Surveys & Tutorials*, vol. 20, no. 4, pp. 2804–2821, 2018.

[177] I. U. Khan, I. M. Qureshi, M. A. Aziz, T. A. Cheema, and S. B. H. Shah, "Smart iot control-based nature inspired energy efficient routing protocol for flying ad hoc network (fanet)," *IEEE Access*, vol. 8, pp. 56 371–56 378, 2020.

[178] G. Asha, V. Vaidhehi, T. Cedric, and S. Balaji, "A review of routing protocols for airborne networks," *International Journal of Innovative Research in Advanced Engineering*, vol. 2, no. 3, pp. 5–10, 2015.

[179] C. Perkins, E. Belding-Royer, and S. Das, "Rfc3561: Ad hoc on-demand distance vector (aodv) routing," 2003.

[180] T. Clausen, P. Jacquet, C. Adjih, A. Laouiti, P. Minet, P. Muhlethaler, A. Qayyum, and L. Viennot, "Optimized link state routing protocol (olsr)," 2003.

[181] J. Wang, C. Jiang, Z. Han, Y. Ren, R. G. Maunder, and L. Hanzo, "Taking drones to the next level: Cooperative distributed unmanned-aerial-vehicular

networks for small and mini drones," *Ieee vehIcular technology magazIne*, vol. 12, no. 3, pp. 73–82, 2017.

[182] P. Jacquet, "Optimized link state routing protocol," *Internet-draft, draft-ietf-manet-olsr-02. txt*, 2000.

[183] C. E. Perkins and P. Bhagwat, "Highly dynamic destination-sequenced distance-vector routing (dsdv) for mobile computers," *ACM SIGCOMM computer communication review*, vol. 24, no. 4, pp. 234–244, 1994.

VITAE

- Name: Gamil Abdullah Mohsen Ahmed
- Nationality: Yemeni
- Date of Birth: 01/01/1979
- Email: *jameel.almoliki@gmail.com*
- Permenant Address: Ibb Yemen
- Education

2018-2022	Ph.D., Computer Engineering May 2022. Faculty of Computer Science and Engineering King Fahd University of Petroleum and Minerals (KFUPM), KSA Thesis Title: ' Internet of Drones Deployment for Intelligent Transportation System Application'
2014-2017	M.Sc., Computer Engineering Sep 2017. Faculty of Computer Science and Engineering King Fahd University of Petroleum and Minerals (KFUPM), KSA Thesis Title: FBNoC: FPGA-based network on chip emulator
2001-2004	B.Sc. Computer Engineering, 2004 The University of Mosul, Mosul, Iraq

- Research Interest

  Wireless Sensor Network, Intelligent Transportation System, Mobile Robotics and Intelligent Systems, Vehicular Ad-hoc Network, Internet of Things, Smart City, multicore simulations using FPGAs., Machine Learning., Deep Reinforcement Learning. My work involves both analysing and enhancing the performance of Intelligent systems. Specifically, most of my previous studies targeted wireless communication networks such as V2I communication of constrained resources such as flying RSU Infrastructure, i.e. Internet of drones (IoD) networks deployment for VANETs Assistance. The key question that drives my research is, how to efficiently utilize these constrained resources to meet the application's requirements in robust and reliable manners. The main thrust of my work during my Ph.D. program is developing collision avoidance protocols for flying Robotic-based networks. Furthermore, enhance the VANETs' communication network using flying Roadside Unit (i.e.UAVs). Improving the performance of such strategies require a strong knowledge. This fact led me to gain a strong background and great interest in collaborative control and decision-making of multi-agent systems.

9.3 Publications

This section presents the publications that have been emanated from this thesis.

9.3.1 Journal Papers

- Ahmed, G., Sheltami, T., Mahmoud, A., Yasar, A. (2020). IoD swarms collision avoidance via improved particle swarm optimization. Transportation Research Part A: Policy and Practice, 142, .260-278
- Ahmed, G., Sheltami, T., Deriche, M., Yasar, A. (2021). An energy efficient IoD static and dynamic collision avoidance approach based on gradient optimization. Ad Hoc Networks, 118, 102519.
- Ahmed, G. A., Sheltami, T. R., Mahmoud, A. S., Imran, M., Shoaib, M. (2021). A Novel Collaborative IoD-Assisted VANET Approach for Coverage Area Maximization. IEEE Access, 9, .61211-61223
- Ahmed, G., Sheltami, T., Yasar, A. A Novel 3D Simulation Model for IoD-To-Vehicles Communication in IoD-Assisted VANET. submitted to Electronics
- Ahmed, G. A., Sheltami, T. R., Mahmoud, A., Yasar, Energy-Efficient UAVs Coverage Path Planning Approach. submitted to Special Issue ”Digital Twins in Smart Transportation and Mobility” in ”Computer Modeling in Engineering Sciences”
- Ahmed, G. A., Sheltami, T. R., Mahmoud, A., Yasar, Performance Evaluation of DSDV, OLSR, and AODV Routing Protocols for Drone Communication Networks. (Drafted).